Analysis of piled bridges at sites prone to liquefaction and lateral spreading in New Zealand

January 2018

C Keepa, G Adhikari, A Murashev, D Novakov
Opus International Consultants Ltd, Wellington

M Cubrinovski, J Haskell
University of Canterbury, Christchurch

NZ TRANSPORT AGENCY
WAKA KOTAHI

ISBN 978-1-98-851287-7 (online)

NZ Transport Agency
Private Bag 6995, Wellington 6141, New Zealand
Telephone 64 4 894 5400; facsimile 64 4 894 6100
bridgemanual@nzta.govt.nz
www.nzta.govt.nz

Keepa, C, G Adhikari, A Murashev, D Novakov, M Cubrinovski and J Haskell (2017) *Analysis of piled bridges at sites prone to liquefaction and lateral spreading in New Zealand*. Wellington: NZ Transport Agency. 161pp.

Keywords: bridge, lateral spread, liquefaction, piles, seismic

Acknowledgements

The funding for the project was provided by the New Zealand Transport Agency. Dr John Wood of John Wood Consulting is thanked for his detailed review of the manuscript. Messrs Nigel Lloyd, John Reynolds and Barry Wright of the New Zealand Transport Agency are gratefully acknowledged for the valuable comments, advice and the support they provided to the research team through the course of the project.

Disclaimer

Abbreviations and acronyms

API	American Petroleum Institute
ASCE	American Society of Civil Engineers
BE	best estimate
BEP	best estimate parameters
BH	borehole
BNWF	beam on non-linear Winkler foundation
CALTRANS	California Department of Transportation
COR	centre of rotation
CPT(s)	cone penetrometer test(s)
DBD	displacement based design
ESA	equivalent static analysis
FBD	force based design
LB	lower bound
LBP	lower bound parameters
LD	lateral displacement
LDI	lateral displacement index
MASW	multi-array surface wave
MBIE	Ministry of Business, Innovation and Employment
NZGS	New Zealand Geotechnical Society
PEER	Pacific Earthquake Engineering Research Centre
PGA	peak ground acceleration
PSA	pseudo-static analysis
PVC	polyvinyl chloride
p-wave	compression wave
RM	reference model
SDOF	single degree of freedom
SESA	substructure equivalent static analysis
SLS	serviceability limit state
SPT	Standard Penetration Test
s-wave	shear wave
UB	upper bound
UBP	upper bound parameters
ULS	ultimate limit state

Contents

Executive summary

Introduction

This report is a result of a follow-on project to the NZ Transport Agency (Transport Agency) research project that culminated in the publication of research report 553 *The development of design guidance for bridges in New Zealand for liquefaction and lateral spreading*. In the research project, methods for the evaluation of bridges on liquefiable sites were assessed and a pseudo-static procedure was developed for the analysis and seismic assessment of piled bridges in New Zealand. This report summarises this procedure and presents two examples of its application. Also included in this report are two examples of the evaluation of liquefaction and lateral spreading and guidance on the scoping of site investigations at bridge sites with liquefaction susceptible geologies.

Liquefaction evaluation examples

Example 1: Tauherenikau Bridge

The first liquefaction evaluation example is for the Tauherenikau River Bridge near Masterton. The 127 m long eight-span concrete bridge is located on deep gravelly alluvium located about 10 km from both the Wellington Fault and the Wairarapa Fault that have recurrence intervals of 715 to 1,575 years (Langridge et al (2011)) and 1,200 years respectively. These faults are capable of producing Mw 7.5 and Mw 8.2 earthquakes. A simple deterministic assessment of ground motions proved useful in the assessment of seismicity at this site where there are known active faults nearby. Comparison of the *Bridge manual*'s 1,000 year return ground motions (peak ground acceleration = 0.45 g, Mw 7.0) with ground motion predictions from rupture of the Wairarapa and Wellington Faults suggests the seismic hazard could be under-represented by the *Bridge manual* at this location.

The importance of understanding whether a) the gravels are clast supported and b) the characteristics of the supporting soil matrix in the liquefaction evaluation of gravelly soils are exemplified in the Tauherenikau Bridge example. Challenges with assessing the density of gravelly soils, and therefore their liquefaction potential using penetration testing techniques, is addressed with the supplementation of triggering evaluation using shear wave velocities and the adjustment of standard penetration tests using blow counts measured in 25 mm increments.

Example 2: Belfast Road Underpass

The second example of liquefaction evaluation is for a site just north of Christchurch where a new underpass is to be constructed. The two-lane, two-span reinforced concrete bridge will take Belfast Road over the new, at grade Christchurch Northern Motorway and has approach embankments that are 8 m high at the abutments with spill through slopes and a central pier.

The site is underlain by variable thinly bedded silty sands, sands and soft organic silts that overlie dense sands and gravels from a depth of about 9.5 m. Little surface manifestation of liquefaction was observed at this site in the Christchurch 2011 or the Darfield 2010 earthquakes yet analysis solely using cone penetrometer tests (CPTs) to assess liquefaction susceptibility suggested extensive liquefaction near the surface. This example demonstrates the importance of assessing the susceptibility of silty soils using measurement and observations of their plasticity and comparing this with the soil behaviour index calculated in using CPTs.

Lateral spread displacements are evaluated using empirical methods and adjusted to account for the limited width of the embankment and the stabilising effect of the continuous crust between the two approach embankments. A simplified method for the prediction of seismic horizontal ground displacements of non-liquefied soils is implemented in the calculation of displacement profiles for each phase of the earthquake.

Examples of the pseudo-static analysis of piled bridges

Example 1: Anzac Bridge

The first pseudo static bridge analysis example is of the existing four-span Anzac Bridge that crosses the Avon River in Christchurch. This bridge is situated on loose to medium dense sands and was damaged by liquefaction and lateral spreading in both the 2010 Darfield and the 2011 Christchurch earthquakes. The response of the bridge in the lateral spreading phase following the February 2011 Mw 6.2 Christchurch earthquake has been analysed with surface ground displacements measured at the site used to develop ground displacement profiles with depth at the pile locations and ground motions derived from nearby strong motion stations.

Comparison of the model predictions of displacement and bending to observations following the earthquake demonstrates that the method captures the key deformation with strutting of bridge deck constraining horizontal ground displacement at the end of the deck, backward rotation of the abutment back-walls about the deck and bending of the abutment piles as the river banks spread toward the middle of the river. Kinematic demands on the pier piles and rotation of the pier columns, consistent with the observed deformation modes, is also captured in the whole bridge analysis.

The predicted back-wall rotation was greater than observed (approximately double) and the level of bending predicted at the top of the piers is inconsistent with the degree of cracking and spalling observed at the top of the pier columns. This suggests, while the method predicts the deformation mechanism, it may overestimate the level of damage in this case although some of this apparent overestimation could be attributed to simplifications made in the model, particularly the degree of fixity at the connections and possibly with transforming the 3D bridge into a 2D model.

Example 2: Belfast Road Underpass

The second pseudo static bridge analysis example is for the Belfast Bridge, the same bridge that is the subject of one of the example liquefaction evaluations. In this example, a method is developed to implement the pseudo-static analysis procedure in the design of a new bridge.

Being a transient problem, the peak ground displacements at different supports of a bridge may or may not occur concurrently and may not be in the same direction as the inertial demands. Different combinations of inertia and kinematic demands for each of the three phases of the ground response are evaluated in the design of the bridge. For the specimen bridge, the lateral spreading phase proved to be critical for the design of the abutment piles. The cyclic liquefaction phase was critical for the design of the pier piles.

The relative merits of single pile vs whole bridge were assessed. The major challenge of a single pile analysis is knowing the conditions (load and displacement) applied at the head of the pile by the superstructure. For the specimen bridge in this example where ground conditions are similar across the site and there is a relatively symmetric distribution of stiffness and mass, analysis of a single pile gave

similar results to the global analysis for the lateral spreading phase and greatly reduced computational effort for this phase.

Inertia demands from the superstructure have been applied either as a force or as displacement. It is difficult to confirm which approach is more realistic. However for the single pile model, imposing displacement makes more sense, as it provides the response that is comparable with the whole bridge model. Where inertial demands are applied as force, an appropriate boundary condition should be assigned at the superstructure level.

Observations

The performance predictions of the pseudo-static analysis method are generally sensitive to the predicted extent of liquefaction and the horizontal ground displacements applied to the soil springs in the analysis. As shown in these examples, ground displacement predictions have a high degree of uncertainty. This is one area where further research is needed to improve the accuracy of the performance predictions using the pseudo-static method. Other aspects of the analysis procedure requiring further evaluation are:

- the evaluation of liquefaction resistance of pumice soils, gravelly soils and sites with thinly interbedded layers
- the assessment of ground displacement profiles at bridge piles for sites with improved ground
- whether the pinning effect of the piles is sufficiently accounted for within the pseudo-static method
- for bridges with approach embankments, how the stiffness of the bridge affects the direction of spreading
- assessing bridge response with kinematic and inertia loading in the transverse and longitudinal directions together.

The examples highlight some of the challenges when applying the recommended methods. There is a high degree of uncertainty associated with the assessment of liquefaction hazards and the response of bridges to lateral spreading. Built-in conservatisms at each step of the analysis to manage this uncertainty is not always transparent and the compounding effect of these can result in overly conservative assessments and designs.

One thing emphasised in this study is the need for parametric studies and sound engineering judgement to envelope the response, gain a good understanding of the likely seismic performance of the bridge and make appropriate design decisions.

Abstract

This report presents a summary of the outcomes of a follow-on project to a research project commissioned by the NZ Transport Agency that culminated in the publication of research report 553 *The development of design guidance for bridges in New Zealand for liquefaction and lateral spreading effects*. This project has involved summarising the pseudo-static approach developed in the research project for the analysis of bridge foundations on sites prone to liquefaction and presents two examples of the evaluation of the liquefaction hazard and two examples of the analysis of piled bridges on sites prone to liquefaction. This report is intended for engineers who are familiar with geotechnical and structural design practice for static and seismic loading of bridges.

1 Introduction

New Zealand state highways serve as connections between communities and many are primary lifelines following natural disasters. The seismic performance of bridges has a substantial effect on post-earthquake response and recovery efforts and on the quality of life of affected communities.

Many New Zealand bridges and highway structures are located on sites with soils that are susceptible to liquefaction and lateral spreading in earthquakes. A large number of recorded cases of damage to bridges from lateral ground displacements and settlements associated with liquefaction have been reported worldwide. There are also recent examples of earthquake damage to bridge structures caused by liquefaction and lateral spreading in Christchurch as a result of the 2010 Darfield and 2011 Christchurch earthquakes.

In current practice, a variety of methods are being used to assess liquefaction, lateral spreading and their effects on piled bridges. With a goal of promoting a consistent approach to assessment and design, the NZ Transport Agency (the Transport Agency) commissioned a research project towards the development of design guidelines for the design of bridges on sites prone to liquefaction and lateral spreading in New Zealand. This work was published in *NZ Transport Agency research report 553* (Murashev et al 2014). The report discusses the effects of liquefaction on bridges and looks in detail at the available methods to analyse liquefaction and lateral spreading effects on bridges in New Zealand.

This report is the result of a follow-on project to the research project. It gives practical advice for scoping site investigations and laboratory testing, summarises the pseudo-static and sub-structure analysis procedures for the analysis of piled bridges on liquefiable sites and presents two examples that demonstrate the use of the procedures.

This report should be read in conjunction with Murashev et al (2014), the *Bridge manual* (NZ Transport Agency 2016) and the MBIE–NZGS modules *Guidelines for earthquake geotechnical engineering practice*. Modules 1, 2 and 3 (MBIE–NZGS 2016a; 2016b; 2016c) covering general aspects of earthquake geotechnical engineering, site investigations and the assessment of liquefaction hazards are the most relevant. In module 5 (MBIE–NZGS 2017) the design of ground improvement for sites prone to liquefaction is specifically for buildings but some advice is also applicable to bridges.

This document has been prepared for qualified professional geotechnical and bridge engineers with a sound background in geo-mechanics, structural mechanics, seismology and liquefaction theory. There is a high degree of uncertainty associated with the assessment of liquefaction hazards and the response of bridges when soils liquefy in earthquakes. Sound engineering judgement must be applied in all cases and the recommendations provided here should be adapted appropriately to the site conditions and project requirements.

This document is not intended to be a detailed treatise of the latest research in geotechnical earthquake engineering. Instead it provides state of practice advice for competent professionals to use on routine projects where bridges are at risk from liquefaction and lateral spreading. More complex studies may be warranted for high-cost or critical structures on lifeline routes for complex sites with a high liquefaction and lateral spreading hazard. Engineers involved in the analysis and design of bridges on liquefiable sites need to keep abreast of continuing research and developments on this subject and adapt design methods accordingly.

2 Site investigations

2.1 Scope

Bridge sites must be thoroughly investigated to allow identification and assessment of all geotechnical hazards, including liquefaction-related hazards. This chapter discusses the scoping of geotechnical investigations for liquefaction assessment purposes. Supplementary investigations may be required to assess other hazards and geotechnical issues but are not discussed here.

Site investigations to assess the liquefaction and lateral spreading hazard at bridge sites are usually staged to get the maximum value from the site investigation. Preliminary assessment of the liquefaction hazard at a site starts with a desktop study to gather information on the site geology including geomorphology, depositional history and seismology. Initial sub-surface investigations are then planned based on the findings of the preliminary assessment. Additional stages of site investigation may be carried out to reduce uncertainties, refine the geotechnical assessment made using the initial investigations or to optimise a design.

Further discussion on the planning of site investigations to assess the site liquefaction hazard is in the MBIE–NZGS (2016b; 2016c) modules 2 and 3. Details on specific requirements for site investigations and laboratory testing can be found in module 2.

2.2 Preliminary investigations

A comprehensive desktop study is the first step in assessing the susceptibility of the site soils to liquefaction and making a preliminary assessment of the liquefaction hazard. The desktop study should include a review of:

- the published geology of the area that describes its geomorphology, stratigraphy and seismicity
- the GNS active faults database
- the *Bridge manual* to determine peak ground accelerations (PGAs)
- liquefaction hazard maps if they available
- previous site investigations carried out in the same geologic units at or near the site
- observations from previous earthquakes (the Canterbury and Napier earthquakes for example)
- if the assessment is for an existing bridge, the bridge as-built drawings and construction records (eg piling records).

2.3 Subsurface investigation planning

The level of site investigation should be appropriate to the geology of the site, the importance of the route, the size of the bridge and the stage of assessment or design (eg concept, developed or detailed design).

The primary investigation techniques for sites prone to liquefaction include electronic static cone penetrometer tests (CPTs) and fully cored machine boreholes with Standard Penetration Test (SPT) measurements.

Except in cases where shallow gravel layers or other inclusions that could cause early refusal of the CPT are expected, the first phase of investigation often involves pushing CPTs to characterise the ground conditions over the length and width of the bridge. Because of their nature of deposition, the soils at sites susceptible to liquefaction are often spatially variable and the CPTs are a relatively cheap and fast method of obtaining information on the ground conditions compared with boreholes. The results of the CPT investigation can then be used to strategically place machine boreholes, plan depths for SPTs, sampling for laboratory testing and plan piezometer installations.

It is advantageous to place some, if not all boreholes adjacent to CPTs to calibrate soil properties such as soil type and fines content interpreted from the CPT measurements against the borehole descriptions and laboratory testing on samples from the boreholes. Look to sample locations with a fairly consistent normalised tip resistance and sleeve friction when establishing or calibrating CPT correlations and carefully measure the depth that the sample is retrieved from.

It is often not possible to push the CPT through layers of gravelly soils. For sites with a predominantly gravel profile, CPT testing is generally not feasible. SPTs in gravels may not be reliable and can indicate loose gravelly layers to be dense when course gravels or boulders are encountered. In these cases, initial investigations could include surface geophysics (eg multi-array surface waves (MASW), spectral analysis of surface waves to make a preliminary assessment of subsurface conditions, identification of layers that could be liquefiable and planning borehole investigations. Shear wave velocities from surface geophysics are typically not suitable for detailed liquefaction triggering analysis because of the difficulty in distinguishing soil layers less than a few metres thick without significant contrasts in shear wave velocity. Downhole or cross-hole measurement of shear wave velocity should be carried out in casings grouted into selected boreholes for detailed assessment of liquefaction triggering at sites containing deep gravel layers.

Where thin gravel layers are encountered, predrilling and casing through the gravel to test underlying sand and silt layers by pushing a CPT through the casing is an option.

3 Summary of procedures for analysis of piles

3.1 Introduction

When evaluating the effects of liquefaction and lateral spreading on the performance of a bridge and its pile foundations using the equivalent static approach (or pseudo-static analysis ((PSA), it is necessary to conduct at least three separate analyses, each addressing a different stage (phase) of the response and using different assumptions in the assessment as recommended in Murashev et al (2014).

1 Cyclic analysis without liquefaction (to estimate the pile-bridge response in the absence of liquefaction)

2 Cyclic analysis considering liquefaction of soils. In this analysis, kinematic loads due to ground displacements and inertial loads from the superstructure need to be simultaneously applied to the pile-bridge system while accounting for stiffness and strength degradation of the soils due to earthquake-generated excess pore water pressures

3 Lateral spreading analysis including effects of liquefaction and lateral spreading on the pile foundations and bridge structure. In this analysis, effects and consequences of liquefaction-induced lateral spreading is considered including substantial stiffness and strength degradation of liquefied soils, and kinematic loads due to large (biased) ground displacements caused by spreading. Inertial loads may also be considered in this analysis.

It is recommended readers become familiar with Murashev et al (2014) before reading this document.

3.2 Method 1: Pseudo-static analysis (recommended)

In the PSA approach, a relatively simple beam-spring model is used for the soil-pile-bridge system to perform an equivalent static analysis (ESA). In this case, the PSA focuses on effects of soil liquefaction and lateral spreading on the response of the bridge and its pile foundations in particular.

3.2.1 Key objectives of PSA

The scope of PSA is limited to the following objectives in the assessment:

1 To provide a simple and practical tool for assessment of piles in liquefying soils undergoing lateral spreading

2 To estimate the maximum pile response (rather than a time history of the response)

3 To estimate the damage to piles for the design earthquake loading (and address some aspects in the seismic performance evaluation)

4 To address uncertainties associated with the complex response of piles in liquefying soils including uncertainties associated with the use of an equivalent static approach (ESA) for its modelling.

The keywords here are: simple, maximum pile response, damage to piles and uncertainties.

The PSA method can be applied either to a single-pile, pile group or the whole bridge.

3.2.2 Uncertainties associated with PSA of piles in liquefying soils

There are three principal sources of uncertainties in the assessment of pile response using PSA:

1 Ground motions (earthquake loads) representative for the site

2 Ground response and soil-structure interaction during the development of excess pore water pressure, evolution of liquefaction, and post-liquefaction

3 Representative input parameters for the PSA.

Item 1 implies that variation in the seismic demand should be considered; item 2 implies that variation in soil stiffness and strength, and interaction loads should be considered; item 3 implies that variation in parameters and results should be considered because of analysis uncertainties.

3.2.3 Principal phases in the pseudo-static analysis of piles

The assessment of piles based on the simplified PSA approach involves three phases (figure 3.1).

- Phase 1: Characterisation of site conditions and earthquake loading (section 3.2.3.1)
- Phase 2: Evaluation of free field ground response
- Phase 3: Evaluation of pile foundations response and bridge performance.

The output from each phase provides key input for the subsequent stage of the assessment and PSA.

3.2.3.1 Phase 1: Characterisation of site conditions and earthquake loading

In phase 1 of the assessment, site characteristics and earthquake load parameters are determined involving the following steps (figure 3.2):

1.1) Identify ground motion parameters based on interpretation of the seismic hazard at the site for relevant return periods. In particular, PGA (a_{max}) and earthquake magnitude (M_w) pairs are required for liquefaction assessment based on simplified procedures. In addition, spectral accelerations at relevant periods for the bridge structure ($S_a(T_b)$) could be used to estimate the bridge response and approximate inertial loads in the PSAs. Guidance for identification of ground motion parameters is provided in the *Bridge manual*.

1.2) Define representative soil profiles for the site based on adequate field investigations and their interpretation specific to the assessment of effects of liquefaction and lateral spreading on pile foundations and bridge structure. Typically this would involve boreholes, CPT, SPT and compression and sheer wave velocity logging followed by geotechnical evaluation and interpretation. Guidance on site investigation procedures for liquefaction assessment is provided in the *Bridge manual* and also in the MBIE–NZGS module 2 (2016b) and module 3 (2016c).

1.3) Identify soils (layers) susceptible to liquefaction (ie soils that have the potential to liquefy during earthquakes) either based on soil index properties (plasticity index (PI) in conjunction with grain-size composition of soils) or using field test parameters such as the CPT-based soil behaviour type index (I_c). Each layer in the adopted representative soil profiles is evaluated separately, and is identified as

susceptible to liquefaction if either $PI \leq 12$ or $I_c \leq 2.6$. Geologic evaluation including details on depositional processes, age of the deposits and geomorphology is essential in the assessment of liquefaction susceptibility.

Figure 3.1 Three principal phases in the simplified assessment of piles based on the PSA approach

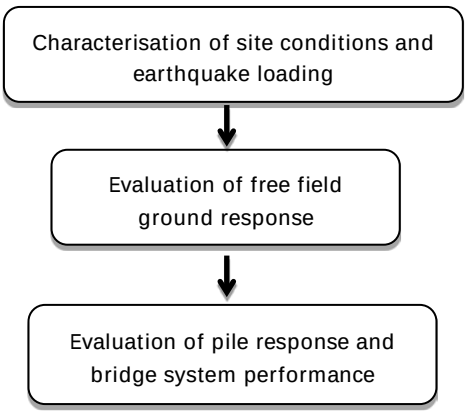

Figure 3.2 Key steps in phase 1 of the assessment: determination of earthquake load parameters for liquefaction assessment, definition of representative soil profiles, and identification of soils (layers) susceptible to liquefaction

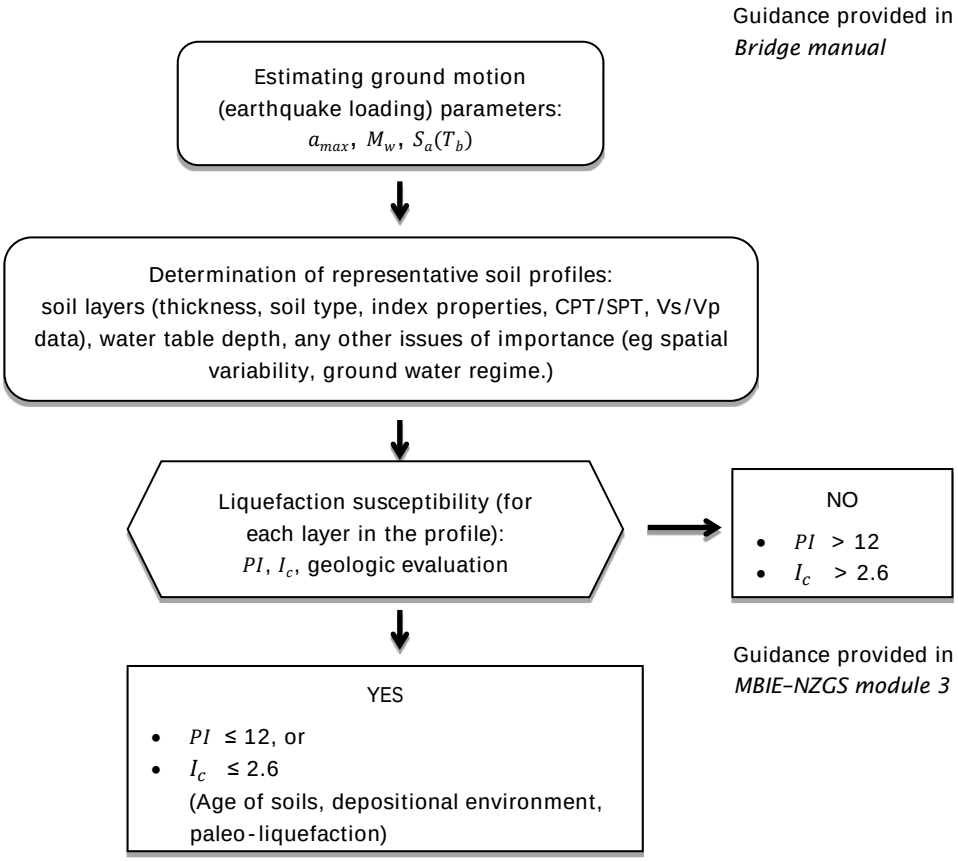

3.2.3.2 Phase 2: Evaluation of free field ground response

In phase 2 of the assessment, the earthquake-induced ground response, including effects of liquefaction and lateral spreading, is evaluated assuming free field ground conditions (ie ignoring the presence and effects of the bridge structure and its foundations). This phase of the analysis aims at identifying first the layers within the soil profile that will liquefy if the site is shaken by the design earthquake, and then estimating consequent ground deformation and displacements, both cyclic (transient, during the shaking) and permanent (residual displacements) due to liquefaction and lateral spreading. This phase of the assessment provides basis for interpretation of the effects of liquefaction on soil stiffness, strength and instability potential. As shown in figure 3.3, this phase involves separate assessments for level ground conditions and lateral spreading.

The free field ground response for assumed level ground conditions is evaluated using conventional liquefaction evaluation procedures based on the simplified (semi-empirical) approach adopted in international and New Zealand professional guidelines (eg MBIE–NZGS 2016c, figure 5.2 outlines the key factors that need to be considered in the liquefaction vulnerability assessment). The simplified liquefaction evaluation approach involves the following steps (figure 3.3):

2.1) Analyse liquefaction triggering (eg Boulanger and Idriss 2014; MBIE–NZGS 2016c). In this step of the assessment, factors of safety against liquefaction triggering (FS) are calculated for each layer (soil) susceptible to liquefaction, for the adopted earthquake load (a_{max} - M_w, pair).

2.2) For each layer in the soil profile, estimate maximum cyclic shear strains ($\gamma_{max-cyc}$), ie maximum ground strains generated during the earthquake shaking, for assumed free field level ground conditions at the site. The methods of Tokimatsu and Asaka (1998), and Ishihara and Yoshimine (1992) can be used to estimate ($\gamma_{max-cyc}$); in these methods, either $CSR_{7.5}$ or FS (calculated in step 2.1) are used as input parameters together with a representative penetration resistance for each soil layer. Here, $CSR_{7.5}$ indicates a cyclic stress ratio converted to $M_w 7.5$.

2.3) Estimate maximum volumetric strains (ε_{v-max}) generated during post-liquefaction re-consolidation of the deposit for each layer susceptible to liquefaction using either the method of Zhang et al (2002) or Ishihara and Yoshimine (1992). In these methods, FS computed in step 2.1 and representative penetration resistance of the layer (computational sub-layer) are needed as input parameters.

2.4) By integrating maximum cyclic shear strains ($\gamma_{max-cyc}$; computed in step 2.2) and maximum volumetric strains (ε_{v-max}; computed in step 2.3), with respect to the depth, profiles of maximum cyclic ground displacements $U_g(z)$ and ground settlements $s(z)$, respectively, are estimated throughout the depth of the deposit.

2.5) Using the representative penetration resistance, computed FS values and liquefaction-induced ground strains and displacements, identify layers within the soil profile showing potential for soil instability due to strain softening or a complete loss of strength.

There are no well-established procedures for assessment of lateral spreading though some guidance is provided in Murashev et al (2014), MBIE–NZGS (2016c) and Cubrinovski and Robinson (2015). The lateral spreading assessment should include the following steps:

2.6) Evaluate free face conditions associated with the dimensions of river channel (free face height and width of channel) and topographic conditions, in particular, maximum gradient of ground surface slope, gradient of the base of liquefied layer, and proximity of topographic features to the free face. Geologic evaluation of deposits, geomorphology and river channel features is essential in this step.

Figure 3.3 Key steps in phase 2 of the assessment: evaluation of free field ground response (without effects of bridge structure) assuming level ground conditions (for liquefaction analysis), and actual free face conditions for lateral spreading

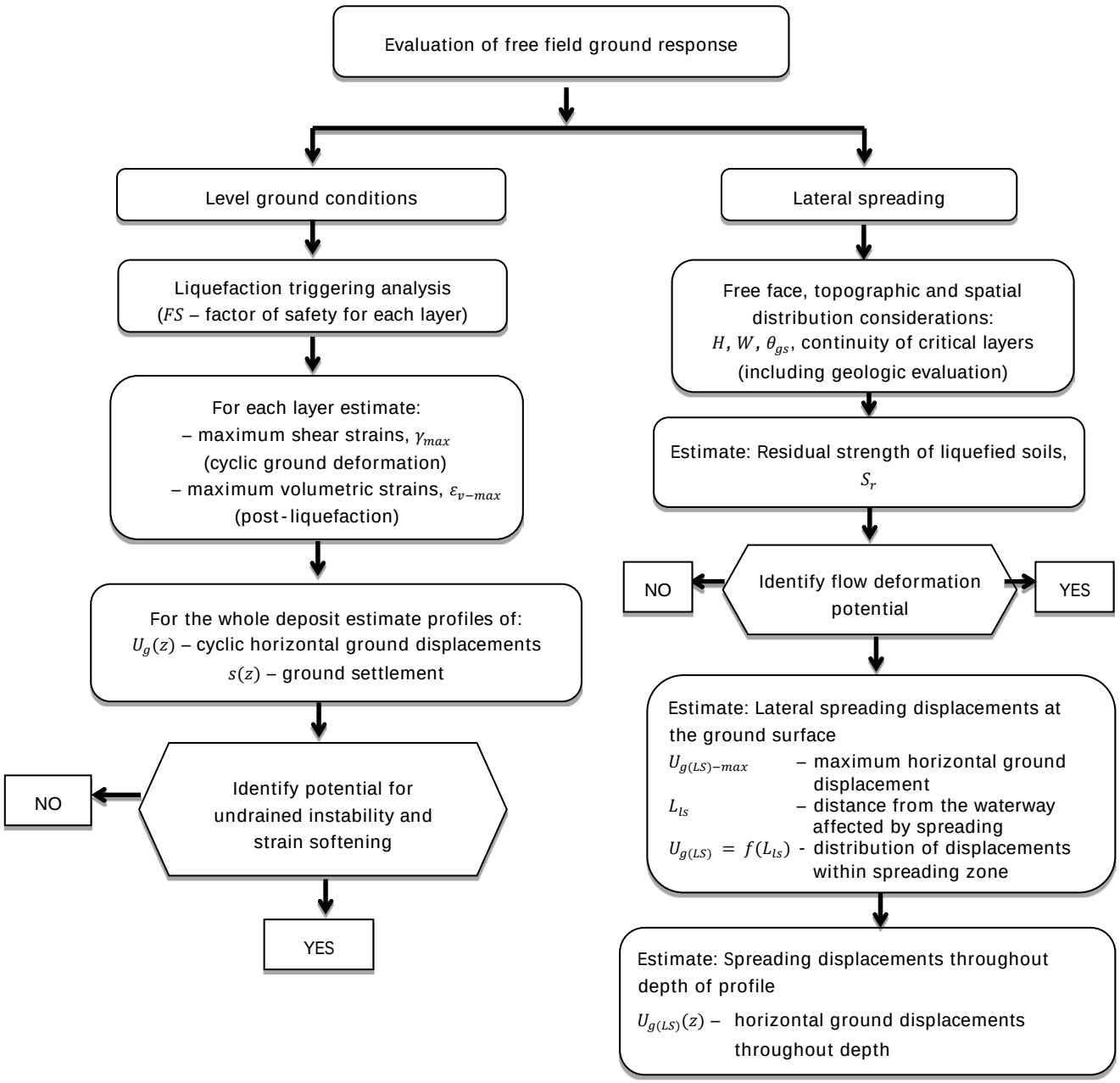

2.7) From the adopted soil profile and triggering analysis, identify critical layer(s) for lateral spreading, and estimate the residual strength (S_r) of these soils assuming they have fully liquefied. Idriss and Boulanger (2008), Olson and Stark (2002) and others provide methods for estimating residual strength of liquefied soils.

2.8) Assess the potential for flow deformation by comparing driving shear stresses with the residual strength of liquefied soils.

2.9) Estimate lateral spreading displacements at the ground surface: a) maximum lateral ground displacement at the free face (river banks); b) zone affected by lateral spreading (ie distance from the waterway affected by permanent ground displacements); c) spatial distribution of permanent ground displacements within the spreading zone (Cubrinovski and Robinson 2015). The methods of Zhang et al (2004), Youd et al (2002) and Tokimatsu and Asaka (1998) can be used for some of these estimates; poor predictability of spreading displacements and uncertainties in the estimates should be addressed through parametric studies.

2.10) Estimate permanent ground displacement profiles throughout depth (eg the methods of Zhang et al (2004) and Tokimatsu and Asaka (1998) allow for such estimates to be made).

3.2.3.3 Phase 3a: Evaluation of pile foundations (single pile analysis)

In phase 3 of the assessment, PSAs are performed to: a) evaluate the response of the pile foundations, and b) evaluate the performance of the bridge system. Separate analyses can be conducted for this purpose using either a single pile model or a whole-bridge model. These analyses are conceptually similar, but do include some considerations specific to the single pile analysis and whole bridge analysis respectively.

The assessment of piles through the use of a single pile model involves the following key steps (figure 3.4):

3.1) Define a computational beam-spring model. A typical beam-spring model for PSA is shown in figure 3.5. In this finite element model, horizontal springs are used to represent the soil while beam elements are used to model the pile. A multi-layered deposit can be considered with different soil properties for each layer. In fact, each spring can have different properties, and hence, depth-dependent soil properties can be modelled. Soil spring parameters can be adjusted to represent both liquefied soils and non-liquefied soils.

i) A non-liquefiable layer at the ground surface (crust) is commonly assumed from the ground surface to the water table; the crust can extend beyond the depth of the water table if the immediate sub-surface is composed of non-liquefiable soils (eg soils with I_c >2.6).

ii) Soil spring parameters are determined using conventional field parameters such as SPT blow count or CPT resistance.

iii) Bi-linear soil springs are used to model load-deformation relationship of soils. Two parameters define the soil spring: stiffness and strength; the latter defines the soil capacity or the maximum pressure that the soil can take (apply) to the pile.

iv) Both stiffness and strength can be degraded due to effects of liquefaction (for liquefied layers) or nonlinear soil response (for non-liquefiable soils).

v) The pile is modelled with a series of beam elements; the length of the beam elements should be equal to the spring spacing, which is preferably 0.1 m and not larger than 0.2 m.

vi) Tri-linear (or bilinear) moment-curvature (M-ϕ) relationship for the pile is used. For a reinforced concrete (RC) pile, the tri-linear relationship indicates threshold levels of concrete cracking (C), yielding of reinforcement (Y) and ultimate state at concrete crushing (U).

vii) Translational and rotational fixity (boundary) conditions should be defined at the top and tip of the pile depending on the particular connection and installation details.

viii) Two equivalent static loads can be applied to the pile: a horizontal ground displacement (U_G), and a lateral force at the pile head (F), representing the kinematic load on the pile due to ground displacements and the inertial load on the pile due to vibration of the superstructure respectively.

The key issue in the implementation of PSA is how to select appropriate values for the soil stiffness, soil strength, and lateral loads applied to the pile in the ESA (ie what are the appropriate values for β_L, p_{max}, U_G and F in the model shown in figure 3.5).

Figure 3.4 Key steps of the assessment in phase 3a (single pile analysis with or without pile- group effects) pseudo- static analyses involving definition of computational model, PSA using best- estimate parameters, parametric PSAs using lower- bound and upper- bound values of critical parameters, evaluation of pile response and damage to piles

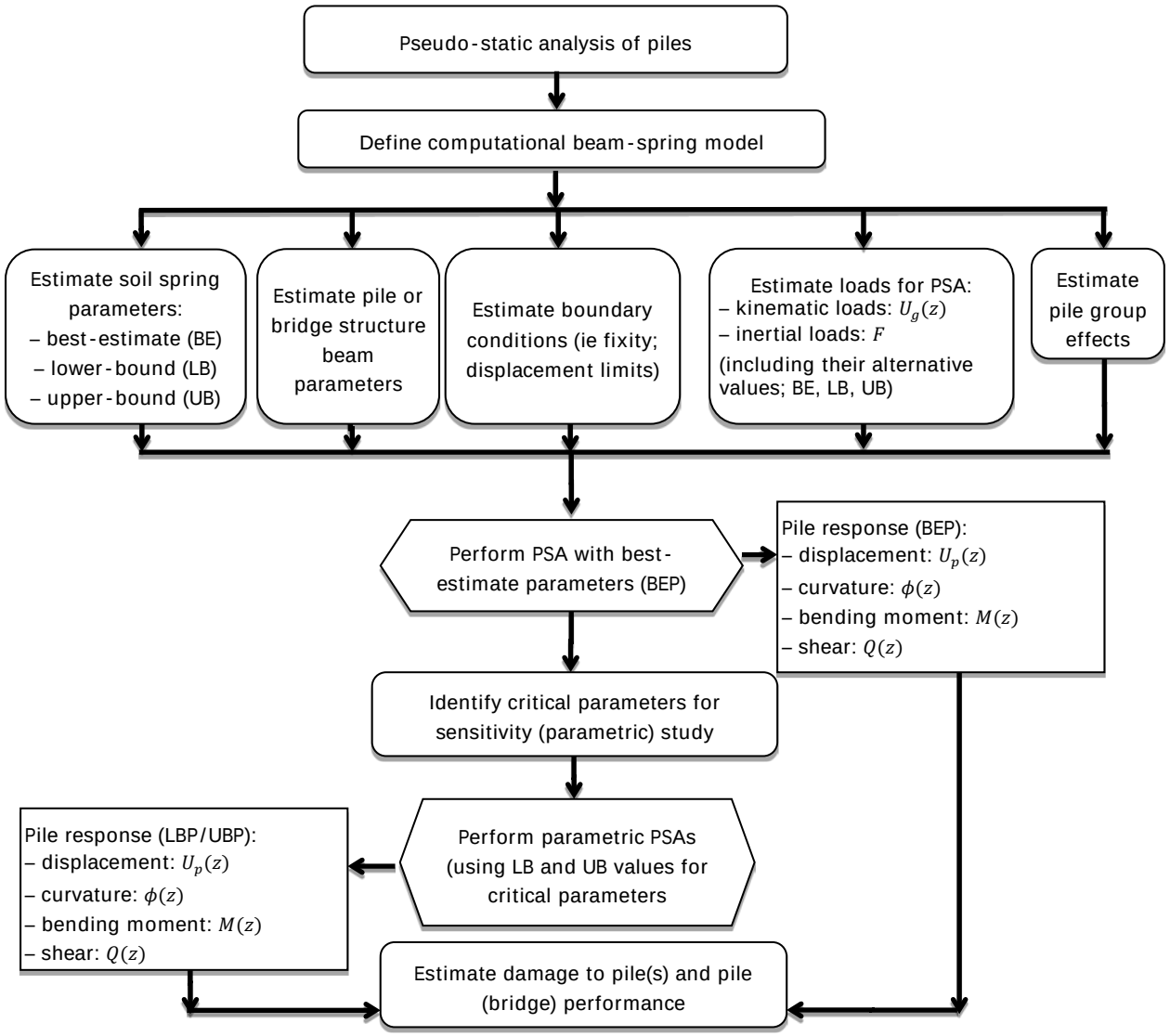

Figure 3.5 Beam- spring model for pseudo- static analysis of piles in liquefying soils: simplified models and parameters for characterisation of nonlinear behaviour (Cubrinovski et al 2009)

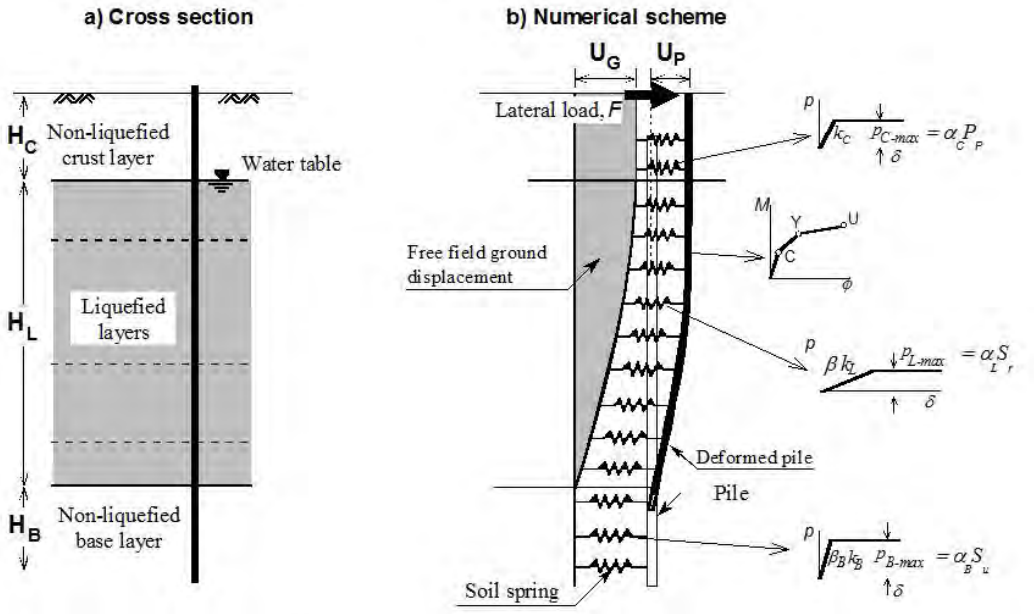

3.2) Determine soil-spring parameters

i) Non-liquefied crust (layers at/near ground surface)

The soil spring stiffness for the crust is given by:

$$K_C = \beta_c \cdot k_C \cdot s \cdot D_0 \qquad \text{(Equation 3.1)}$$

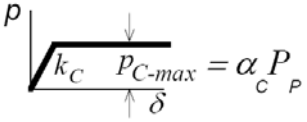

where K_C = spring stiffness (MN/m), β_c = degradation factor ($\beta_c \leq 1.0$), s = spring spacing (m), D_0 = pile diameter (m), and k_c = horizontal subgrade reaction coefficient given by:

$$k_C = 56 \cdot N \cdot (100 D_0)^{-3/4} \qquad (N/m^3) \qquad \text{(Equation 3.2)}$$

where N = SPT blow count (uncorrected, as measured in the field, assumed to correspond to 60% energy efficiency, N_{60}). The subgrade reaction coefficient in equation 3.2 represents the stiffness at 25 mm horizontal displacement. The spring stiffness can be degraded by assuming values of β_c = 0.5 to β_c = 1.0, for greater levels of relative displacement between the soil and pile.

The yield force of the soil spring corresponding to the ultimate soil pressure is given by:

$$P_{C-max} = p_{c-max} \cdot s \cdot D_0 = \alpha_c \cdot P_p \cdot s \cdot D_0 \quad \text{(for non-cohesive soils)} \qquad \text{(Equation 3.3)}$$

$$P_{C-max} = p_{c-max} \cdot s \cdot D_0 = 9 \cdot S_u \cdot s \cdot D_0 \quad \text{(for cohesive soils)} \qquad \text{(Equation 3.4)}$$

where p_{c-max} - yield strength of soil spring, P_p – Rankine passive pressure, s – spring spacing, D_0 – pile diameter, S_u – undrained strength of soil, and α_c = scaling factor accounting for 'wedge effect' on individual piles, as compared with the Rankine pressure for an equivalent continuous wall (P_p).

Cubrinovski et al (2009) recommend use of:

α_c = 4.5 as a reference value; α_c = 3 lower-bound, and α_c = 5 upper-bound values. (Equation 3.5)

Note that α_c = 1.0 is used for the springs connected to a pier or abutment (wall). Alternatively, force deformation curves determined by Caltrans (2013), or as proposed by Mokwa (1991), could be used. This choice is based on the following reasoning. The adopted method assumes large lateral ground displacements associated with spreading, and consequently large relative displacements between the wall/abutment and the surrounding soils. Hence, the mobilised passive pressure should be associated with large shear strains corresponding to the critical (steady) state of deformation of soils. Also, it is postulated that the key mechanism of lateral spreading is associated with kinematic loads due to ground displacement, and not by inertial loads associated with dynamic actions and response of the soil-structure system. Under these assumptions, and considering all the approximations involved, the use of the Rankine passive pressure seems to be a rational estimate for the passive pressure, in the simplified model.

ii) Non-liquefied deeper soils

The soil spring parameters for deeper non-liquefied soils are determined using an identical approach as for the crust (at the ground surface) except for the following modification due to a reduction or loss of the 'wedge effect':

$$P_{B-max} = p_{B-max} \cdot s \cdot D_0 = \alpha_c \cdot P_p \cdot s \cdot D_0 \quad \text{(for non-cohesive soils)} \qquad \text{(Equation 3.6)}$$

Note: α_c = 1.0 (instead of 3) could be used, and is the preferred choice at larger depths based on a reasoning that a wedge cannot develop at large depths; in some cases, this choice may have substantial effects on pile displacements and bending moments. It is important to note that non-liquefied layers of cohesionless soils are expected to develop excess pore water pressures during the earthquake, which may substantially reduce both stiffness and strength of these layers. In addition, at the interface between the liquefied layer and underlying non-liquefied sandy soil, a substantial stiffness and strength reduction may occur due to pore water flow and loss of shearing resistance, confinement and constraint from the liquefied soil just above the interface. Hence, theoretical and empirical solutions derived based on the plastic flow assumption and experiments involving non-liquefiable soils are not directly applicable for the characterisation of non-liquefied layers of cohesionless soils in the adopted PSA involving liquefied soils.

iii) Liquefied soils

The soil spring parameters for liquefied soils are determined using similar procedure as for the non-liquefied soils but with the following modifications:

The spring stiffness is reduced by a degradation factor β_L and is given by:

$$K_L = \beta_L \cdot k_L \cdot s \cdot D_0 \qquad \text{(Equation 3.7)}$$

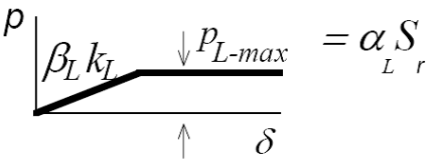

$= \alpha_L S_r$

in which K_L = spring stiffness, s = spring spacing, D_0 = pile diameter (width), k_L = subgrade reaction coefficient (equation 3.2) and β_L is defined as:

For cyclic loading (transient phase):		For lateral spreading (post-liquefaction spreading):		
β_L = 0.05	– reference value	β_L = 0.01	– reference value	
β_L = 0.02	– lower bound value	β_L = 0.001	– lower bound value	(Equation 3.8)
β_L = 0.10	– upper bound value	β_L = 0.02	– upper bound value	

The recommended ranges of values for β_L are based on back-calculations of case histories from the 1995 Kobe earthquake (Ishihara and Cubrinovski 1998a 1998b; Ishihara and Cubrinovski 2004) and benchmark liquefaction experiments on full-size piles (Cubrinovski et al 1999; Cubrinovski et al 2006).

The soil spring yield force for the liquefied soil is given by:

$$P_{L-max} = p_{L-max} \cdot s \cdot D_0 = \alpha_L \cdot S_r \cdot s \cdot D_0 \quad \text{(Equation 3.9)}$$

In which p_{L-max} - yield strength of soil spring, s - spring spacing, D_0 - pile diameter (width), and S_r - residual strength of liquefied soil. α_L = 1.0 is provisionally adopted as a reference value (best estimate, BE), and lower-bound (LB) value; α_L > 1.0 values could be used in parametric evaluations, but this would be generally conservative.

S_r can be estimated using empirical correlations between S_r and SPT blow count N (Idriss and Boulanger 2008; Olson and Stark 2002; Seed and Harder 1990) or S_r and CPT resistance (Idriss and Boulanger 2008; Olson and Stark 2002). While there is no consensus on the particular relationship to use, Idriss and Boulanger (2008) could be adopted as a reference relationship until further updates are provided. Whichever relationship is adopted, it is most important to consider the uncertainty in the analysis associated with estimates of the residual strength of liquefied soils. For example, BE values (average), UB and LB values for S_r should be used considering a relevant range of values in the empirical correlation.

3.3) Estimate pile beam parameters: The *M-ϕ* relationship for the pile should be determined using conventional procedures for cross-section analysis with simplified elastic-plastic stress-strain relationships for concrete and steel. Determine the moment-curvature relationship for the particular cross-section dimensions and details, yield strength and threshold strains of materials, axial loads and pre-stress levels of the piles.

3.4) Determine boundary conditions for the pile. The boundary conditions should reflect translational and rotational constraints imposed on the pile by the superstructure, structural members and pile-soil or pile-structure interfaces. For example, in the case of a rigidly connected pile into a cap, a fixed rotation at the pile head should be specified; it is common to define fixed translation and free rotation at the tip of the pile, which in turn means soil properties (springs) of the base layer will practically define the rotational constraints near the tip of the pile.

3.5) Estimate the kinematic loads due to permanent lateral spreading displacements.

i) Free field lateral spreading displacement estimated in steps 2.9 and 2.10, $U_{g(LS)}(z)$, is applied at the free end of the soil springs (as illustrated in figure 3.5).

ii) Common assumptions in the analyses are: all of the ground surface displacement is accommodated within the liquefied layer; the crust and other non-liquefied layers move as rigid blocks on top of the underlying liquefied layers; the base non-liquefied layer does not move (is stationary). However, there are no restrictions imposed by the model in this regard, and the

method allows the designer to apply various magnitudes and distribution patterns of lateral ground displacements in any soil layer.

iii) A range of ground displacements should be considered in the lateral spreading analyses to address the uncertainties associated with the estimate of spreading-induced displacements. For example: best-estimate (BE), lower-bound (LB) and upper bound (UB) values could be determined; as a practical approach in the absence of accurate estimates, the LB and UB values could be 50% and 200% of the best-estimate values for lateral spreading ground displacements.

iv) The displacements estimated in step 2.10 are free-field ground movements unaffected by the presence of piles and bridge structure. Reduction of soil displacements due to pinning and strutting effects should be considered for stiff and strong bridge structures with sufficient capacity to resist large lateral loads/movements. Cubrinovski et al (2014a; 2014b) found that in the 2010–2011 Canterbury earthquakes pinning (strutting)-effects reduced the displacements of the foundation soils to 50% of the corresponding free-field displacements of the river banks. (Note: 'pinning' refers to a resistance to ground movement provided by the superstructure. Pinning effects could be provided by global effects, eg from the strutting of the superstructure between the two abutments, or by structural members such as cantilevering of the piles above non-liquefied soils).

3.6) Estimate inertial loads due to vibration of the superstructure:

i) An estimate for the dynamic response of the bridge is needed, and in particular, the peak horizontal acceleration response or spectral acceleration at a relevant period of the bridge.

ii) A portion of this acceleration can be used to calculate the equivalent horizontal static force. This force can be applied at the top of the pile considering the total number of piles, and distribution of the total inertial load on the piers, abutments and their piles (ie by estimating the tributary load on the pile).

iii) A combined ground displacement (kinematic load) and inertial load should be applied for the transient (cyclic) phase of the response. Inertial loads may or may not be considered in the lateral spreading analysis, at discretion of the engineer.

The selection of appropriate equivalent static loads (steps 3.5 and 3.6) is one of the most difficult tasks in the PSA, because these inputs in effect require estimation of the seismic response of the ground and superstructure respectively. Tokimatsu et al (2005) and Boulanger et al (2007) provide some guidance for the selection of combined kinematic and inertial loads on the pile while considering the predominant periods of the ground motion and structure. As commonly acknowledged for equivalent static approaches targeting seismic problems, the particular kinematic-inertial load combination that produces the critical (peak) pile response in liquefying soils cannot be predicted with any high degree of certainty. However, it is recommended that all assumptions adopted in the analysis, such as those related to the stiffness, strength and displacement magnitude of liquefied soils, and maximum accelerations, inertial loads and structural response, should be compatible and consistent with the particular response scenario adopted in the analysis.

3.7) Estimate pile-group effects

Pile group effects generally arise due to two separate mechanisms: a) obstruction of ground movement by adjacent and surrounding piles, and b) cross-interaction and transfer of loads amongst piles through structural members (ie pile caps, grade beams or rafts).

Shadowing effects (obstruction of ground movement by the frontline and adjacent piles) and *overlapping of wedges* (reduced pressure on the pile due to shared wedge-zone with adjacent piles in the row) affect both the movement of the foundations soils and the imposed kinematic loads from the soil on the pile.

i) Soil-pile interaction effects in non-liquefied soils depend on the pile spacing and number of piles in the group. For spacing of six diameters or greater ($s \geq 6D_0$), pile group effects due to shadowing and overlapping of wedges could be ignored.

ii) Also, pile group effects in liquefied soils associated with shadowing and overlapping of wedges could be ignored.

iii) The beam-spring model used in the analysis including the effects from inertial and kinematic loads can reflect pile group effects through modification of soil spring parameters, and also through a change in the magnitude and distribution of loads per pile while considering the load characteristics, and configuration of the bridge and foundation piles.

3.8) Perform PSA with best-estimate parameters. In this analysis, reference values or best-estimate parameters for the soil springs and loads are used, and pile response (ie horizontal pile displacements, curvatures, bending moments and shear) is estimated throughout the length of the pile.

3.9) Identify critical parameters for sensitivity study. In most of the cases the pile response will be particularly sensitive to only a few parameters. Critical parameters that should be scrutinised in sensitivity studies are: a) magnitude of lateral ground displacements, and b) strength parameters of soil springs for the crust layer, in cases where relatively large loads are applied from the crust layer on the pile/structure. In some cases other parameters such as properties of liquefied layer may become important/critical.

3.10) Perform parametric PSAs using LB and UB values for the identified critical parameters in step 3.9. The sensitivity study should be done systematically so the effects of variation of different parameters are rigorously examined and quantified. In these analyses, a range of pile responses are obtained for a relevant range of values for key parameters of the soil-spring model.

3.11) Using the computed pile responses in steps 3.8 and 3.10, assess the level of damage to the pile by comparing the computed curvatures to threshold curvatures associated with characteristic damage states such as: concrete cracking (C), yielding of reinforcement (Y), and ultimate state at concrete crushing (U), for RC piles (as defined by the *M-ϕ* relationship in step 3.3). The assessment of damage is performed throughout the length of the pile thus providing estimates for both severity and location of the damage.

3.2.3.4 Phase 3b: Evaluation of bridge performance (whole bridge analysis)

The assessment utilising a whole bridge model involves the following key steps (figure 3.6):

3.12) In principle, the soil and pile modelling for the whole bridge model is identical to the single-pile model. The global bridge analysis can provide more realistic simulation of the distribution of force and displacement demands throughout the bridge while considering the interaction between different components of the bridge, complex spatial distribution of subsurface conditions, foundation characteristics and ground movements along the bridge alignment.

i) The bridge superstructure can be modelled either as elastic or elastic-plastic, using linear or nonlinear beam elements, with adequate stiffness and strength of structural members.

ii) Gaps between the deck and the abutment can be modelled as well as deck-pinning or deck-strutting effects through the use of appropriate interface elements and boundary conditions. Abutments can be modelled as rigid members (beams).

iii) Liquefaction analysis and estimate of ground displacement profiles are required for each foundation (ie pile group for each abutment and pier). Lateral spreading displacements at the ground surface at the location of piers in the riverbed can be estimated by interpolating between the estimated spreading displacements at the river banks and assuming zero displacement at the centre axis of the riverbed.

3.13) The focus in the whole bridge analysis should be on the interaction effects and bridge-system influence on the response and damage to pile foundations. The analysis may allow estimating overall bridge movements including bias in residual deformations and displacements.

3.14) P-delta effects, potential buckling, dynamic effects of soil-foundation-structure interaction, and 3-D effects could be considered by separate checks and analyses, if deemed potentially significant.

The interpretation of damage to piles and overall bridge performance should integrate all results and findings from the analyses including assumptions made and treatment of uncertainties across all three phases in the assessment.

Figure 3.7 Key steps of the assessment in phase 3b (whole bridge analysis): determination of a whole bridge model including relevant loads and boundary conditions; analysis and interpretation of results focusing on bridge- system effects on damage and performance of pile foundations

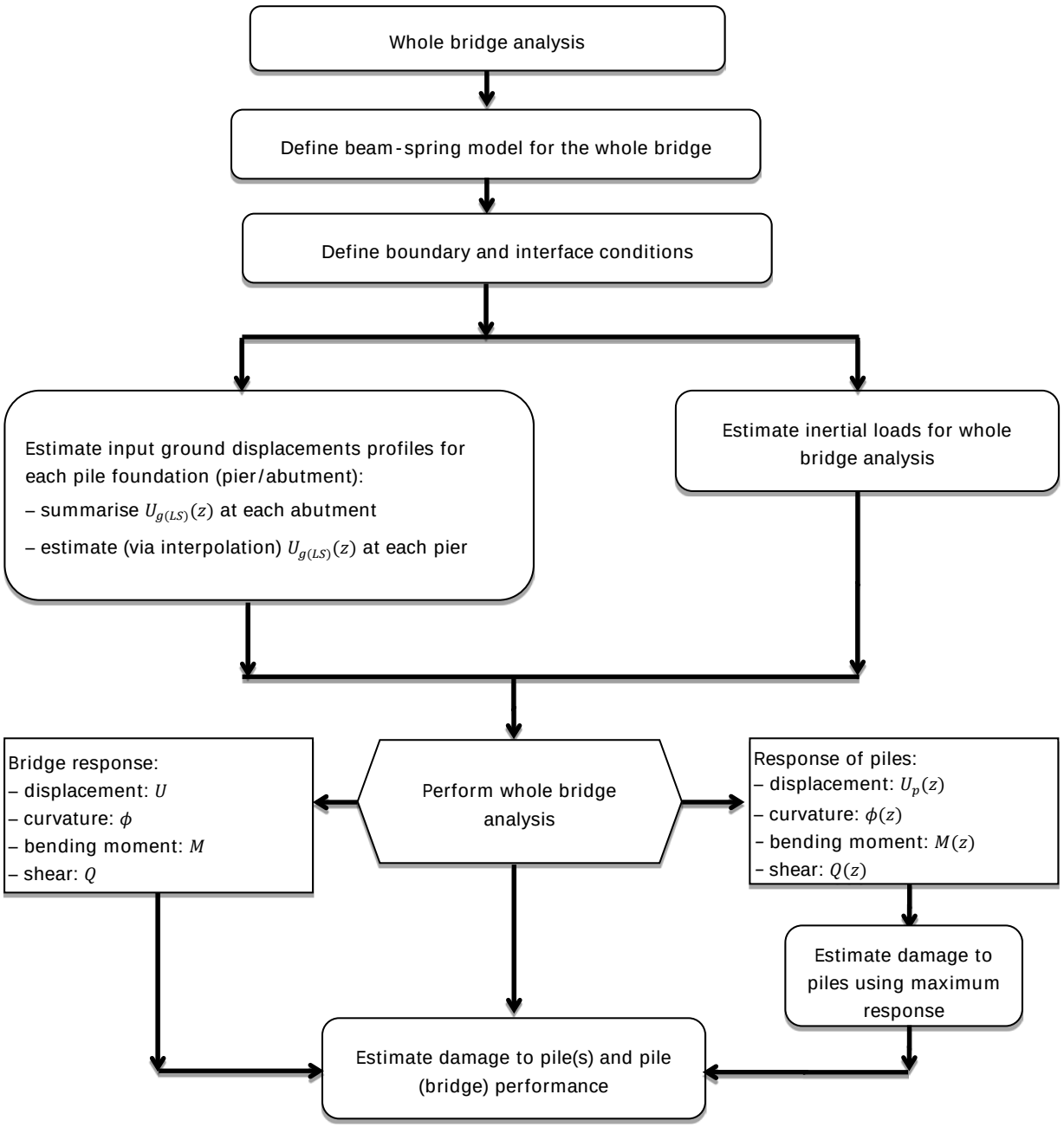

3.3 Method 2: Bridge substructure equivalent static analysis (overview)

3.3.1 Substructure equivalent static analysis (SESA) approach

The SESA method to assess the response of piled bridge abutments or piers in areas prone to liquefaction and laterally spreading is described by Ashford et al (2011) and Armstrong and Boulanger (2014). There

are several similarities between this approach and the PSA method. The susceptibility of the site soils to liquefaction, whether liquefaction will be triggered or not, the residual strength of the soil when liquefied and free-field ground response are assessed in the same ways described in the PSA method in section 3.2.3, phases 1 and 2. The key differences between the methods and the limitations of each are discussed in Murashev et al (2014).

The steps involved in calculating embankment displacement, Δ_{emb} and pile bending and shear demands for piled bridge foundations in laterally spreading slopes using the SESA approach are summarised in figure 3.8 and essentially involve three steps:

1 Calculate the slope displacements for a range pile and bridge restraining forces

2 Calculate the pile and bridge restraining forces for a range of embankment displacements

3 Find the embankment displacement and displacement compatible restraining force by comparing the results of steps 1 and 2.

Figure 3.8 Sub- structure analysis method for piled abutments (Armstrong et al 2014)

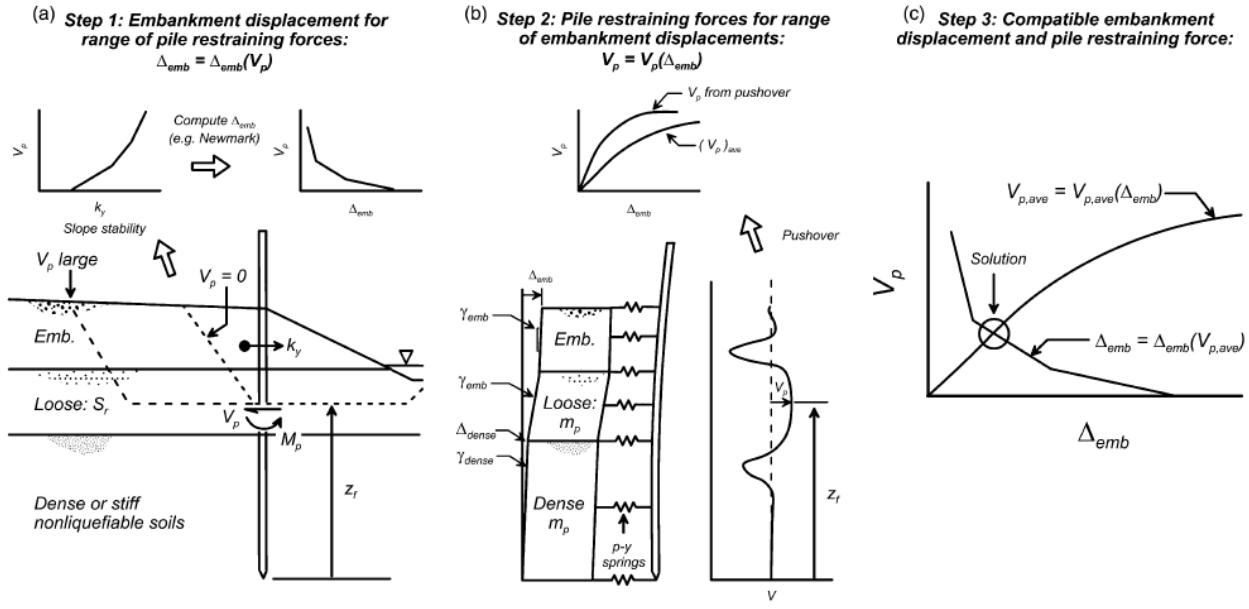

Each of these steps is discussed in more detail in the following sections.

3.3.2 Phase 1: Calculation of embankment displacements

In this step, embankment displacements are estimated using the Newmark sliding block method for a range of pile and bridge restraining forces. This involves calculating slope yield accelerations, k_y in a series of limit equilibrium slope stability analysis each with a different effective pile-pinning force and each with residual undrained strengths for layers expected to liquefy. The yield acceleration is calculated by finding the horizontal acceleration that produces a factor of safety of 1 in each slope stability analysis. Embankment displacements are a function of k_y and are calculated using a regression model such as Ambraseys and Srbulov (1995) or Bray and Travasarou (2007) or by integration of accelerations exceeding yield for several representative earthquake acceleration records. Ground improvement can be included within the slope stability analyses. This is usually achieved by assigning average effective improved ground strengths to the area of improved ground.

A range of possible failure surfaces intersecting the piles should be considered including circular and non-circular failure surfaces. The limit equilibrium method selected should satisfy both equilibrium of moments and horizontal forces. The pile restraining force can be applied as a single horizontal force at the centre of a row of piles or distributed over the width of a pile group. Application of large horizontal restraining forces can cause numerical problems in limit equilibrium analyses. In this situation, the restraining force can be distributed over some length of the failure surface. The slice base normal forces and the inter-slice forces should be carefully examined and adjustments made to the restraining force distribution when necessary.

Where there is a bending moment in the piles at their intersection with the slip surface that improves the stability of the slope, the shear force can be shifted vertically by a distance M_p/V_p to account for the pile bending effects. Restraint from propping by the deck should not be included in the pseudo-static slope stability analysis.

In some cases the sliding mass increases proportionately to the increase in the restraining force and a point is reached where there is little apparent reduction in slope displacement with increasing restraint. In reality the extents of the sliding mass will be limited by the topography, stratigraphy, the extent of liquefaction and the inconsistency of the inertia of the sliding mass reducing its average inertia. Recognising these limitations, Ashford et al (2011) recommend limiting the length of the sliding mass to four times the thickness of the embankment.

The calculated displacement versus restraining force are per unit width of the embankment. These displacements are factored by the tributary width for the embankment mass restrained by the abutment piles to establish a common dimension between the force-displacement relationships for the embankment and for the pile foundation/bridge superstructure.

The piles and bridge superstructure will restrain movement of an embankment mass that includes the full height portion across the embankment crest width, plus a portion of the side slope masses. This is accounted for by adopting an equivalent tributary width whose mass includes a portion of the side slope masses as shown in figure 3.9. Ashford et al (2011) recommended one-half of the side slope mass as a reasonable value of the contributing mass for design.

Figure 3.9 Embankment tributary mass

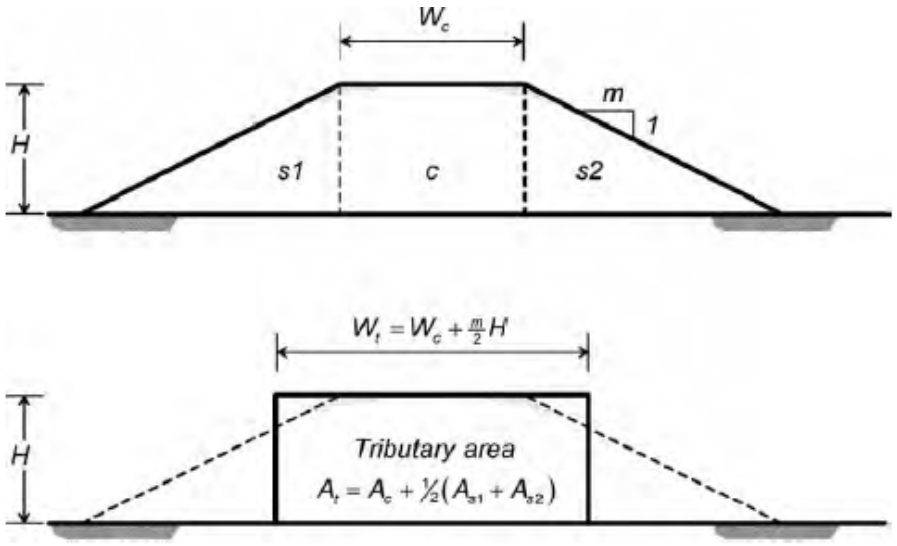

3.3.3 Phase 2: Calculation of pile effective pinning forces

Pile-pinning forces are estimated from a beam-spring pushover analysis of the pile foundation similar to the analysis described in phase 3 of the PSA method. The piles and pile caps are modelled as elastic or elasto-plastic beam elements and springs are used to represent the soils. Displacements are applied to the free field end of the springs in increments to calculate the effective pinning force in the piles for each increment of slope displacement.

To account for the influence of soils either side of the pile group and not just the soil directly behind the group, the properties of the pile elements are factored down. A $P-\Delta$ transformation can be used to account for bending induced in the piles from axial loads acting on the deformed piles.

Non-linear load – displacement curves for the soil springs can be approximated as p-y and t-z springs calculated using methods by the American Petroleum Institute (1993) and Mosher (1984). For layers expected to liquefy, p-y and t-z curves are calculated by factoring curves for the non-liquefied soil by the so called p-multiplier, m_p.

3.4 Method 3: Dynamic analysis (overview)

3.4.1 Introduction

As discussed in Murashev et al (2014), there are three general approaches to analysing bridges and piles in liquefying soils:

1 PSA or ESA

2 Direct dynamic (time history) analysis using the effective stress principles (ie effective stress analysis)

3 Substructure analysis methods which use some features of PSA, effective stress analysis and total stress dynamic analyses but are essentially hybrid approaches tailored to address specific aspects in the performance assessment.

This section provides a very brief summary of the seismic effective stress analysis. Indeed it is a very general overview including a brief outline of some aspects of effective stress analysis, which otherwise is a complex subject that would require a comprehensive coverage of all phases and important details of the analysis.

3.4.2 Brief outline of effective stress analysis characteristics

The reader is referred to the relevant sections and Murashev et al (2014, table 6.1) before reading this document.

3.4.2.1 Key objectives of effective stress analysis

Effective stress analysis has the following objectives in the assessment:

- To provide an advanced tool for assessment of the effects of soil liquefaction (including lateral spreading) on geotechnical and soil-structure systems (in this case, bridges)

- To realistically simulate the dynamic process of pore pressure build-up, development of liquefaction and post-liquefaction effects on soil stiffness, strength, deformation and stability.
- To simulate and assess the above soil liquefaction effects on the performance of foundations, superstructure and overall soil-structure system (bridge).

The keywords here are: advanced, dynamic soil-structure interaction, pile response, system performance.

Effective stress analysis is commonly applied to the whole soil-structure (bridge) system, but could be applied to a subsystem as well.

3.4.2.2 Principal phases of effective stress analysis

Seismic effective stress analysis involves the following principal phases (stages) in the assessment:

1 Characterisation of site conditions and earthquake loading. In principal this is similar to the intent presented in section 3.2.3.1 for PSA, though there are substantial differences in details, and importantly, additional information and inputs are needed for effective stress analysis. The key additional requirements are: i) For each soil layer considered in the analysis, parameters describing the dynamic behaviour of soils and explicitly specifying the liquefaction resistance of soils should be provided; ii) the ground motion must be defined as an acceleration (velocity) time history (hence, use of recorded or artificially generated ground motions is needed as input in the dynamic analysis).

2 Definition of numerical model. In this analysis phase, appropriate element types, mesh (element) sizes, boundary conditions, interface elements and initial stress state of the soil must be selected or computed. Here, one needs to consider the geometry of the structure, stratification of the soil deposit, objectives of the analysis and anticipated behaviour in order to define a numerical model which will facilitate rather than restrain the analysis.

   a Boundary/interface conditions and initial stress state of the soil may have a pivotal influence on the performance of the constitutive model and numerical analysis. Namely, one of the key advantages of the seismic effective stress analysis (and numerical analysis in general) is that no postulated failure and deformation modes are required as an input, as these are produced ('predicted') by the analysis itself. In this context, the selection of appropriate boundary conditions along end-boundaries or soil-foundation-structure interfaces is critically important in order to allow development of unconstrained response and deformation/failure modes.

   b Similarly, an initial stress analysis is required to determine gravity-induced stresses in the soil and account for their effects on the stress-strain behaviour, liquefaction resistance of soils and consequent transient and residual ground displacements.

3 Determination of constitutive model parameters. In this analysis phase, parameters of the constitutive model need to be determined using data from field investigations and results from laboratory tests on soil samples. The types and number of laboratory tests required for the parameters of the constitutive model may vary significantly and are model dependent. In general, however, all models have the same target, to model as accurately as possible the development of the excess pore water pressure and its effects on the relevant stress-strain relationships of the soil. Key steps in this process are:

   a Securing high-quality, representative and relevant field and laboratory data for the soils at the site.

   b Determining constitutive model parameters directly from field/laboratory data.

c Performing element-test-simulations to calibrate the remaining constitutive model parameters and identify their best-fit values that accurately simulate experimentally observed liquefaction resistance of soils.

4 Dynamic analysis and interpretation. In this final phase of the assessment, the acceleration time history defined under item a) is used as an input motion, and a dynamic analysis is performed. This involves (the list below is not an exhaustive list of important tasks):

a Selecting numerical parameters such as computational time increment, integration scheme and numerical damping

b Running the analysis

c Post-processing including extraction of results (time histories and maximum values for a large number of elements/nodes) and visualization of results to depict key response features and assess analysis performance and specific response details.

d Interpreting analysis results in the context of engineering assessment.

The analysis is quite demanding on the user in all phases including the final stages of post-processing and interpretation of results since it requires an in-depth understanding of the site, structure, phenomena considered, constitutive model used and particular features of the numerical procedures adopted in the analysis. More details on some key elements of effective stress analysis can be found in Cubrinovski (2011). Figure 3.10 outlines key phases and steps in the seismic effective stress analysis.

The analysis phases outlined above should not be considered in isolation, but rather they should be seen as essential components of an integrated process. This realisation is very important and suggests that good understanding and coherent treatment of all phases and details in the analysis are pivotal for a successful application of effective stress analysis to liquefaction problems.

Figure 3.10 Principal steps of the assessment of bridges (pile foundations) in liquefying (lateral spreading) soils using the seismic effective stress analysis (modified from Cubrinovski 2011)

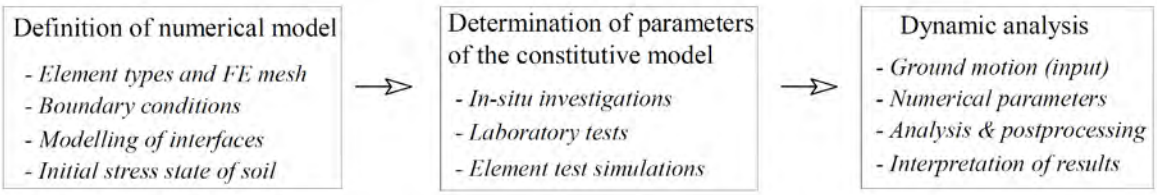

4 Liquefaction and lateral spreading evaluation examples

4.1 Introduction

This chapter presents two examples that demonstrate liquefaction evaluation at New Zealand bridge sites. The scenarios given in the examples aim to show how to approach the assessment of liquefaction and lateral spreading for two sites with different soil types and seismicity in New Zealand. The calculations are not presented in detail, rather the key judgement decisions and the reasoning behind these are provided for each case study.

The first example is for the Tauherenikau Bridge on SH 2 in the Wairarapa. This bridge is in an area of high seismicity, near active faults and is situated on a wide river plain with deep gravel alluvium. This example demonstrates the use of shear wave velocity to assess liquefaction of gravels for specific fault rupture scenarios.

In the second example, the liquefaction and lateral spreading hazard are evaluated for Belfast Road Over-bridge that is part of a grade-separated intersection for the proposed Christchurch Northern Arterial. This site is underlain by approximately 9.5 m of highly variable, thinly bedded silty sands, low plasticity silts and organic silts. Potential conservatisms in the evaluation of liquefaction for sites with thinly interbedded clay and sand like silty soils are discussed as is the use of site response analysis to assess cyclic stresses generated in the soil profile and cyclic triaxial testing to assess the soil's liquefaction resistance and behaviour under cyclic loading. The influence of the bridge propping and the limited width of the slopes at the abutments on the direction and magnitude of spreading of approach embankments at the abutments are also discussed.

4.2 Example 1: Tauherenikau Bridge

4.2.1 Preamble

The Tauherenikau Bridge is located approximately 70 km north of Wellington on SH 2 between Featherston and Greytown. The bridge is approximately 127 m long comprising eight equal spans across the Tauherenikau River and was constructed between 1968 and 1970. As part of the national bridge seismic screening and assessment programme, a detailed assessment of the seismic performance of this bridge was carried out in 2011. Figure 4.1 shows a photo of the bridge.

The site is in an area of high seismicity for New Zealand and is underlain by alluvium in excess of 100 m thick. The upper alluvial soils typically comprise a combination of recent well graded flood plain gravels consisting of layers of poorly to moderately graded gravel. Minor sand or silt layers commonly underlie aggradational and degradational terraces. These strata overlie progressively older, undifferentiated alluvial fan gravel deposits.

Tauherenikau Bridge is a reinforced concrete structure with partially precast hollow units spanning between hammer-head piers, supported by sunk-by-excavation cylinders. The bridge is straight in horizontal alignment and almost completely horizontal in vertical alignment with a gradient of 1 in 500 in the vertical plane. Overall the deck width is 9.25 m and carries two lanes of traffic.

The bridge superstructure consists of simply supported spans with nine precast pre-stressed double 'U' units and cast-in-situ deck. Diaphragms are provided at each end of the girders, and also at each mid-span. Each reinforced concrete abutment is supported by two sunk-by-excavation cylinders. The cylinders are constructed of reinforced concrete with steel casing extending to the soffit of the capping beams. Each hammerhead type concrete pier is supported by a single sunk-by-excavation reinforced concrete cylinder with a steel casing. The abutment and pier pile cylinders have a diameter of 1.4 m.

Figure 4.1 SH 2 Tauherenikau River Bridge

4.2.2 Site investigations

Boreholes were drilled in 1965 to investigate ground conditions for the design of the bridge. The descriptions on the bore logs are not to current conventions but show the site to be underlain by gravels and boulders mixed with varying portions of sand, silt and clay that are described as loose in some areas although typically have an SPT N value greater than 60. The characteristics of the hammer used for the SPT testing are not described and the SPTs are therefore of little value in the assessment of liquefaction resistance and further investigations were commissioned.

Because of the abundant gravels and boulders, CPTs are not practical at this site and SPTs can over-state the density of gravelly soils when the sampler is driven into large gravel or boulders. Liquefaction triggering was therefore evaluated using an empirical method based on shear wave velocity as well as a more conventional SPT-based method.

The site investigation programme carried out for the detailed seismic assessment of the bridge included:

- Mapping of dewatered pits excavated to extract gravels and sands up to a depth of 8 m below road level in the quarry adjacent the western abutment and soils exposed in scoured sections of the river.
- MASW geophysical testing to get a general overview of ground conditions along and across the bridge, to locate buried terraces, over bank deposits, previous channels or oxbows with lenses of loose sands or silts.

- Three boreholes, each with SPT testing at 0.5 m depth intervals and downhole shear wave (s-wave) and compression wave (p-wave) testing in casings grouted into the boreholes.

Because of the presence of gravels, PQ size holes were drilled to reduce the chance of gravels getting jammed in the end of the barrel. Despite careful drilling, the finer soils were not recovered in some layers and there has been some reliance on the experience of the driller and observations of changes in the wash water in assessing the sand and fine fractions. With the availability of sonic drilling and its capability to drill these materials with near full core recovery, sonic drilling would be preferable from the perspective of assessing the particle size distribution and constituents of the soil matrix. There is however a trade off in the quality of SPT tests with sonic drilling as sonic vibrations can disturb soil well in advance of the bit and bias the SPT penetration resistance.

SPT blow counts were measured in 25 mm intervals. For this project manual measurements were taken. For better accuracy, an optical pile driving monitor could be used. Examination of the blow counts per 25 mm gives insight into the SPTs that are affected by isolated gravels within a sand, silt or clay matrix. Almost all the SPTs refused with blow counts greater than 50 for 300 mm. In cases where gravels have clearly affected the SPT, the SPT is adjusted using the surrounding penetration resistances per 25 mm. Figure 4.2 shows how the SPT at a depth of 7.5 m in borehole (BH) 2 was adjusted for the effects of a large gravel or cobble encountered in the sandy gravel matrix during the SPT test. The measured SPT N was 41 blows per 300 mm and the adjusted is 24 blows per 300 mm.

Figure 4.2 Example of SPT N adjustment

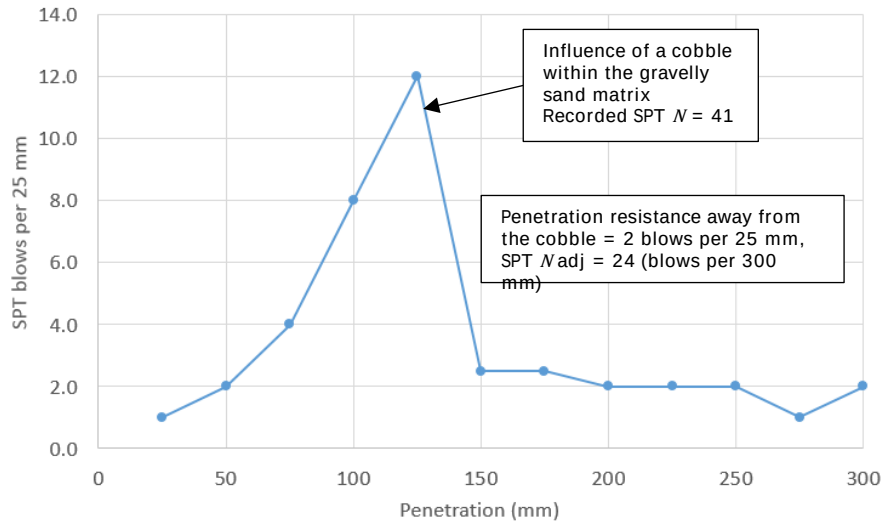

Downhole s-wave and p-wave testing was undertaken in the boreholes as MASW testing, while useful for detecting subsoil features with contrasting stiffness, may not determine s-wave velocities with suitable resolution or accuracy for liquefaction evaluation. A polyvinyl chloride (PVC) casing was grouted into each borehole with the bottom 1.5 m section of each slotted, backfilled with sand and capped with bentonite so the casing had a dual purpose of a piezometer and a conduit for installing geophones for downhole testing. The casing was grouted from the bentonite plug with care to ensure there were no voids between the casing and the surrounding ground. Before the s-wave testing, the casings were sealed above the screen using air-filled packers and dewatered to eliminate tube waves masking the s-waves. S-wave velocities were measured using a string of geophones attached to a length of PVC and held tightly against the casing with air-filled packers.

4.2.3 Ground conditions

The ground conditions are assessed in the context of the published geological description of the area and the results of the site investigations. The alluvial deposits generally comprise bedded silty sandy gravels, gravels and cobbles with occasional interbedded silty sand lenses up to a few metres thick. The cobbles and boulders are typically rounded and less than 0.5 m diameter. The gravels are predominantly fine to coarse, sub-angular to rounded sandstone.

Figure 4.3 Geotechnical long- section – Tauherenikau Bridge

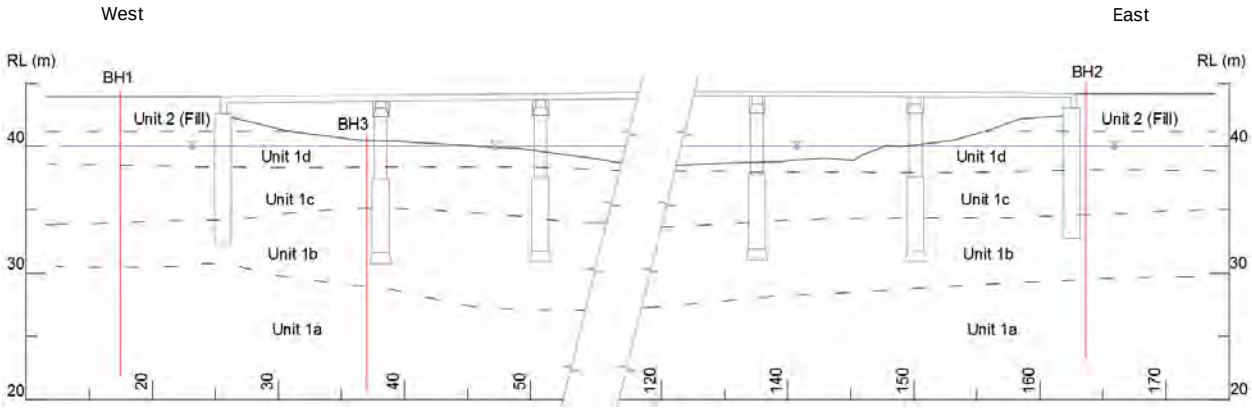

Figure 4.4 Generalised borehole, s- wave velocities, adj SPT N_{60} profiles

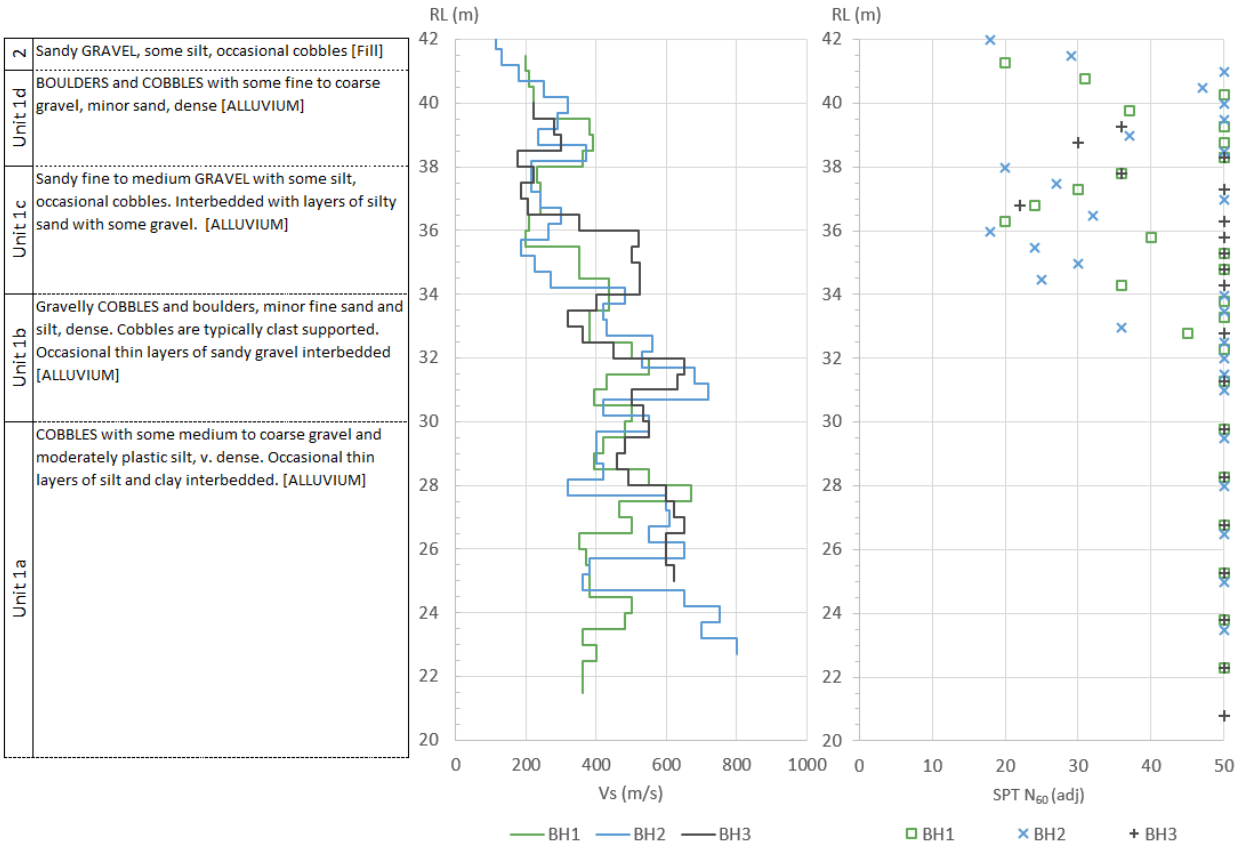

The composition of the gravel deposits needs to be carefully evaluated. Rough-faced gravels that are clast supported with no fine sands or silt fraction and good interlock between particles typically have high

permeability, strength and stiffness and are more resistant to liquefaction than other non-plastic soils. Where the gravels are supported in a matrix of sandy soils, the sands dictate the liquefaction resistance of the deposit (MBIE–NZGS (2016c) module 3).

Due to the nature of deposition, the composition of the gravels varies greatly across the river and with depth. There are lenses of medium dense to dense silty sand matrix supported gravels intermixed with lenses of dense clast supported interlocking gravels and boulders with minor sand filling the voids. From observations in the quarry adjacent to the western approach and scoured sections of the river bank upstream and downstream, the compositions of the gravels can vary considerably over distances of only several metres. The resolution of the site investigation is therefore not sufficient to define the extent of lenses of either matrix or clast-supported gravels. The generalised ground model for the site is shown in figure 4.3 together with the locations of the site investigations.

The bridge approach embankments that are typically less than a few metres high, consist of gravelly sand and sandy gravel that was likely won from the river bed or surrounding alluvial terraces.

Groundwater levels correspond with the Tauherenikau River levels, and therefore fluctuate with the changes in the river level. The annual average ground water level is at about 39 m.

4.2.4 Engineering soil properties

Engineering soil properties for the bridge assessment were determined from the site investigation results, empirical correlations with penetration resistance and experience with similar materials. Engineering soil properties determined for each unit are presented in table 4.1.

Table 4.1 Engineering soil properties for Tauherenikau Bridge

Geology unit	Sub unit	Description	γ (kN/m³)	Vs (m/s)	c' (kPa)	ϕ' (°)
Fill	2	Sandy GRAVEL , medium dense	19	150–220	0–3	30–35
Alluvium	1d	BOULDERS and COBBLES with some fine to coarse gravel, minor sand, dense	20	220–380	0	36–40
	1c	Sandy fine to medium GRAVEL with some silt, occasional cobbles. Interbedded with layers of silty sand with some gravel.	20	185–300	0–3	32–35
	1b	Gravelly COBBLES and boulders, minor fine sand and silt, dense. Cobbles are typically clast supported. Occasional thin layers of sandy gravel interbedded	22	380–550	0–5	38–43
	1a	COBBLES with some medium to coarse gravel and moderately plastic silt, very dense. Occasional thin layers of silt and clay interbedded.	22	360–800	0–10	40–45

Literature references used for the assessment of soil properties using empirical correlations include: Sabatini et al (2002) *Geotechnical Engineering Circular no.5 FHWA-IF-02-0-34*, Kulhawy and Mayne (1990) *Report no. EPRI EL-6800* and Look (2007) *Handbook of geotechnical investigation and design tables*.

4.2.5 Seismicity

The site is situated in an area of relatively high seismicity for New Zealand with the active Wairarapa Fault and the Wellington Fault, capable of producing earthquakes of M8.2 and M7.5 respectively located within 5 km and 11 km of the site. Recurrence intervals for the Wellington and Wairarapa Faults are 715 to 1,575 years, Langridge et al (2011) and 1,150 years respectively. There are several other known faults including the Masterton Fault, Huangarua Fault and Mokonui Fault within 30 km that could cause strong ground shaking at this site.

The 1,000 year return period PGA, unweighted for magnitude, calculated using the method in the *Bridge manual* is 0.45 g for this class D site. Figure 6.2c of the *Bridge manual* suggests an effective magnitude of 7.0 is appropriate for a design 1 in 1,000 year event.

Ground motion characteristics in the *Bridge manual* have been generalised from a country-wide probabilistic study. As both the Wairarapa and the Wellington Faults are major contributors to the seismic hazard at this site, ground motion characteristics for these two specific rupture scenarios have also been calculated and compared with the motions calculated from the *Bridge manual*.

There is a range of ground motion models that can be used for estimating ground motions each with their advantages and limitations. Van Houtte et al (2016) assessed the performance of several ground motion models against New Zealand data and found the Chiou and Youngs (2014) model fits the data well. Median PGAs at this site from rupture of the Wairarapa and Wellington Faults, calculated using the Chiou and Youngs (2014) ground motion prediction equations, are 0.55 g and 0.35 g respectively with 84th percentile PGAs of 0.90 g and 0.58 g. Clearly, rupture of either fault, both with recurrence intervals near to 1,000 years could generate motions that are more severe than those derived from the *Bridge manual* and warrant specific consideration in the assessment of seismic performance of this bridge.

4.2.6 Liquefaction evaluation

All the soils within the depth of interest have low plasticity and are considered susceptible to liquefaction.

As CPTs were not practical and large gravels and boulders can bias SPT readings, liquefaction triggering analysis was carried out using a procedure based on s-wave velocity as well as the SPTs. The factor of safety against liquefaction triggering has been evaluated from the measured s-wave velocities using the Kayen et al 2013 method and representative SPTs using the method by Boulanger and Idriss (2014) for the 1,000 year seismicity as determined from the *Bridge manual* and the estimated 84th percentile ground motions from rupture of the Wairarapa Fault.

The method by Kayen et al (2014) is a semi-empirical method based on case histories of mostly sandy soil sites around the world. While the database of sites used to develop the empirical relationship between s-wave velocity and cyclic resistance is not as comprehensive as databases used to establish similar relations with CPT or SPT and does not contain many gravel sites, measured s-wave velocities are unlikely to be biased by the presence of large gravels or cobbles as they are with some SPTs.

The fines content of the soils have been determined from the borehole descriptions or taken as 5% where recovery was not sufficient to ascertain the fines content. The liquefaction factor of safety calculated from the triggering analysis for both the *Bridge manual* seismic loading and the 84th percentile Wairarapa Fault scenario for each of the three boreholes from both the s-wave velocity analysis and the SPT analysis are shown in figure 4.5.

Figure 4.5 Liquefaction factor of safety

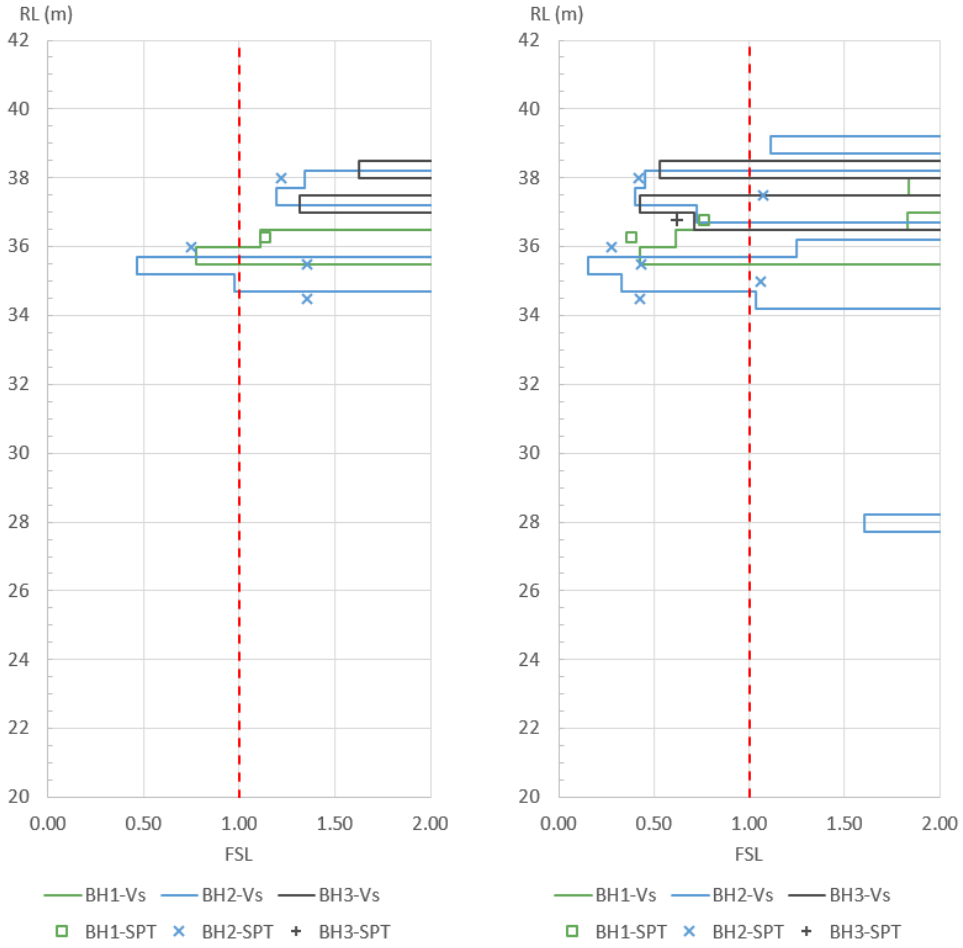

a) BM 1,000 year

b) Wairarapa Fault 84th percentile

From the liquefaction triggering analysis, it can be seen that:

- Both the downhole shear wave testing and the MASW testing show s-wave velocities in the soils in unit 1b below an elevation of 35 m exceed 300 m/s with normalised velocities exceeding 250 m/s and factors of safety typically exceeding 2 for both earthquake scenarios. Therefore, liquefaction or the production of any significant excess pore water pressure below elevation 35 m in strong earthquakes is unlikely.
- Above elevation 35 m and below the water table at elevation 39 m, there are localised layers typically less than 2 m thick that could liquefy in a 1,000 year (according to the *Bridge manual*) earthquake at each abutment. No liquefaction was predicted at BH 3 indicating that the liquefiable layers are not laterally extensive. This is consistent with site observations and the highly variable depositional environment.
- More extensive liquefaction is anticipated in a Wairarapa Fault earthquake with up to 50% of soils between elevations 35 m and 39 m anticipated to liquefy.

4.2.7 Slope stability and seismic slope displacements

Stability of the river banks and the potential for lateral spreading has been evaluated using limit equilibrium analysis in slope/W for both the *Bridge manual* 1,000 year earthquake and 84th percentile ground motions and for rupture of the Wairarapa Fault. For the *Bridge manual* 1,000 year earthquake, two different extents of liquefaction have been evaluated which represent the approximate extents at the west and east abutments. Factors of safety have been calculated for cases with and without liquefaction for each earthquake scenario. The factor of safety is calculated for both the post-earthquake static condition with no inertia and with PGA with residual strengths for liquefied layers. Critical accelerations have also been calculated for cases where the post-earthquake factor of safety is greater than 1.0. Free field slope displacements have then been calculated using the regression based methods by Bray and Travasarou (2007), Ambraseys and Srbulov (1995) and Jibson (2007) with the critical accelerations calculated from the limit equilibrium analysis.

The method by Ozener (2012), an empirical method based on the back analysis of liquefiable, typically sandy soil slopes have been used to calculate the liquefied soil residual undrained strength for use in the limit equilibrium analysis. Taking a normalised s-wave velocity, V_{s1} of 215 m/s, a median normalised liquefied soil strength (s_{ur}/σ'_v) of 0.20 has been calculated for the liquefied layers. For the range of normalised s-wave velocities of the liquefiable layer and considering the confidence limits presented by Ozener, the liquefied soil strength ratio may range from 0.1 to 0.3. A minimum undrained strength of 2 kPa has been adopted for the liquefied layer. Because the liquefied layers are not liquefied from the beginning of the earthquake, the strength of liquefied layers is increased by 20% for the calculation of critical accelerations.

Where there is an appreciable volume of soil with a factor of safety against liquefaction greater than 1 but less than 1.5, a pore pressure ratio has been assigned to these layers for calculation of the post-earthquake stability to account for the development of excess pore water pressures during the earthquake shaking.

The shape of the river bed will change over time with each flood. A moderately conservative estimate of the river cross-section profile at the time of an earthquake has been assessed for the analysis based on past observations of the translational movement of the river channel. Sensitivity analysis indicates that the stability of the banks is not particularly sensitive to the likely profile of the river bed at the time of an earthquake.

Analysis results for the post-earthquake case for each earthquake scenario are shown in figures 4.6 and 4.7 respectively. The results of the limit equilibrium analysis for all cases and the calculated yield accelerations and mean slope displacements for both earthquake scenarios are summarised in table 4.2.

Figure 4.6 Slope stability analyses – *Bridge manual* 1,000 year return period seismicity and liquefaction

a) West abutment

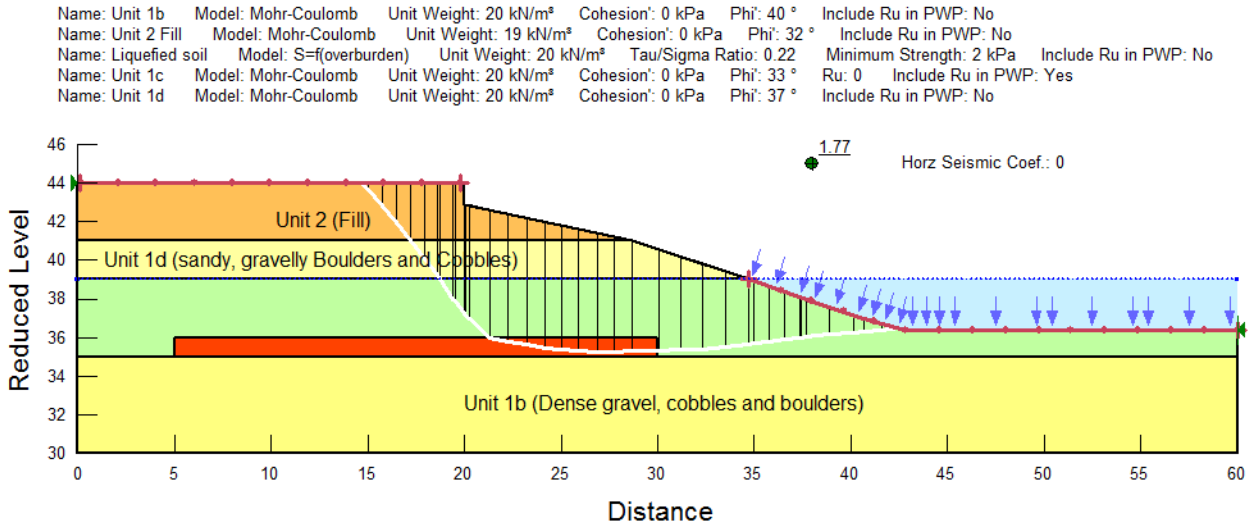

b) East abutment

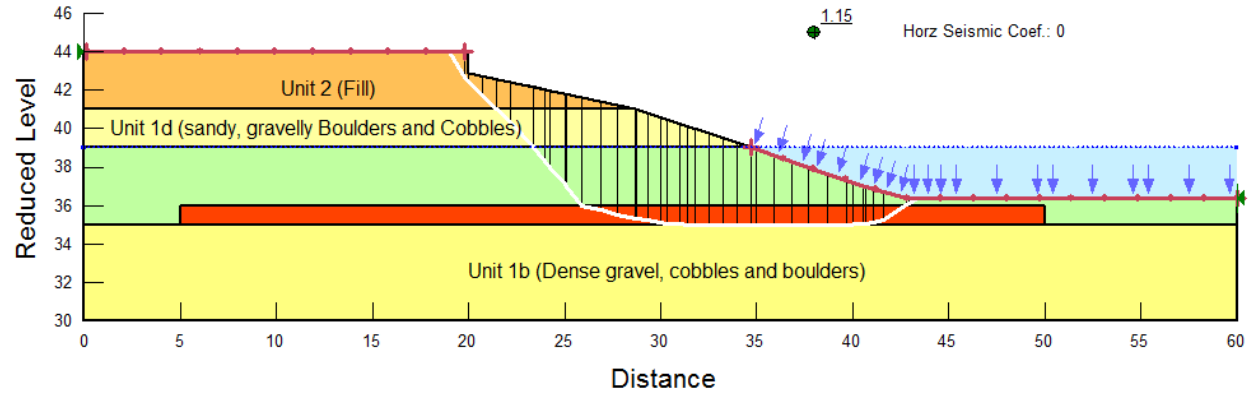

Figure 4.7 Slope stability analysis results – Wairarapa Fault event, 84th percentile motions

a) West abutment

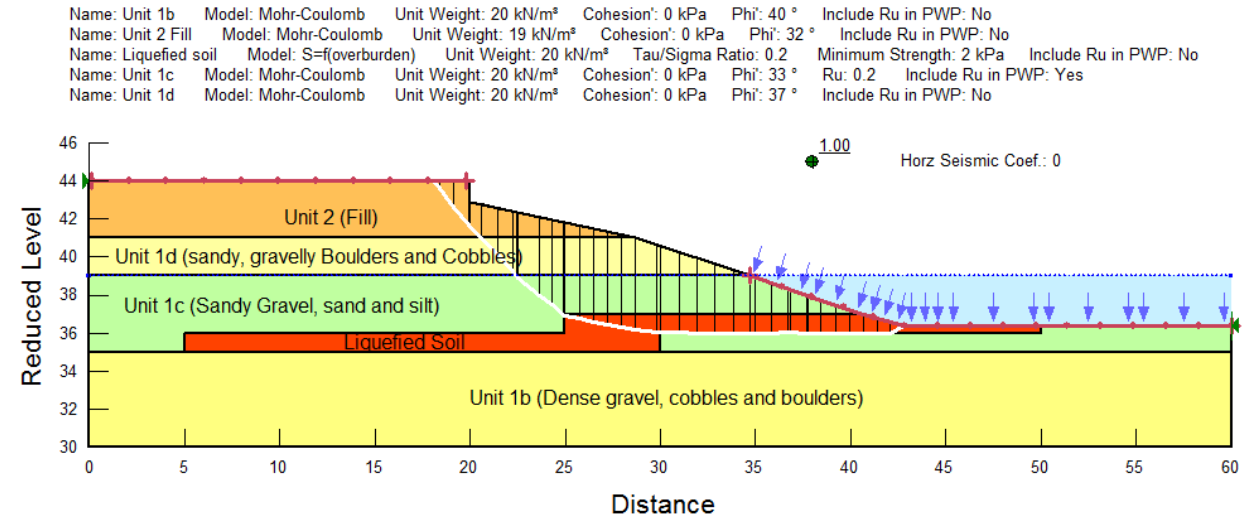

b) East abutment

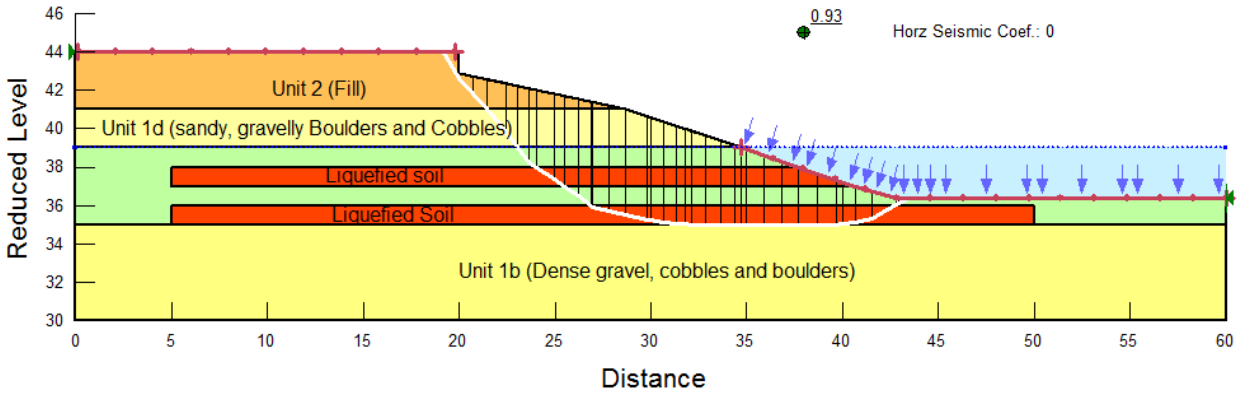

Table 4.2 Summary of slope stability results

Liquefaction scenario	Factor of safety		Critical accel (g)	Slope displacement (m)[a]		
	Post EQ[b] static	PGA[c]		B and T (2007)	A and S (1995)	Jibson (2007)
***Bridge manual* 1,000 year return period, M7.0, 0.45 g, d = 10 km**						
No liquefaction	2.00	0.59	0.205	0.02	0.01	0.03
With liquefaction (west)	1.77	0.50	0.205[d]	0.02	0.01	0.03
With liquefaction (east)	1.15	0.27	0.030	0.43	0.84	0.72
Wairarapa Fault, 1,200 year recurrence interval, M8.2, 0.9 g, d = 11 km						
No liquefaction	2.00	0.31	0.205	0.14	0.29	0.45
With liquefaction (west)	1.00	0.19	0.014	1.9	2.65	1.3
With liquefaction (east)	0.93	0.15	–	–	–	–

Notes: EQ = earthquake; B and T = Bray and Travasarou (2007); A and S = Ambraseys and Srbulov (1995)

[a] Displacements are the mean displacement calculated by each method

[b] No inertia included in the analysis

[c] PGA used to calculate soil inertia in factor of safety calculation

[d] For the BM seismicity, at the western abutment the location of the critical failure surface is outside of the zone of liquefaction and hence the displacement magnitudes are apparently unaffected by liquefaction

4.3 Example 2: Belfast Underpass, North Christchurch

4.3.1 Preamble

This example demonstrates the analysis of a proposed bridge that is part of a grade-separated intersection on a relatively flat site with thinly interbedded soils in Northern Christchurch. The two-span bridge takes Belfast Road over the four-lane expressway with approach embankments up to 8 m high that spill through slopes at the abutments. The abutments and pier are supported on piles that are founded in

dense sandy gravels about 28 m deep. Section 5.3.1 presents the PSA of the bridge and gives further details of the proposed structure.

4.3.2 Site investigations and laboratory testing

The site investigations for this project were carried out in stages as the project developed from conception through to detailed design. Figure 4.8 is a plan showing the site investigation locations near the bridge. The investigations shown in blue were undertaken as part of the initial stage of investigations for the scheme design phase. Investigations in black were carried out for detailed design. The site investigations include:

- seven electronic CPTs, two with s-wave recordings at 0.5 m intervals
- four fully cored BHs, BH 501a (not shown) was adjacent to BH 501 and used to collect undisturbed samples
- two plate dilatometer profiles with readings at 0.5 m intervals.

Figure 4.8 Site investigation plan

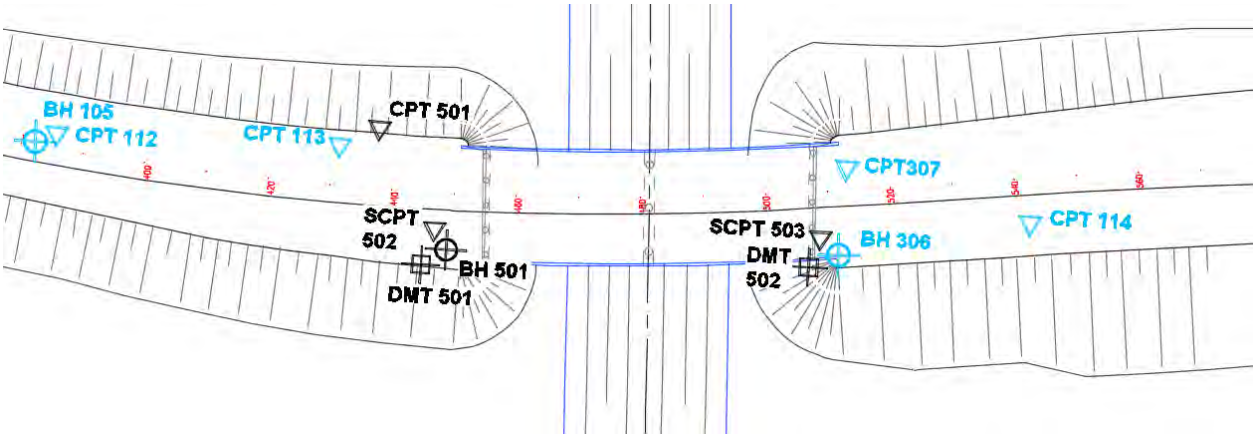

Laboratory testing included:

- 13 Atterberg limit tests (to determine plastic limit, liquid limit and natural water content)
- 15 particle size distribution tests
- 1 multi-stage consolidated undrained triaxial
- 1 unconsolidated, undrained triaxial
- 2 oedometer tests.

4.3.3 Ground conditions

The ground conditions at the site are summarised in table 4.3 and on a longitudinal section through the bridge in figure 4.9. The site is underlain by 9.5 m of interbedded and laterally variable alluvial sand and silt over bank and flood channel deposits of the Springston Formation. Underlying the Springston Formation, from a depth of 9.5 m is the Christchurch Formation which extends to a depth of about 23 m and overlies the Riccarton Gravels. The Christchurch Formation comprises beach and dune sand deposits along with

undifferentiated estuarine, lagoon and coastal swamp deposits of gravel, sand, silt, clay, shell and peat. The Riccarton Gravels, encountered from a depth of about 23 m, comprise sandy and silty coarse gravel glacial outwash deposits interbedded with occasional layers of stiff to hard silt. The Riccarton Gravels are part of a series of Pliocene-Pleistocene marine sediments that are estimated to extend to a depth of about 580 m and are underlain by the Kowhai formation sediments (McVerry et al 2014).

Figure 4.9 Geotechnical long section

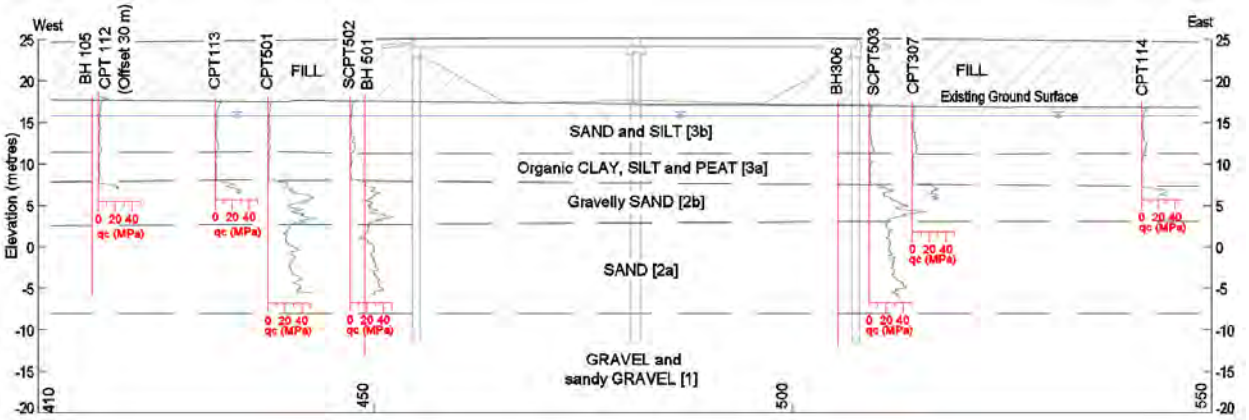

Table 4.3 Ground conditions

Geology unit	Sub-unit	Depth top[1]	Elev top	Thickness	Description
[Springston Formation]	3b	0 m	17.2 m	6.0 m	Interbedded silty fine SAND, loose, and low to medium plasticity sandy SILT
	3a	6 m	11.2 m	3.5 m	Organic CLAY, SILT and PEAT, soft
[Christchurch Formation]	2b	9.5 m	7.7 m	5 m	Fine – coarse gravelly SAND, medium dense – dense
	2a	14.5 m	2.7 m	8.5 m	Fine – med SAND, dense
[Riccarton Gravels]	1	25.5 m	-8.3 m	> 100 m	Fine to coarse GRAVEL and sandy GRAVEL, some cobbles, dense to very dense

4.3.3.1 From pre- construction ground level

The average groundwater level in the Springston Formation is assumed to be approximately 1.5 m below the ground level but may fluctuate seasonally by approximately 1 m. The piezometer in BH 105 and heaving of the base of the borehole observed during drilling BH 306 through the Christchurch Formation medium dense sands indicates slight sub-artesian conditions in units 2a and 2b with the piezometeric level near to the natural ground surface.

4.3.4 Engineering soil properties

Engineering soil properties and other soil indices (eg SPT N_{60}) used in the analysis have been calculated at 0.2 m intervals using common empirical correlations with CPT such as those by Robertson (2015), Cubrinovski and Ishihara (2001), McGann et al (2015) that have been calibrated to direct measurements where possible. For example, the factor N_k used to calculate undrained shear strength of unit 2b has been calibrated against unconsolidated, undrained triaxial and downhole shear vane measurements of

undrained strength in boreholes adjacent to the CPTs and the s-wave velocity, V_S was calibrated to measured velocities in the seismic CPTs.

The ground conditions are relatively uniform across the site. Representative parameter values (shown as black dots) for each 0.2 m thick laterally extensive layer have been taken as the average across all CPTs, adjusted where outliers are biasing the average or where conditions are outside the limits applicable to the empirical correlations. Profiles of the key parameter values are shown in figures 4.10 and 4.11.

Figure 4.10 Soil behaviour index (i_c), SPT N_{60} and relative density (D_r)

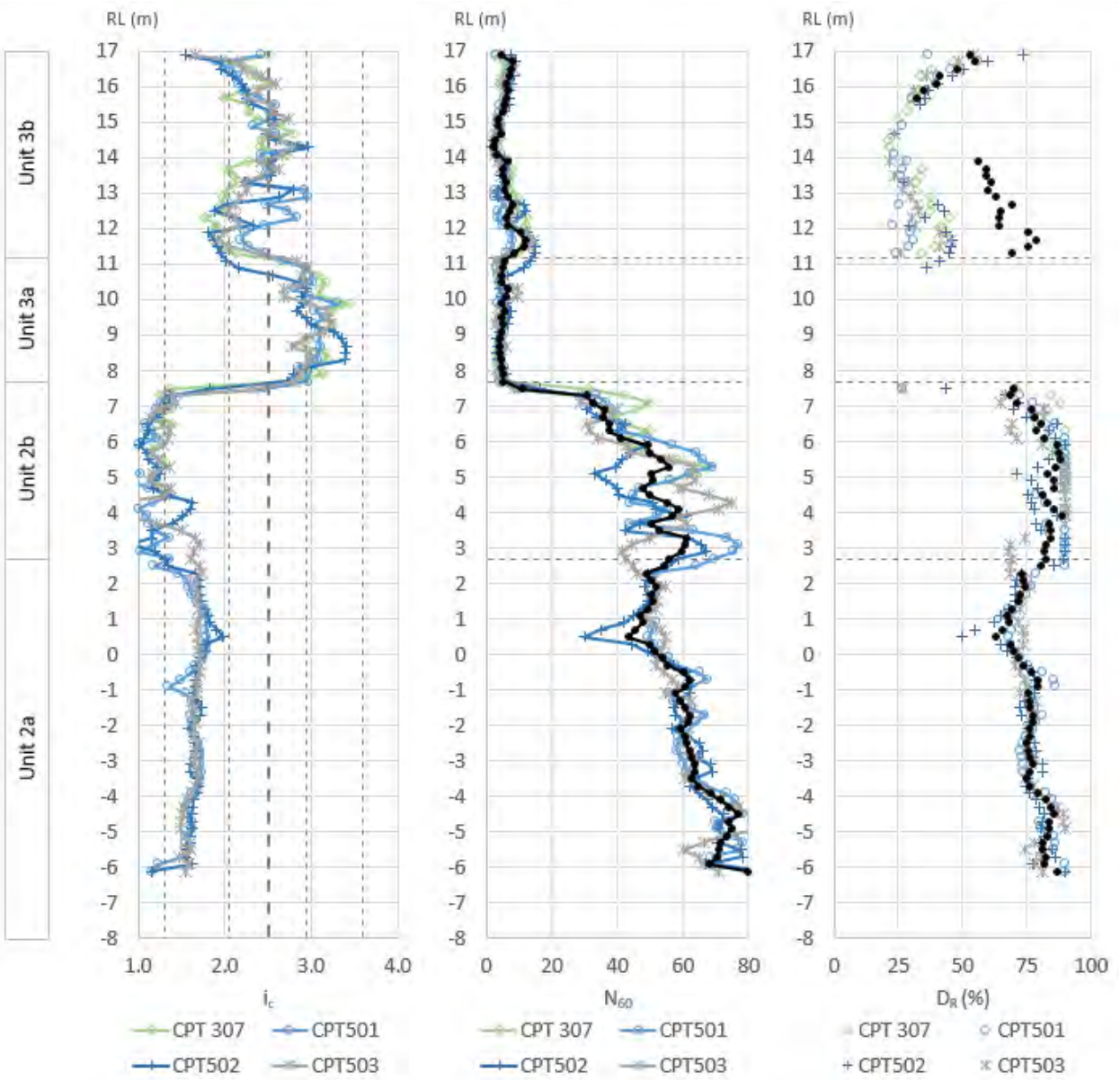

Figure 4.11 Shearwave velocity (V_s), soil friction angle (ϕ) and undrained strength (s_u)

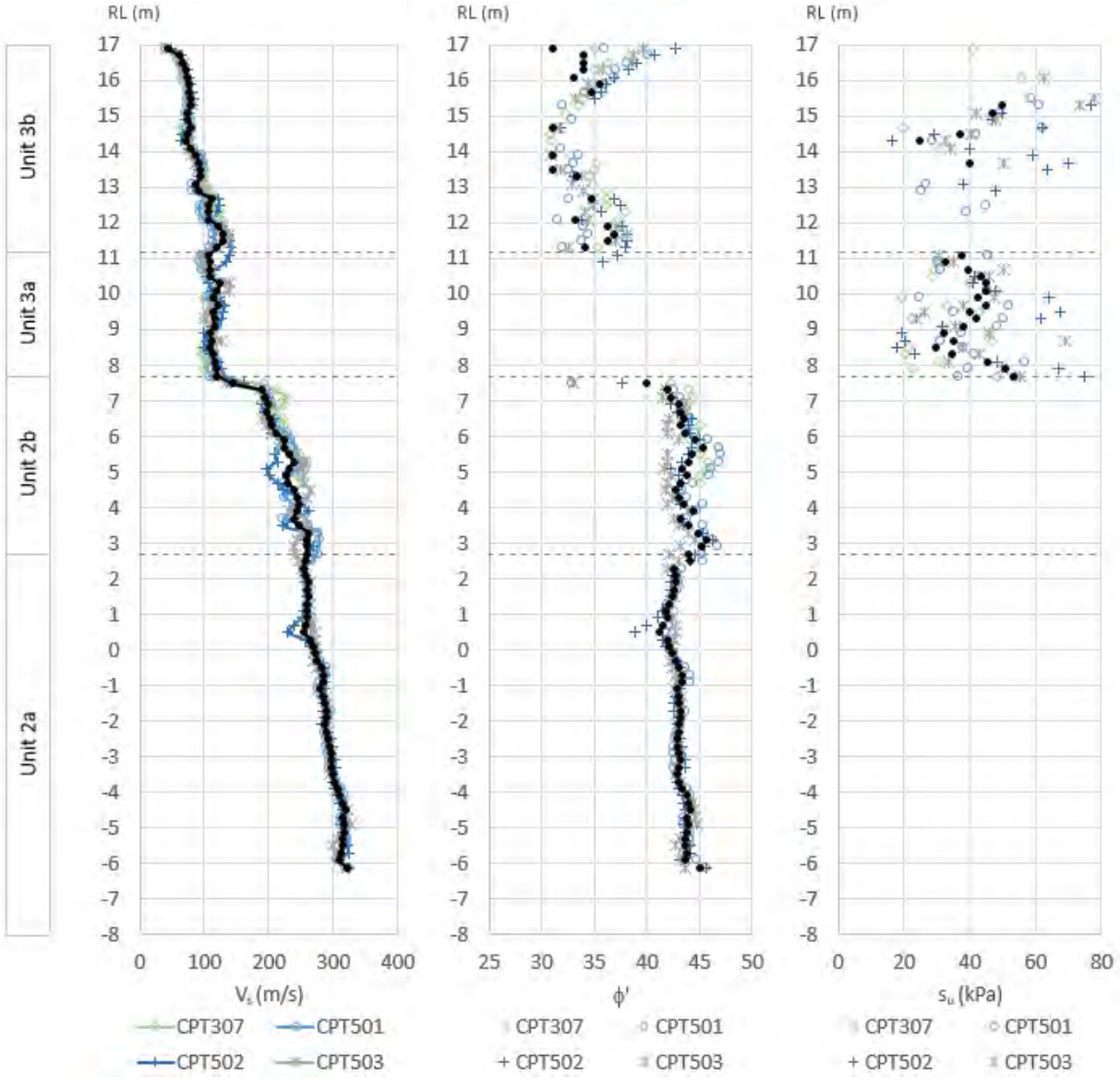

4.3.5 Earthquake ground motions

For PSA, PGA (a_{max}) and earthquake magnitude (M_w) are used to characterise earthquake ground motions. The PGA and earthquake magnitude determined using the *Bridge manual* (method 1 described in MBIE–NZGS (2016a) module 1) for a 1,000 year return period are used in this example of liquefaction evaluation.

Based on ambient noise records at the two nearest seismometer stations (Wotherspoon et al 2014), the fundamental period of the soils from bedrock level is likely to be in the order of 0.6 s. Using the measured s-wave velocities, the period of the soils above the Riccarton Gravels is 0.63 s. These site period estimations show the site period to be above the 0.6 s threshold for site class C and considering that this site is underlain by alluvium to a depth of at least 400 m, the site is classified as site class D in accordance with NZS1170.5.

The PGA for a 1,000 year earthquake calculated using the *Bridge manual* charts is 0.35 g. The effective earthquake magnitude for a 1,000 year return period is 6.25 for northern Christchurch.

4.3.6 Liquefaction evaluation

4.3.6.1 Soil susceptibility to liquefaction

Geologically young sands and low plasticity silts are most susceptible to liquefaction. Clays and silts with a plasticity index ≥ 12 have been found not to be susceptible to liquefaction and this is the primary criteria used to distinguish between soils that are or are not potentially liquefiable. The soil behaviour index i_c calculated from the CPTs is frequently used to assess a soil liquefaction susceptibility with soils having an i_c greater than 2.6 typically deemed clay like and not liquefiable. The actual i_c at which a soil's behaviour changes from sand like to clay like ranges between about 2.4 and 2.7. For sites with silty sandy soils, such as this site, adopting a cut off of 2.6 can give an over or under estimation of the extent of liquefaction and have a significant impact on the seismic performance assessment of the bridge when i_c is relied upon as the sole means of assessing a soil's liquefaction susceptibility.

Figure 4.12 Comparison of boreholes, CPT i_c and plasticity index

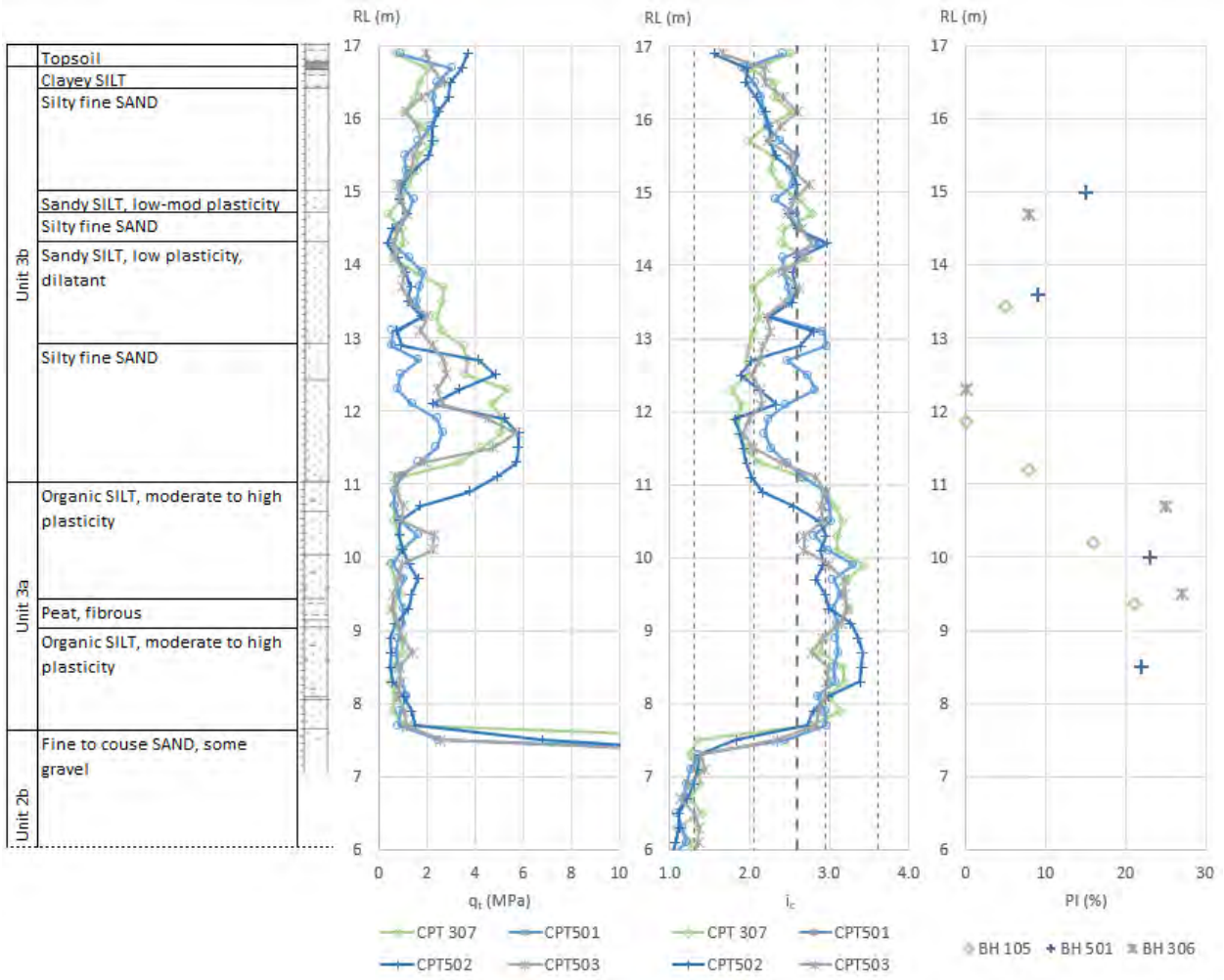

For this example, susceptibility to liquefaction is evaluated from plasticity indices of samples taken from the boreholes, the soil behaviour index i_c, calculated using the CPTs and the soil descriptions on the

borehole logs. Figure 4.12 shows a typified borehole log, profiles of i_c for the four CPTs nearest the bridge and the plasticity index of carefully selected samples from the three nearest boreholes, all of which are used to assess the susceptibility of soils in units 3a and 3b to liquefaction.

The relationship between i_c and plasticity index for the soils of units 3a and 3b is also examined to see if there was reason to adjust the i_c cut-off criteria from the conventional value of 2.6. To look at the relationship between soil behaviour index and plasticity index, i_c was plotted against measured plasticity indices as shown in figure 4.13. All samples are taken from boreholes within 2 m of a CPT and have a reasonably consistent i_c over the depth of the sample. Inspection of figure 4.13 suggests an i_c of 2.5 is appropriate to distinguish soils that exhibit sand like behaviour from clay like soils. Reducing the i_c cut-off from 2.6 to 2.5 reduces the extent of liquefaction susceptible soils by approximately 30% at this site. An i_c cut off of 2.5 has been adopted for this assessment.

Figure 4.13 Soil behaviour index (i_c) vs plasticity index (PI)

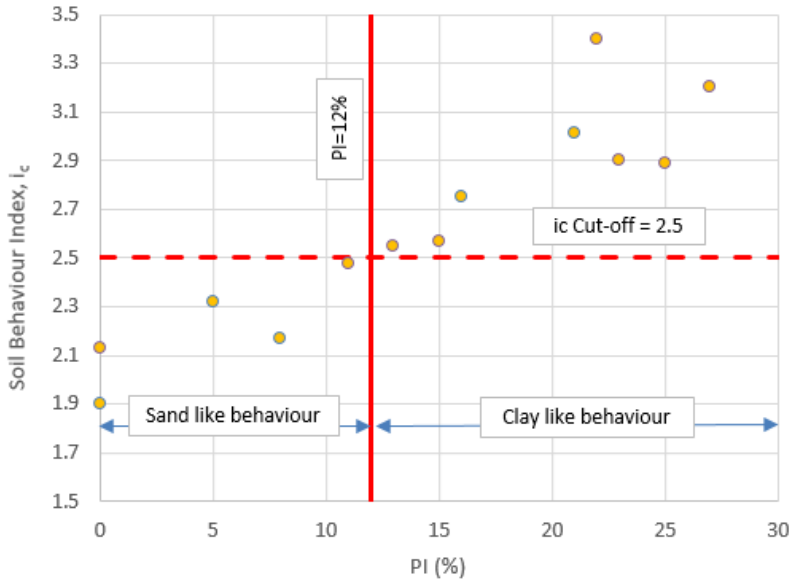

Figure 4.12 shows the organic silts of unit 3a have a measured plasticity index of 16 to 27, are described as moderately to highly plastic in the borehole logs and generally have an i_c well above 2.5. Unit 3a is therefore not considered susceptible to liquefaction.

Soils in unit 3b are thinly bedded comprising layers of fine to medium sands and low to moderate plasticity sandy silt and silt. Between elevations 11.2 m and about 13.5m, i_c is typically between 1.8 and 2.4 with measured plasticity indices below 9. Apart from some thin seams of plastic silts eg 13.0 m in CPT 501 and 502, these soils are considered susceptible to liquefaction. Above an elevation of 13.5 m to the water table at an elevation of 15.5 m, i_c typically varies between 2.4 and 2.8 and the plasticity index varies between 8 and 15. These soils are generally more plastic than other soils in unit 3b and are typically less susceptible to liquefaction.

Below elevation 7.7 m, the soils of unit 2a and unit 2b comprise sands and gravels with an i_c typically less than 2 so are clearly susceptible to liquefaction.

4.3.6.2 Triggering of liquefaction in a design earthquake

Once the layers susceptible to liquefaction have been determined, the propensity for significant excess pore water pressures or liquefaction to be generated in these layers in a design earthquake needs to be assessed. The extent of liquefaction triggered at this site in a 1,000 year return period earthquake was assessed from conventional empirical analysis using the CPT results and moderated against observations of liquefaction in the Canterbury earthquake sequence both at this site and other sites with similar ground conditions.

As case studies from the Canterbury earthquake sequence were used in the development of the empirical method by Boulanger and Idriss (2014), triggering analysis was carried out using this method and the CPT data. In the CPT tests, measurements of each metric were taken at 0.02 m depth intervals. To reduce calculations, measurements from the CPT were averaged over 0.2 m depth increments. A comprehensive description of this method is given in Boulanger and Idriss (2014). Further background information is included in Idriss and Boulanger (2008) and the important differences between the Boulanger and Idriss (2014) and Idriss and Boulanger (2008) methods are discussed in MBIE–NZGS (2016c) module 3.

In conventional empirical triggering analysis methods that use penetration resistance, the liquefaction resistance of silty sandy soils is sensitive to fines content which, in Boulanger and Idriss (2014) is derived from i_c. The relationship between i_c and fines content is poorly defined and should be scrutinised against measured fines content when these are available. Where necessary, adjustments can be made by calibration of the i_c – fines relationship using the factor C_{FC} or by manual adjustment. To determine C_{FC}, measured fines content from particle size analyses on samples from boreholes next to CPT tests are compared against calculated i_c (see figure 4.14) for units 2a, 2b and 3a. Regression of i_c against fines content for units 2a, 2b and 3a to establish the C_{FC} gives values of 0.39, 0.13 and 0.12 respectively.

Figure 4.14 Relationship between fines content and i_c

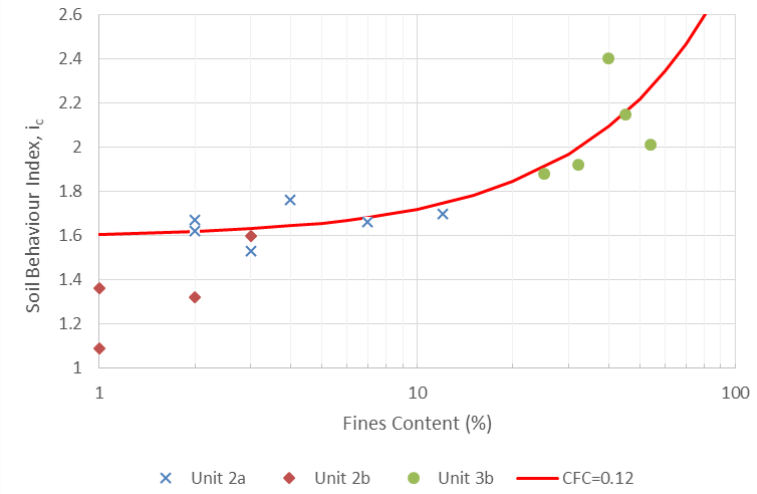

The calculated C_{FC} of 0.39 for unit 2b takes the relationship outside 1 standard deviation (0.29) for the dataset used to establish this relationship in Idriss and Boulanger (2014). This is because of the low fines content of these soils and the gravels affecting penetration resistance and i_c. A C_{FC} value of 0.12 has been adopted for all layers.

The weight of the embankment will both compress and alter the initial stress state and the cyclic shear stresses experienced in the ground underlying the embankment. Liquefaction triggering has therefore

been evaluated for free-field conditions (no embankment) and under the centreline of the 8 m high approach embankments. Note that in areas near the edge of heavy structures, for example near the toe of embankments, the relatively high ratio of shear stress to overburden pressures can greatly reduce liquefaction resistance.

For calculation including the weight of the embankment, the CPT end bearing resistance has been increased proportionally to the square root of the increase in effective overburden pressure using a factor calculated from pre and post penetration resistance measurements for embankments at other sites with similar ground conditions in this area. The result is an approximately 15% increase in penetration resistance in the Springston Formation sands and silts above 9.5 m depth and no increase in the underlying Christchurch Formation medium dense sands.

Figures 4.15 and 4.16 summarise the results of the liquefaction triggering analysis for the free field and embankment case respectively. The first two plots in each figure show the calculated normalised penetration resistance $qc1N$, and the clean sand equivalent $(qc1N)_{cs}$ showing the fines correction made to each soil layer. The earthquake applied cyclic stress ratios, cyclic resistance ratios and liquefaction factors of safety (FS_L) are plotted for the for the 1 in 1,000-year earthquake ground motion characteristics determined from the *Bridge manual*.

Figure 4.15 Results of triggering analysis – free field (without embankment)

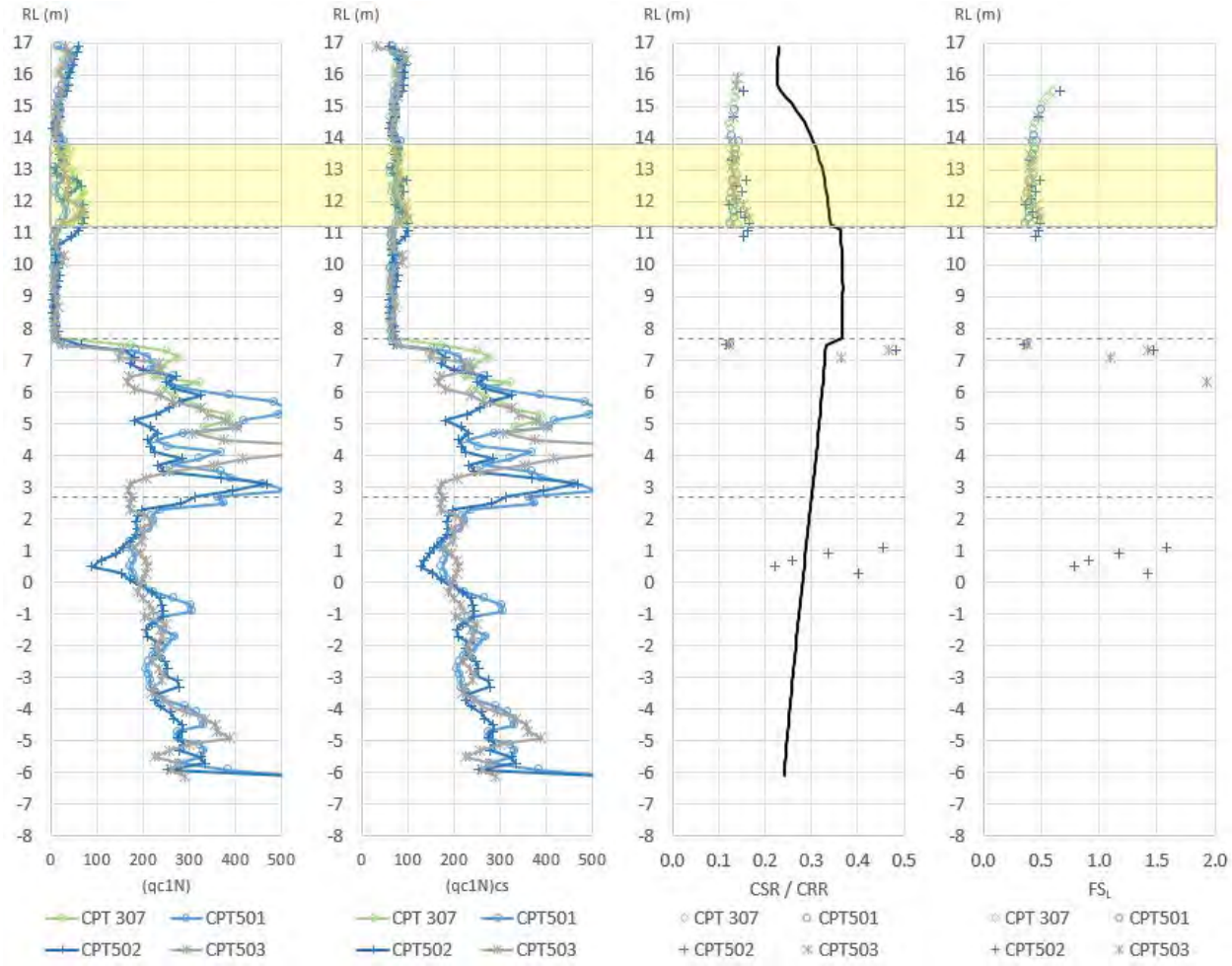

Figure 4.16 Results of triggering analysis – beneath the centre of the 8 m high embankment

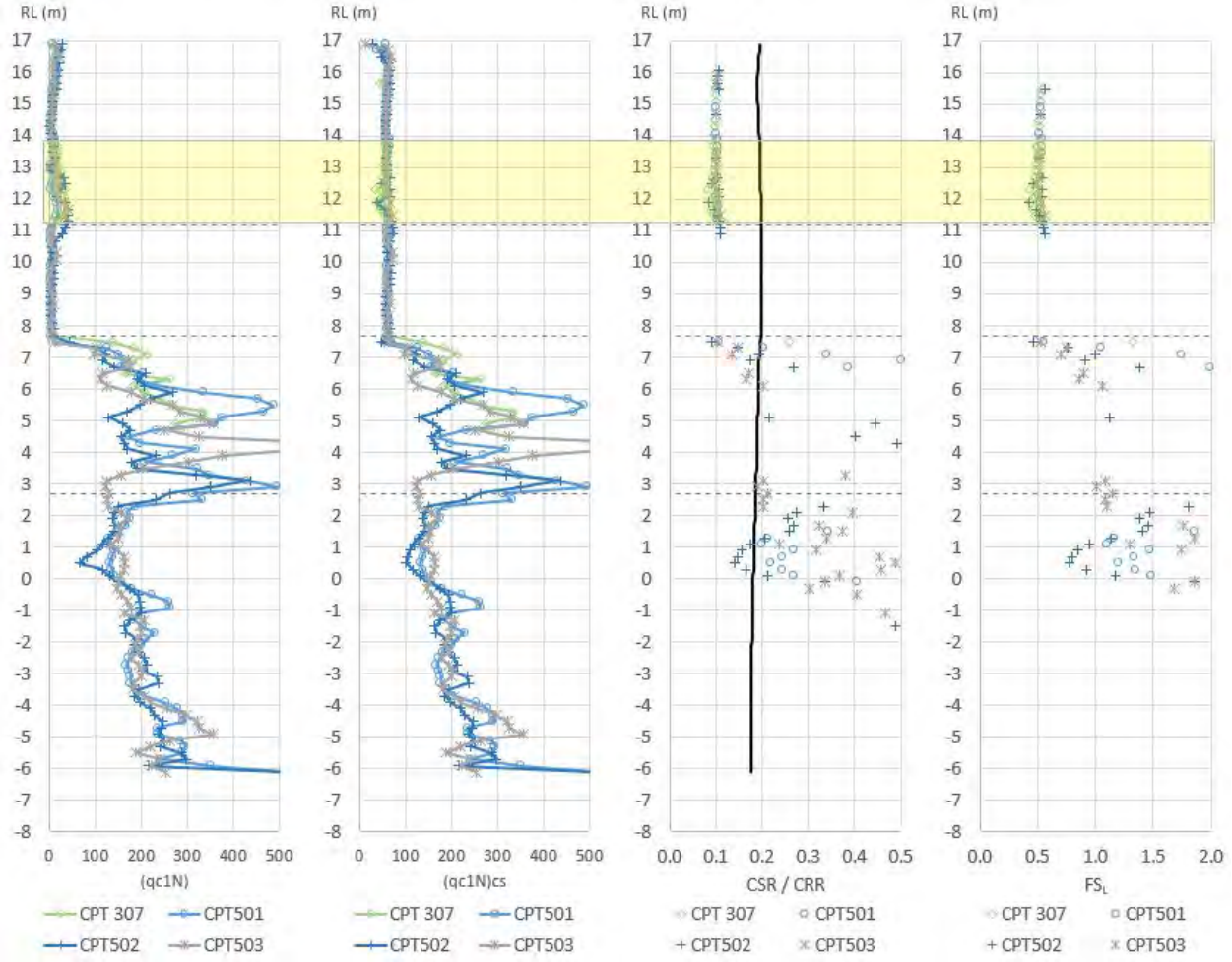

All CPTs analysed in figures 4.15 and 4.16 indicate that apart from two thin localised layers of silt on the western side of the bridge at elevation 12.5 m and 13.0 m, all layers between elevation 11.2 m and 14.0 m would liquefy in a 1,000-year earthquake. Between elevation 14.0 m and the water table at an elevation of 15.5 m the analysis of each CPT indicates liquefaction of some layers. Typically these have a combined depth of less than 0.4 m and do not appear to be laterally extensive. The exception is CPT 307 where most of these soils are predicted to liquefy in a 1,000 year return period earthquake. Note that more detailed plots were used to identify that the liquefaction between 14 and 15.5 m was only in thin layers that were not laterally extensive. For this assessment, the extent of soils anticipated to liquefy in a 1 in 1,000 year return period earthquake is highlighted in yellow.

There was relatively little surface evidence of the manifestation of liquefaction at this site following both the September 2010 Darfield M 7.1 earthquake and the February 2011 M6.2 Christchurch earthquake indicating that liquefaction was not extensive near the surface. Note that PGAs at the nearest recorder were of the order of 0.3 g in the Darfield earthquake. Furthermore, observations following the Canterbury earthquake sequence indicate the simplified methods over-predict the extent of liquefaction at sites with thinly layered silty soils similar to this site. One reason postulated is that the soils in the upper interbedded layers may not be fully saturated and hence more resistant to liquefaction. Another contributing factor to the over-prediction of liquefaction is that the thin bedding of these soils can affect the measured CPT end bearing resistance and the density of soils interbedded within or near boundaries

with soft soils may be under-represented by their measured penetration resistance. This particular site is further complicated by the soft organic soils below the liquefiable sand which may somewhat insulate the overlying layers from cyclic stresses. For these reasons liquefaction is not expected to be triggered above elevation 14.0 m.

4.3.7 Residual undrained strength of liquefied soils

The residual undrained strength ratio and residual undrained strength of liquefied layers can be assessed using the empirical relationships by Olson and Stark (2002), Idriss and Boulanger (2008) and Kramer and Wang (2015). Figure 4.17(a) gives a comparison between the calculated stress (strength) ratios using each method for CPT 307. The pseudo-static pile analysis is typically not sensitive to the strength of liquefied soils. This is not necessarily the case for the sub-structure Pacific Earthquake Engineering Research Centre (PEER) method where ground displacements calculated using the sliding block method are sensitive to the undrained strength of liquefied layers.

For this example, strength ratios have been calculated using the method by Idriss and Boulanger (2008) for each CPT and then reference values selected for each 0.2 m thick liquefiable layer. The soils are thinly bedded containing low permeability seams that could affect the distribution of excess pore water pressure during and after earthquake shaking and so strengths have been calculated with void redistribution. However, as can be seen from figure 17(a), this has little impact on the strength in this case given the comparatively low density of the liquefiable soils.

Figure 4.17 Residual undrained strength ratio and strength for liquefied layers

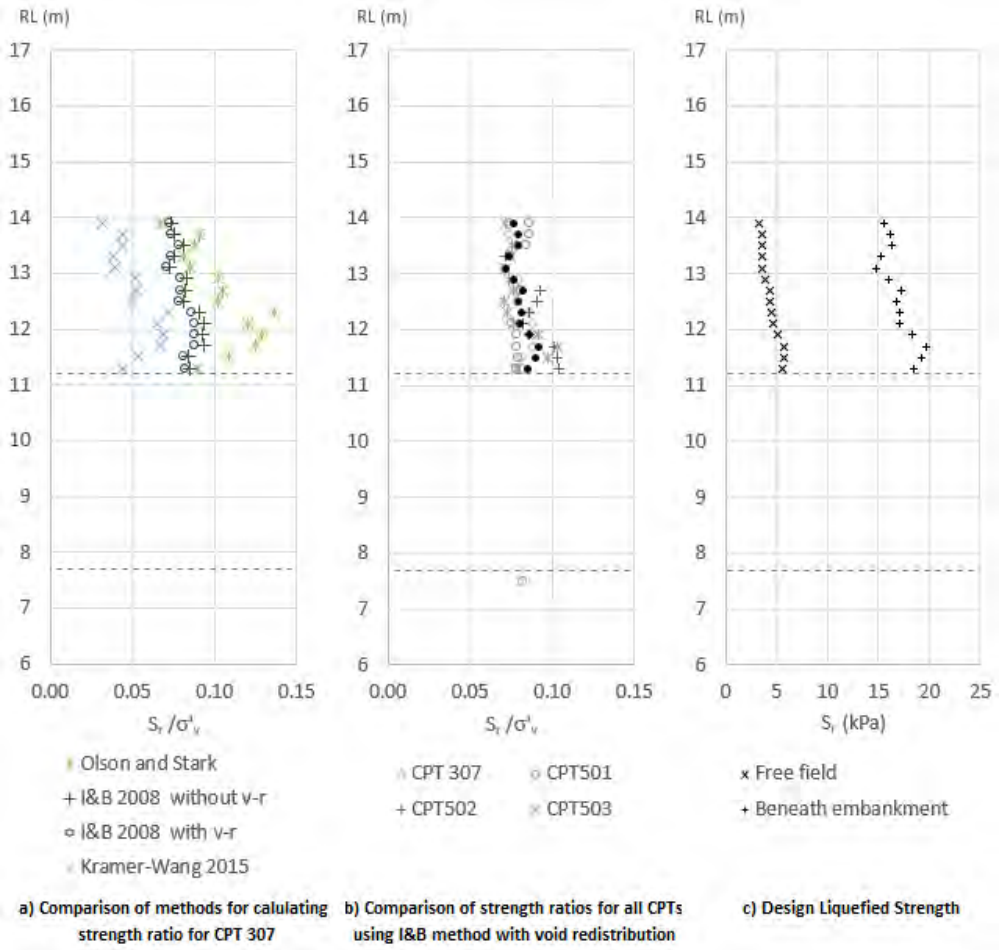

a) Comparison of methods for calulating strength ratio for CPT 307

b) Comparison of strength ratios for all CPTs using I&B method with void redistribution

c) Design Liquefied Strength

4.3.8 Seismic ground strains

4.3.8.1 Maximum cyclic shear strains, γ_{cyc}

Maximum cyclic shear strains (γ_{cyc}) in soils that are not liquefied have been calculated for both the level ground free-field case and the case at the abutments with the approach embankments using the following equation:

$$\gamma_{cyc-max} = \frac{\tau_{max}}{G} \quad \text{(Equation 4.1)}$$

Where the secant shear modulus, G for each soil layer is calculated as $\beta \cdot G_0$ with β, a non-linearity factor varying between 0.25 and 0.4 depending on the layers propensity for strain. G_0, the low strain shear modulus was calculated from density and s-wave velocity of each layer as $G_0 = \rho V_s^2$.

Consolidation of soils beneath the embankment will increase their shear stiffness. For layers in units 3a and 3b, the low strain shear modulus calculated from the pre-construction level ground s-wave velocities was increased proportionally to the square root of their increase in effective stress from the construction of the embankments resulting in an 18% to 20% increase in the low strain modulus. The low strain shear modulus of the approach embankment fill was calculated assuming the fill to have a normalised s-wave velocity, V_{s*1} of 300 and a unit weight of 22 kN/m^3 giving s-wave velocities ranging from 173 m/s at the top of the 8 m high fill to 308 m/s at the base. Note that $V_{s*1} = V_S.(Pa/\sigma'_{v0})^{0.25}$.

The maximum cyclic shear stress, $\tau_{cyc-max}$ is calculated from the magnitude unweighted cyclic stress ratio, CSR_M as:

$$\tau_{cyc-max} = \frac{CSR_M.\sigma'_{v0}}{0.65} \quad \text{(Equation 4.2)}$$

Separate profiles of cyclic stress ratio and initial effective vertical stresses σ'_{v0} are calculated for each layer for both the level ground case and at the centre of the abutments with the full height of the approach embankment. Profiles of maximum shear strains for non-liquefied soil conditions are presented in figure 4.19.

4.3.8.2 Cyclic shear strains for liquefied layers, $\gamma_{cyc-liq}$

Maximum cyclic shear strains that develop in liquefied soil layers during earthquake shaking can be estimated using the simplified methods by Tokimatsu and Asaka (1998), Ishihara and Yoshmine (1992) and Zhang et al (2004), refer to figure 4.20.

Figure 4.20 shows the estimated maximum cyclic shear strains for each layer expected to liquefy in a 1,000 year design earthquake for the free-field conditions at the pier and beneath the embankment fill at the abutments. In the method by Tokimatsu and Asaka, $\gamma_{cyc-liq}$ is calculated using the cyclic stress ratio adjusted to magnitude 7.5 and the overburden corrected SPT N. For the Ishihara and Yoshmine method and the method by Zhang, $\gamma_{cyc-liq}$ is a function of soil relative density and the factor of safety against liquefaction. Some correlations between CPT penetration resistance and soil relative density tend to under estimate the relative density of silty sands. In this example relative densities for silty sands have been calculated for each layer using the method by Cubrinovski and Ishihara (2001) where:

$$D_R = \sqrt{(N_1)_{60}/C_D} \quad \text{(Equation 4.3)}$$

with the factor, C_D equal to 25 for sand with some silt and SPT penetration resistance calculated from the CPTs.

Figure 4.18 Maximum cyclic strains

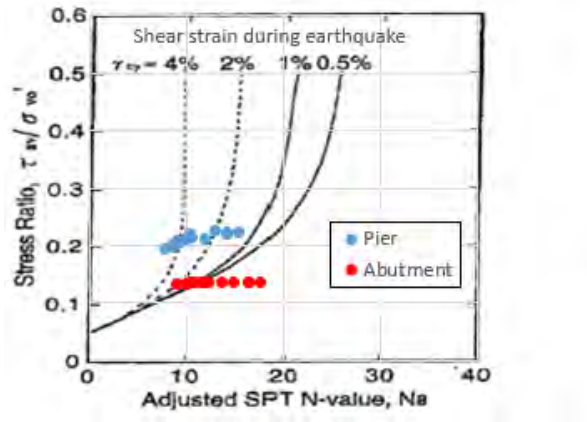

a) Tokimatsu and Asaka (1998)

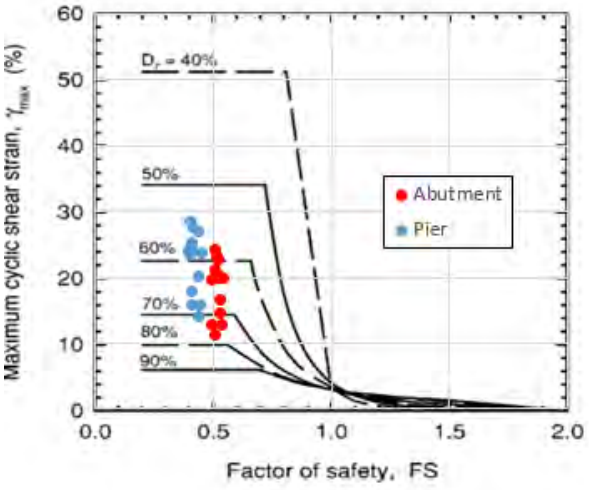

b) Zhang (2004)

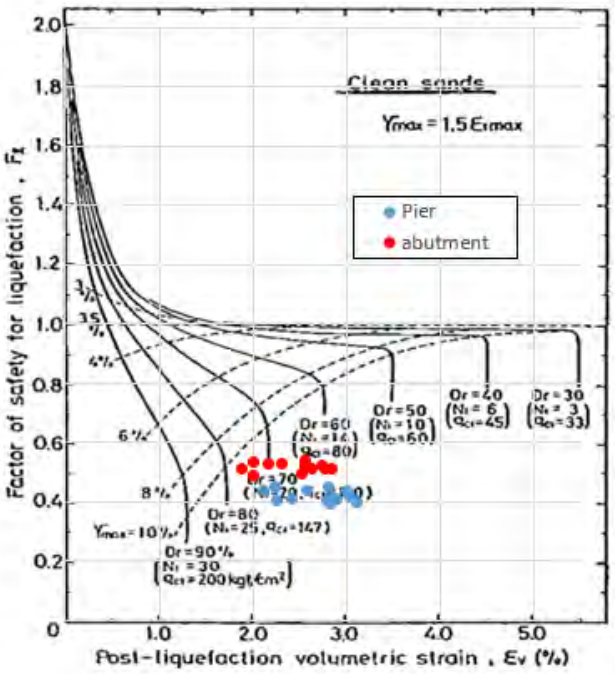

c) Ishihara and Yoshmine (1998)

Both the method by Zhang and the method by Ishihara and Yoshimine indicate maximum cyclic shear strains for all liquefied layers to be in excess of 10% for both the free-field conditions and beneath the embankment with shear strain up to 28% suggested in the Zhang method. Cyclic ground displacements calculated using strains of this magnitude appear to be unreasonably high when they are compared with surface ground displacements measured in the Canterbury earthquake sequence, even when recognising the difference in shaking intensity. The Tokimatsu and Asaka method gives much lower maximum shear strains of about 1.2% to 5% for the free-field conditions, a 5th to a 10th of shear strains calculated using the method by Zhang. The difference is even greater for the case beneath the embankment, however, for some liquefied layers the method by Tokimatsu and Asaka suggests shear strain to be less than 0.5%, less than the calculated peak cyclic shear strain for the soils when they are not liquefied.

So it appears that for this case the Tokimatsu and Asaka method underestimates peak cyclic shear strains in some of the liquefied soils beneath the embankments and the Zhang method appears to over-predict the magnitude of shear strains but probably gives a reasonable estimate of the relative magnitude of stain throughout the depth of liquefiable soil. For this example, maximum cyclic shear strains for liquefied layers have been calculated by dividing cyclic shear strains calculated using the method by Zhang by a factor of 6.

4.3.8.3 Volumetric strains in liquefied layers, ε_v

Free-field volumetric strains from post-earthquake reconsolidation of liquefied soils have been evaluated using the method by Zhang et al (2002). A 0.5% volumetric strain has been applied in the non-liquefiable layers in unit 3b and unit 3a as some development of excess pore water pressure from cyclic loading is anticipated in these layers although liquefaction is not expected.

4.3.8.4 Summary of seismic ground strain profiles

Calculated peak post-earthquake volumetric strains and cyclic strains for each 0.2 m thick soil layers above elevation 6.0 m are shown in figure 4.19. The black dots on the plot of volumetric strain represent those selected for the assessment.

Figure 4.19 Seismic ground strain profiles

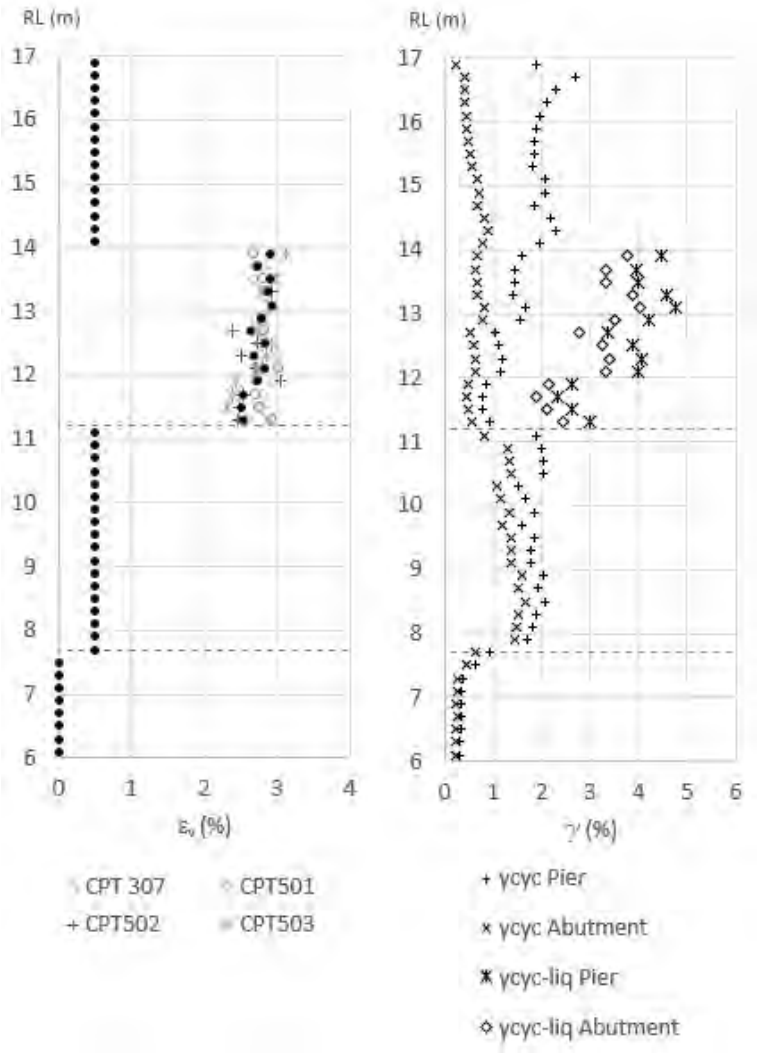

4.3.9 Post-earthquake stability

The post-earthquake stability of the approach embankments is assessed both along the bridge and transversely. In the stability analysis the residual undrained strength ratio of the liquefied soil and cyclically softened strength for the organic soils are used with no soil inertia (ie the horizontal seismic

coefficient is set to zero). In the longitudinal direction, the opposing abutments will counteract each other and slip circle exit points have therefore been restricted to the mid-point between the two embankments.

The result from the analysis in the bridge longitudinal direction is shown in figure 4.20. Bridge and site are practically symmetric about the central pier so the one analysis is applicable to the embankments at both abutments. Both circular and non-circular failure surfaces have been assessed using the Morgenstern-Price method and the computer software Geostudio 2012.

Figure 4.20 Post earthquake stability analysis – bridge longitudinal direction

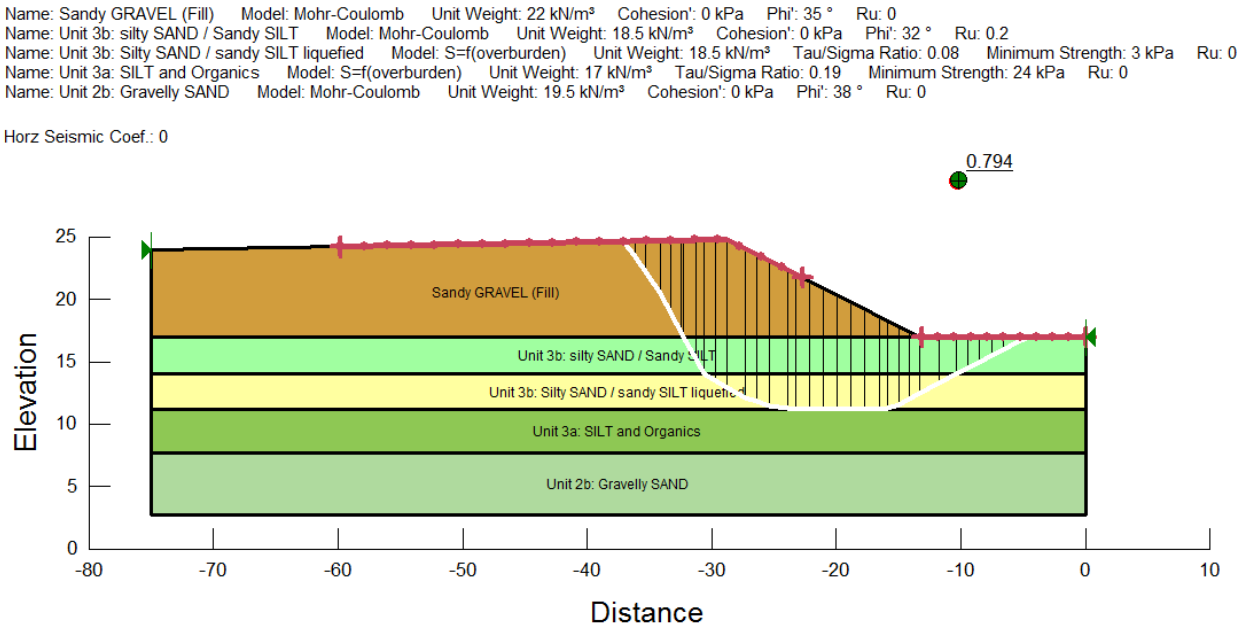

Inspection of the slope stability analysis in the bridge longitudinal direction shows that the critical slip surface intersects the top of the fill less than the width of the embankment away from the crest. Therefore the slope factor of safety will be the same in the transverse and longitudinal directions. The post-earthquake factor of safety in both the longitudinal and transverse direction of 0.8 is less than 1 indicating potential for flow type lateral spreading in both directions.

4.3.10 Seismic ground displacements

4.3.10.1 Cyclic ground displacements, U_{g-cyc} and $U_{g-cyc\,liq}$ and subsidence U_z

Profiles of free-field horizontal cyclic ground displacements at the pier and the abutment for both the non-liquefied and liquefied cases have been calculated by integrating the cyclic shear strains in section 4.3.8 times the thickness of each layer (0.2 m) over the depth of the profile. Post-earthquake subsidence from reconsolidation of liquefied and non-liquefied soils is calculated in a similar manner using the volumetric strains. As the pseudo-static pile analysis is not sensitive to the vertical ground displacements, we have used the same volumetric strain profile at both the abutments and the pier.

Profiles of cyclic horizontal ground displacements and subsidence at the pier and the abutments for non-liquefied and liquefied soil conditions are presented in figures 4.22 and 4.23.

4.3.10.2 Lateral spreading, U_{g-lat}

The post-earthquake stability analysis indicates potential for lateral spreading of the approach embankments. Most of the established simple methods for estimating lateral spreading displacements are empirical and have been developed from observations of lateral spreading of river banks, coastal margins or gently sloping ground. In the estimate of seismic displacement of approach embankments on level liquefiable sites it is important to consider that:

- the main driving force, the embankment fill, is of limited width and its height reduces with distance from the abutments
- there is a continuous non-liquefied crust overlying the liquefied soil that constrains spreading
- the pinning and strutting by the bridge between the embankments may bias the direction of spreading.

This case is further complicated by the soft organic soils below the liquefiable sand which may also soften somewhat with cyclic loading and may also develop sizeable permanent shear strains in earthquakes.

Examination of the charts produced by Tokimatsu and Asaka 1998 indicates lateral spreading shear strains are 10 times the estimated cyclic shear strains in the liquefied soils. Considering the limited lateral extent of the embankment and the containment effect of the non-liquefied crust, for this example lateral spread shear strains in the liquefied soils have been calculated as eight times the cyclic liquefied shear strains shown in figure 4.19. The profile of lateral spread shear strains is shown in figure 4.21.

For comparison, lateral spread strains have also been calculated using the method by Zhang et al (2004). In this method, the lateral displacement depends on the distance from the free face with displacements decreasing with distance away from the face. Lateral spread shear strain in each liquefiable layer can be calculated by multiplying the layers cyclic shear strain from figure 4.18(b) by the LD/LDI ratio. Figure 4.21 shows the lateral spread shear strain profiles through the liquefiable layer at the abutments calculated using the method by Zhang et al (2004) with an LD/LDI factor of 2.5.

There is a sizable difference (factor of 2.2) between estimates using the two alternative approaches. The spread in the data used by Zhang et al to derive LD/LDI relationships indicates lateral spreading calculated using this method could also vary by a factor of two. Upper and lower bound displacement profiles for parametric studies need to be selected recognising the differences between the approaches and the uncertainty in each.

Figure 4.21 Shear strains in the liquefiable layer at the abutments

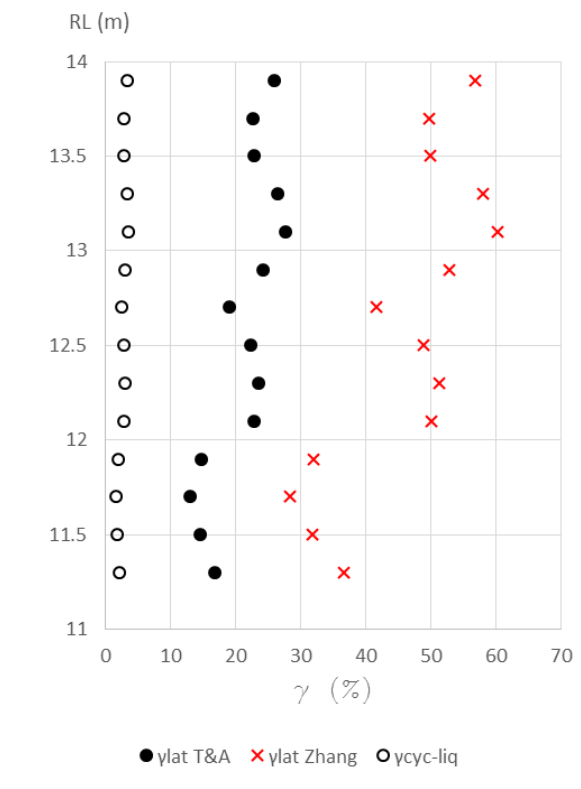

Permanent horizontal ground displacement of the soils below an elevation of 7.7 m (the base of the soft organic soils) is assumed to be negligible as the relatively strong and stiff medium dense sands will constrain spreading to the soils above this layer.

With the lack of simplified methods available to estimate permanent horizontal displacement in the soft organics and non-liquefied silts above elevation 7.7 m, permanent horizontal ground displacements of nodes in these layers have been taken to be 1.5 times the maximum cyclic ground displacement.

Profiles of lateral spread ground displacements and subsidence at the pier and the abutments for non-liquefied and liquefied soil conditions are presented in figures 4.22 and 4.23.

4.3.10.3 Summary of seismic ground displacement profiles

Profiles of free-field ground displacements from cyclic shear during an earthquake with and without liquefaction, ground subsidence from reconsolidation following the dissipation of excess pore water pressures developed during the earthquake and lateral spreading are presented in figures 4.22 and 4.23 for the pier location and the abutment respectively. These are reference values. For parametric assessment of sensitivity a factor of 0.33 and 3 could be applied to calculate lower and upper bound displacements.

Figure 4.22 Free- field ground displacements at the pier

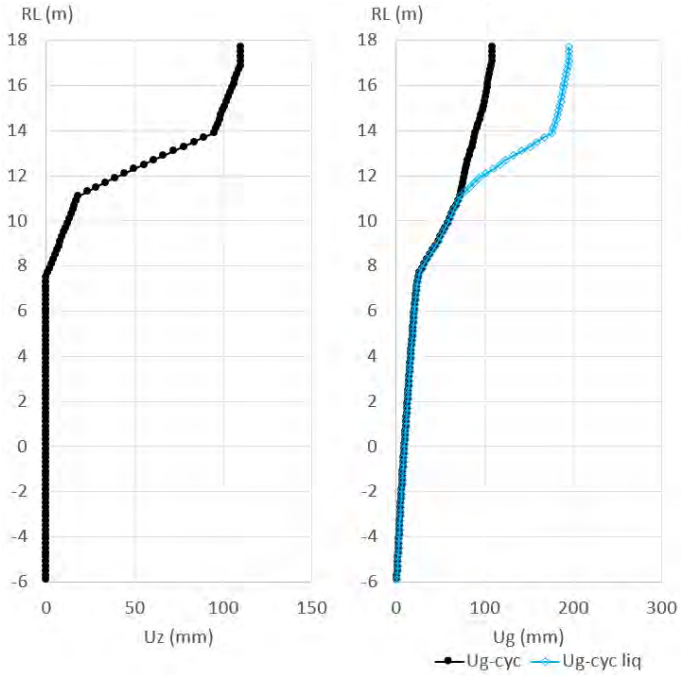

Figure 4.23 Free- field ground displacements at the abutment

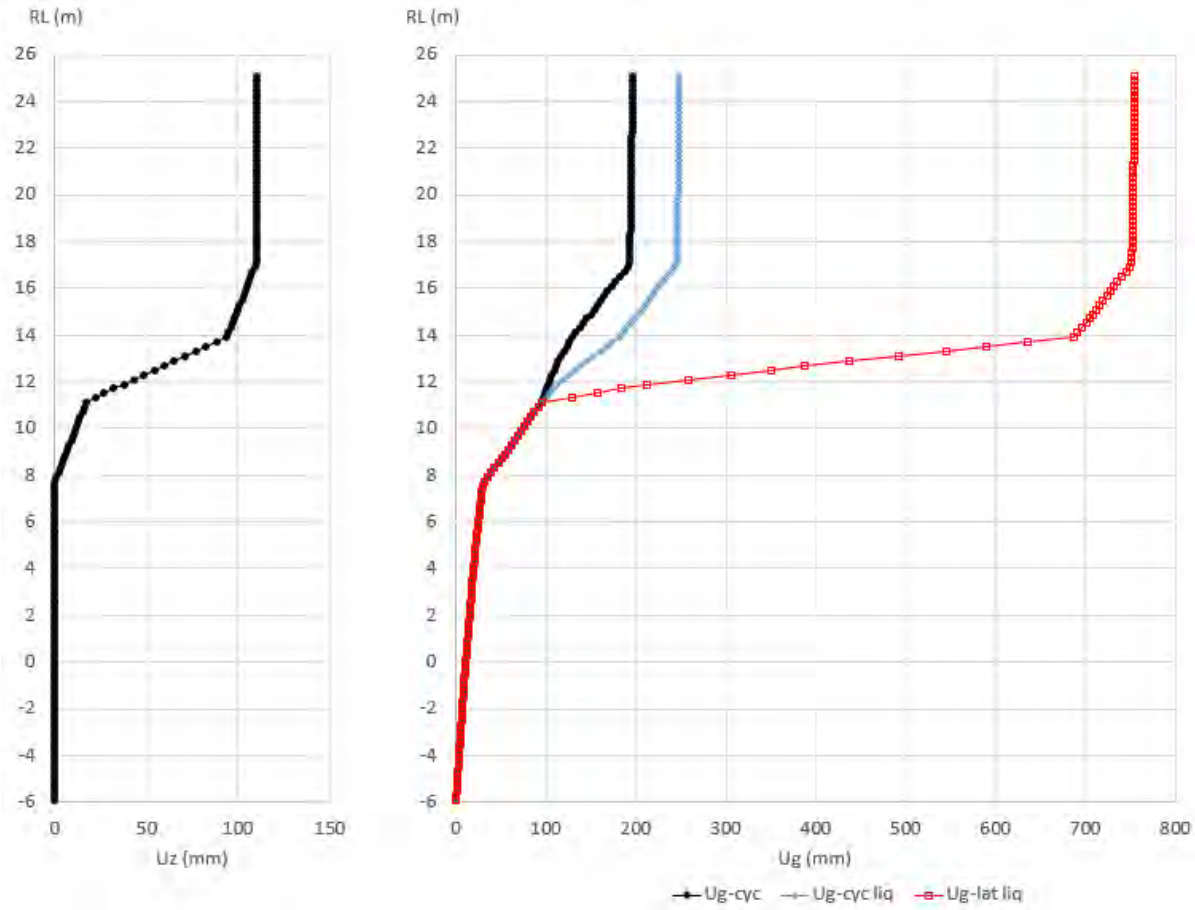

5 Bridge pile analysis examples

5.1 Introduction

As a main objective of this report, two examples of PSA of piled bridges at sites susceptible to liquefaction and lateral spreading are presented to illustrate the recommended PSA procedure described in chapter 3 and in Murashev et al (2014).

The first example is a PSA of an existing bridge, ANZAC bridge, a four-span reinforced concrete bridge crossing the Avon River in Christchurch. This bridge was severely affected by liquefaction and lateral spreading in the September 2010 M7.1 Darfield earthquake and the February 2011 M6.2 Christchurch earthquake. In this example of a single pile analysis for the lateral spreading case, phase 3a of the PSA procedure, the assessment of the response of the bridge abutment piles to lateral spreading is demonstrated.

The second example illustrates PSA and seismic design procedures for a proposed new two-span bridge constructed on level ground as part of a grade separated intersection, where kinematic loading of the piles as a result of liquefaction is the critical load case. Seismic assessment in the longitudinal direction of the bridge is presented in this example as the liquefaction induced ground movements generally have the most significant effect on the bridge design in this direction. In the second example, comparisons are made between the results of a sub-structure and dynamic analysis of the structure and design of the seismic resisting elements to comply with the *Bridge manual*.

5.2 Example 1: Anzac Bridge

5.2.1 Preamble

The following example analysis illustrates the key steps of a phase 3a assessment of a pile foundation in laterally spreading soil. The subject of the analysis is the Anzac Bridge in Christchurch. Anzac Bridge crosses the Avon River and is located in an area that was severely affected by liquefaction and lateral spreading during the Canterbury earthquake sequence. Detailed descriptions of the performance of Anzac Bridge in the Canterbury earthquakes can be found in Cubrinovski et al (2014a; 2014b), Haskell (2014), and Haskell et al (2013).

The phase 3a pile analysis makes use of outputs from phase 1 and 2 characterisation and free-field ground response analyses, specifically the identification of liquefiable and non-liquefiable soil layers and the estimated lateral spreading ground displacements. These preceding analyses are not the main focus of this example, so are not illustrated in detail here; they are the subject of detailed scrutiny in chapter 4 of this report. Rather, it is assumed that phase 1 and 2 analyses have been undertaken for the site and the outputs are available to be used as the starting point for the phase 3a analysis.

The first part of the example covers the procedure for undertaking the reference model analysis using best-estimate parameters. Following this, the sensitivity analysis procedure is illustrated. Finally, some concepts and results from a whole-bridge analysis for the example structure are presented.

5.2.2 The scenario

Anzac Bridge was built in 2000 and is located 4.2 km upstream of the mouth of the Avon River in Christchurch. It carries two lanes of traffic in each direction and comprises three spans of 14.9, 18.6 and 14.9 m length. Aligned in a north-south direction, the south abutment of the bridge is located on the inside bank of a gentle bight of the river. The deck is constructed of precast prestressed reinforced concrete hollowcore units. It is supported on reinforced concrete abutments at the river banks plus two three-bay reinforced concrete bents in the centre of the river (figure 5.1). The 1 m x 1 m trapezoidal columns of the central bents are each founded on a single 20 m long 1.5 m diameter steel-encased reinforced concrete pile. The abutments are supported by 15 (or 16, for the north abutment) 22 m UC 310x137 kg/m steel H-piles which are spaced at 1.5 m centres and arranged in a single row. At both banks of the river the abutment piles pass through layers of liquefiable loose to medium-dense fine to medium sand (from approximately 2–12 m at the south bank, and 2–16 m at the north bank), into more dense layers of coarse sand below.

Figure 5.1 Side elevation of Anzac Bridge showing superstructural, abutment, and foundation details and dimensions (Haskell 2014)

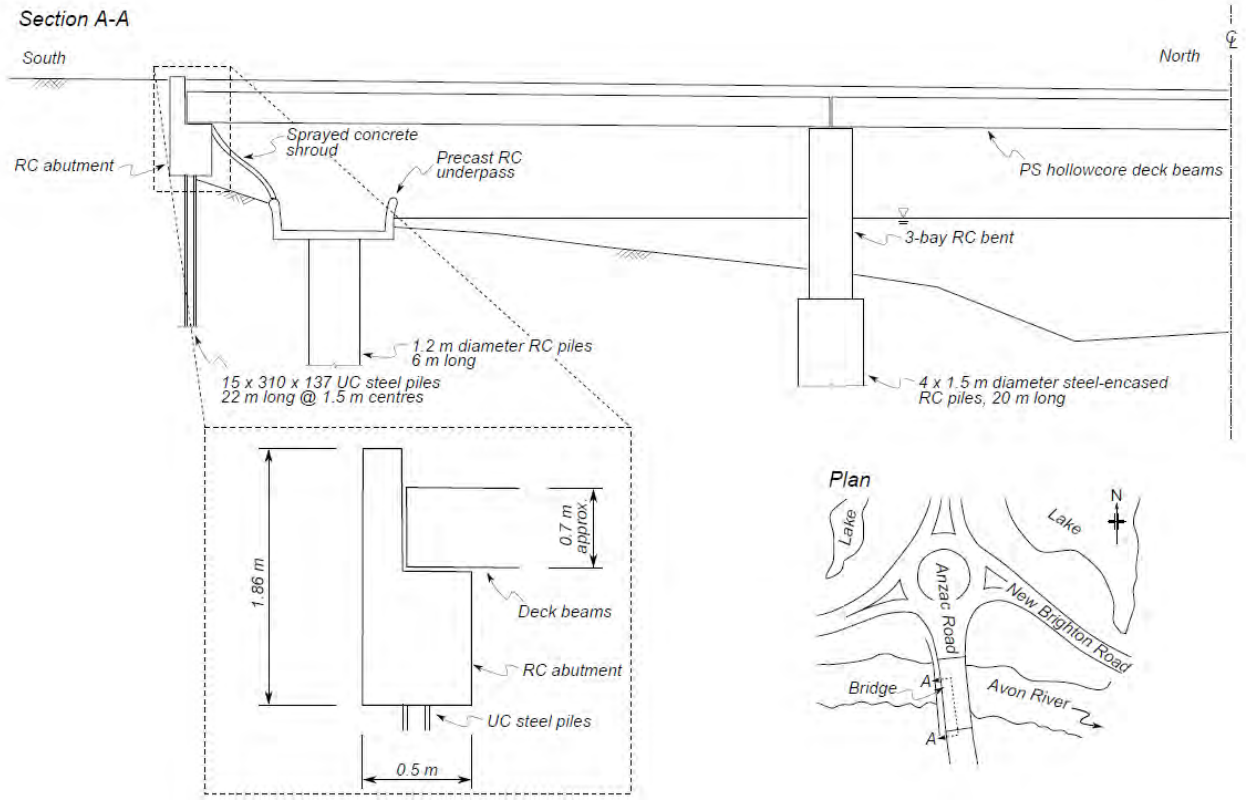

Original CPT from the time of construction for the southern bank of the river (ie south bridge abutment) is shown in figure 5.2. The borelog also includes SPT blowcount values alongside the soil profile; however, this data is missing the associated energy efficiency values for the equipment, so cannot be used directly to calculate soil spring parameters for the PSA.

Figure 5.2 CPT profiles for south abutment direct from design documents

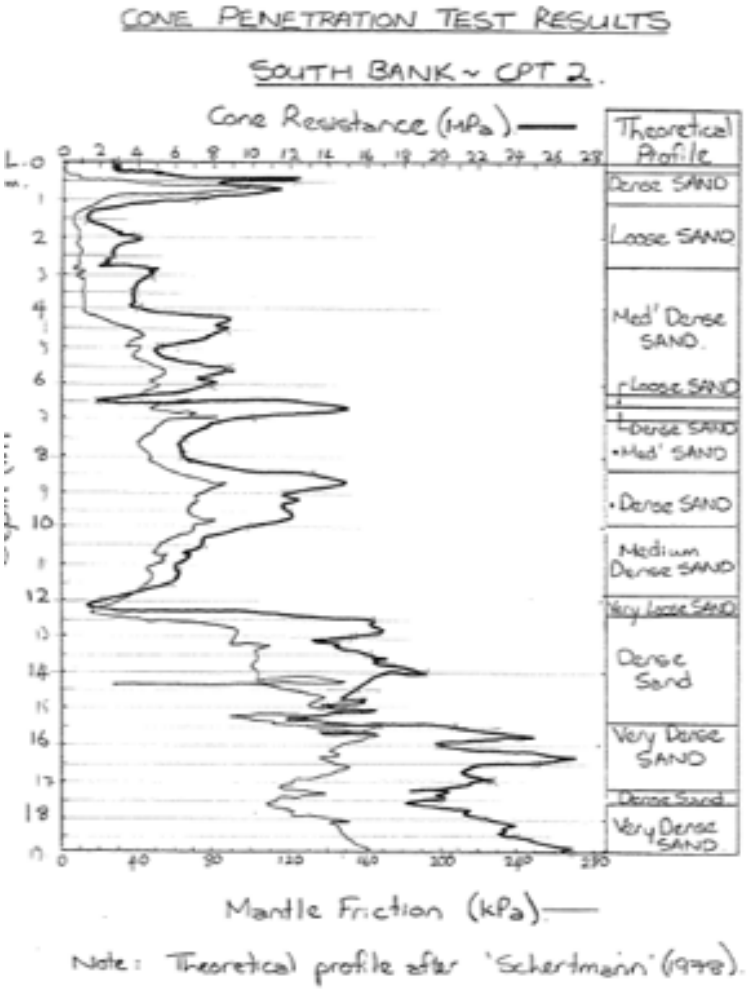

Important notes concerning this example analysis:

1 The original SPT data has not been used for any of the calculations. Instead, the available CPT data has been converted to equivalent SPT values, which are subsequently used to calculate the soil spring parameter values. The equivalent SPT values that have been calculated in this way and which are used in subsequent calculations of soil spring properties are provided in figure 5.3 'adopted profile for analysis'.

2 The method for estimating the horizontal ground displacement demand for the PSA for this example deviates from the general method described in phase 2. This is because measurements of ground surface lateral spreading displacement were available for the 22 February 2011 Christchurch earthquake (which would not normally be the case for a predictive analysis). However, the distribution of lateral spreading displacement as a function of depth remains unknown, yet is required for the phase 3a analysis, so a modified phase 2 analysis has been used to estimate the lateral displacements below the ground surface. The precise method that has been followed here for estimating the lateral spreading displacement profile is as follows:

   a The phase 1 site characterisation and earthquake loading analysis were undertaken for the 22 February 2011 Christchurch earthquake ground motion. Using the available soil data and local geological information, the soil layers susceptible to liquefaction were identified (figure 5.3). A

PGA of 0.28g was used for the triggering analysis, and was based on records from nearby strong ground motion stations and an empirical ground motion equation.

b The distribution of horizontal lateral spreading displacement as a function of depth was determined according to the method described in phase 2.

c This distribution was normalised by the ground surface displacement value from the phase 2 analysis, resulting in a non-dimensionalised distribution of horizontal lateral spreading displacement versus depth.

d The non-dimensionalised horizontal lateral spreading displacement distribution was scaled by the ground surface displacement measured at the south abutment during post-earthquake reconnaissance.

e The resulting scaled horizontal lateral spreading displacement was applied to the abutment piles in the PSA.

5.2.3 Idealisation of the soil profile

The first step of the phase 3a analysis is the idealisation of the soil profile. The aim of the idealisation process is to divide the soil profile into a series of discrete layers, each of which will be represented by its own soil spring material properties. Simplification of the soil profile has to be undertaken in the context of the phase 1 and 2 analyses and should consider all parameters relevant to the liquefaction analyses. Particular attention should be given to discriminating between layers likely to exhibit sand-like behaviour versus clay-like behaviour, clear identification of groundwater table depth, and the specification of each layer as either 'liquefied' or 'non-liquefied' (which will depend on the severity of the input seismic demand used in the phase 1 and 2 analyses).

The idealisation of the soil profile at the south abutment of Anzac Bridge is illustrated in figure 5.3. Note in particular that multiple data sources were used to discriminate between different soils, including CPT tip resistance data, CPT-based soil behaviour type I_c, borelog soil information, and factor of safety against liquefaction triggering values.

Once the simplified soil layering has been determined, the remaining step in the idealisation process involves assigning representative parameters (in this case SPT N values) to each layer for use in subsequent calculations of soil spring properties.

As can be seen in figure 5.3, all layers except for a thin seam at ~14 m depth have I_c values suggesting sand or silty-sand-like behaviour, which is consistent with the soil type information from the nearby borelog. Soil layers above the groundwater table are identified as non-liquefiable, while factor of safety against liquefaction triggering values have been used to determine which layers below the water table at a depth of 3.5 m should be treated as liquefiable in the pile analysis. Liquefiable layers are shown in blue in figure 5.3.

Figure 5.3 Anzac bridge south abutment in situ soil data, liquefaction triggering results (CHC – 22 Feb 2011 Christchurch earthquake; DAR – 10 Sep 2010 Darfield earthquake), adopted soil profile, and lateral soil displacement distribution

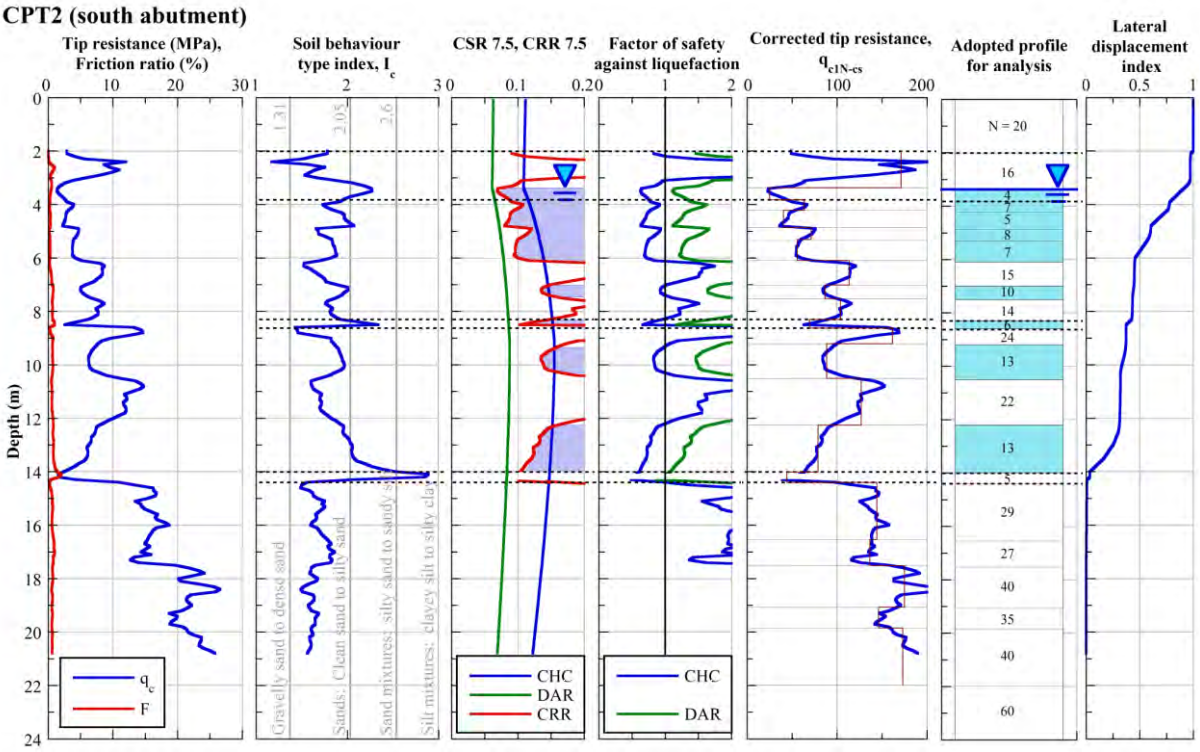

5.2.4 Define computational beam-spring model

5.2.4.1 Specifying the beam- spring mesh

Node array

In a single pile analysis, the pile is represented as a series of beam elements connected at node points arranged in a vertical array. For practical reasons, typically the nodes would be equally spaced, and hence the beam elements would all be of equal length. Each beam node (ie horizontal degree of freedom) is connected to its adjacent spring node by a soil spring (figure 3.5). The soil spring spacing is thus determined by the beam node spacing and is equal to the length of the beam elements. For the case of Anzac Bridge, the piles and the abutments are included in the beam array.

For this example, a vertical node spacing of 0.1 m has been adopted, meaning that each beam element is 0.1 m long and the soil springs are spaced 0.1 m apart. For all cases encountered in practice, this spacing is considered to be appropriate.

Pile head and pile tip fixity

A critical step in the development of the node array is the specification of the fixity conditions of the pile head/abutment top and pile tip nodes. Rotational and translational fixity can be independently specified, meaning that the following fixity conditions can be achieved at each of the pile head/abutment top and pile tip:

- fully fixed against rotation and translation

- pinned (free to rotate, but not translate)
- restrained against rotation but free to translate
- free to rotate and translate (unrestrained).

For the case of the Anzac Bridge south abutment, the node array has been developed as follows:

- The topmost node corresponds to the centre of rotation (CoR) of the abutment about the bridge deck. In this example the CoR is located 0.5 m below the true top of the abutment, based on post-earthquake observations and measurements of the deformed shape of the bridge. In the analysis, the topmost node (located at the CoR) is assigned a 'depth' of 0 m for simplicity.
- Based on the structural details of the connection between the abutment and the bridge deck, the topmost node is considered free to rotate, but is constrained against lateral translation by the axially-stiff bridge deck. This abutment-bridge deck connection is an important feature of the superstructure design that can have a significant influence of the mode of deformation of the entire bridge, including the foundations (Haskell 2014; Haskell et al 2013).
- The bottom abutment node is located 1.4 m below the topmost abutment node. The nodes below 1.4 m correspond to the abutment pile.
- The pile tip is specified as free to translate and rotate as the piles are not socketed into rock nor otherwise rigidly fixed.

5.2.4.2 Beam material parameters

When developing the array of beam elements intended to represent the pile and abutment, the beam material type must be specified for each beam element. For the case of Anzac Bridge south abutment single pile analysis described here, two separate beam material types are required – one for the pile and another for the abutment. For the whole-bridge analysis described in section 3.2.3, additional beam material types are required for the other structural components (ie bridge deck, central piers and pier piles).

Pile beam material type

The abutment piles are UC 310x137 kg/m steel H-piles. The beam element moment-curvature values for yield and ultimate states can be obtained from the section properties. Moment-curvature relationships for each element were calculated using the computer software CUMBIA (Montejo and Kowalsky 2007). The moment-curvature relationship as specified in the PS model is illustrated in figure 5.4. Note that these have been scaled to be representative of a 1.5 m tributary bridge width.

Abutment material type

The concrete abutment is assumed to remain in the elastic range, hence has a linear moment-curvature relationship in the PS analysis. The flexural stiffness (EI) is found by multiplying Young's modulus (E) of concrete by the second moment of area (I).

Note on tributary width

When idealising a three-dimensional structure as a two-dimensional plane strain representation, all beam and spring materials must correspond to the same 'tributary width' for the analysis to be valid. For a single pile analysis, such as the example illustrated here, it is convenient to take the tributary width as

equal to the centre-to-centre spacing of the piles. This means that the abutment beam and spring material strengths must correspond to an abutment width of 1.5 m.

Figure 5.4 Moment curvature relationships

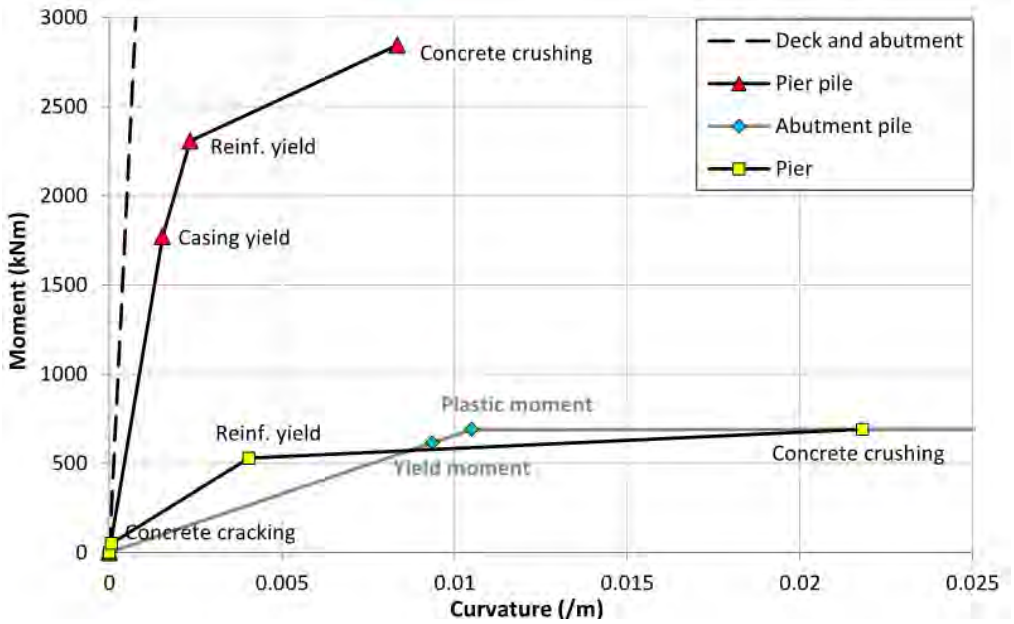

5.2.4.3 Soil spring material parameters

Specification of the soil spring material parameters is done on a layer-by-layer basis. The relationships used to calculate the spring parameters depend on the characteristics of the layer, specifically:

- whether or not the layer has been identified as liquefied
- if non-liquefied, whether the layer exhibits sand-like or clay-like behaviour
- for sand-like non-liquefied layers, the depth of the layer.

Example liquefied layer

To illustrate the calculation of liquefied soil spring parameters, consider the liquefied layer at the south abutment, approximately 3.4–3.8 m depth that has been assigned a representative SPT blowcount, N_{60}, of 4. For the initial analysis, best-estimate values for N_{60}, β_L, and α_L are used.

Soil spring stiffness:

$N_{60} = 4 \qquad \beta_L = 0.01 \qquad s = 0.1$ m $\qquad D_0 = 0.309$ m

$$k_L = 56 \cdot N \cdot (100 D_0)^{-3/4}$$

$$k_L = 56 \cdot 4 \cdot (100 \times 0.309)^{-3/4}$$

$$k_L = 17.1 \text{ MNm}^{-3}$$

$$K_L = \beta_L \cdot k_L \cdot s \cdot D_0$$

$$K_L = 0.01 \times 17.1 \times 0.1 \times 0.309$$

$$K_L = 5.28 \times 10^{-3} \text{ MNm}^{-1}$$

Soil spring yield force:

Using Seed and Harder (1990) to estimate S_r, which requires N_{60} to be converted to the clean sand equivalent, normalised blowcount, $(N_{60})_{1-CS}$:

$(N_{60})_{1-CS} = 10$ $S_r = 15.5$ kPa $\alpha_L = 1$

$$P_{L-max} = p_{L-max} \cdot s \cdot D_0 = \alpha_L \cdot S_r \cdot s \cdot D_0$$

$$P_{L-max} = 1 \times 15.5 \times 0.1 \times 0.309$$

$$P_{L-max} = 0.479 \text{ kN}$$

Example non-liquefied layer (sand-like, crust)

For cohesionless non-liquefied layers at the ground surface, the increase in shear strength of the soil with depth (ie with effective stress) is taken into account. This is done by specifying a different yield strength for each individual spring in the crust layer. The crust layer at Anzac Bridge consists of a layer of engineered backfill behind the concrete abutment. The backfill extends to a depth of 0.6 m below the bottom of the abutment (corresponding to a depth in the analysis of 2.0 m below the topmost node in the node array). The relative density and unit weight of the backfill material were assumed to be 70–80% and 18 kNm^{-3}, respectively. Note also that the 'depth' referred to in the calculations below is relative to the topmost node in the node array. As described earlier, this node is located at the CoR of the abutment, and is 0.5 m below the ground surface. For this reason it is necessary to account for the additional vertical stress due to the 0.5 m of soil above the top node (equal to 9.2 kPa) when calculating the σ'_{v0} values for the soil springs.

$N_{60} = 20$ $\gamma_{Fill} = 18$ kNm^{-3} surcharge = 9.2 kPa

Calculations for two crust springs (at 0.5 and 1.5 m depth) are illustrated here. Note that the calculations below would need to be repeated for every spring in the crust layer at 0.1 m spacing.

Spring at 0.5 m depth ($z = 0.5$)

$D_0 = 1.5$ m (abutment segment tributary width = pile spacing), $\beta_C = 1.0$

Soil spring stiffness

$$k_C = 56 \cdot N \cdot (100 D_0)^{-3/4}$$

$$k_C = 56 \cdot 20 \cdot (100 \times 1.5)^{-3/4}$$

$$k_C = 26.1 \text{ MNm}^{-3}$$

$$K_C = \beta_C \cdot k_C \cdot s \cdot D_0$$

$$K_C = 1.0 \times 26.1 \times 0.1 \times 1.5$$

$$K_C = 3.92 \text{ MNm}^{-1}$$

Soil spring yield strength

σ'_{v0} at depth of 0.5 m below topmost node

$$\sigma'_{v0} = 9.2 + 0.5 \times 18$$

$$\sigma'_{v0} = 18.2 \text{ kPa}$$

Taking $\phi' = 37°$

$K_P = \frac{1+\sin\phi'}{1-\sin\phi'}$

$K_P = 4.0$

At a depth of 0.5 m the soil is behind the abutment, so $\alpha_C = 1.0$

$P_{C-max} = p_{C-max} \cdot s \cdot D_0 = \alpha_C \cdot K_P \cdot \sigma'_{v0} \cdot s \cdot D_0$

$P_{C-max} = 1.0 \times 4.0 \times 18.2 \times 0.1 \times 1.5$

$P_{C-max} = 10.9$ kN

Spring at 1.5 m depth ($z = 1.5$)

$D_0 = 0.309$ m (pile width) $\beta_C = 1.0$

Soil spring stiffness

$k_C = 56 \cdot N \cdot (100D_0)^{-3/4}$

$k_C = 56 \cdot 20 \cdot (100 \times 0.309)^{-3/4}$

$k_C = 85.5$ MNm^{-3}

$K_C = \beta_C \cdot k_C \cdot s \cdot D_0$

$K_C = 1.0 \times 85.5 \times 0.1 \times 0.309$

$K_C = 2.64$ MNm^{-1}

Soil spring yield strength

σ'_{v0} at depth of 1.5 m below the topmost node

$\sigma'_{v0} = 9.2 + 1.5 \times 18$

$\sigma'_{v0} = 36.2$ kPa

Taking $\phi' = 37°$

$K_P = \frac{1+\sin\phi'}{1-\sin\phi'}$

$K_P = 4.0$

At a depth of 1.5 m the soil is behind the pile, so $\alpha_C = 4.5$

$P_{C-max} = p_{C-max} \cdot s \cdot D_0 = \alpha_C \cdot K_P \cdot \sigma'_{v0} \cdot s \cdot D_0$

$P_{C-max} = 4.5 \times 4.0 \times 36.2 \times 0.1 \times 0.309$

$P_{C-max} = 20.1$ kN

Example non-liquefied layer (sand-like, deep)

For cohesionless non-liquefied layers at depth, the calculation procedure follows that for the crust layer, except that each individual spring does not need to be individually specified. Here the calculations are undertaken for the centre spring of the layer in question, and then the same properties are used for all springs in that layer as the layer is relatively thin. As a practical guide, if a deep, non-liquefied layer is thicker than approximately 1 m or two pile diameters (whichever is the larger), then splitting the layer into sub-layers for the purpose of specifying soil spring properties is recommended.

Taking as an example the layer between approximately 8.6 and 9.2 m depth, which has an SPT N_{60} value of 24:

$N_{60} = 24 \qquad D_0 = 0.309$ m $\qquad \beta_B = 1.0$

Soil spring stiffness

$$k_B = 56 \cdot N \cdot (100 D_0)^{-3/4}$$

$$k_B = 56 \cdot 24 \cdot (100 \times 0.309)^{-3/4}$$

$$k_B = 103 \text{ MNm}^{-3}$$

$$K_B = \beta_B \cdot k_B \cdot s \cdot D_0$$

$$K_B = 1.0 \times 103 \times 0.1 \times 0.309$$

$$K_B = 3.16 \text{ MNm}^{-1}$$

Soil spring yield strength

$$\sigma' v0 = 121 \text{ kPa}$$

Taking $\phi' = 37°$

$$K_P = \frac{1+\sin\phi'}{1-\sin\phi'}$$

$$K_P = 4.0$$

At greater depths a wedge mechanism cannot form around the pile, so $\alpha_B = 1.0$

$$P_{B-max} = p_{B-max} \cdot s \cdot D_0 = \alpha_B \cdot K_P \cdot \sigma'_{v0} \cdot s \cdot D_0$$

$$P_{B-max} = 1.0 \times 4.0 \times 121 \times 0.1 \times 0.309$$

$$P_{B-max} = 15.0 \text{ kN}$$

5.2.4.4 Inertial and ground displacement demands

Lateral spreading ground displacement profile

As already discussed, a modified procedure based on Zhang et al (2004) was used to estimate the lateral spreading displacement profile for the south abutment of the bridge. The resulting normalised soil displacement profile is shown in figure 5.5 and is multiplied by the surface ground displacement of 0.66 m and applied to the soil springs.

Inertial demand from the superstructure

This example analysis considers the lateral spreading phase of the foundation response, hence no equivalent static inertial demand is applied to the foundation. Note that effects of the inertial demand from the superstructure should be evaluated using a separate cyclic liquefaction analysis (section 3.2.3).

5.2.5 Performing pile analysis with best estimate parameters and interpretation of results

The pile analysis is carried out using a custom-built computer code that can simulate the elastic and plastic behaviour of the structural elements. Figure 5.5 summarises the pile displacement and bending moment results of the reference model (RM) analysis. Particular features of the results to note are:

1 The displacement at the top of the abutment is zero. Recall that in this single pile analyses, the abutment is modelled by rigid beam elements, and is constrained laterally at the point contact between the abutment and the bridge deck. This pattern of abutment and foundation deformation is a result of the boundary condition specified at the abutment top, which was based on the assumption that the bridge deck is axially stiff.

2 The horizontal displacement at the top of the pile is approximately 35 cm, indicating that the abutment base was pushed towards the river. This, combined with the restraint of the abutment top results in a backward tilt of the abutment – a mode of displacement that matches field observations of the bridge following the 22 February earthquake. The angle of abutment back-rotation from the RM analysis is approximately 13.5. We note that this is somewhat greater than the 5° rotation observed following the earthquake. This suggests that, while the mode of deformation predicted is similar to that observed, the analysis may be over predicting the level of damage in this example.

3 There is a concentration of curvature at the interface between the non-liquefied crust layer and the uppermost liquefied soil layer. This corresponds with the location of maximum bending moment in the pile. The bending moment demand at this location reaches the ultimate moment of the steel H-piles.

4 There is a second concentration of curvature at depth, the location of which approximately coincides with interface between the lowest liquefiable layer and the non-liquefied soil below. Again the bending moment demand at this location approaches the ultimate capacity of the abutment piles.

Together, these results suggest the demand on the pile from the laterally deforming spring soil is severe, and the crust layer may represent a significant component of this demand. Note that this result was obtained using the best estimate parameters for the model under the assumption of a ground displacement of 0.66 m acting on the abutment and uppermost part of the abutment piles. The example sensitivity analyses that follow explore this interpretation in more detail.

Figure 5.5 Pile deformation and bending moment results for the single pile analysis of the Anzac Bridge south abutment piles, including results of the sensitivity analyses

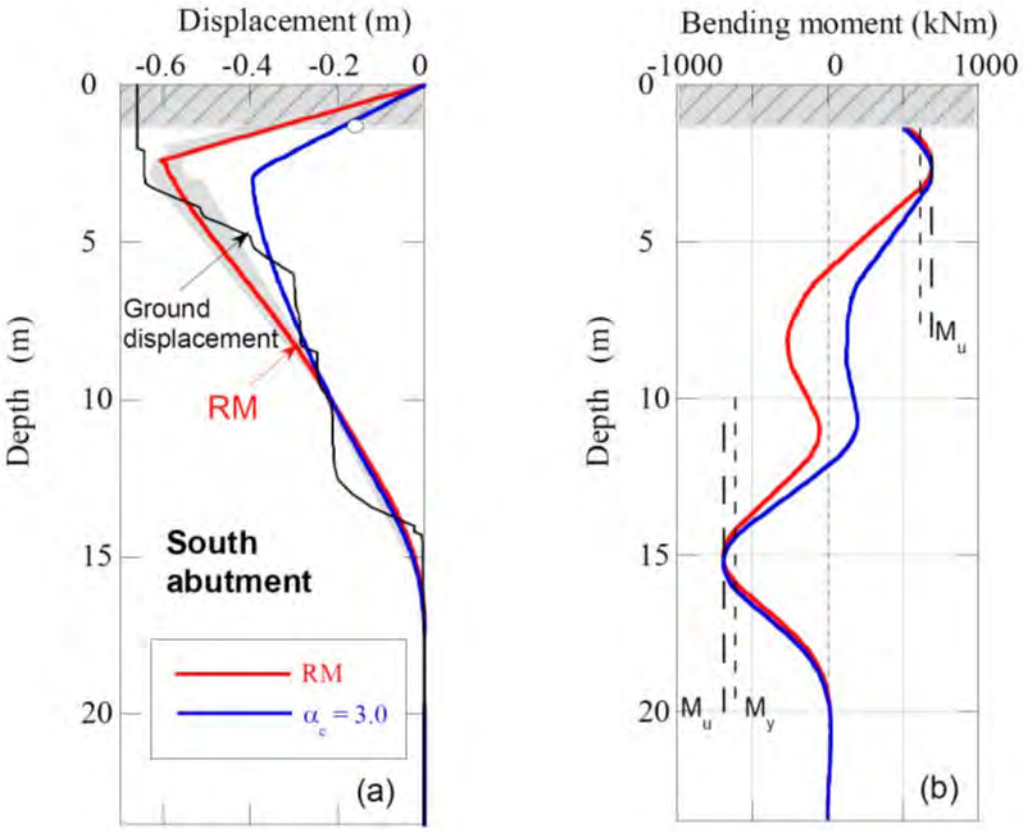

5.2.6 Parametric sensitivity analyses and interpretation of results

The procedure for undertaking a parametric sensitivity analysis is described in sections 3.2.2 and 3.2.3.3. Having already completed the RM analysis using best-estimate values for all parameters, a series of analyses is then performed in which the value of each parameter, in turn, is set first at its lower bound (LB) and then at its upper bound (UB) value, with all other parameters kept at their RM values. In this way, the sensitivity of the pile response to each particular parameter can be examined.

5.2.6.1 Example sensitivity analysis – crust parameters

Figure 5.5 presents the results of the analyses investigating the effects of crust parameters on the pile response (α_c and β_c). The reference LB and UB values for these parameters are summarised below:

α_c LB: 3.0 ref: 4.5 UB: 5.0

β_c LB: 0.3 ref: 1.0 UB: 1.0

5.2.6.2 Interpretation of sensitivity results

As already discussed, the RM response, shown with the solid lines, indicates horizontal displacement at the top of the south abutment pile (figure 5.5) of approximately 35 cm. When varying the stiffness parameter of the crust β_c, the pile response only changes slightly and remains within the shaded area along the RM response, shown in figure 5.5. However, the pile response does change when $\alpha_c = 3.0$ is used

with RM values for all other parameters, indicating the large sensitivity of the pile response to this crust strength parameter. More specifically, the use of a lower value for α_c leads to a reduction in demand from the crust layer compared to the RM analysis. This in turn results in a reduction in the predicted peak pile displacement. It is interesting to note that the predicted peak pile bending moments at the critical locations along the pile are not much affected by the use of a lower α_c value, indicating that the flexural pile demand is still large enough to exceed the yield moment of the abutment piles, even when a lower α_c value is assumed. The piles are therefore still predicted to suffer significant damage and plastic hinging, though the rotation at the plastic hinges and overall abutment displacement are somewhat reduced.

Additional sensitivity analyses should also be performed in which parameters of the liquefied and deep non-liquefied layers are varied between their LB and UB values. For the Anzac Bridge south abutment, such analyses (not shown) indicate there is an insignificant influence of the liquefied and non-liquefied layer parameters on the abutment pile response. The results of these analyses varied within a few percent from the RM response of the abutment piles shown in figure 5.5.

Putting all of these results together, it is clear that the modelling of the crust (in particular the maximum size of the load from the crust on the abutment/pile) strongly influences, and practically governs the abutment pile response.

Further sensitivity analyses should also be undertaken to evaluate the influence of the lateral spreading displacement demand on the predicted pile response. This is because there is considerable uncertainty in the estimation of the magnitude of the lateral spreading ground displacements (ie the phase 2 analysis). Such analyses show the governing influence of the magnitude of the applied ground displacement on the abutment pile response (Cubrinovski et al 2014b).

5.2.7 Whole-bridge analysis (key considerations)

The next stage in the procedure is to model the response of the entire bridge including both the superstructure and the foundations. A global bridge analysis would be undertaken in order to account for the effects of soil-pile-pier/abutment-superstructure interaction and variation in the liquefaction-induced ground displacements acting on the abutment and pier piles. The procedure is essentially an extension of the single pile analysis, with the bridge superstructure modelled using a series of beam elements; however, when developing a global bridge model there are several important considerations to take into account:

- One of the main considerations is the specification of the lateral spreading ground displacements for each of the abutments and central piers. In this example global bridge analysis, the ground displacement at the top of the pier piles is assumed to be 50% of that at the respective elevation for the abutment piles. The distribution of lateral ground displacement with depth has been evaluated using the triggering and normalised displacement calculation, as previously discussed.

- Another important consideration is the tributary width selected for the two-dimensional idealisation of the bridge. For a global bridge analysis the most straightforward approach is to model the full width of the bridge, meaning the beam and spring material properties for each individual component type should represent the ‘lumped’ strength corresponding to the entire bridge width.

- The boundary conditions/node fixities in the node array also require careful specification. For example, unlike for the single pile model, the node located at the CoR of the abutment no longer requires lateral restraint, as the interaction between the abutment and deck is modelled explicitly in the global bridge model. Care is required when specifying fixities at internal joints and connections, taking into account the structural design and construction details. Based on the connection details of

Anzac Bridge, the connections between the deck and each abutment are modelled as pinned, while the connections between the deck and each central pier are modelled as rigid, an approximation of semi-integral connection between the piers and the deck.

A schematic view of the global bridge model for the Anzac Bridge, including a summary of the applied ground displacements and computed bridge displacements and bending moments for the piers and pier piles is shown in figure 5.6.

Results from the global bridge analysis indicate that the pier piles approach yield level at large depth (approximately 16.5 m depth below the bridge deck elements for the south pier piles and 10 m depth for the north pier piles). It is predicted that the piers themselves experience bending moments exceeding yield and approaching ultimate level at the tops of the piers (ie at the connection to the deck) and a similar but somewhat smaller level of damage at the base of the piers. The computed moments at the tops of the piers probably overestimate the actual pier moments because a fully restrained connection between the deck and pier-cap was adopted in the analysis.

Interestingly, the global bridge analysis indicates that the entire bridge displaces approximately 3 cm to the north. It is also interesting to note that the peak bending demands at the north pier exceed those at the south pier, in spite of the smaller lateral spreading soil displacement at the north pier. This is due to the system response of the bridge, where the global displacement of the bridge structure to the north imposes a displacement at the top of the north pier, that is, in the opposite direction to the lateral spreading displacement of the soil around the north pier piles. This in turn results in the larger than expected bending demand on the north pier and north pier piles.

Figure 5.6 Results from whole- bridge analysis of Anzac Bridge showing deflected shapes of abutment and pier piles, and pier pile bending moment distributions and damage locations

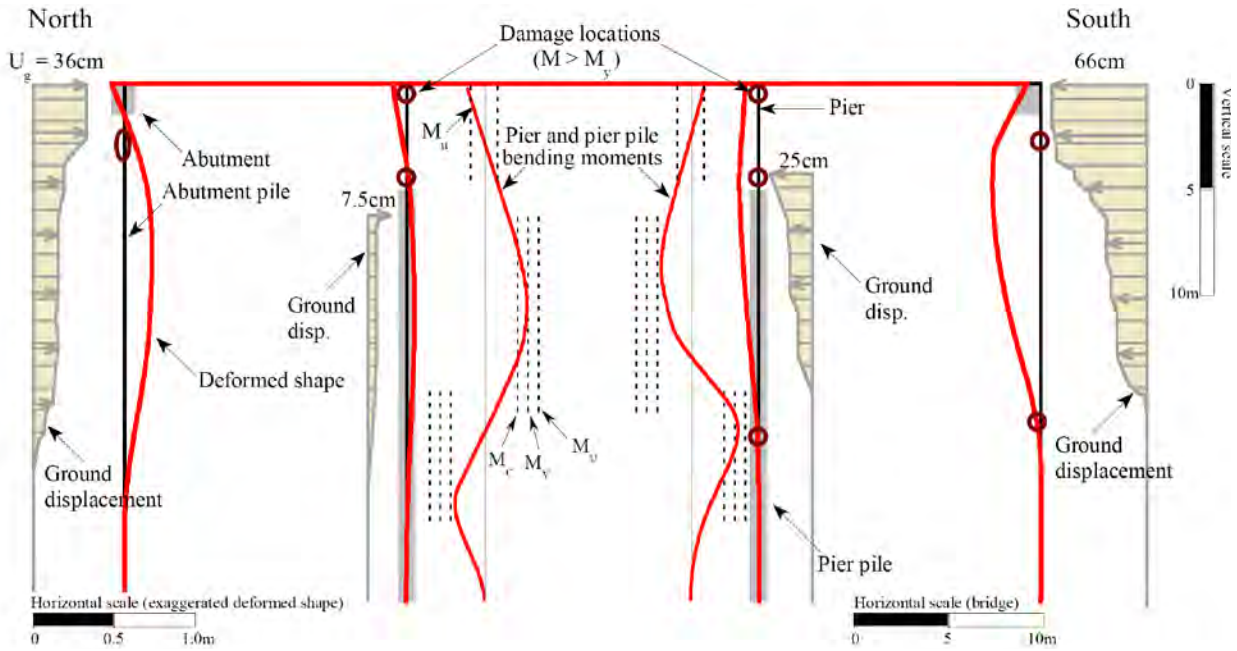

5.3 Example 2: Belfast Road Underpass

5.3.1 Bridge and site description

This example demonstrates the PSA and design of a proposed bridge at a grade separated intersection on a relatively flat, liquefaction susceptible site. The two-lane, two-span bridge takes a local road over a four-lane expressway and has approach embankments up to 8 m high with spill through slopes at the abutments. The abutments and piers are supported on piles that are founded in dense sandy gravels about 28 m deep.

The bridge is 52.5 m long, (2x26.250 m spans) with integral abutments, as shown in figure 5.7. The superstructure comprises 16 900 mm deep, single hollow core units resting on elastomeric strip bearings at the pier and connected integrally to the abutment cap. The foundation system comprises three 1,200 mm concrete bored piles at the pier and five 900 mm concrete bored piles at each abutment, pinned to the capping beam. Each pile at the pier supports a concrete column of 900 mm diameter and 6.25 m height. The pier piles are about 24 m long whereas the piles at each abutment are about 30 m long.

Figure 5.7 Typical longitudinal (above) and cross section (below) of the bridge

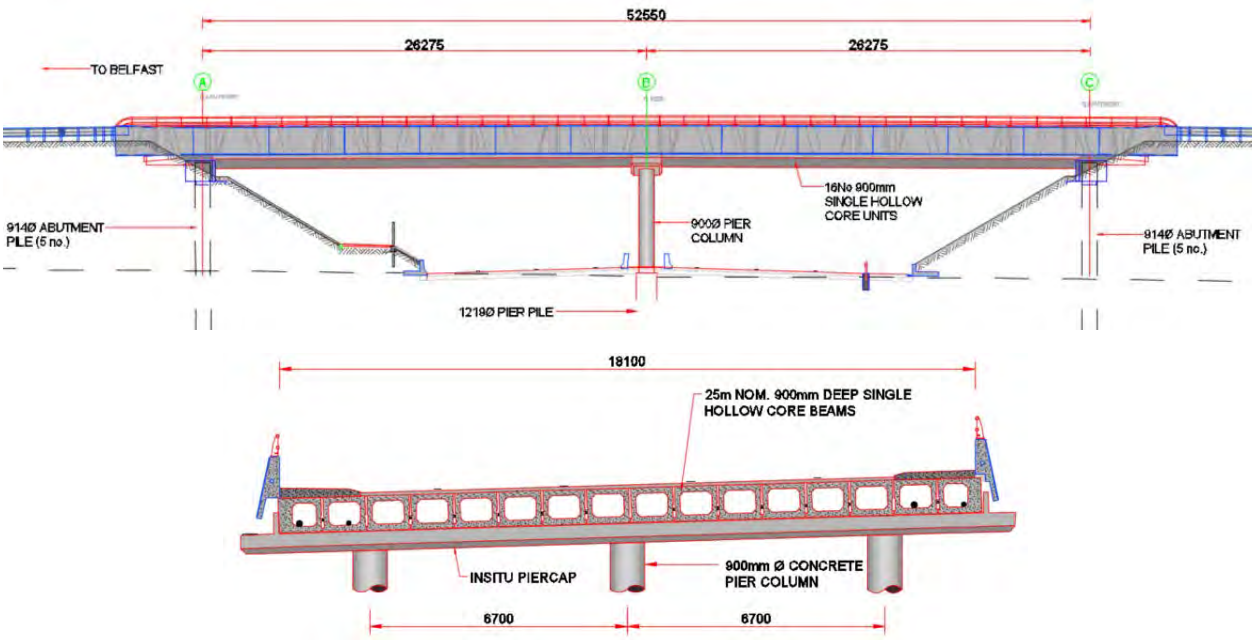

The site is underlain by about 9.5 m of interbedded typically loose sands, silt and soft organics with medium dense sands and dense gravels at depth. Ground water level is typically about 1.5 m below ground level. Further details of the ground conditions at this structure are presented in section 4.2.3.

This study focuses only on the longitudinal response of the bridge as the response will be critical in this direction for this relatively short bridge.

5.3.2 Liquefaction and lateral spreading hazard

The laterally extensive layer of fine silty sand between elevations of 14 m and 11.2 m is anticipated to liquefy at the ultimate limit state (ULS) earthquake (1 in 1,000 year) shaking levels causing ground subsidence and

lateral spreading of the approach embankments. Free-field, level ground subsidence of 110 mm is predicted in a 1 in 1,000 year earthquake and lateral spreading at the abutments is anticipated to be in the order of 750 mm. Full details of the liquefaction and lateral spreading hazard at this bridge are described in section 4.3.

5.3.3 Seismic performance requirements

The *Bridge manual* specifies qualitatively a set of minimum seismic performance requirements for a bridge based on the earthquake severity, post-earthquake functions and reparability (*Bridge manual*, table 5.1). Following an ultimate limit state earthquake, the bridge should be available for emergency traffic and capable of being reinstated to carry its full design load. The design earthquake severity is determined from the importance of the structure (*Bridge manual*, table 2.1). Where the bridge is located on ground susceptible to liquefaction and lateral spreading, an additional set of requirements is given in the *Bridge manual*, section 6.1.2.

The minimum performance requirements are deemed to be satisfied if a bridge is designed and detailed as per the relevant New Zealand codes of practice. The *Bridge manual* allows formation of plastic hinges in the piles. The preferred location for hinges is at the top of piles where they are easily accessible for inspection and repair after an earthquake. Hinging is also acceptable at depths with a limited displacement ductility of 3 (for vertical piles).

For information, the US design standard for ports and wharfs (ASCE 61 2014) prescribes, qualitatively, a set of strain limits for plastic hinges formed in reinforced concrete piles at different depths depending on the design requirements, as presented in table 5.1. Furthermore, in the recent *Memo to designers* (California Department of Transportation 2016), Caltrans allows formation of two plastic hinges with allowable ductility demands up to five for new bridges subjected to lateral spreading. For existing bridges, the memo also prescribes allowable drift limits and differential settlement requirements.

Allowing piles to yield under a design level of shaking may lead to significant damage to bridge foundations and to the bridge itself. However, in the case of a major earthquake event, allowing yielding in piles may be a practical alternative. Therefore, the designer has to consider the consequences of the formation of plastic hinges in the piles at different levels of earthquake severity and design accordingly to satisfy the necessary performance requirements in the *Bridge manual*.

Table 5.1 Summary of strain limits for various damage states per ASCE 61 (2014)

Damage states (earthquake severity)	Component	Hinge location		
		Top of pile	In ground (<10D)	Deep in ground (>10D)
Minimal damage (serviceability limit state SLS event)	Concrete	$\varepsilon_c \leq 0.005$	$\varepsilon_c \leq 0.005$	$\varepsilon_c \leq 0.008$
	Reinforcement	$\varepsilon_s \leq 0.015$		
Controlled and repairable damage (ULS event)	Concrete	$\varepsilon_c \leq 0.005 + 1.1\rho_s \leq 0.025$	$\varepsilon_c \leq 0.005 + 1.1\rho_s \leq 0.008$	$\varepsilon_c \leq 0.012$
	Reinforcement	$\varepsilon_s \leq 0.6\varepsilon_{su} \leq 0.06$		
Life safety protection (major event)	Concrete	No limit	$\varepsilon_c \leq 0.005 + 1.1\rho_s \leq 0.012$	No limit
	Reinforcement	$\varepsilon_s \leq 0.8\varepsilon_{su} \leq 0.08$		

5.3.4 Design earthquake data

Ideally, characterisation of the seismic hazard at a bridge site should be carried out using a site specific study. In design practice, however, the seismic hazard is often characterised by the code prescribed design response spectrum anchored at a point representative of the site hazard and the earthquake severity.

The example bridge is located near Christchurch. According to NZS 1170.5, the bridge site was assessed to be class D and the zone factor Z is 0.30. The *Bridge manual* classifies the bridge to be an important level 2 structure and, accordingly, the design seismic actions are as shown in table 5.2.

Table 5.2 Seismic design parameters for piles in liquefiable soils per *Bridge manual*

	SLS event	ULS event	Major event
Risk factor R	1.3/4 = 0.325	1.3	1.5 x 1.3 = 1.95
Zone factor Z	0.30	0.30	0.30
Structure performance factor S_p	0.7 (FBD) 1.0 (DBD)	0.7 (FBD) 1.0 (DBD)	0.7 (FBD) 1.0 (DBD)
Allowable ductility μ	None (FBD) Strain limits (DBD)	≤ 3.0 (FBD) Strain limits (DBD)	No collapse (FBD) Strain limits (DBD)

Note. FBD is force based design method, and DBD is displacement base design method.

Note that, in the draft revised section 5 (NZ Transport Agency 2017) of the *Bridge manual* (as at the time of preparing this report), the structural performance factor S_p is effectively replaced by the foundation damping which is used to scale down the design spectrum. In this example, we are following the traditional force based approach with the S_p factor as a function of site class.

5.3.5 Soil springs and ultimate loads

Three types of soils spring and ultimate loads are used to model the interaction between the soil and the piles, one for the horizontal response, one for sleeve friction and one for the pile base resistance. The reference vertical and horizontal springs and ultimate loads that have been calculated for a node spacing of 0.2 m are shown in figures 5.8 and 5.9 for the pier and abutment respectively.

The soil properties derived from the CPT tests shown in figures 4.10 and 4.11 have been used to calculate the spring constants and ultimate loads. Note that the soil properties are similar at both abutments and the pier and properties at each node have typically been taken as the average derived from the correlations with CPT across the site.

The horizontal soil springs and ultimate pressures have been calculated using the procedure described in section 3.2.3. Vertical springs have been evaluated as follows:

5.3.5.1 For non- cohesive soils:

The ultimate skin resistance is given by:

$$t_u = K_s \tan\delta' \, \sigma'_v(z, z_{cr})\pi D \qquad t_{max} = t_u \, \Delta L$$

where, the angle of wall friction δ' is $3/4\phi'$ and the effective lateral pressure coefficient K_s is taken as $1.5K_0$ and K_0 is $1 - \sin\phi'$. Skin friction has been limited to 120 kPa.

The displacement at which 50% of the ultimate resistance is mobilised is given in API (1993) as:

$z_{50} = 0.05 \ * 25.4\ mm = 1.3\ mm$

5.3.5.2 For cohesive soils

The ultimate skin resistance is given by

$t_u = \alpha_u s_u \pi D \qquad t_{ult} = t_u \Delta L$

where, the adhesion factor α_u is given by the following relations as given in Verification Method B1/VM4 (MBIE 2017) or Kulhawy and Phoon (1993).

The displacement at which 50% of the ultimate resistance is mobilized is given by the following relation as given in API (1993)

$z_{50} = 0.0031\ D$

For layers predicted to liquefy, the side resistance is computed using the post-liquefaction residual undrained strength S_r from figure 4.17.

Note that the embankments will be constructed and preloaded and surcharged before construction of the piles. We have therefore assumed that there will be no locked in stresses in the pile from down drag of the embankment prior to an earthquake. Furthermore, we have assumed there will be no subsidence within the cyclic phase of the earthquake. The subsidence will occur in the lateral spreading phase with the redistribution of excess pore water pressures.

Figure 5.8 Secant soil spring constants and ultimate loads at the pier nodes

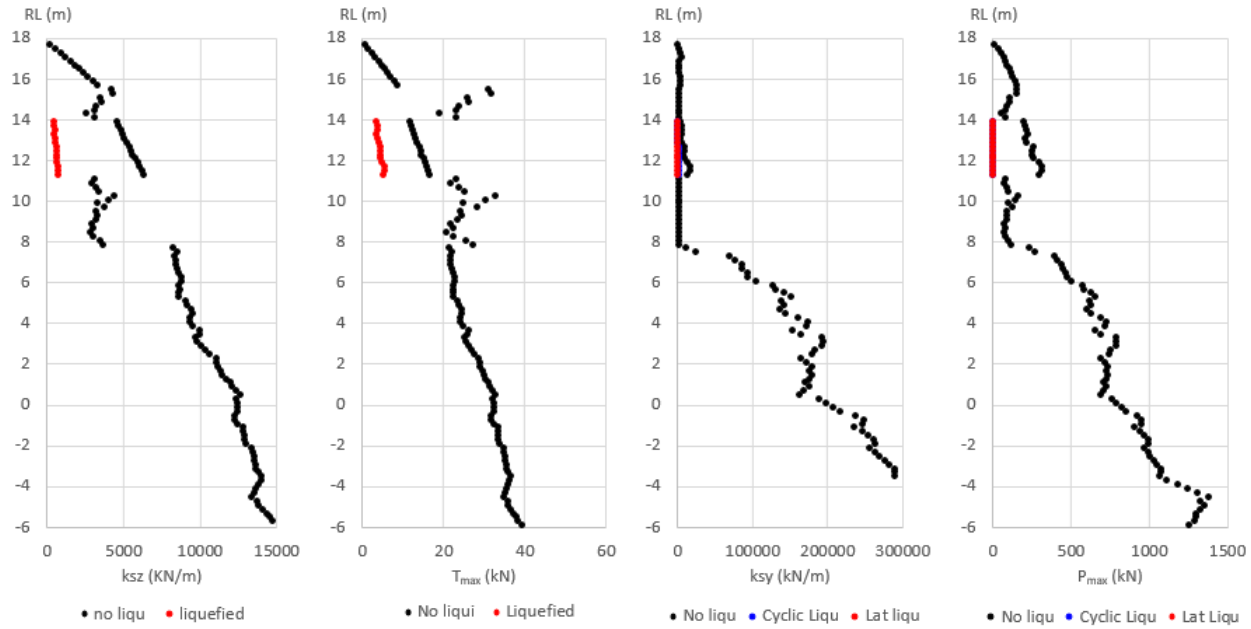

Figure 5.9 Secant soil spring constants and ultimate loads at the abutment nodes

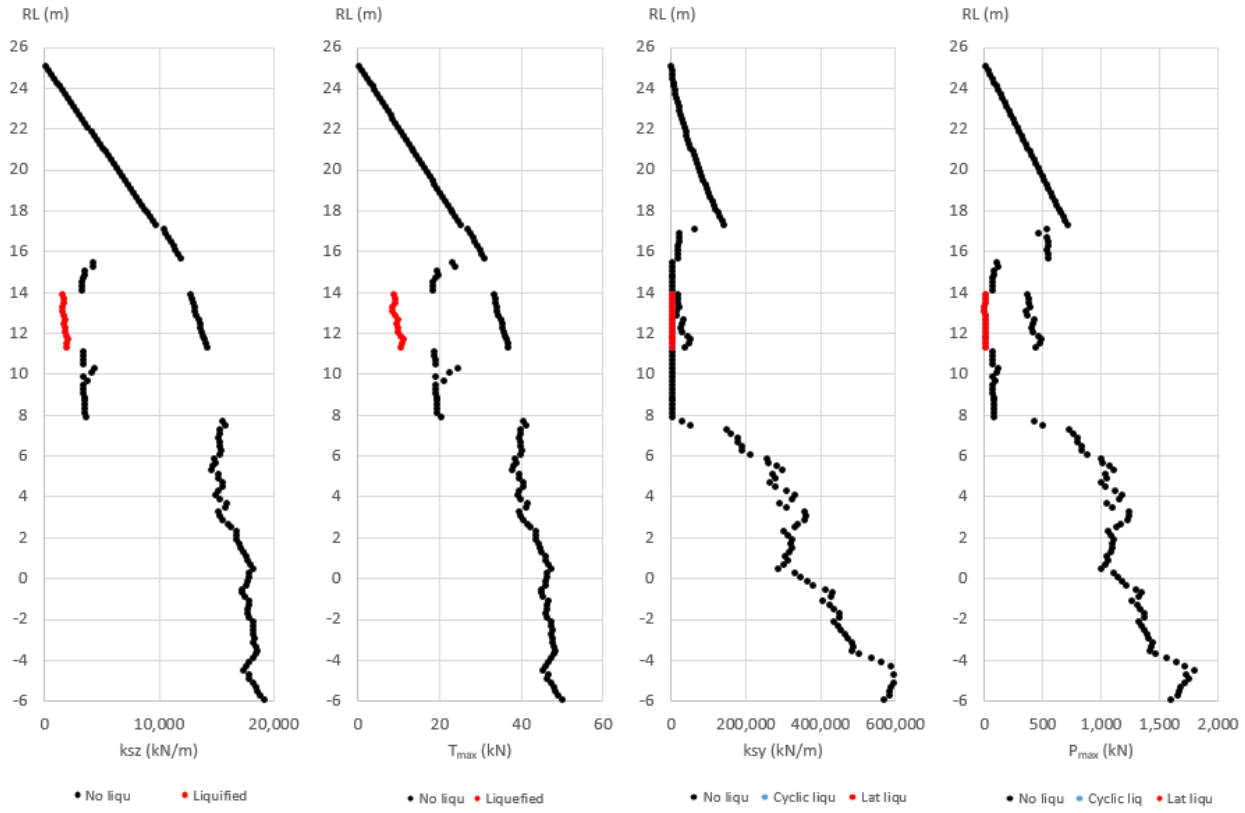

5.3.6 Kinematic demands

Profiles of horizontal ground displacement at the abutment and the pier used in the three phases of the structural analysis presented in this section are shown in figure 5.10. These displacements were derived from free-field dynamic finite element analysis that is not discussed in detail here. The profile is similar in shape to those calculated from the simplified method shown in figures 4.22 and 4.23, but is lower in magnitude and could be considered LB estimates from the simplified method. The reduced displacements primarily result from seismic isolation of the liquefiable silt by the underlying soft organic silt limiting the strains in the liquefiable layer. Vertical ground displacements used in the structural analysis are the vertical displacements shown in figures 4.22 and 4.23.

Figure 5.10 Horizontal ground displacements

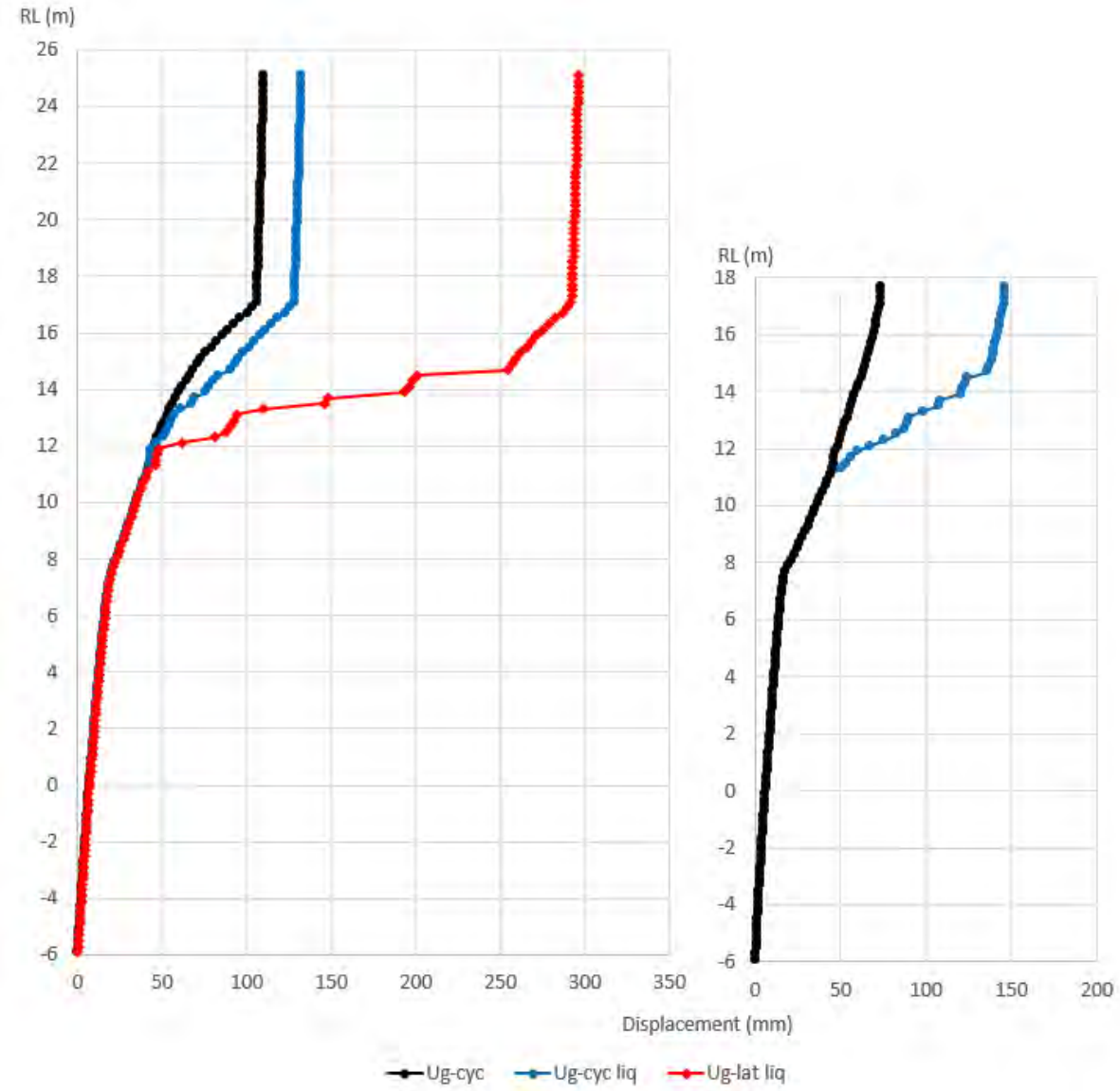

a) Abutment **b) Pier**

5.3.7 Determination of inertial demand

The *Bridge manual* recommends two analysis/design methods to determine the inertial demand from the superstructure. These are the conventional force based design (FBD) method as presented in section 5 of the *Bridge manual*, and the displacement based design (DBD) method as given in the draft section 5. A brief description of both methods follows.

5.3.7.1 Force based design method

In the FBD method, an elastic analysis model is developed based on the effective stiffness (secant stiffness to yield displacement) of the lateral load resisting elements to determine the elastic fundamental natural period. The inertial demand is then computed corresponding to that period from the design response spectrum scaled down by a ductility factor to include the effect of hysteresis energy dissipation within the

structure. The energy dissipation through surrounding soil is incorporated via the structural performance (S_p) factor (*Bridge manual*, table 5.4). Note that in the draft section 5 of the *Bridge manual*, the S_p factor is effectively replaced by foundation damping. The total inertial demand is distributed to the different lateral load resisting elements according to their relative effective lateral stiffness.

5.3.7.2 Displacement based design method

In the DBD method, the secant stiffness of the lateral load resisting elements is determined from the permissible displacement at the bridge deck level. The permissible displacements are generally determined from the material strain limits at the potential plastic hinge locations. An equivalent single degree of freedom (SDOF) system is then derived using a compatible displacement profile scaled to the displacement limit of the critical member(s). The equivalent SDOF system is characterised by the displacement demand and equivalent viscous damping representative of the various forms of energy dissipation in the structure. With the known displacement demand and equivalent viscous damping, the secant period of the structure is derived from the design displacement spectrum and subsequently, the inertial demand on the structure. Where the response of the foundations contribute significantly to the deck displacement, it is preferable to carry out a non-linear pushover analysis to determine the inertial demands on the structure.

5.3.7.3 Analysis model – the whole bridge model or the single pier/abutment bent model

Both design methods can be applied to individual members in isolation, such as only one pier or one abutment, or to a global model of the whole bridge or part of it (for long multi-span bridges).

For short to moderately long bridges, most of the reliable longitudinal response comes from the leading abutment system via passive resistance of the abutment backwall and lateral resistance of piles, if the abutment is supported on pile foundations. The single pier or abutment model in isolation would not reflect the longitudinal seismic response of the whole bridge and could lead to calculation of an inappropriate inertial demand. Therefore, for short-to-moderately long bridges, it is preferable to determine the inertial response, irrespective of the design method, from a global model of the bridge that includes all lateral load resisting elements and soil-structure interaction.

Where nonlinear soil springs are included in the analysis model, gravity loads sustained during the design earthquake should be imposed on the analysis model before carrying out a modal analysis, for the FBD method, or a pushover analysis, for DBD method. This is to ensure the appropriate state of lateral stiffness is included in the analysis model.

5.3.7.4 Determination of inertial demands for this example

In this example, the structure inertia has been calculated using both the force based and displacement based methods. For the force based design method, a modal analysis of the whole bridge was carried out to determine the fundamental translation period (in the longitudinal direction) after imposing the sustained gravity loads. The piles were assumed to resist elastically a design level of shaking without the effects of liquefaction, and thus the seismic base shear was determined for a displacement ductility of one using the equivalent static method (*Bridge manual*, section 5.2.6). The design spectrum was scaled by the site class dependent S_p factor.

In the DBD method, due to complex soil-pile interaction, a pushover analysis was carried out on the same analysis model (as used for the modal analysis) to determine the dynamic properties of the equivalent SDOF system. Since most of the longitudinal seismic resistance comes from the passive resistance of the leading abutment backfill soil and lateral resistance of the piles, a 15% equivalent viscous damping was

assumed to determine the seismic base shear demand, as proposed in the draft section 5 of the *Bridge manual*.

Since the two design methods incorporate the effects of energy dissipation during shaking differently, the estimated inertia demands from these two methods are not equal.

5.3.7.5 Description of the analysis models

The following sections provide a brief description of information related to materials, section properties, soil springs, and modelling assumptions related to the analysis models.

5.3.7.6 Material data

The following material properties conforming to relevant New Zealand standards were used. Note that, in the FBD method, flexural capacity of a member is computed based on the characteristic strength of materials and then reduced by a strength reduction factor as recommended in NZS 3101. In the DBD method, flexural capacity is computed based on the probable strength with a strength reduction factor of 1.0. The overstrength material properties were used to determine the maximum feasible flexural strength at the potential plastic hinge locations to prevent undesirable brittle failure mode due to shear. Tables 5.3 and 5.4 summarise relevant strengths used in this assessment.

Table 5.3 Properties of concrete in different structural components

Structure components	Characteristic strength	Probable strength	Over- strength
Superstructure	50 MPa	1.3 x 50 = 65 MPa	1.7 x 50 = 85 MPa
Pier column and piles	40 MPa	1.3 x 40 = 52 MPa	1.7 x 40 = 68 MPa

Table 5.4 Properties of reinforcement in different structural components

Reinforcement	Characteristic strength	Probable strength	Over- strength
Flexural rebars	500 MPa	1.1 x 500 = 550 MPa	1.3 x 500 = 650 MPa
Transverse rebars	500 MPa	1.0 x 500 = 500 MPa	1.0 x 500 = 500 MPa

5.3.7.7 Member sizes

Based on the gravity load design and preliminary seismic design, following member sizes were adopted as a first guess to develop the analysis model of the bridge.

Table 5.5 Preliminary member sizes used in the analysis

Components	Gross dimensions
Superstructure	16 900 mm deep single hollow core units
Pier column	Three 900 mm diameter column per pier bent
Pier pile	Three 1,200 mm diameter pile per pier bent
Abutment pile	Five 900 mm diameter pile per abutment
Bent cap	1,100 mm wide x 1400mm deep beam

5.3.7.8 Seismic weight

The seismic weight was determined based on the tributary length for each abutment and pier. It was assumed that the seismic weight comprised 100% weight of the superstructure and bent cap (for

abutments and pier) along with 33% weight of the pier columns, with no contribution from piles (for abutments and pier). Accordingly, the following table summarises the seismic weight per support.

Table 5.6 Summary of seismic weights

Components	Pier bent	Each abutment bent	Total
Seismic weight (kN)	9,900	7,000	23,900

5.3.7.9 Modelling of structural elements

All structural elements were modelled with appropriate stiffnesses. The main lateral load resisting elements, namely, pier columns and abutment piles, were modelled using the effective stiffness accounting for the stiffness degradation due to cracking. The other elements that are also part of the lateral load path but formation of plastic hinge is prevented following the capacity design principle, were modelled using the gross stiffness. Such members are bridge deck, bent caps and pier piles. Since member stiffness is a function of reinforcement content, the reinforcement percentage required to carry gravity loads was assumed as a first trial. Subsequently, depending on the seismic demands, the reinforcement percentage is modified. The geometric nonlinearity was included to capture the effect of large lateral displacement demand on the piles, especially in the lateral spreading phase.

Once all elastic analyses were completed for all ground response phases and the location of potential plastic hinges were identified, for the initial plastic hinge design, elastic moment demands at the plastic hinges were reduced by the assumed rotational ductility. The plastic hinge locations were then designed for the reduced moments. A pushover analysis is carried out in later stages to check whether the rotational demands satisfy the capacities at the respective performance limit states

Subsequently, a set non-linear pushover analyses was carried out to ascertain the assumed rotation ductility for various performance limit states. In SAP2000, a fibre hinge section was introduced at the location of plastic hinges. The fibre hinge is capable of accounting for the variable axial load and corresponding axial load – moment interaction. An alternative option, where axial load variation is not significant, is to define the moment-rotation curve at the plastic hinge location.

The rotation capacities of plastic hinges under various performance limit states were computed in accordance with table 5.1. Note that similar strain limits are also prescribed for reinforced pier columns in the draft section 5 of the *Bridge manual*.

5.3.7.10 Modelling of soil- pile interaction

The soil-pile interaction was modelled using the beam on nonlinear Winkler foundation (BNWF) approach. The pile was modelled using beam elements and nonlinear soil springs, to represent the vertical and lateral response of the surrounding soil. The material inelasticity and geometric nonlinearity of the pile elements were included in the analysis model, wherever appropriate. A schematic diagram showing soil-pile interaction using the BNWF method is presented in figure 5.11. The soil springs are spaced at 0.2 m centre to centre, as recommended in Murashev et al (2014, section 6.2.1.2).

Three types of soil springs were employed to simulate the lateral and vertical responses of the surrounding soil. The lateral soil resistance was modelled using the p-y springs. The t-z springs represented the skin friction along the pile shaft and the q-z spring simulated the end bearing response. All springs were assumed uncoupled, ie response of one spring depends only on the respective soil deformation at the spring location and is not influenced by the response of other springs.

To simulate the uncoupled vertical and lateral responses of the soil springs, three nodes of same coordinates are required to define a zero length spring element with uniaxial translational spring triplet as shown in the figure below. The pile nodes are part of the pile elements. The soil spring connects the slave and the fixed nodes. The slave nodes are connected to the pile nodes via kinematic constraints of relevant degrees of freedom.

The force-deformation curve of each soil spring can be defined either by a simplified elastic-perfectly plastic curve (as recommended in Murashev et al 2014) or by a hyperbolic curve (as recommended in API 1993). In this example, bi-linear springs were used. Details of soil spring are presented in section 5.3.5 of this report.

The passive resistance behind the abutment backwall was also modelled using a row of soil springs. The force deformation curve for these can be modelled either as a simplified bi-linear curve (as recommended in the Caltrans' seismic design criteria (California Department of Transport 2013), or as a hyperbolic curve as proposed by Khalili-Tehrani et al (2010). In this example, the strength and stiffness of the abutment soil spring was determined following the Caltrans' recommendations for new bridges. A complete analysis model developed in SAP2000 is presented in figure 5.12.

Figure 5.11 An idealised pile model using the BNWF approach

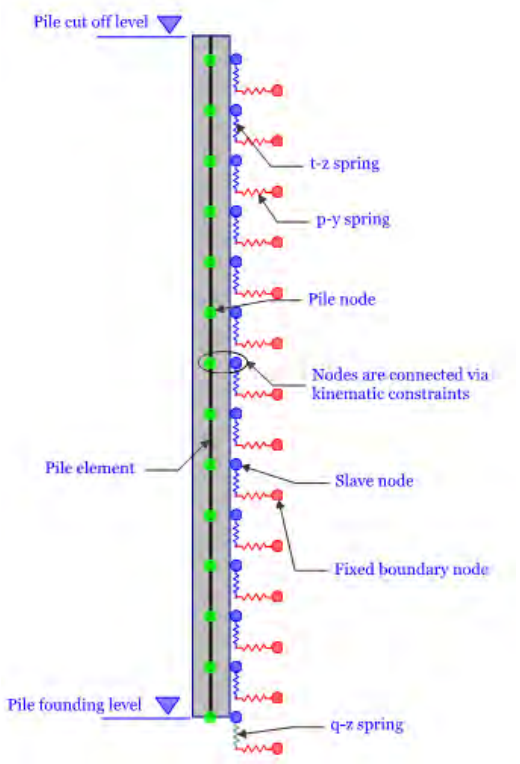

Figure 5.12 An isometric view of the complete analysis model in SAP2000

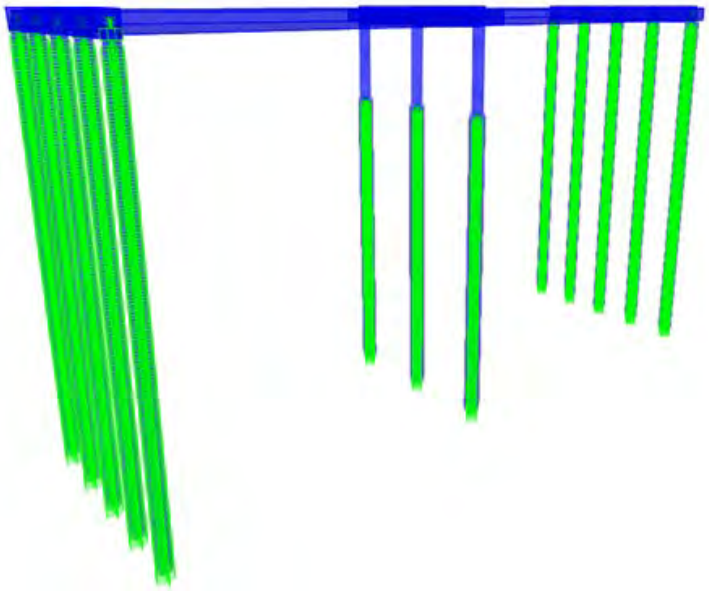

5.3.8 Analysis specific to the pile foundation

When PSA is carried out to derive the design forces in piles, the *Bridge manual* recommends consideration of three different phases of ground response as described below.

Phase 1. Pre- liquefied phase. This is the initial phase of the response to ground shaking before onset of liquefaction. The piles are analysed for the inertial demands from the superstructure. Kinematic demands can be applied in this phase.

Phase 2. Cyclic phase. This is the second phase of the response to ground shaking when liquefaction or cyclic softening has developed. In this phase, piles are subjected to the inertial demands from the superstructure as well as the kinematic loading due to cyclic ground movement. The analysis model should include the liquefaction compatible soil springs with reduced strength and stiffness. Since the peak inertial demand and peak cyclic ground displacement are momentarily in nature, it is unlikely that both peaks will occur at the same time. To allow for this in the PSA, design standards recommend a fraction of the inertial demands to be combined with the kinematic loading. For example, the *Bridge manual* recommends the full kinematic loading to be combined with 80% of the inertial demands. Note that there is no such recommendation in the PEER method (Ashford et al 2011) for this phase.

Phase 3. Lateral spreading phase. This is the last phase, when lateral spreading due to liquefaction has fully developed. This typically occurs after the strongest portion of the design ground shaking is over. Piles, in this phase, are mainly subjected to the large monotonic unidirectional ground displacement (both lateral and vertical) due to lateral spreading. The inertial demands from the superstructure may, or may not, exist at this phase, depending on the nature of shaking.

The *Bridge manual* recommends consideration of 25% of the peak inertial demands or the plastic hinge overstrength forces, whichever is less, to be combined with the full kinematic loading due to lateral spreading. This is if, for the ULS or maximum considered earthquake, the contribution to the PGA by a magnitude 7.5 or greater earthquake is more than 20%. This can be obtained by de-aggregation of results from a seismic hazard study. If a hazard study is not carried out, then the requirement to apply this load

should be assessed qualitatively considering the proximity, recurrence interval and magnitude of faults in the region and the sensitivity of the system response to this load Otherwise, the inertial demands from the superstructure can be ignored. The PEER method (Ashford et al 2011), on the other hand, recommends two empirical scaling factors for the inertial demands. The values of these factors depend on the frequency content of the ground motion which is given by the ratio of elastic spectral acceleration (5% elastic damping) to the corresponding PGA. The first empirical factor C_{cc} accounts for the phasing effect between peak inertia and kinematic loadings. The second empirical factor C_{liq} accounts for the reduction in seismic demands due to softening of soil strength and stiffness due to liquefaction. In this example, the ratio of elastic spectral acceleration at 1.0s time period to PGA is about 1.20, and thus the empirical factors C_{liq} and $C_{cc}$are 0.55 and 0.65 respectively for inertial demands from the superstructure. The overall reduction factor in the inertial demand during the lateral spreading phase is therefore 0.36.

Table 5.7 summarises recommendations of the *Bridge manual* and the PEER method (referred to as PEER) for combining the inertial demands with the kinematic loadings at different phases of ground response.

Table 5.7 Combination of inertial demands and kinematic loading in different phases

	Phase 1. Pre liquefaction phase	Phase 2. Cyclic phase		Phase 3. Lateral spreading phase	
		Bridge manual	**PEER*[1]**	***Bridge manual***	**PEER**
Inertial demands	100%	80%	$C_{cc}C_{liq}$ (~36%)	25%	$C_{cc}C_{liq}$ (~36%)
Kinematic loading	None	100%	100%	100%	100%

Note *[1]. In the absence of any recommendations in the cyclic phase, the combination recommended in the lateral spreading phase is used for the cyclic phase also, for comparison only.

5.3.8.1 Analysis model – the whole bridge model or the single pile model

The pile responses under the kinematic loadings (phases 2 and 3) can be determined either from the analysis model of the whole bridge or by modelling a single pile with appropriate boundary conditions at the top. Both analysis models have advantages and disadvantages.

The main issue with the whole bridge model is how the kinematic loadings on different supports (eg at the piers and abutments) are to be considered in the analysis. Being a transient problem, the peak ground displacements at different supports of a long bridge may or may not occur concurrently and may not even be in the same direction as with the inertial demands. Also, in phase 3, lateral spreading may occur only at one abutment with some residual cyclic displacement demand on the pier piles; or at both abutments, but to a different extent. There is no general consensus about how to consider different peak ground displacements at different supports together with the inertial demands from the superstructure in the PSA. Therefore, a significant amount of engineering judgement, as well as time-consuming analyses of the whole bridge model, are required to envelope all the possible design cases.

The single pile model, on the other hand, provides a much simpler approach as only a few cases to estimate an envelope of critical responses may be analysed. However, the challenging aspect of the single pile analysis is to determine the boundary conditions at the pile top so that the derived responses are representative of the whole bridge. Therefore, it is not advisable to use the single pile model in phases 1 and 2. This can only be used for the lateral spreading phase.

In this example, for the sake of comparison purpose, we considered only two sets of ground displacement profiles for phases 2 and 3, respectively. There could be many other possible sets of ground displacement

profiles. Figure 5.13 presents schematically the whole bridge analysis model for different phases and different sets of ground displacement profiles.

Figure 5.13 Schematic representation of all analysis cases for the whole bridge model

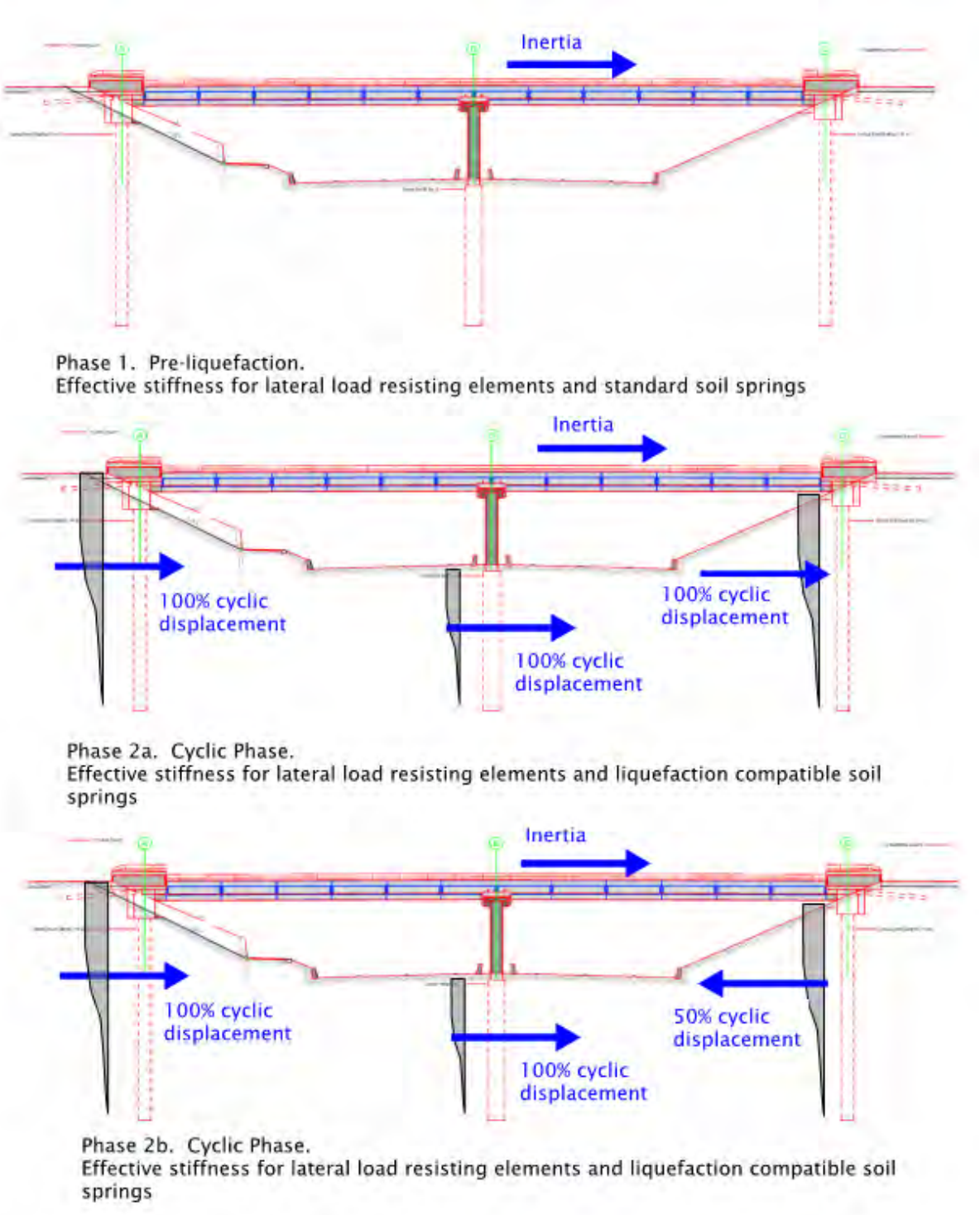

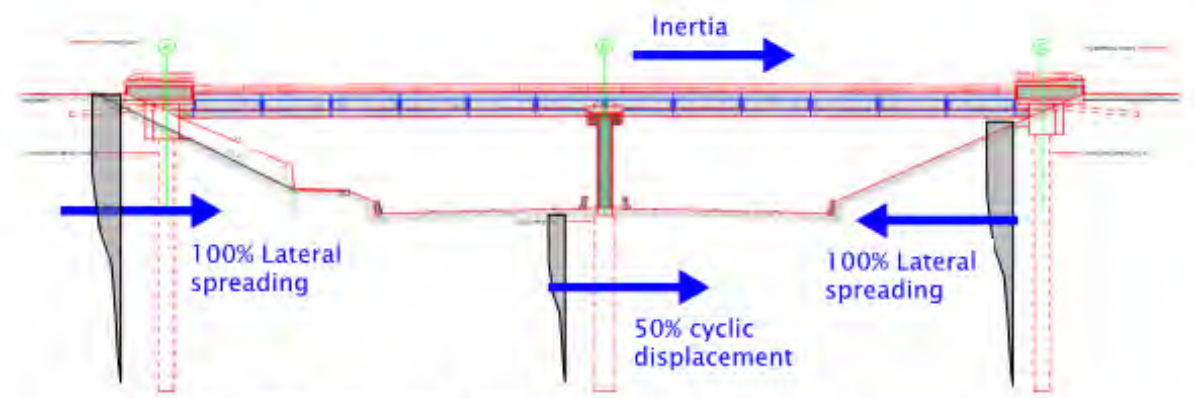

Phase 3a. Lateral spreading Phase.
Effective stiffness for lateral load resisting elements and lateral spreading compatible soil springs

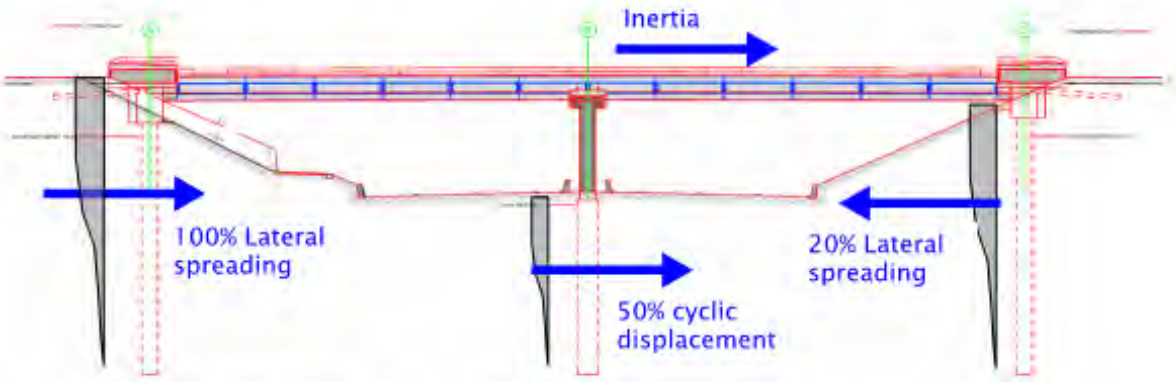

Phase 3b. Lateral spreading Phase.
Effective stiffness for lateral load resisting elements and lateral spreading compatible soil springs

5.3.8.2 Combination of inertial demand with kinematic loading

Another issue is how to impose the inertial demands from the superstructure in combination with the kinematic loading. Being a nonlinear analysis, the principle of superposition is not applicable. There could be three alternative ways to combine both loadings in the PSA. The first two are to apply the inertial demands and then the kinematic loading and vice versa, respectively. The third alternative is to impose both loadings together gradually on the analysis model. In this example, we followed the third alternative.

5.3.8.3 Inertial demand applied as force or displacement to the analysis model

Inertial demands on the bridge model can be applied in two ways. The first way is to apply the inertia as a force which is determined by multiplying the tributary mass by the spectral acceleration at the first fundamental period. The second way is by applying the spectral displacement, corresponding to the same fundamental period. In a linear elastic system both approaches yield the same results. However, for a nonlinear system, the results can vary significantly.

For a single pile model, imposing displacement as an inertial demand could be an attractive option, as this is compatible with the deformation of the whole bridge. When the inertial demand is applied as force, the pile top displacement may not be compatible with the overall deformation of the whole bridge. The *Bridge manual* recommends imposing the inertial demand as force, whereas the PEER method (Ashford et al

2011) recommends the displacement to be applied on the model. Therefore, for both the single pile and whole bridge models, three analyses were carried out for each design phase, as presented schematically in figure 5.14.

- Case 1. No inertial demands from the superstructure
- Case 2. Inertial demands applied as a displacement
- Case 3. Inertial demands applied as a force.

Figure 5.14 Schematic representation of all analysis cases for the single pile model

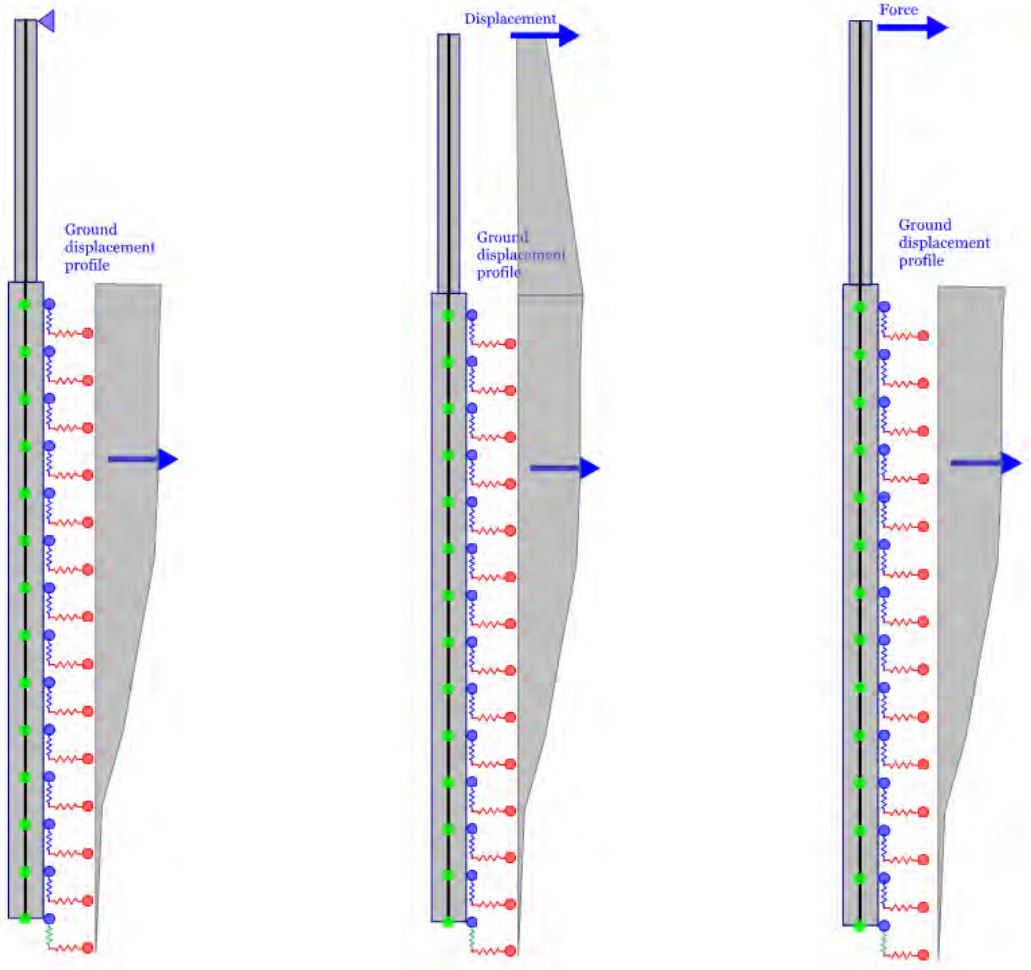

Case 1. No inertia. For the single pile model, top is assumed to be restrained by the deck.

Case 2. Displacement (inertial demand) is applied at the deck level

Case 3. Force (inertial demand) is applied at the deck level

5.3.8.4 Summary of the analysis process

Figure 5.15 summarises the key steps for the design of piled bridges in liquefied soils with relevant involvement of the geotechnical engineer and the structural engineer. Parametric studies to determine the sensitivity of the structures response to different parameters can follow the same basic steps.

Figure 5.15 A summary of steps for design of piled bridges in liquefied soils. GE = geotechnical engineer and SE = structural engineer

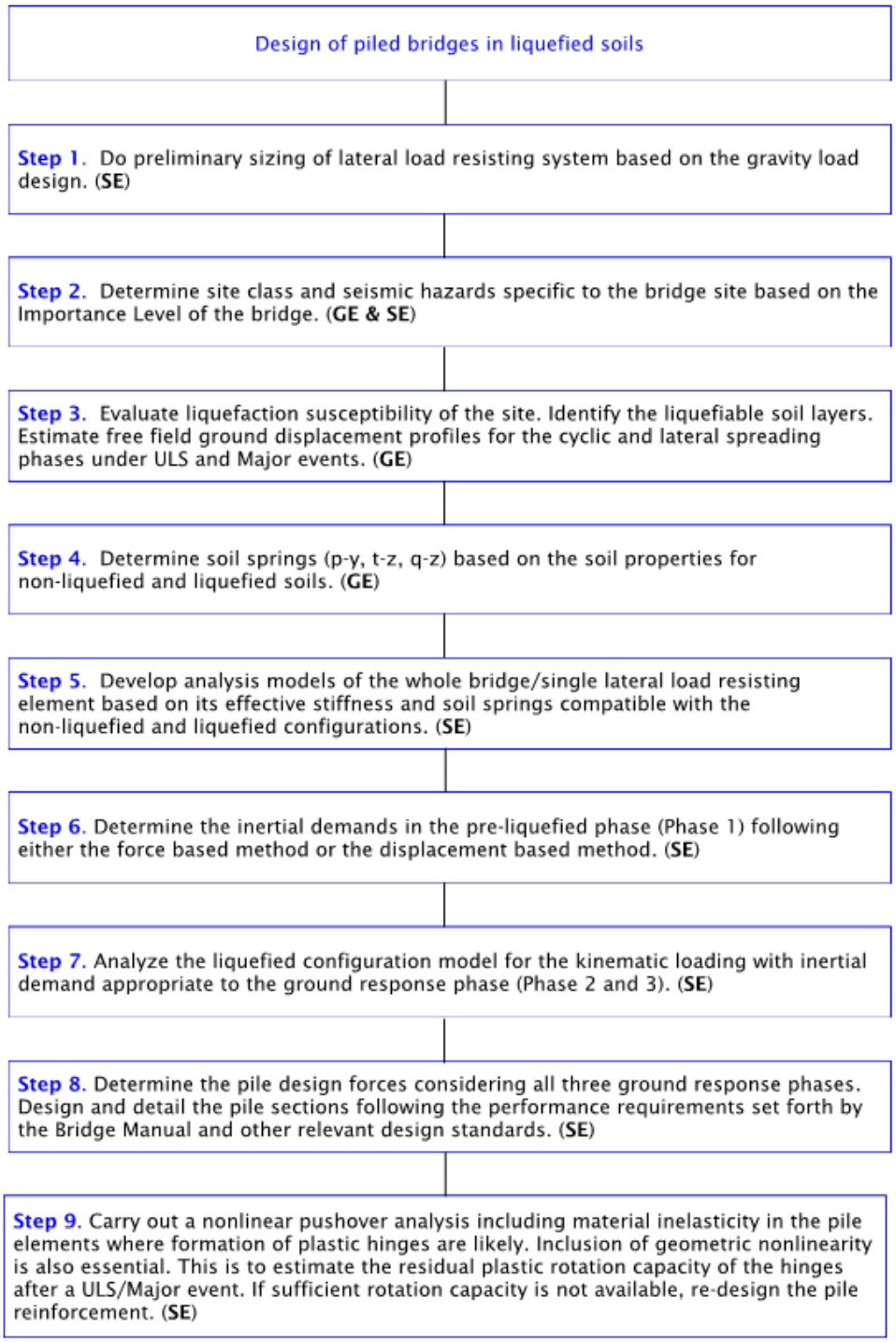

Figure 5.16 presents a summary of analyses that were carried out in this example. Note that the PEER method is presented here only for comparison. The pile design was carried out based on the *Bridge manual* recommendations. The inertial demand was determined from the DBD method. For comparison purposes, the inertial demand from the FBD method is also presented. Following both code

recommendations, a minimum of three analyses is required. The inertial demand is determined from one analysis, followed by two separate analyses for two phases of ground response.

Figure 5.16 Summary of pseudo- static analyses for piled bridges in liquefied soils

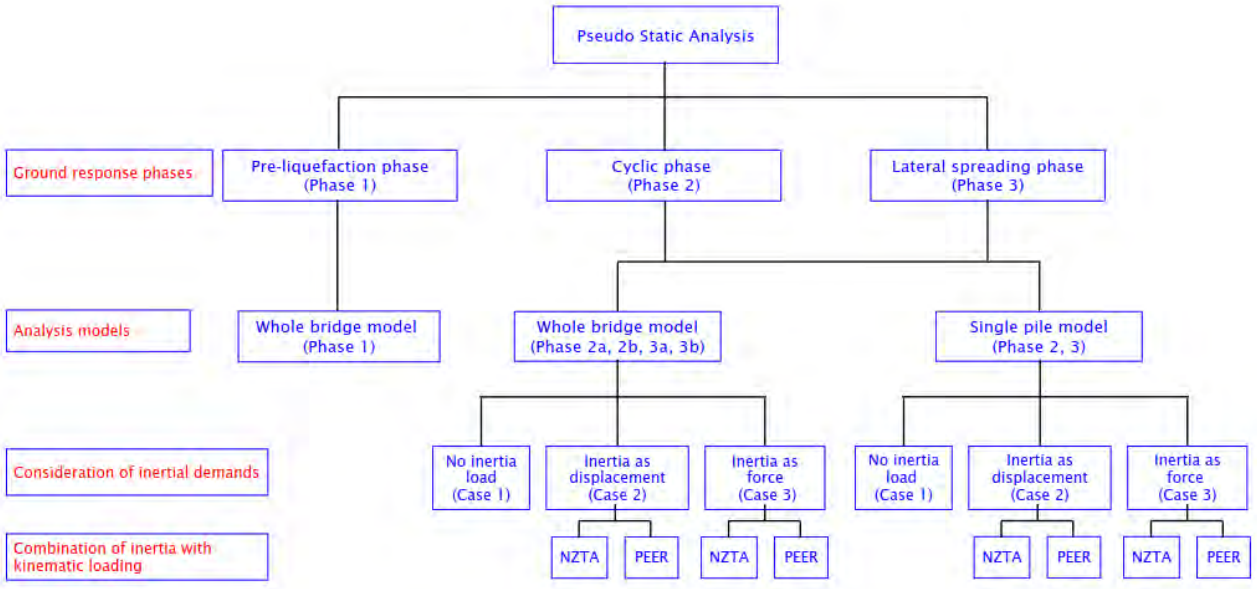

5.3.9 Analysis results for the pre-liquefied phase (phase 1)

The inertial demands were determined following both FBD and DBD methods, as given in the *Bridge manual*. The seismic design parameters are presented in sections 5.3.4 and 5.3.7. Table 5.8 summarises the base shear demands estimated from two design methods. Plots showing force (bending moment and shear force) and deformation (lateral displacement and vertical settlement) distributions along the pile are presented in appendix A. A summary of design forces and deformations for phase 1 are presented in table 5.9. The piles in non-liquefied soils are designed for these responses only.

Table 5.8 Summary of base shear demands at pre- liquefaction phase (phase 1)

	Force based method (50% gross stiffness)	Displacement based method (15% damping)
Time period (s)	0.31	0.49
Spectral acceleration (g)	0.82	0.75
Spectral displacement (mm)	20.00	51.00
Total base shear (kN)	19,575	17,925

Table 5.9 Summary of the demands at the pre- liquefaction phase (phase 1)

	Abutment pile		Pier pile	
	FBD	DBD	FBD	DBD
Max moment (kNm)	3192	2781	1156	890
Max shear force (kN)	1542	1400	151	145
Disp (mm) at pile top	49	79	15	18

5.3.9.1 Inertial demand to be used for the subsequent phases (phases 2 and 3)

The *Bridge manual* requires inertial demands for phases 2 and 3 to be determined with appropriate soil springs accounting for liquefaction. Since the lateral response of the bridge depends mainly on the lateral stiffness of soils in the top few metres from the surface, it is unlikely that any considerable difference in the inertial demands compared with the non-liquefied phase will be observed, if the liquefied layer is located at a significant depth. The PEER method, on the other hand, includes the reduction in inertial demands due to soil softening via an empirical scaling factor that reduces the inertial demand of the non-liquefied configuration.

In this example, the liquefied soil layer is at such a depth that no noticeable changes in the elastic inertial demands were observed. Therefore, the inertial demand estimated using the non-liquefied springs was used for the subsequent phases. Table 5.10 summarises the inertial demands used in the different phases of ground response following the *Bridge manual* and PEER methods.

Table 5.10 Summary of inertial demands (from displacement based method) at different phases

	Phase 1	Phase 2		Phase 3	
		Bridge manual	**PEER**	***Bridge manual***	**PEER**
% of inertia at non-liquefied case	100%	80%	36%	25%	36%
Displacement at the bridge deck (mm)	51	41	19	13	19
Shear force (kN) per abutment pile	1,400	1,100	495	345	495
Shear force (kN) per pier pile	145	116	52	36	52

5.3.10 Analysis results for the cyclic phase (phase 2)

Analyses were carried out for the three structure inertia cases illustrated in figure 5.14. Both single pile and whole bridge models were employed to determine various response demands for the piles. The single pile model was considered for both pier and abutment piles with various boundary conditions at the bridge deck level, as shown in figure 5.14. Two sets of ground displacement profile, as shown in figure 5.13, were imposed on the liquefaction compatible analysis model with the inertial demands as recommended by the *Bridge manual* and the PEER method.

Table 5.11 summarises the results of single pile analysis for different boundary conditions and code recommendations. Results of the whole bridge analysis are presented in tables 5.12 and 5.13. Plots showing distribution of moment, shear force, displacement and soil reactions along the pile length are presented in appendix A.

Table 5.11 Summary of single pile analysis during cyclic phase (phase 2)

Element	Response parameter	Case 1. No inertia, pile top restrained by deck	Case 2. Apply inertia demand as displacement		Case 3. Apply inertia demand as force	
			Bridge manual	PEER	*Bridge manual*	PEER
Abutment pile	Moment (kNm)	**5,445**	4,417	4,984	2,014	1,765
	Shear (kN)	**2,226**	1,929	2,096	1116	685
	Max disp (mm)	148	148	148	170	152
Pier pile	Moment (kNm)	2,862	2,704	2,736	**3,617**	3,600
	Shear (kN)	669	746	697	**989**	988
	Max disp (mm)	76	93	84	**180**	172

Table 5.12 Summary of whole bridge analysis during cyclic phase (phase 2a, figure 5.13)

Element	Response parameter	Case 2. Apply inertia demand as displacement		Case 3. Apply inertia demand as force	
		Bridge manual	PEER	*Bridge manual*	PEER
Abutment pile	Moment (kNm)	4,417	4,984	1,785	1,765
	Shear (kN)	1,929	2,096	949	685
	Max disp (mm)	148	148	**163**	152
Pier pile	Moment (kNm)	2,704	2,736	**3,484**	3,442
	Shear (kN)	746	697	**961**	949
	Max disp (mm)	93	84	**139**	135

Table 5.13 Summary of whole bridge analysis during cyclic phase (phase 2b, figure 5.13)

Element	Response parameter	Case 2. Apply inertia demand as displacement		Case 3. Apply inertia demand as force	
		Bridge manual	PEER	*Bridge manual*	PEER
Abutment pile	Moment (kNm)	4,537	4,984	**6,430**	5,751
	Shear (kN)	1,993	2,096	**2,523**	2,340
	Max disp (mm)	148	148	147	147
Pier pile	Moment (kNm)	2,704	2,736	3,321	3,120
	Shear (kN)	746	697	916	860
	Max disp (mm)	93	84	126	115

5.3.11 Analysis results for the lateral spreading phase (phase 3)

In this phase, analyses similar to these in phase 2 were carried out with different magnitudes of ground displacement profiles and inertial demands. The settlement of non-liquefied crust overlying the liquefied layer was also included in the analysis. This down drag increases axial load demand on the piles.

Table 5.14 summarises the results of single pile analysis for different boundary conditions and code recommendations. Results of the whole bridge analysis are presented in tables 5.15 and 5.16.

Table 5.14 Summary of single pile analysis during lateral spreading phase (phase 3)

Element	Response parameter	Case 1. No inertia, pile top restrained by deck	Case 2. Apply inertia demand as displacement		Case 3. Apply inertia demand as force	
			Bridge manual	PEER	*Bridge manual*	PEER
Abutment pile	Moment (kNm)	**8,819**	8,586	8,476	4,472	4,473
	Shear (kN)	**3,081**	3,025	2,999	1,775	1,775
	Axial force (kN)	3,513	3,513	3,513	3,513	3,513
	Max disp (mm)	314	315	315	313	315

Table 5.15 Summary of whole bridge analysis during lateral spreading phase (phase 3a, figure 5.13)

Element	Response parameter	Case 1. No inertia	Case 2. Apply inertia demand as displacement		Case 3. Apply inertia demand as force	
			Bridge manual	PEER	*Bridge manual*	PEER
Abutment pile	Moment (kNm)	9,020	9,046	9,152	**10,274**	10,766
	Shear (kN)	3,129	3,135	3,160	**3,416**	3,524
	Axial force (kN)	3,513	3,513	3,513	3,513	3,513
	Max disp (mm)	314	315	315	315	316
Pier pile	Moment (kNm)	1,904	1,942	1,866	**1,865**	1,856
	Shear (kN)	519	519	520	**518**	514
	Axial force (kN)	3,576	3,576	3,576	3,576	3,576
	Max disp (mm)	58	57	59	73	78

Table 5.16 Summary of whole bridge analysis during lateral spreading phase (phase 3b, figure 5.13)

Element	Response parameter	Case 1. No inertia	Case 2. Apply inertia demand as displacement		Case 3. Apply inertia demand as force	
			Bridge manual	PEER	*Bridge manual*	PEER
Abutment pile	Moment (kNm)	6254	8586	8476	7276	7654
	Shear (kN)	2441	3025	2999	2705	2800
	Axial force (kN)	3513	3513	3513	3513	3513
	Max disp (mm)	313	314	314	313	313
Pier pile	Moment (kNm)	1853	1942	1866	1834	1832
	Shear (kN)	513	519	520	505	503
	Axial force (kN)	3576	3576	3576	3576	3576
	Max disp (mm)	80	57	59	**89**	93

Figures 5.17 and 5.18 present displacement and bending moment profiles of abutment pile and pier pile for phases 1, 2a and 3a of the ground response for the whole bridge analysis. Further plots showing distribution of moment, shear force, displacement and soil reactions along the pile length for each ground response phase for the single pile are presented in appendix A. Note that for the whole bridge analysis, the results are for a single pile.

Figure 5.17 Comparison of displacement and moment profiles of the abutment piles for phases 1, 2a and 3a of ground response for the whole bridge analysis

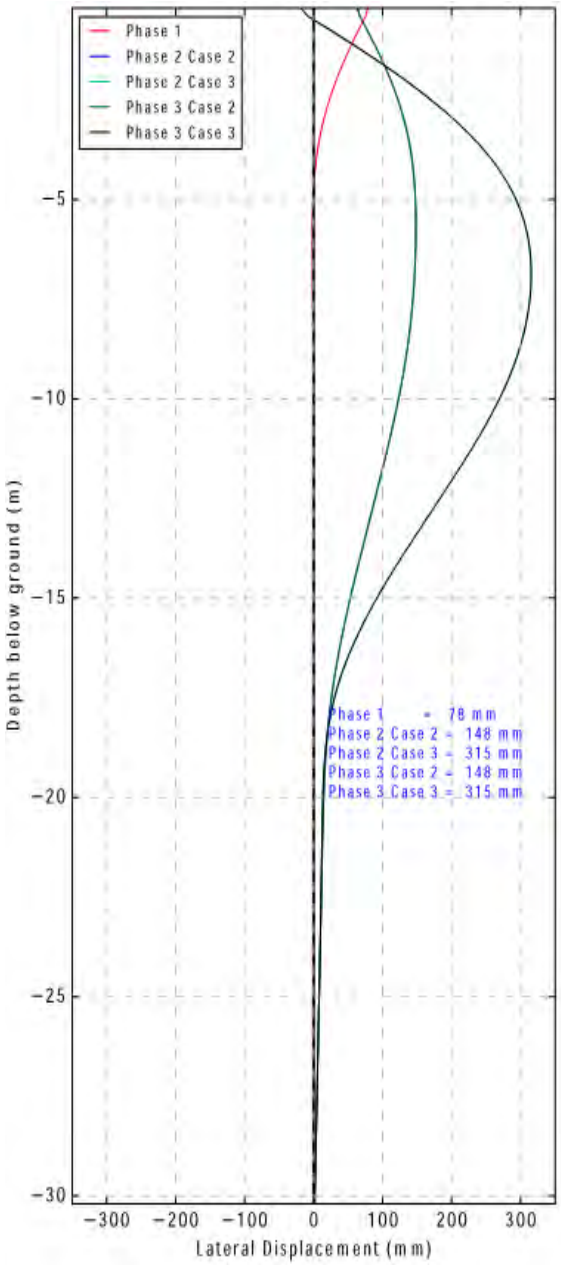

a) Displacement profile

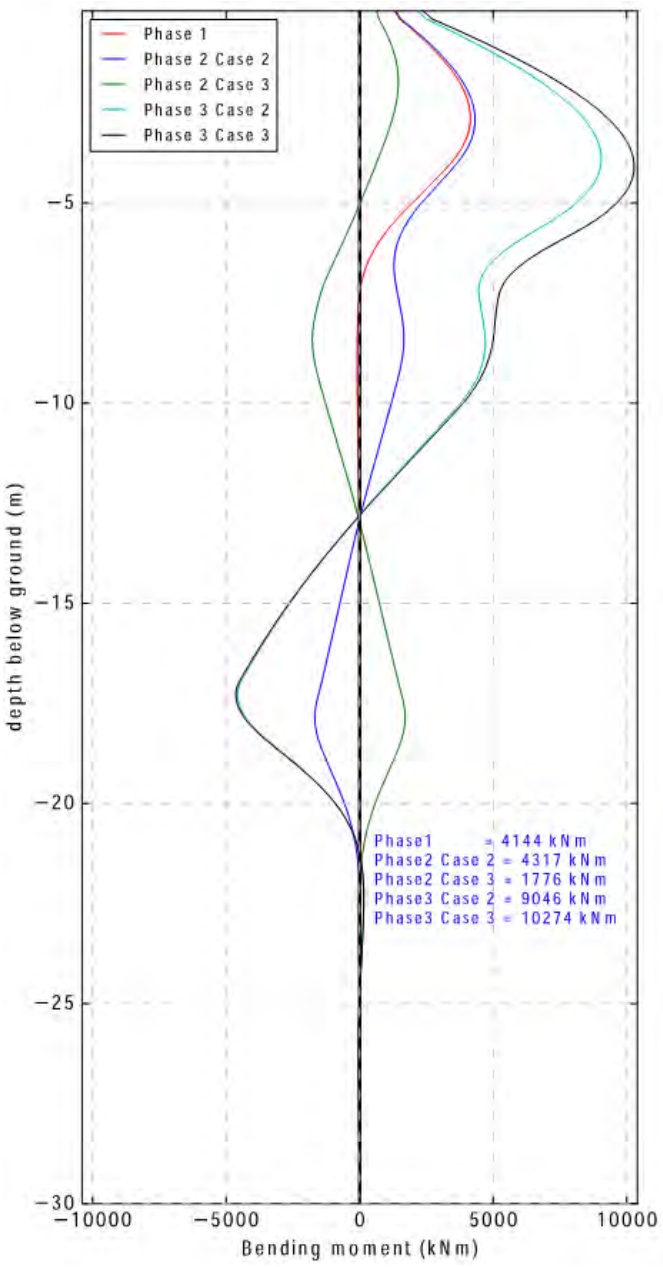

b) Moment profile

Figure 5.18 Comparison of displacement and moment profiles of pier pile for various phases of ground response

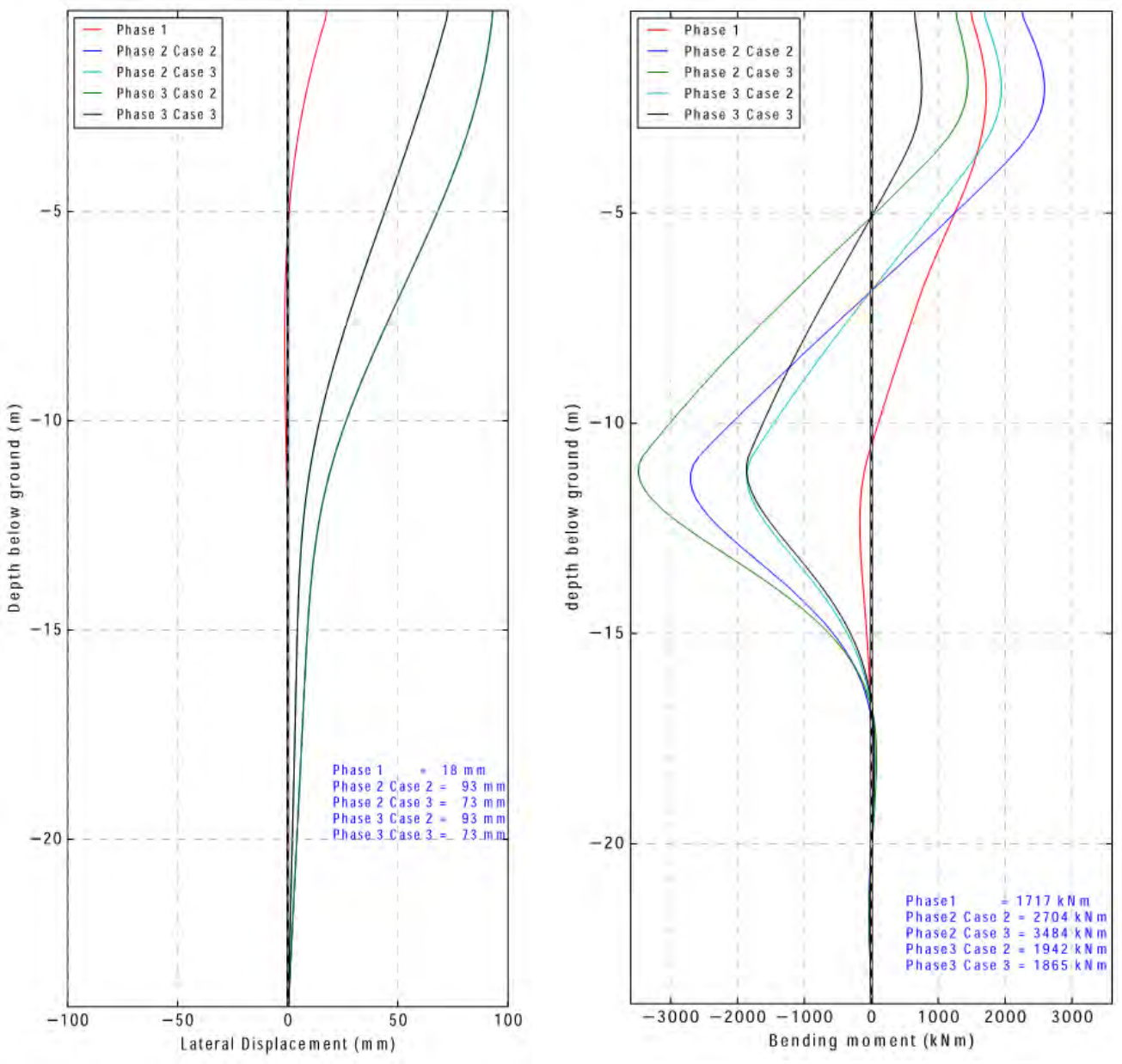

a) Displacement profile **b) Moment profile**

5.3.12 Structural design of the pile

5.3.12.1 Summary of peak pile demands from different ground response phases

Table 5.17 summaries the maximum elastic force demands in the piles at different phases of the ground response under a ULS level of shaking following the *Bridge manual's* recommendations. The results following the PEER method shown in the previous tables are for comparison purposes only. Since the *Bridge manual* recommends the inertial demand to be applied as a force, the results obtained by imposing displacement are not considered in the pile design.

Table 5.17 Summary of maximum elastic forces in the piles based on the *Bridge manual*

Element	Response parameter	Phase 1. Pre liquefaction phase		Phase 2. Cyclic phase		Phase 3. Lateral spreading phase	
		Single pile*	Whole bridge	Single pile	Whole bridge	Single pile	Whole bridge
Abutment pile	Moment (kNm)	Not analysed	2781	5445	**6430**	8819	**10274**
	Shear (kN)		1400	2226	**2523**	3081	**3416**
	Axial force (kN)		1400	1400	1400	3513	3513
	Max disp (mm)		79	170	163	314	315
Pier pile	Moment (kNm)		890	**3617**	3484	--	1865
	Shear (kN)		145	**989**	961	--	518
	Axial force (kN)		3300	3300	3300	--	3576
	Max disp (mm)		18	180	139	--	89

* Design actions for phase 1 are taken from the whole bridge analysis

5.3.12.2 Design philosophy of pile sections for flexure

The pile sections are to be designed and detailed to satisfy the performance requirements set by the *Bridge manual*. It is economically impractical to design the abutment piles elastically for the lateral spreading loading (phase 3), where the flexural demands are at a maximum. On the other hand, allowing the formation of plastic hinges in the pier piles during the cyclic phase (phase 2) may lead to the collapse of the bridge due to the significant $P-\Delta$ effect during the lateral spreading phase (phase 3). Therefore, the design of piles should consider the consequences of allowing yielding under a ULS design event or a maximum considered earthquake.

A reasonable trade-off between economy and the post-earthquake performance would be that the abutment piles are designed to achieve limited ductility (minimal damage) for the cyclic phase (phase 2) and accept controlled and repairable damage for the lateral spreading phase (phase 3), as recommended in ASCE (2014). There should also be sufficient margin in the pile's ductility capacity so that collapse could be prevented under a major event (1.5 times the design event), as required by the *Bridge manual*. Note that Caltrans allows formation of two plastic hinges in the pile with a displacement ductility of 5. The designer must also check whether the post-earthquake repair of any unstable mechanism formed by allowing yielding of abutment piles may not be economically viable.

The pier piles, on the other hand, are subjected to much fewer demands compared with the abutment piles due to ground movement. It may therefore be prudent to design the pier piles elastically (minimal damage) or maybe allow limited yielding so that stability of the pier is not jeopardised in phase 3.

5.3.12.3 Application of the capacity design principle

The next stage of pile design is to prevent any sort of brittle failures even under a major event. This can be achieved by following the code prescribed detailing though the pile. The pile section should also have sufficient shear resistance to prevent a brittle type failure. If a plastic hinge is formed in the pile section, the shear design demand should be derived from the over-strength flexural demand of the plastic hinge with appropriate soil resistance above it. Alternatively, the pile section can be designed for the critical shear demand as determined from the analysis of different phases. The critical shear demand for abutment piles is likely to be from the lateral spreading phase (phase 3) and for pier piles, it is the cyclic

phase (phase 2). Note that, as proposed in the draft DBD section 5, the shear capacity should be determined based on the characteristic strength with a strength reduction factor of 0.90 (section 5.6.1 draft section 5), while the flexural capacity should be determined using the probable strength with a strength reduction factor of one (*Bridge manual*, table 5.5, draft section 5).

The pile sections, where plastic hinge formation is likely, are to be detailed for confinement of core concrete and prevent buckling of longitudinal reinforcement, following the recommendations of *NZS 3101:2006* (NZS 3101) (Standards New Zealand).

5.3.12.4 Pile design forces

Table 5.18 summarises the actions used in the initial design of the pile reinforcement. For the abutment piles in this example, the maximum rotational ductility in the cyclic phase is 1.5 and in the lateral spreading phase it is 2.0. The pier piles were designed for a rotational ductility of 1.0. Standard design and detailing procedures in accordance with NZS 3101 were followed. Rotational ductility (the ratio of calculated rotation to the rotation at yield) is used here instead of displacement ductility as it is difficult to assess displacement ductility in piles when hinges form at depth.

Table 5.18 Summary of pile design forces

Demand parameters	Pile design forces	
	Abutment	Pier
Rotational ductility	2.0	1.0
Moment (kNm)	6,500	3,700
Shear (kN)	3,500	1,000
Axial force (kN)	1,400	3,300

5.3.12.5 Computation of plastic curvature capacity at the hinges

Once the reinforcement content at the plastic hinges locations was determined, a set of moment-curvature analyses was carried out based on the probable material strengths as given in tables 5.2 and 5.3. The Mander's model (Mander et al 1988 was adopted to determine the confining effects provided by spirals. The plastic hinge length for in-ground hinges was taken as two times the pile diameter, as given in section 6.6.4.1 of ASCE (2014). Figures 5.19 and 5.20 present the moment-curvature plots at the hinges locations in the abutment and pier piles respectively. The figures also show the curvature capacities at various performance limit states. The curvature capacities were computed based on the strain limits presented in table 5.1. Similar values are also recommended in the draft section 5 of the *Bridge manual*.

Figure 5.19 Moment- curvature plot of 900mm diameter abutment pile section

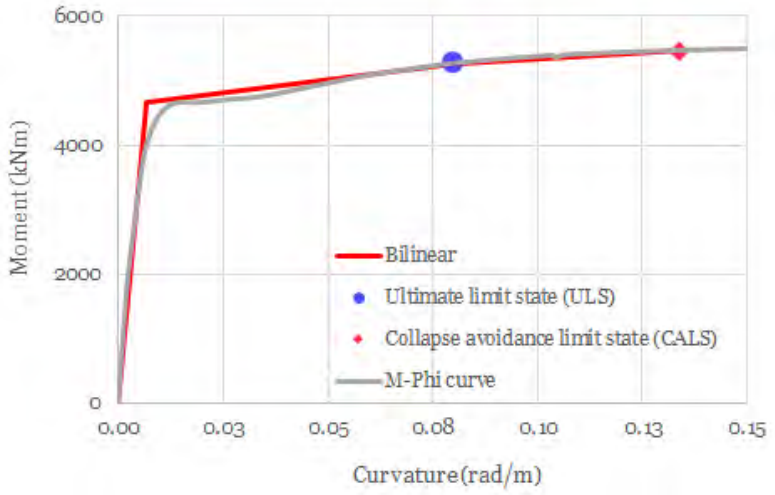

Figure 5.20 Moment- curvature plot of 1,200mm diameter pier pile section

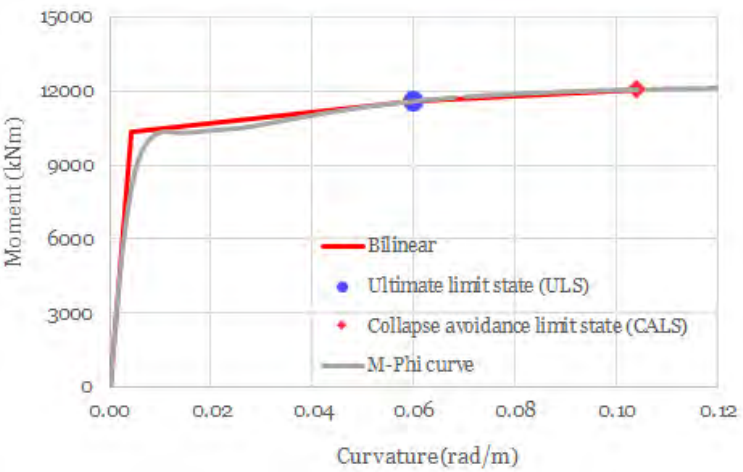

Note the moment curvature plots shown in figures 19 and 20 are based on the initial hinge reinforcement design.

5.3.12.6 Assessment of the rotational ductility capacity

A further analysis of the whole bridge model was carried out to verify the rotational ductility demand in the abutment piles in the lateral spreading phase. The previous analysis model was modified with the plastic hinge elements in the locations where formation of plastic hinge is likely. The analysis showed that the plastic curvature demand on the abutment piles was in the order of 0.07 rad/m which is less than the curvature capacity for the ULS. Since we analysed for kinematic loadings from a ULS level shaking, similar procedure can be followed for the collapse avoidance limit state, if required.

5.3.13 Observations

Based on the PSA of different phases of ground response, the following observations are made.

- The single pile model predicts fairly accurately the responses obtained from the whole bridge model. Given the uncertainties associated with the input parameters, such as soil springs, ground

displacement profiles, and the complexity of analysing a whole bridge model, the single pile model can be used for the design purposes.

- The cyclic ground response (phase 2) governs the design of pier piles, whereas the lateral spreading phase (phase 3) determines the design forces for abutment piles.

The inertial demand from the superstructure can be applied either as force or as displacement. It is difficult to confirm which approach is more realistic. However for the single pile model, imposing displacement makes more sense, as it provides the response that is comparable with the whole bridge model. Where inertial demands are applied as force, an appropriate boundary condition should be assigned at the superstructure level.

6 References

Ambraseys, N and M Srbulov (1995) Earthquake-induced displacements of slopes. *Soil Dynamics and Earthquake Engineering 14*, no.1: 59–71.

American Association of State Highway and Transportation Officials (2011a) *AASHTO guide specifications for LRFD seismic bridge design – section 3.2 performance criteria*. Washington DC: American Association of State Highway and Transportation Officials.

American Association of State Highway and Transportation Officials (2011b) *AASHTO guide specifications for LRFD seismic bridge design – section 3.4.3 performance criteria*. Washington DC: American Association of State Highway and Transportation Officials.

American Association of State Highway and Transportation Officials (2011c) *AASHTO guide specifications for LRFD seismic bridge design – section 3.5 selection of seismic design category*. Washington DC: American Association of State Highway and Transportation Officials.

American Association of State Highway and Transportation Officials (2011d) *AASHTO LFRD bridge design specifications – section 10.5.4 extreme events limit states*. Washington, DC: American Association of State Highway and Transportation Officials.

American Association of State Highway and Transportation Officials (2014) *AASHTO LFRD bridge design specifications*. 7th ed. Washington, DC: American Association of State Highway and Transportation Officials.

American Petroleum Institute (API) (1993) Recommended practice for planning, designing, and constructing fixed offshore platforms. *API recommended practice 2A (RP-2A)*, 20th ed. Washington DC: American Petroleum Institute.

American Society of Civil Engineers (ASCE) (2014) Seismic design of piers and wharves. *Standards ASCE/COPRI 61-14*. US: ASCE.

Applied Technology Council, Multidisciplinary Center for Earthquake Engineering Research (2001) Comprehensive specification for the seismic design of bridges – revised LRFD design specifications (seismic provisions), *NHCRP report 12–49* (third draft of specifications and commentary). Washington DC: American Association of State Highway and Transportation Officials.

Applied Technology Council, Multidisciplinary Center for Earthquake Engineering Research (2002) Comprehensive specification for the seismic design of bridges. *NCHRP report 472*, Washington DC: American Association of State Highway and Transportation Officials.

Applied Technology Council, Multidisciplinary Center for Earthquake Engineering Research (2003a) *Design examples – recommended LRFD guidelines for the seismic design of highway bridges*. Washington DC: National Cooperative Highway Research Program.

Applied Technology Council, Multidisciplinary Center for Earthquake Engineering Research (2003b) Liquefaction study report – recommended LRFD guidelines for the seismic design of highway bridges. MCEER/ATC-49-1. Washington DC: American Association of State Highway and Transportation Officials.

Applied Technology Council, Multidisciplinary Center for Earthquake Engineering Research (2003c) *Recommended LRFD guidelines for the seismic design of highway bridges – part 1: specifications*. MCEER Research Highway Project 094 Task F3-1, Washington DC: Federal Highway Administration.

Architectural Institute of Japan (AIJ) (2001) *Recommendations for design of building foundations*, p65 (in Japanese).

Armstrong, RJ, RW Boulanger and MH Beaty (2014) Equivalent static analysis of piled bridge abutments affected by earthquake induced liquefaction. *Journal of Geotechnical and Geoenvironmental Engineering 140*, no.8.

Ashford, SA, RW Boulanger and SJ Brandenberg (2011) *Recommended design practice for pile foundations in laterally spreading ground*. Berkeley, California: Pacific Earthquake Engineering Centre.

Bertlett, S and T Youd (1992) Empirical analysis of horizontal ground displacement generated by liquefaction-induced lateral spreads, *Technical report NCEER-0021*. Utah: Brigham Young University.

Blake, T, R Hollingsworth and J Stewart (2002) *Recommended procedures for implementation of DMG special publication. 117 guidelines for analyzing and mitigating landslide hazards in California*. Los Angeles: Southern California Earthquake Center.

Boulanger, RW, D Chang, SJ Brandenberg, RJ Armstrong and BL Kutter (2007) Seismic design of pile foundations for liquefaction effects. Pp 277–302 in *Proceedings of 4th International Conference on Earthquake Geotechnical Engineering.* KD Pitilakis (Ed) Springer.

Boulanger, RW and IM Idriss (2014) CPT and SPT based liquefaction triggering procedures. *Report no. UCD/CMG-14/01*. Department of Civil & Environmental Engineering, University of California at Davis.

Bray, JD and T Travasarou (2007) Simplified procedure for estimating earthquake induced deviatoric slope displacements. *Journal of Geotechnical and Geoenvironmental Engineering 133*, no.4:381–392.

British Standards International (2004) *Euro code 8: Design of structures for earthquake resistance – part 5: Foundations, retaining structures and geotechnical aspects. BS EN 1998-5:2004*. London, UK: British Standards International.

California Department of Transportation (Caltrans) (2011) *Guidelines on foundation loading and deformation due to liquefaction induced lateral spreading*. Los Angeles, California: California Department of Transportation.

California Department of Transportation (Caltrans) (2013) *Seismic design criteria*. Version 1.7, Los Angeles, California: California Department of Transportation.

California Department of Transportation (Caltrans) (2016) Caltrans LRFD lateral spreading analysis for new and existing bridges. *Memo to designers 20-15*. Accessed 29 November 2017. www.dot.ca.gov/des/techpubs/manuals/bridge-memo-to-designer/page/section-20/20-15.pdf

California Geological Survey (2008) *Guidelines for evaluating and mitigating seismic hazards in California*. California: California Geological Survey.

Chapman, H, P North and R Park (1980) Seismic design of bridges, section 3. Capacity design principles and practice. *Bulletin for the New Zealand National Society for Earthquake Engineering 13*, no.3: 242–247.

Chiou, B, and R Youngs (2014) Update of the Chiou and Youngs NGA model for the average horizontal component of peak ground motion and response spectra. *Earthquake Spectra 30*, no.3: 1087–1115.

Cubrinovski, M (2011) Seismic effective stress analysis: modelling and application. *5th International Conference on Earthquake Geotechnical Engineering*, Santiago, Chile, January 2011.

Cubrinovski, M and K Ishihara (2001) *Correlation between penetration resistance and relative density of sandy soils*.

Cubrinovski, M and K Robinson (2015) Lateral spreading: evidence and interpretation from the 2010–2011 Christchurch earthquakes. *SDEE special issue: 6ICEGE invited papers 91*: 187–201.

Cubrinovski, M, K Ishihara and K Furukawazono (1999) Analysis of full scale tests on piles in deposits subjected to liquefaction. *2nd International Conference on Earthquake Geotechnical Engineering*. Lisbon, Portugal, June 1999. 6pp.

Cubrinovski, M, K Ishihara and H Poulos (2009). Pseudostatic analysis of piles subjected to lateral spreading. Special issue, *Bulletin of NZ Society for Earthquake Engineering 42*, no.1: 28–38.

Cubrinovski, M, T Kokusho and K Ishihara (2006) Interpretation from large-scale shake table tests on piles undergoing lateral spreading in liquefied soils. *Soil Dynamics and Earthquake Engineering 26*: 275-286.

Cubrinovski, M, J Haskell, A Winkley, K Robinson and L Wotherspoon (2014a) Performance of bridges in liquefied deposits during the 2010–2011 Christchurch (New Zealand) earthquakes. *ASCE Journal of Performance of Constructed Facilities 28*, no.1: 24–39.

Cubrinovski, M, A Winkley, J Haskell, A Palermo, L Wotherspoon, K Robinson, B Bradley, P Brabhaharan and M Hughes (2014b) Spreading-induced damage to short-span bridges in Christchurch, New Zealand. *Earthquake Spectra 30*, no.1: 57–83.

Dash, SR, S Bhattacharya and A Blakeborough (2010) Bending–buckling interaction as a failure mechanism of piles in liquefiable soils. *Soil Dynamics and Earthquake Engineering 30,* no.1: 32–39.

Dickenson, S (2005) *Recommended guidelines for liquefaction evaluations using ground motions from probabilistic seismic hazard analyses*. Salem, Oregon: Oregon Department of Transportation.

Dickenson, S, N McCullough, M Barkau and B Wavra (2002) *Assessment and mitigation of liquefaction hazards to bridge approach embankments in Oregon.* Salem, Oregon: Oregon Department of Transport Research Group.

Finn, W and A Wightman (2007) Logical evaluation of liquefaction potential using NBCC 2005 probabilistic ground accelerations. Pp1984–1993 in *Proceedings of the 9th Canadian conference on Earthquake Engineering*, Ontario, Canada.

Gadeikis, S, K Dundulis, G Zarzojus, S Gadeikyte, D Urbaitis D Gribulis and S Sliaupa (2012) Correlation of shear-wave velocities and cone resistance of quarternary glacial sandy soils defined by seismic cone penetration test (SCPT). *Journal of Vibroengineering 14*: 715–722.

Haskell, JJM (2014) *Guidance for the design of pile groups in laterally spreading soil*. PhD, University of Cambridge, Cambridge, United Kingdom.

Haskell, JJM, SPG Madabhushi, M Cubrinovski and A Winkley (2013) Lateral spreading-induced abutment rotation in the 2011 Christchurch earthquake: observations and analysis. *Géotechnique 63*, no.15: 1310–1327.

Holzer, TL, S Toprak and MJ Bennett (2002) Liquefaction potential index and seismic hazard mapping in the San Francisco Bay area, California. Pp1699–1706, vol 2 in *Proceedings of Urban Earthquake Risk, National Conference on Earthquake Engineering*, Boston.

Idriss, IM and RW Boulanger (2008) *Soil liquefaction during earthquakes*. MNO-12. Oakland, California: Earthquake Engineering Research Institute.

Ishihara, K and M Cubrinovski (1998a) Performance of large-diameter piles subjected to lateral spreading of liquefied deposits. *13th Southeast Asian Geotechnical Conference*, December 1998, Taipei.

Ishihara, K and M Cubrinovski (1998b) Soil-pile interaction in liquefied deposits undergoing lateral spreading. *11th Danube European Conference on Soil Mechanics and Geotechnical Engineering*, Porec, Croatia, May 1998.

Ishihara, K and M Cubrinovski (2004) Case studies of pile foundations undergoing lateral spreading in liquefied deposits: *5th International Conference on Case Histories in Geotechnical Engineering*, New York, NY, USA, April 2004, 9pp.

Ishihara, K and M Yoshimine (1992) Evaluation of settlements in sand deposits following liquefaction during earthquakes. *Soils and Foundations 32*, no.1: 173–188.

Jibson, RW (2007) Regression models for estimating coseismic landslide displacement. *Engineering Geology 91*, no.2–4: 209–218.

Khalili-Tehrani, P, E Taciroglu and A Shamsabadi (2010) *Backbone curves for passive lateral response of walls with homogeneous backfills, soil-foundation-structure interaction.* London: Taylor and Francis Group.

Kawashima, K (2004) An analysis on the seismic performance levels of bridges. Pp77–88, vol 2004 in *Proceedings of International Workshop on Performance-Based Seismic Design,* Bled, Slovenia.

Kayen, R, R Moss, E Thompson, R Seed, K Cetin, A Kiureghian, Y Tanaka and K Tokimatsu (2013) Shear-wave velocity–based probabilistic and deterministic assessment of seismic soil liquefaction potential. *Journal of Geotechnical and Geoenvironmental Engineering 139*, no.3: 407–419.

Kramer, S and CH Wang (2015) Empirical model for estimation of the residual strength of liquefied soil. *Journal of Geotechnical and Geoenvironmental Engineering 141*, no.9.

Kramer, SL, RT Mayfield and YM Huang (2006) Performance-based liquefaction potential: a step toward more uniform design requirements. In *Proceedings of US–Japan Workshop on Seismic Design of Bridges*, Bellevue, WA.

Kramer, SL, RT Mayfield and YM Huang (2008) *Performance-based liquefaction potential evaluation*. USGS project no. 06HQGR0041. Reston, Virginia: US Geological Survey.

Kramer, S, R Mayfield and R Mitchell (2003) Ground motions and liquefaction –the loading part of the equation. In *Proceedings of the US-Taiwan Workshop on Soil Liquefaction*, Hsinchu, Taiwan, 3–5 November 2003.

Kulhawy, FH and PW Mayne (1990) Manual for estimating soil properties for foundation design. *Report no. EPRI EL-6800.* Palo Alto, California: Electric Power Research Institute (EPRI).

Kulhawy, FH and K-K Phoon (1993) Drilled shaft side resistance in clay soil to rock. Pp172–183 in *Design and performance of deep foundations: piles and piers in soil and rock.* P Nelson, T Smith and E Clukey (Eds) ASCE GSP no. 38.

Langridge, R, R Van Disen, D Rhoades, P Villamor, T Little, N Litchfield, K Clark and D Clark (2011) Five thousand years of surface ruptures on the Wellington fault, New Zealand: implications for recurrence and fault segmentation. *Bulletin of the Seismological Society of America 101*, no.5: 2088–2107.

Ledezma, C and J Bray (2008) *Performance-based earthquake engineering design evaluation procedure for bridge foundations undergoing liquefaction-induced lateral ground displacement*. Berkeley, California: Pacific Earthquake Engineering Centre, University of California,

Ledezma, C and J Bray (2010) Probabilistic performance-based procedure to evaluate pile foundations at sites with liquefaction-induced lateral displacement. *Journal of Geotechnical and Geoenvironmental Engineering 136*, no. 3: 464–476.

Look, BG (2007) *Handbook of geotechnical investigation and design tables*. London: Taylor and Francis Group.

Mackie, KR and B Stojadinović (2006) Post-earthquake functionality of highway overpass bridges. *Earthquake Engineering & Structural Dynamics 35*, no.1: 77–93.

Mander, JB, MJN Priestley and R Park (1988) Theoretical stress-strain model for confined concrete. *Journal of Structural Engineering 114*: no.8: 1804–1826.

Martin, GR (2000) *Annual report for research year 1, June 1, 1999 to September 30, 2000*. MCEER highway project 094: seismic vulnerability of the highway system. Multidisciplinary Centre for Earthquake Engineering Research. New York.

Maula, BH, L Zhang, T Liang, G Xia, X Peng-Ju, Z Yong-Qiang, J Kang and S Lei (2011) *Comparison of current Chinese and Japanese design specification for bridge pile in liquefied ground*. New Mexico, USA: World Academy of Science, Engineering and Technology.

MBIE (2017) Acceptable solutions and verification methods B1 – structure. Wellington: Ministry of Business, Innovation and Employment.

MBIE–NZGS (2016a) *Guidelines for earthquake geotechnical engineering practice, module 1: overview of the guidelines.* Wellington: Ministry of Business, Innovation and Employment.

MBIE–NZGS (2016b) *Guidelines for earthquake geotechnical engineering practice, module 2: geotechnical investigation for earthquake engineering*. Wellington: Ministry of Business, Innovation and Employment.

MBIE–NZGS (2016c) *Guidelines for earthquake geotechnical engineering practice, module 3: identification, assessment and mitigation of liquefaction hazards*. Revision 1. Wellington: Ministry of Business, Innovation and Employment.

MBIE–NZGS (2016d) *Guidelines for earthquake geotechnical engineering practice, module 4: earthquake resistant foundation design*. Wellington: Ministry of Business, Innovation and Employment.

MBIE–NZGS (2017) *Guidelines for earthquake geotechnical engineering practice, module 5: ground improvement of soils prone to liquefaction*. Wellington: Ministry of Business, Innovation and Employment.

McGann, CR, BA Bradley, ML Taylor, LM Wotherspoon, and M Cubrinovski (2015) Development of an empirical correlation for predicting shear wave velocity of Christchurch soils from cone penetration test data. *Soil Dynamics and Earthquake Engineering 75*: 66–65.

McVerry, GH, A Christophersen, C Muller and N Perrin (2014) Christchurch northern arterial and western bypass – probabilistic seismic hazard analysis. *GNS science report 2014/33.*

Mokwa, RL (1999) *Investigation of the resistance of pile caps to lateral loading*. PhD thesis, Virginia Polytechnic Institute and State University.

Montejo, LA and MJ Kowalsky (2007) CUMBIA. *Set of codes for the analysis of reinforced concrete members (computer programme)*. Raleigh, NC: Department of Civil, Construction and Environmental Engineering, North Carolina State University.

Mosher, RL (1984) *Load transfer criteria for numerical analysis of axial loaded piles in sand*. Vicksburg, MS: US Army Engineering Waterways Experimental Station, Automatic Data Processing Centre.

Murashev, AK, DK Kirkcaldie, C Keepa and JN Lloyd (2013) Proposed amendments to geotechnical requirements of NZTA *Bridge manual*. *Proceedings of 19th New Zealand Geotechnical Society Geotechnical Symposium*, Queenstown, New Zealand.

Murashev, A, D Kirkcaldie, C Keepa, M Cubrinovski and R Orense (2014) The development of design guidance for bridges in New Zealand for liquefaction and lateral spreading effects. *NZ Transport Agency research report 553*. 142pp.

National Technical Information Service (1986a) *Seismic design of highway bridge foundations, volume 1. Executive summary.* Springfield, Virginia: US Department of Transportation.

National Technical Information Service (1986b) *Seismic design of highway bridge foundations, volume 3. Example problems and sensitivity studies*. Springfield, Virginia: US Department of Transportation.

New Zealand Transport Agency (2016) *Bridge manual*. 3rd ed. Wellington: New Zealand Transport Agency.

New Zealand Transport Agency (2017) *Bridge manual*. Draft section 5 for amendment 3 (last accessed version 3.3.1). Wellington: New Zealand Transport Agency.

Olson, SM and TD Stark (2002) Liquefied strength ratio from liquefaction flow failure case histories. *Canadian Geotechnical Journal 39*, no.3: 629–647.

Oregon State Department of Transportation (2005) *Seismic foundation design practice, bridge engineering section*. Salem, Oregon: Oregon State Department of Transportation.

Oregon State Department of Transportation (2010) *Geotechnical design manual - chapter 6 seismic design*. Salem, Oregon: Oregon State Department of Transportation.

Oregon State Department of Transportation (2011) *Seismic vulnerability of Oregon state highway bridges – mitigation strategies to reduce major mobility risks*. Salem, Oregon: Oregon State Department of Transportation.

Ozener, P (2012) Estimation of residual shear strength ratios of liquefied soil deposits from shear wave velocity. *Earthquake Engineering and Engineering Vibration 11*: 461–484.

Palermo, A, L Wotherspoon, J Wood, H Chapman, A Scott, L Hogan, A Kivell, E Camniso, M Yashinsky, M Bruneau and N Chouw (2011) Lessons learnt from 2011 Christchurch earthquakes: analysis and assessment of bridges. *Bulletin of the New Zealand Society for Earthquake Engineering 44*: no.4: 319–333.

Park, R (1996) New Zealand perspectives on seismic design of bridges. *Paper no. 2111 presented at the Eleventh World Conference on Earthquake Engineering*. Mexico.

Robertson, P (2015) *Guide to cone penetration testing for geotechnical engineering*. 6th ed. California: Gregg Drilling & Testing.

Sabatini, PJ, RC Bachus, PW Mayne, JA Schneider and TE Zettler (2002) Evaluation of soil and rock properties. *Geotechnical Engineering Circular no.5, FHWA-IF-02-034*. US: Federal Highways Association.

Seed, RB, KO Cetin, RE Moss, AM Kammerer, J Wu, JM Pestana, MF Riemer, RB Sancio, RE Kayen and A Faris (2003) Recent advances in soil liquefaction engineering: a unified and consistent framework. In *Proceedings of the 26th Annual ASCE Los Angeles Geotechnical Spring Seminar*: Long Beach, California.

Seed, RB and LF Harder (1990) SPT-based analysis of cyclic pore pressure generation and undrained residual strength. In *Proceedings of the H. Bolton Seed Memorial Symposium 2*: 351–376.

Standards NZ (2006) *NZS 3101:2006 Concrete structures standard.*

Standards NZ (2004) *NZS 1170.5:2004 Seismic design actions, part 5: Earthquake actions – New Zealand.*

Stirling, M, G McVerry, K Berryman, P McGinty, P Villamore, R Van Dissen, D Dowrick, J Cousins and R Sutherland (2000) Probabilistic seismic hazard assessment of New Zealand: new active fault data, seismicity data, attenuation relationships and methods. *Institute of Geological and Nuclear Sciences client report 2000/53*. Wellington: Earthquake Commission Research Foundation.

Tamura, K (2013) Design requirements of highway bridges for soil liquefaction. Pp49–61 in *Proceedings of the International Symposium for Bridge Earthquake Engineering in Honor of Retirement of Professor Kazuhiko Kawashima*, Tokyo, Japan.

Tasiopoulou, P, N Gerolymos, T Tazoh and G Gazetas (2013) Pile-group response to large soil displacements and liquefaction: centrifuge experiments versus a physically simplified analysis. *Journal of Geotechnical and Geoenvironmental Engineering 139*, no.2: 223–233.

Tasiopoulou, P, E Smyrou, I Bal and G Gazetas (2012) Bridge pile – abutment – deck interaction in laterally spreading ground: Lessons from Christchurch. *Proceedings of the 15th World Conference on Earthquake Engineering*, Lisbon, Portugal.

Tokimatsu, K and Y Asaka (1998) Effects of liquefaction-induced ground displacements on pile performance in the 1995 Hyogoken-Nambu earthquake. *Special Issue of Soils and Foundations*, no.2: 163–177.

Tokimatsu, K, H Suzuki and M Sato (2005) Effects of inertial and kinematic interaction on seismic behavior of pile with embedded foundation. *Soil Dynamics and Earthquake Engineering 25*: 753–762.

Unjoh, S and T Terayama (Eds) (1996) *Design specifications of highway bridges – part V seismic design*. Tokyo: Japan Road Association.

Van Houtte, C, S Bannister, C Holden, S Bouguignon and G McVerry (2016) *Overview of the New Zealand strong motion database project and performance of ground motion models*.

Waldin, J, J Jennings and P Routledge (2012) Critically damaged bridges and concepts for earthquake recovery. *Paper no.104 in the New Zealand Society for Earthquake Engineering Annual Technical Conference*, Christchurch, New Zealand, 2012.

Washington State Department of Transportation (2010) *Geotechnical design manual – chapter 6 seismic design*. Washington DC: Washington State Department of Transportation.

Werner, SD, S Cho and RT Eguchi (2008) *The ShakeOut scenario supplemental study: analysis of risks to Southern California highway system*. Menlo Park, California: United States Geological Survey.

Wood, J (2012) Analyses of state highway bridges damaged in the Darfield and Christchurch earthquakes. *Paper no.018 in the New Zealand Society for Earthquake Engineering Annual Technical Conference*, Christchurch, New Zealand, 2012.

Wotherspoon, L, R Orense, B Bradley, B Cox, C Wood and R Green (2014) Geotechnical characterisation of Christchurch strong motion stations V2. *Earthquake Commission report, project no. 12/629*.

Youd, T and I Idriss (Eds) (1997) Proceedings of the NCEER workshop on evaluation of liquefaction resistance of soils. *Technical report NCEER-97-0022*. Utah, USA.

Youd, TL and IM Idriss (2001) Liquefaction resistance of soils: summary report from the 1996 NCEER and 1998 NCEER/NSF workshops on evaluation of liquefaction resistance of soils. *Journal of Geotechnical and Geoenvironmental Engineering 127*, no.4: 297–313.

Youd, TL, CM Hansen and SF Bartlett (2002) Revised multi-linear regression equations for prediction of lateral spread displacement. *Journal of Geotechnical and Environmental Engineering 128*, no.12: 1007–1017.

Zhao, M (2011) *Response of bridges to lateral spreading and earthquake shaking*. PhD thesis, Los Angeles: University of California.

Zhang, G, PK Robertson and RWI Brachman (2002) Estimating liquefaction-induced ground settlements from CPT for level ground. *Canadian Geotechnical Journal 39*: 1168–1180.

Zhang, G, PK Robertson and RWI Brachman (2004) Estimating liquefaction-induced lateral displacements using the standard penetration test or cone penetration test. *Journal of Geotechnical and Geoenvironmental Engineering 130*, no.8: 861–871.

Appendix A: Results of pseudo- static analysis of Belfast Bridge

A1 Results of the whole bridge model for the pre-liquefied phase (Phase 1)

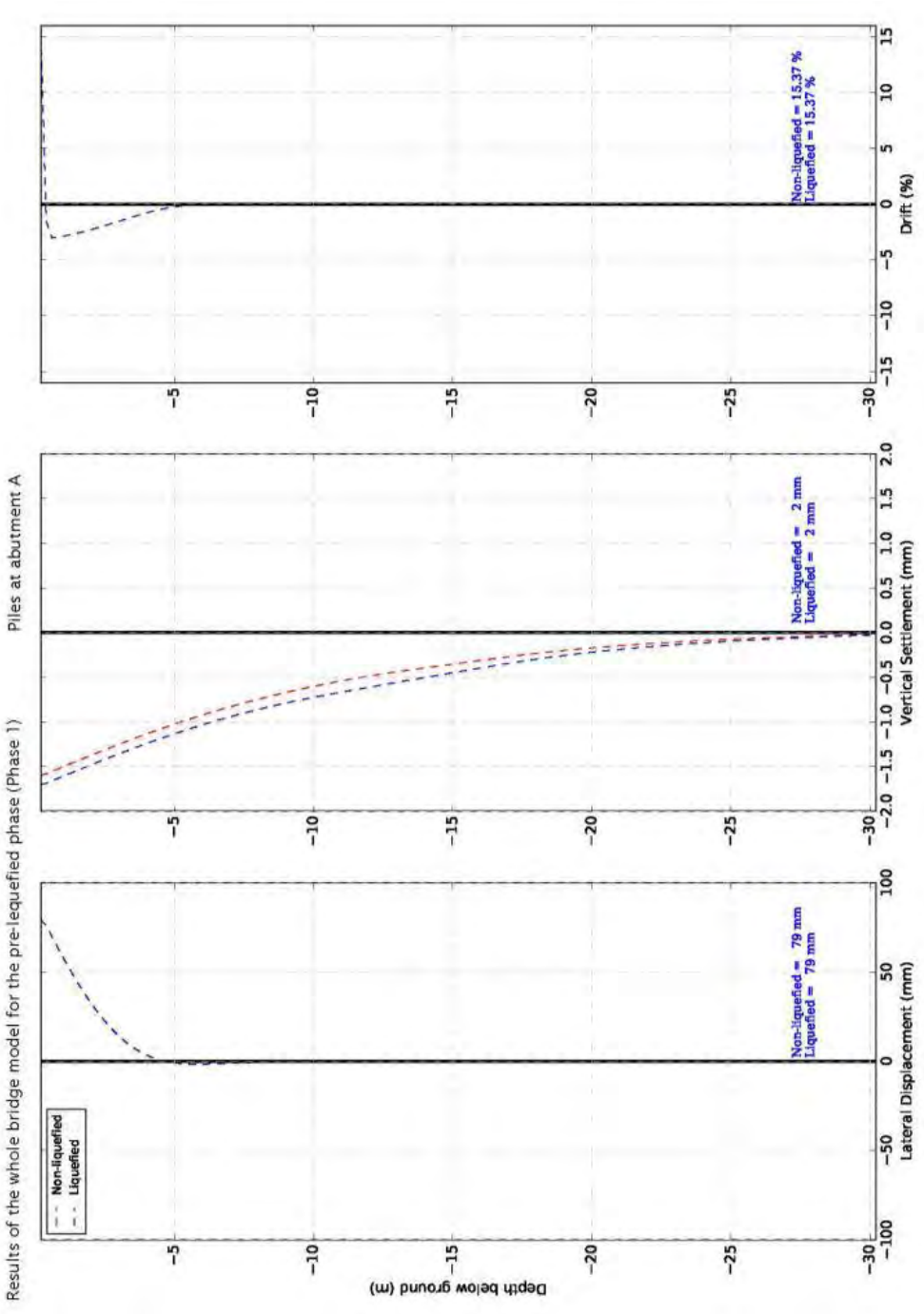

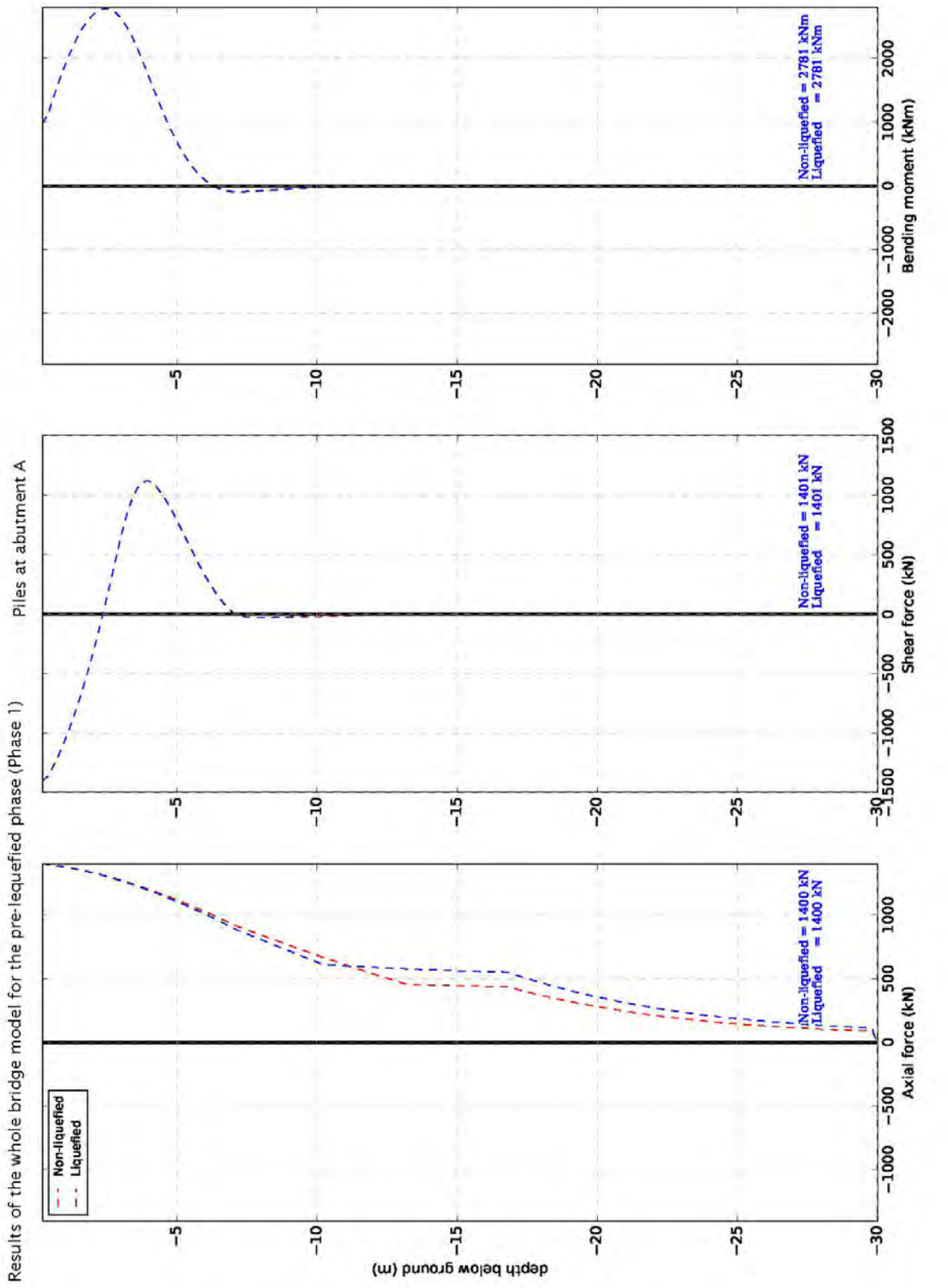
Results of the whole bridge model for the pre-lequefied phase (Phase 1)
Piles at abutment A
depth below ground (m)
Axial force (kN)
Shear force (kN)
Bending moment (kNm)
Non-liquefied
Liquefied
Non-liquefied = 1400 kN
Liquefied = 1400 kN
Non-liquefied = 1401 kN
Liquefied = 1401 kN
Non-liquefied = 2781 kNm
Liquefied = 2781 kNm

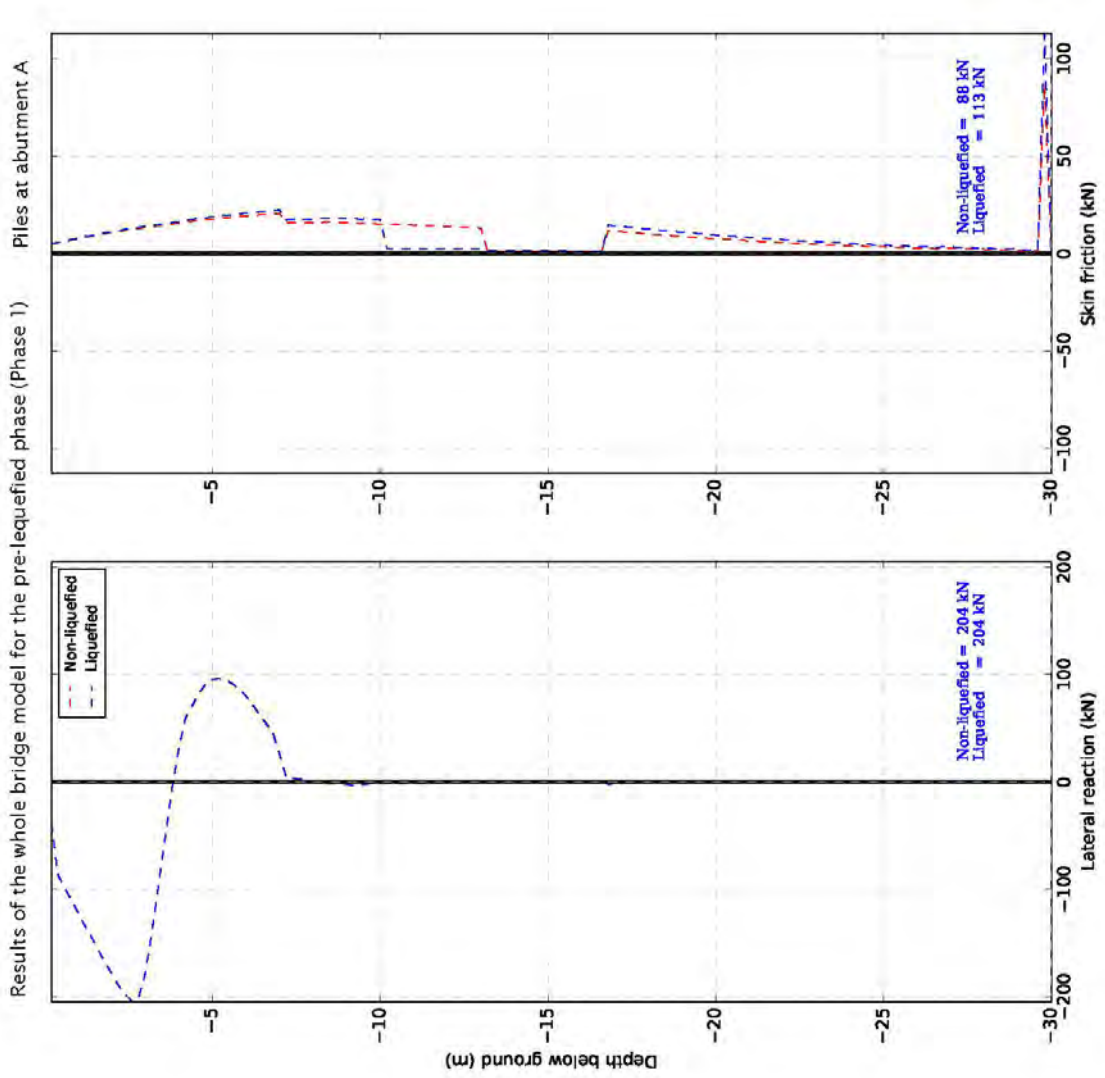
Results of the whole bridge model for the pre-lequefied phase (Phase 1)
Piles at abutment A
Non-liquefied
Liquefied
Non-liquefied = 88 kN
Liquefied = 113 kN
Non-liquefied = 204 kN
Liquefied = 204 kN
Skin friction (kN)
Lateral reaction (kN)
Depth below ground (m)

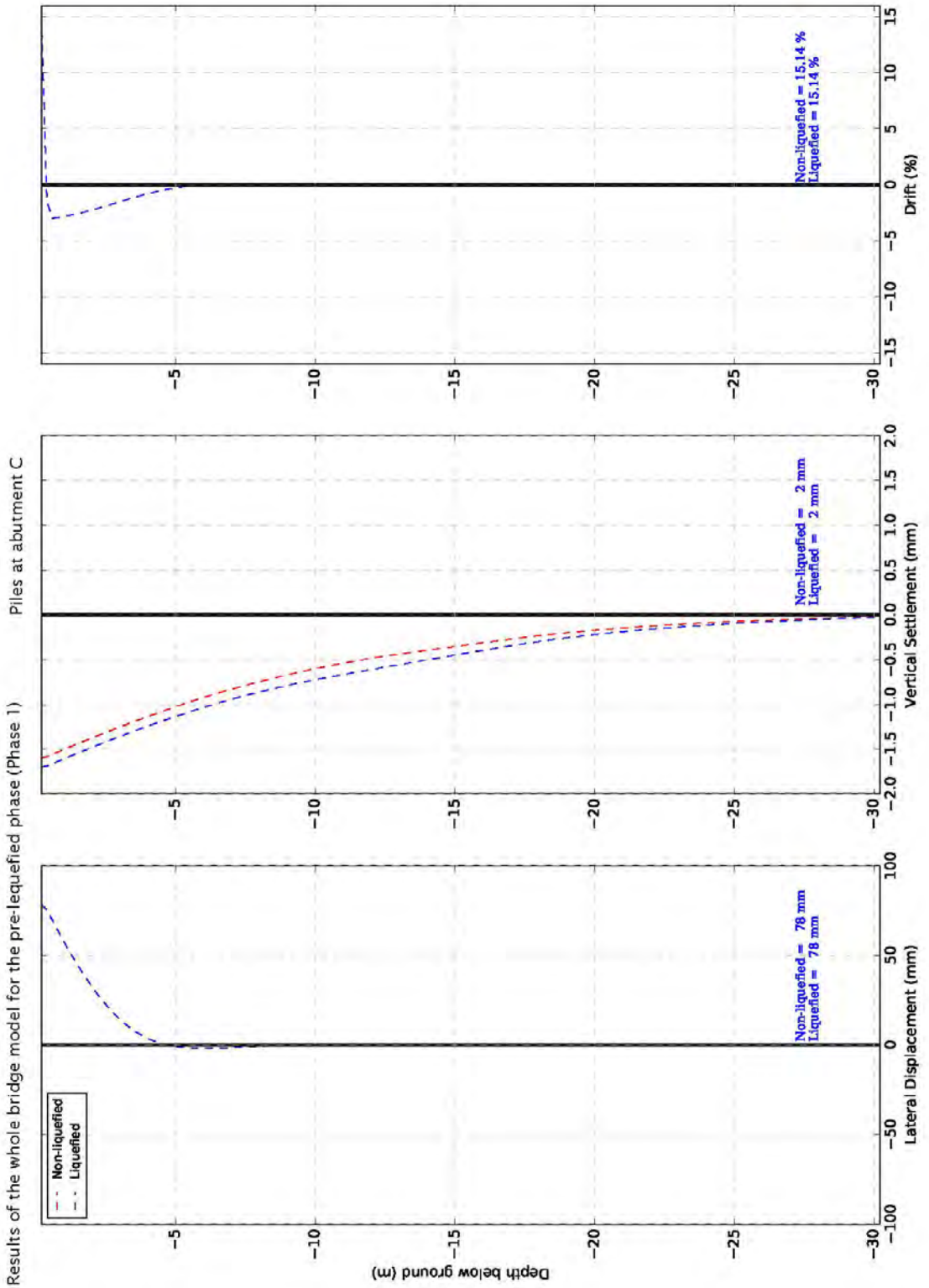
Results of the whole bridge model for the pre-lequefied phase (Phase 1)
Piles at abutment C
Depth below ground (m)
Non-liquefied
Liquefied
Non-liquefied = 78 mm
Liquefied = 78 mm
Lateral Displacement (mm)
Non-liquefied = 2 mm
Liquefied = 2 mm
Vertical Settlement (mm)
Non-liquefied = 15.14 %
Liquefied = 15.14 %
Drift (%)

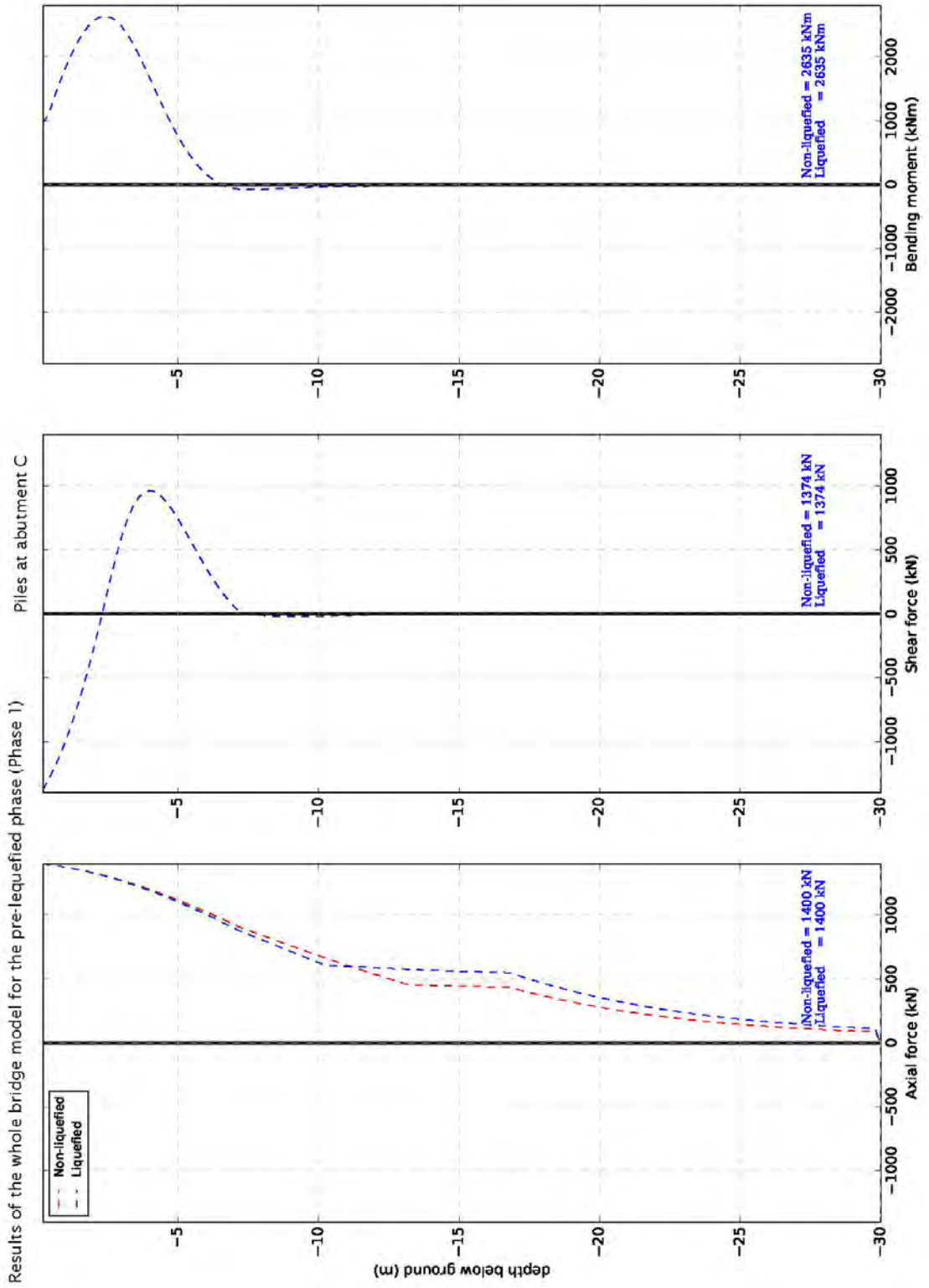
Results of the whole bridge model for the pre-lequefied phase (Phase 1)
Piles at abutment C
Non-liquefied
Liquefied
Non-liquefied = 1400 kN
Liquefied = 1400 kN
Axial force (kN)
Non-liquefied = 1374 kN
Liquefied = 1374 kN
Shear force (kN)
Non-liquefied = 2635 kNm
Liquefied = 2635 kNm
Bending moment (kNm)
depth below ground (m)

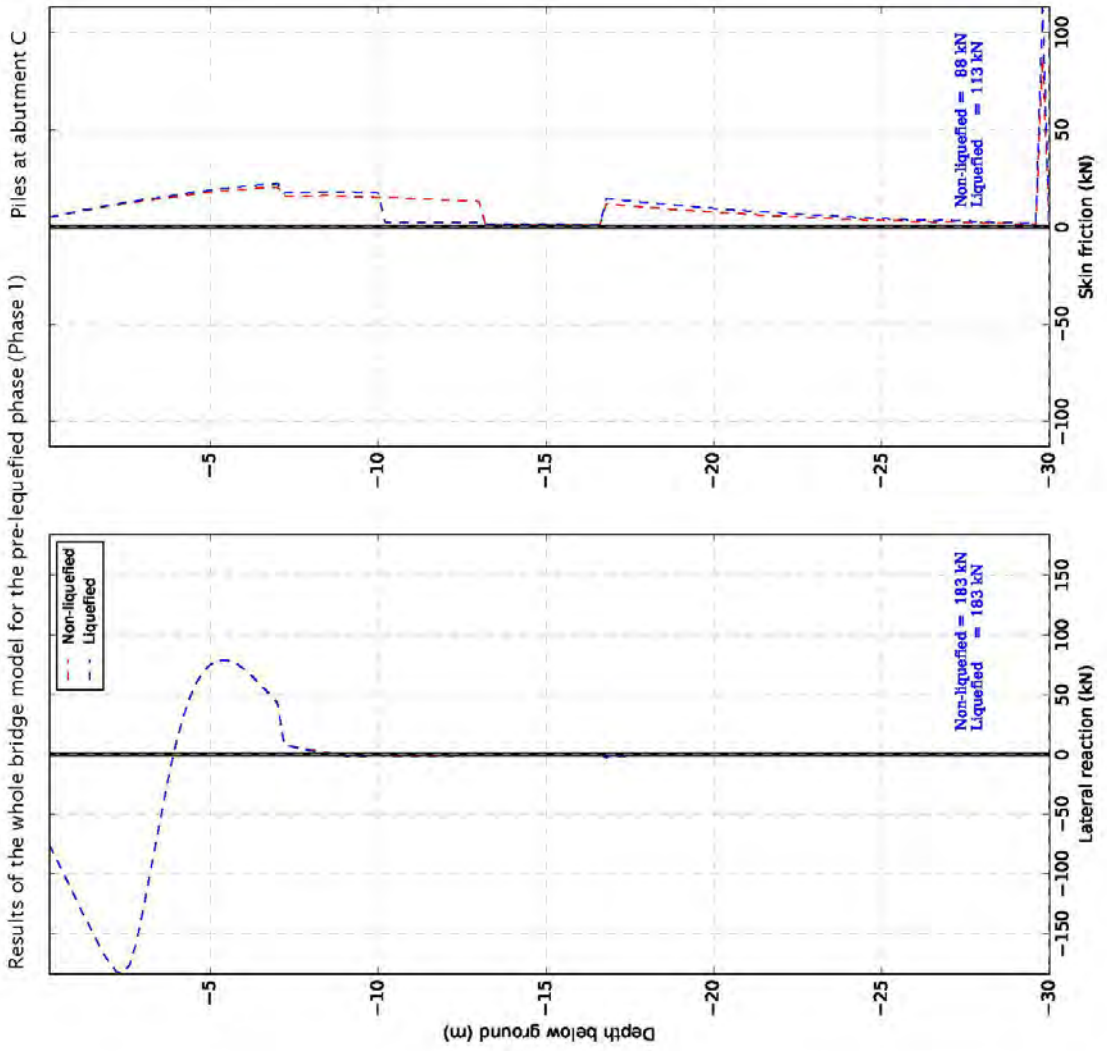
Results of the whole bridge model for the pre-lequefied phase (Phase 1)
Piles at abutment C
Non-liquefied
Liquefied
Non-liquefied = 183 kN
Liquefied = 183 kN
Lateral reaction (kN)
Non-liquefied = 88 kN
Liquefied = 113 kN
Skin friction (kN)
Depth below ground (m)

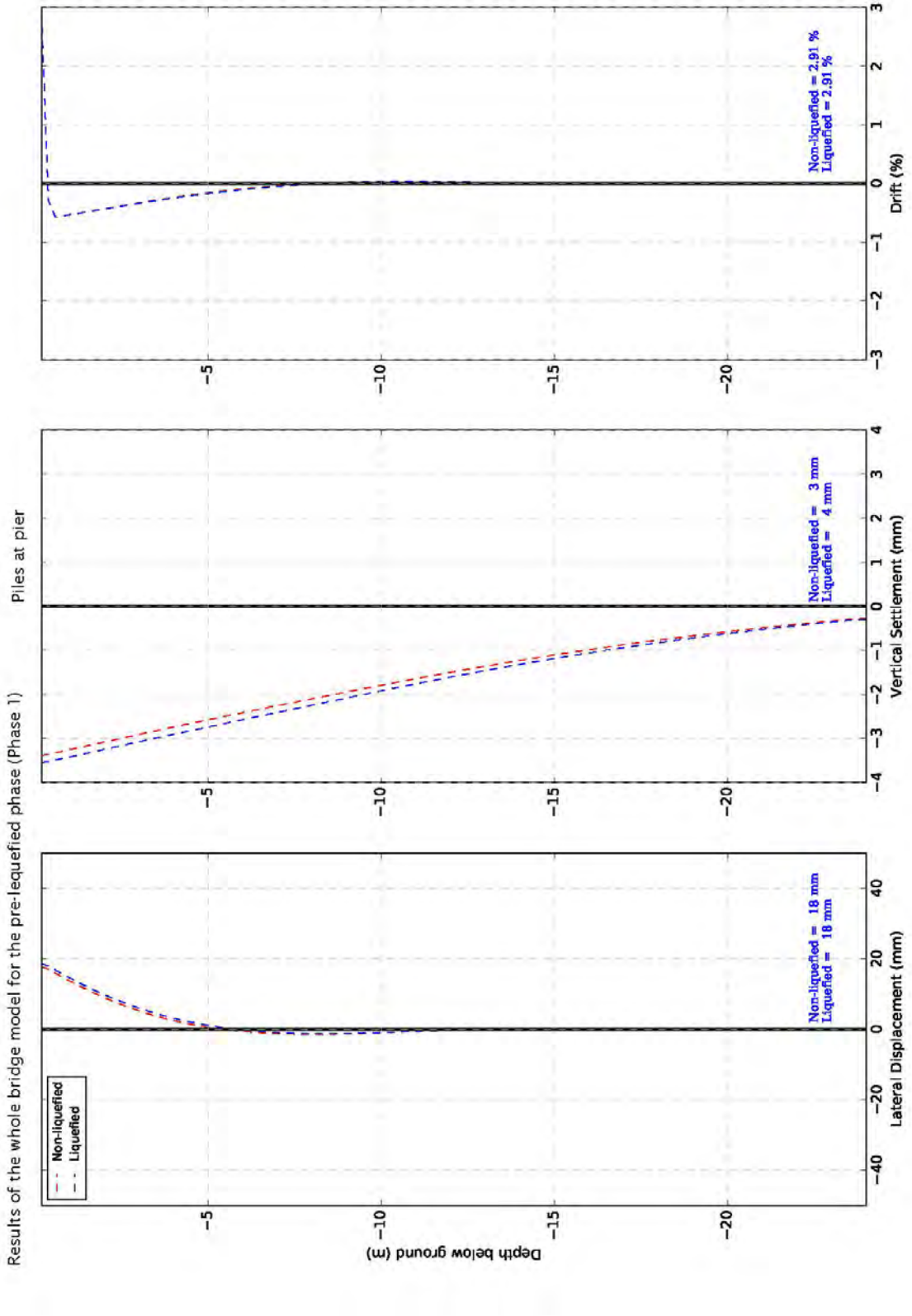
Results of the whole bridge model for the pre-lequefied phase (Phase 1)
Piles at pier
Depth below ground (m)
Non-liquefied
Liquefied
Non-liquefied = 18 mm
Liquefied = 18 mm
Lateral Displacement (mm)
Non-liquefied = 3 mm
Liquefied = 4 mm
Vertical Settlement (mm)
Non-liquefied = 2.91 %
Liquefied = 2.91 %
Drift (%)

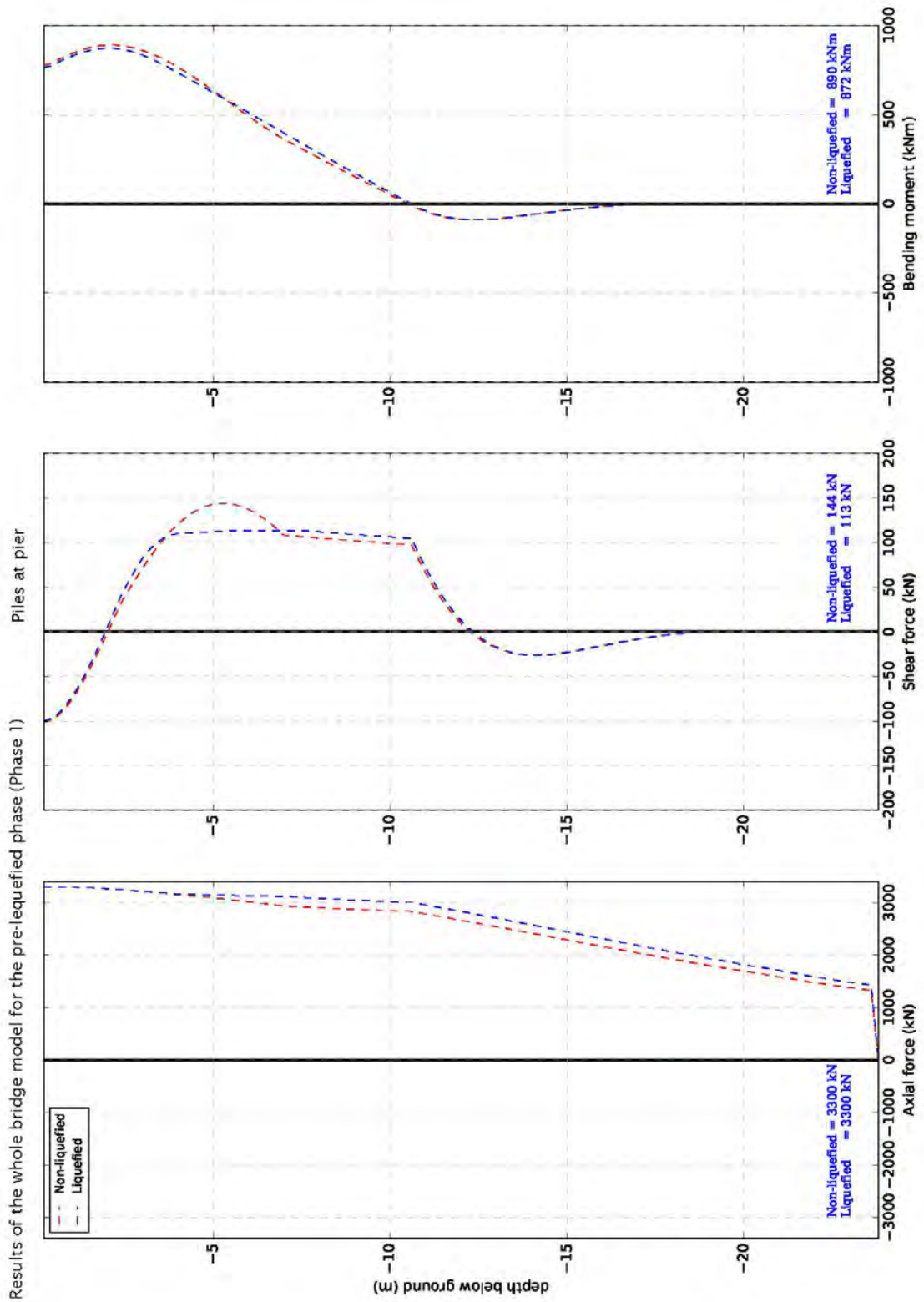
Results of the whole bridge model for the pre-liquefied phase (Phase 1)
Piles at pier
Non-liquefied
Liquefied
depth below ground (m)
Axial force (kN)
Non-liquefied = 3300 kN
Liquefied = 3300 kN
Shear force (kN)
Non-liquefied = 144 kN
Liquefied = 113 kN
Bending moment (kNm)
Non-liquefied = 890 kNm
Liquefied = 872 kNm

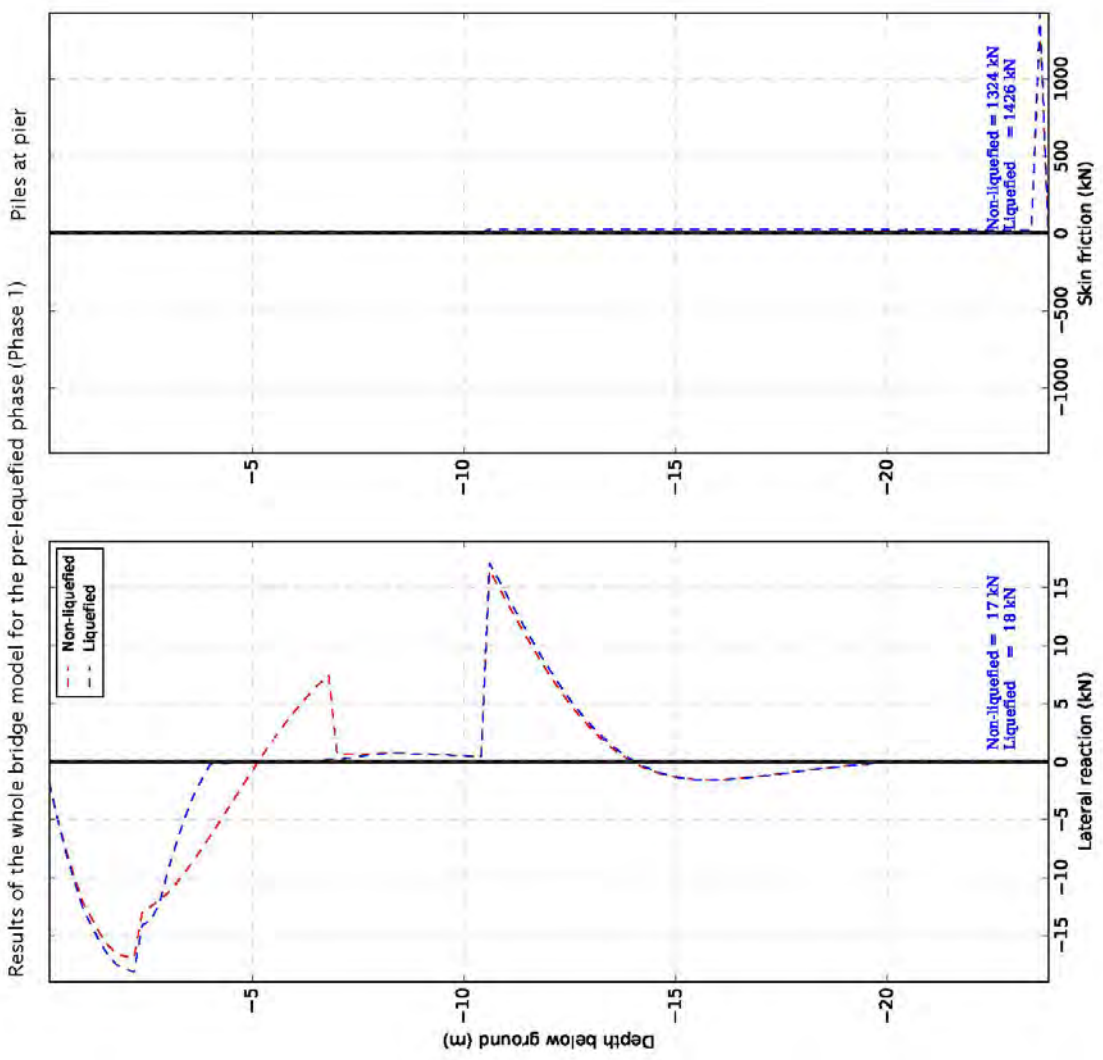
Results of the whole bridge model for the pre-liquefied phase (Phase 1)
Piles at pier
Non-liquefied
Liquefied
Non-liquefied = 17 kN
Liquefied = 18 kN
Lateral reaction (kN)
Depth below ground (m)
Non-liquefied = 1324 kN
Liquefied = 1426 kN
Skin friction (kN)

A2 Results of the single pile model for the cyclic phase (Phase 2)

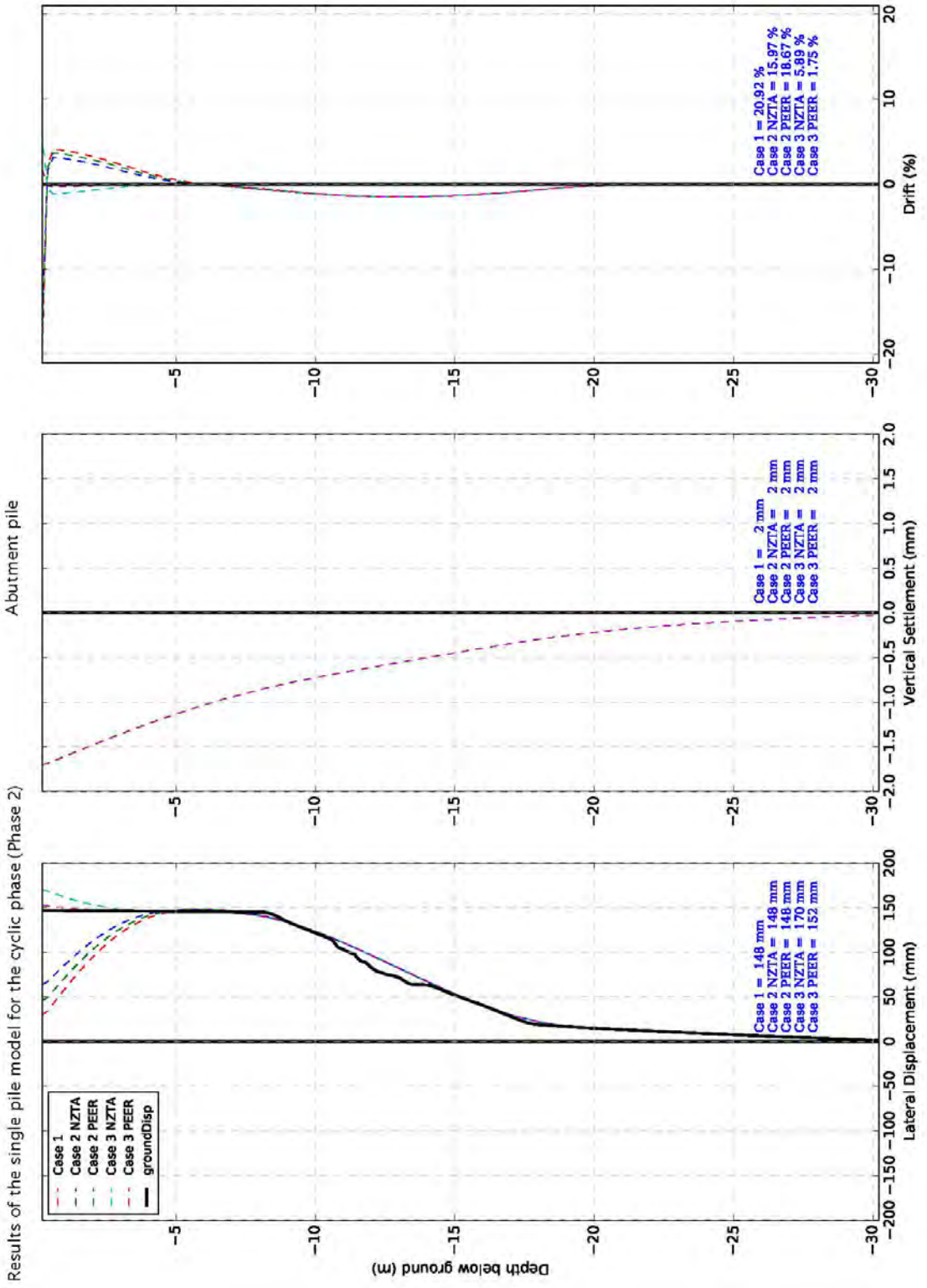

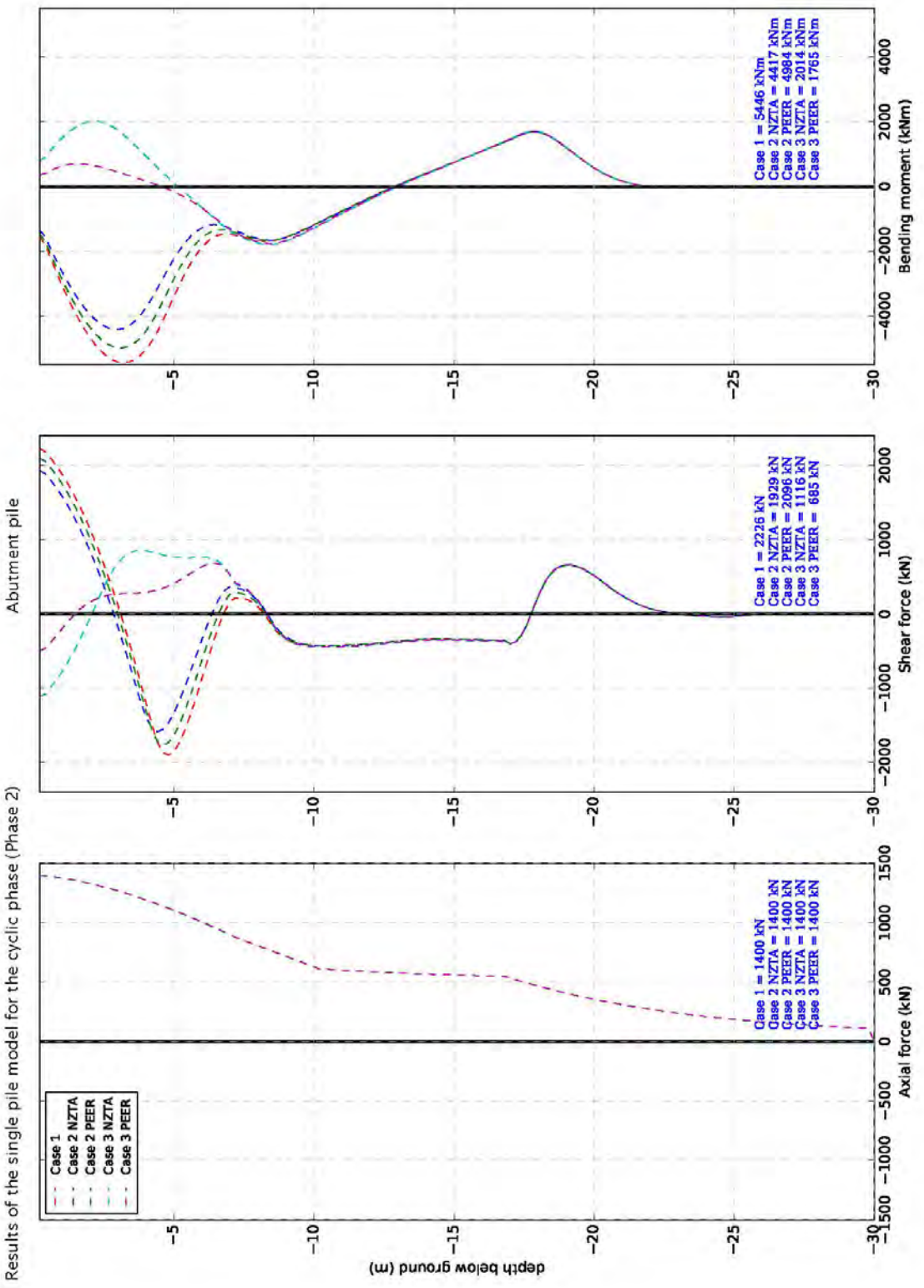
Results of the single pile model for the cyclic phase (Phase 2)
Abutment pile
Case 1
Case 2 NZTA
Case 2 PEER
Case 3 NZTA
Case 3 PEER
Case 1 = 5446 kNm
Case 2 NZTA = 4417 kNm
Case 2 PEER = 4984 kNm
Case 3 NZTA = 2014 kNm
Case 3 PEER = 1765 kNm
Bending moment (kNm)
Case 1 = 2226 kN
Case 2 NZTA = 1929 kN
Case 2 PEER = 2096 kN
Case 3 NZTA = 1116 kN
Case 3 PEER = 685 kN
Shear force (kN)
Case 1 = 1400 kN
Case 2 NZTA = 1400 kN
Case 2 PEER = 1400 kN
Case 3 NZTA = 1400 kN
Case 3 PEER = 1400 kN
Axial force (kN)
depth below ground (m)

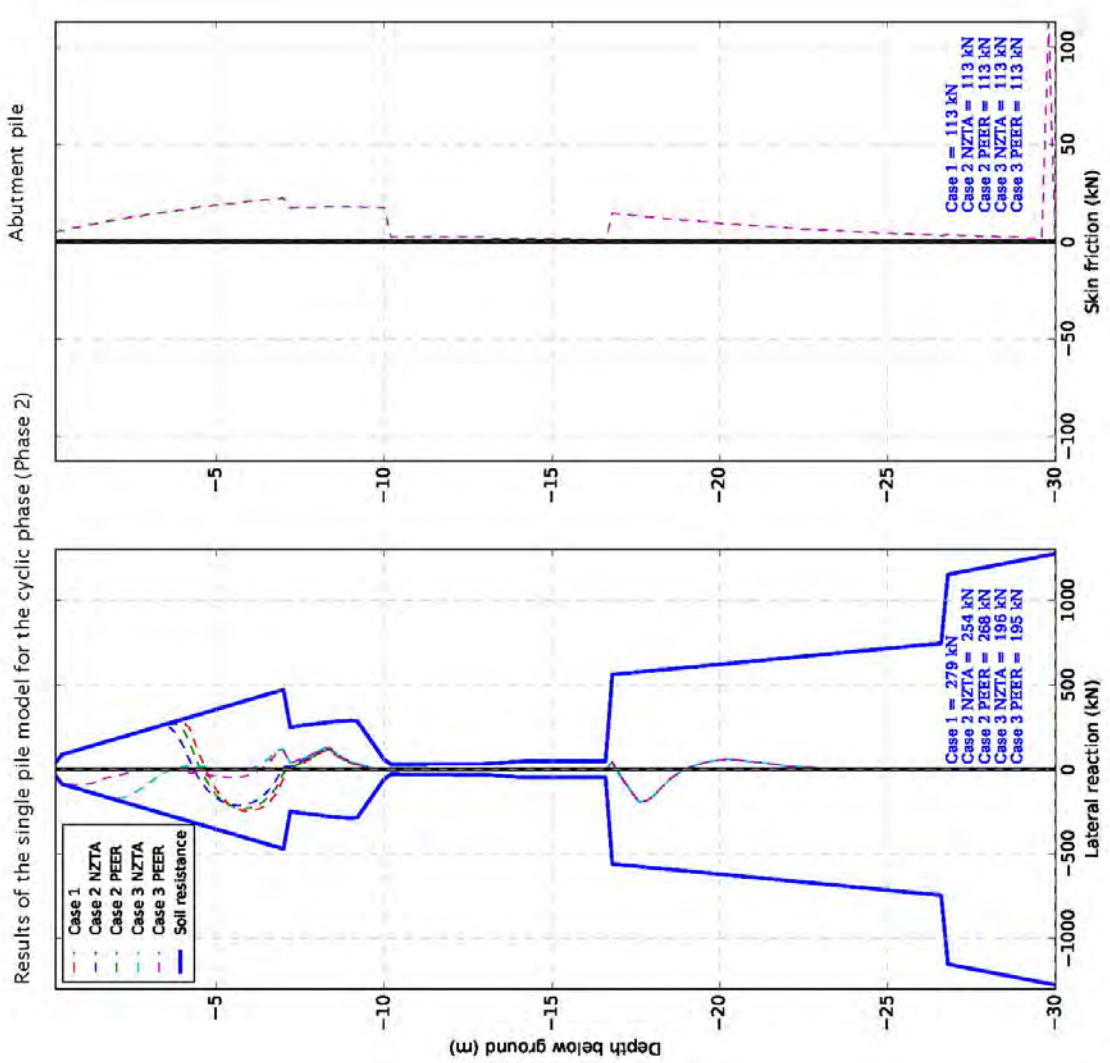
Results of the single pile model for the cyclic phase (Phase 2)
Abutment pile
Depth below ground (m)
Lateral reaction (kN)
Skin friction (kN)
Case 1
Case 2 NZTA
Case 2 PEER
Case 3 NZTA
Case 3 PEER
Soil resistance
Case 1 = 279 kN
Case 2 NZTA = 254 kN
Case 2 PEER = 268 kN
Case 3 NZTA = 196 kN
Case 3 PEER = 195 kN
Case 1 = 113 kN
Case 2 NZTA = 113 kN
Case 2 PEER = 113 kN
Case 3 NZTA = 113 kN
Case 3 PEER = 113 kN

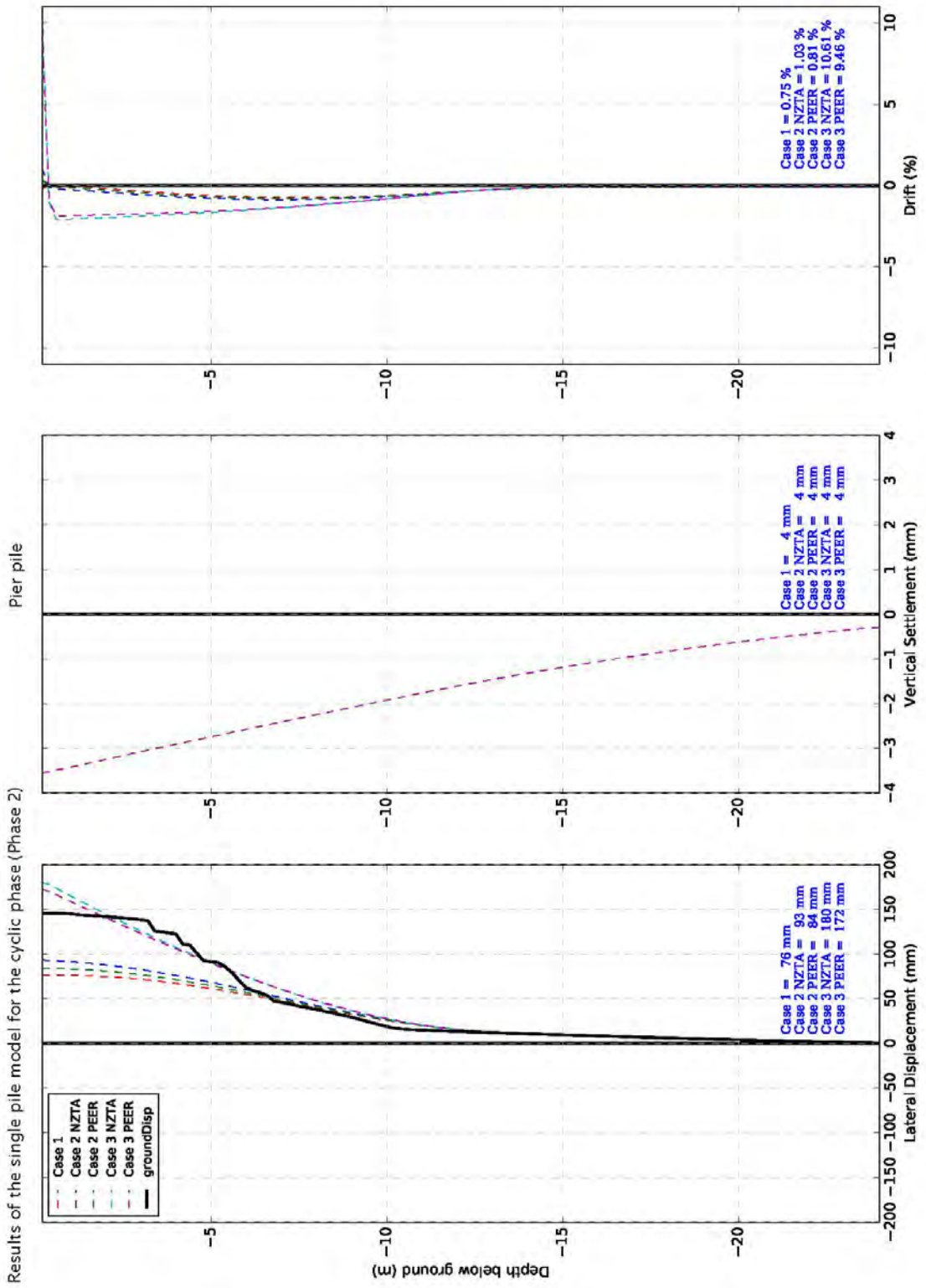
Results of the single pile model for the cyclic phase (Phase 2)
Pier pile
Depth below ground (m)
Lateral Displacement (mm)
Vertical Settlement (mm)
Drift (%)
Case 1
Case 2 NZTA
Case 2 PEER
Case 3 NZTA
Case 3 PEER
groundDisp
Case 1 = 76 mm
Case 2 NZTA = 93 mm
Case 2 PEER = 84 mm
Case 3 NZTA = 180 mm
Case 3 PEER = 172 mm
Case 1 = 4 mm
Case 2 NZTA = 4 mm
Case 2 PEER = 4 mm
Case 3 NZTA = 4 mm
Case 3 PEER = 4 mm
Case 1 = 0.75 %
Case 2 NZTA = 1.03 %
Case 2 PEER = 0.81 %
Case 3 NZTA = 10.61 %
Case 3 PEER = 9.46 %

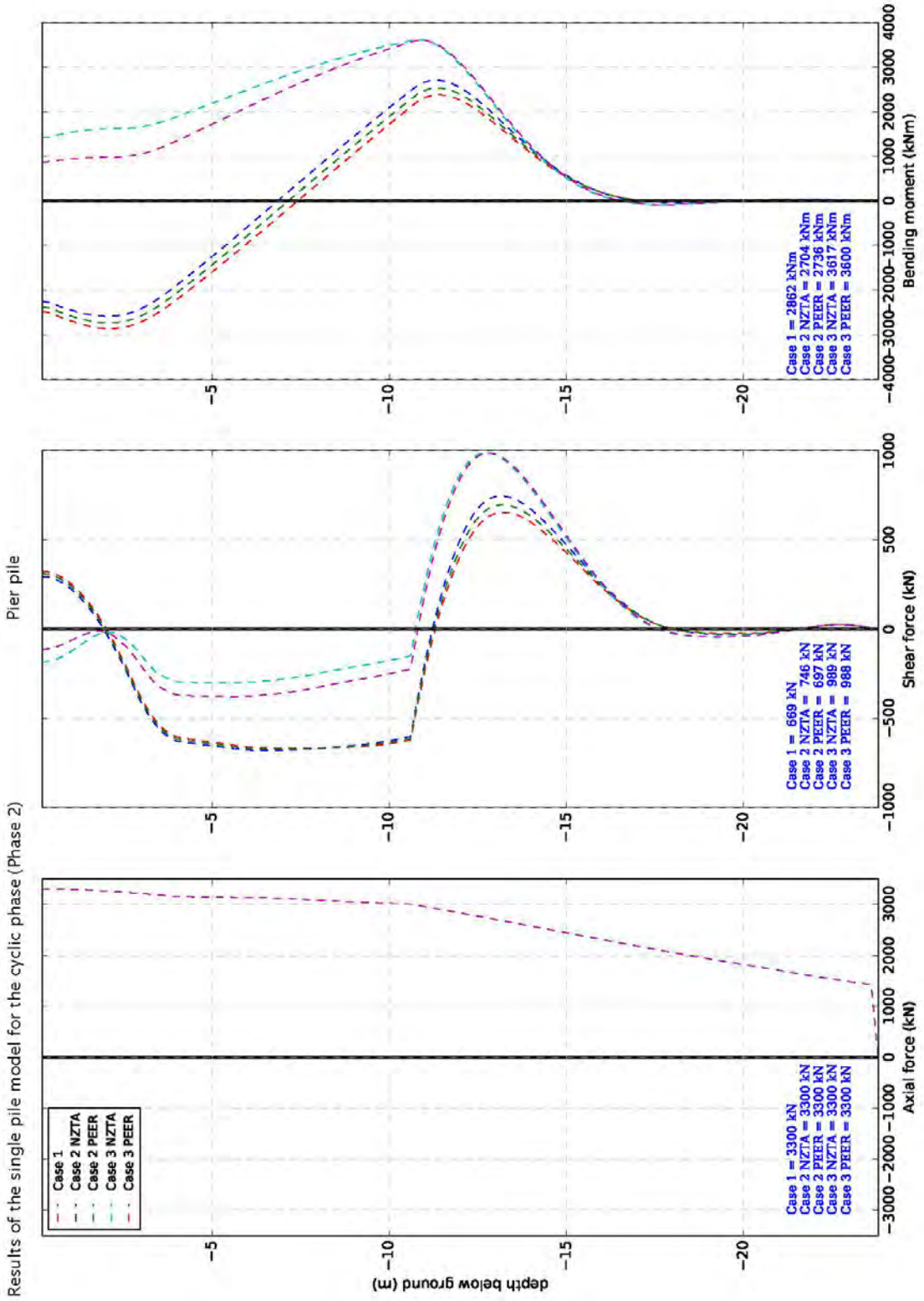
Results of the single pile model for the cyclic phase (Phase 2)
Pier pile
depth below ground (m)
Bending moment (kNm)
Shear force (kN)
Axial force (kN)
Case 1
Case 2 NZTA
Case 2 PEER
Case 3 NZTA
Case 3 PEER
Case 1 = 2862 kNm
Case 2 NZTA = 2704 kNm
Case 2 PEER = 2736 kNm
Case 3 NZTA = 3617 kNm
Case 3 PEER = 3600 kNm
Case 1 = 669 kN
Case 2 NZTA = 746 kN
Case 2 PEER = 697 kN
Case 3 NZTA = 989 kN
Case 3 PEER = 988 kN
Case 1 = 3300 kN
Case 2 NZTA = 3300 kN
Case 2 PEER = 3300 kN
Case 3 NZTA = 3300 kN
Case 3 PEER = 3300 kN

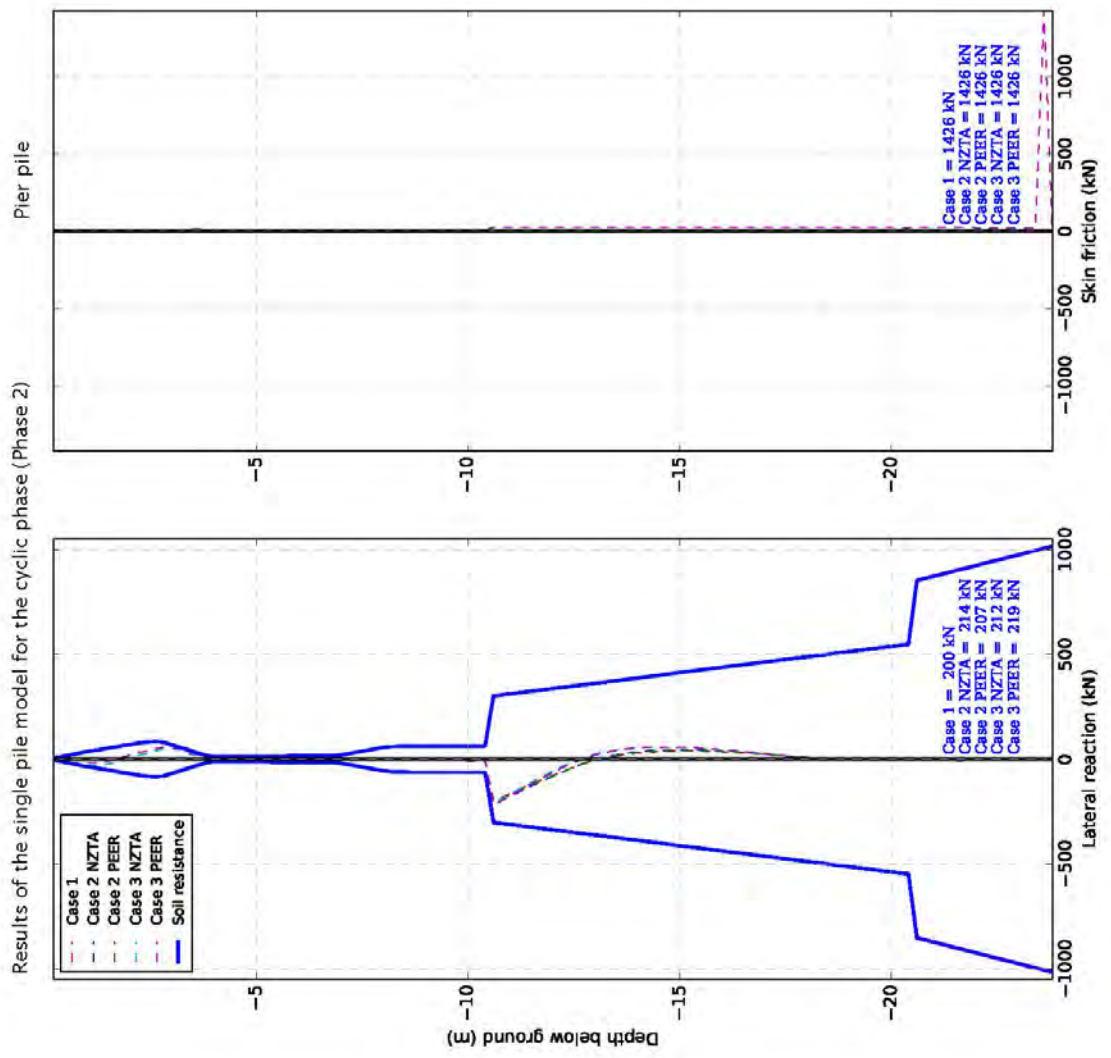
Results of the single pile model for the cyclic phase (Phase 2)
Pier pile
Case 1
Case 2 NZTA
Case 2 PEER
Case 3 NZTA
Case 3 PEER
Soil resistance
Depth below ground (m)
Lateral reaction (kN)
Case 1 = 200 kN
Case 2 NZTA = 214 kN
Case 2 PEER = 207 kN
Case 3 NZTA = 212 kN
Case 3 PEER = 219 kN
Skin friction (kN)
Case 1 = 1426 kN
Case 2 NZTA = 1426 kN
Case 2 PEER = 1426 kN
Case 3 NZTA = 1426 kN
Case 3 PEER = 1426 kN

A3 Results of the whole bridge model for the cyclic phase (Phase 2a)

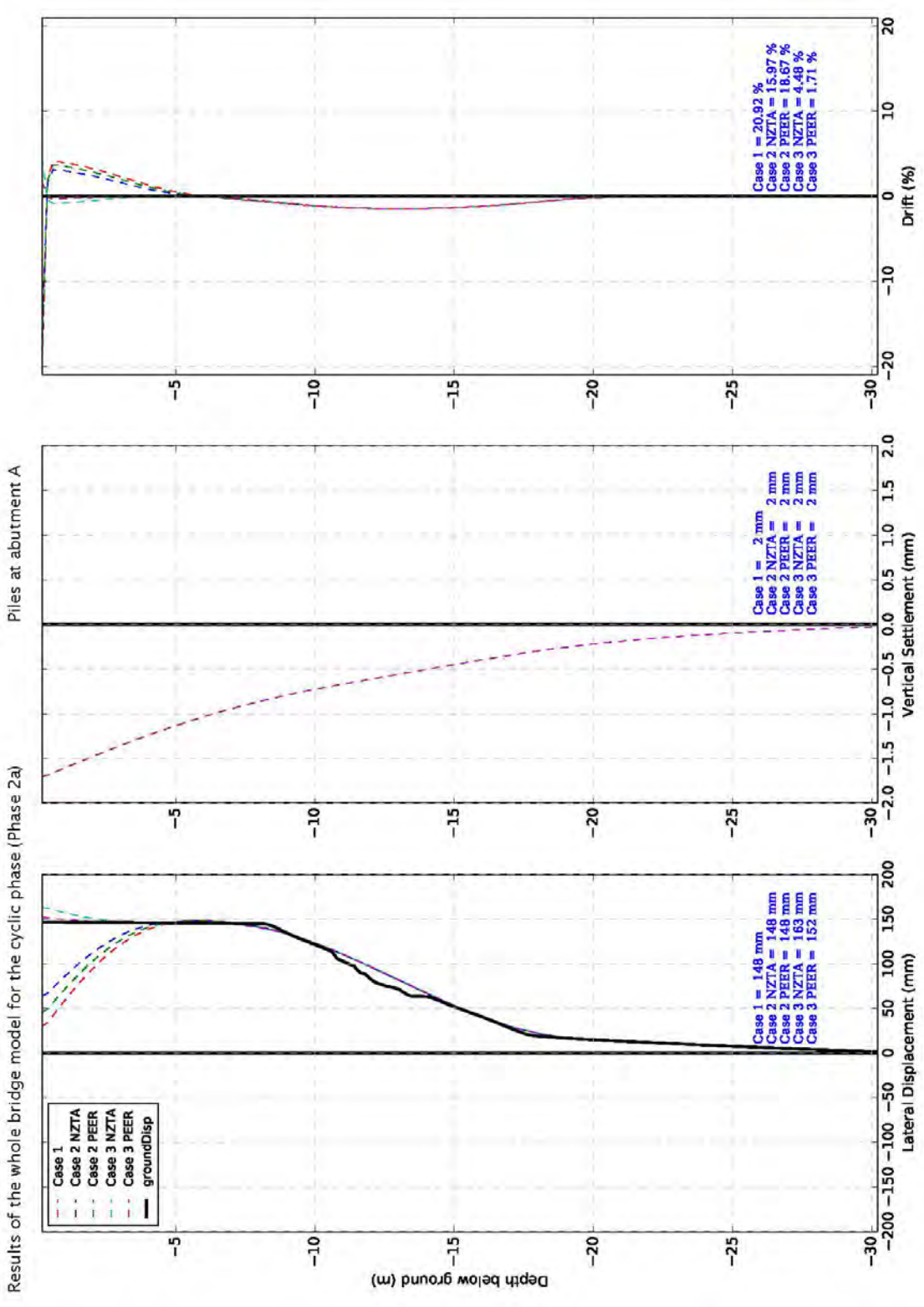

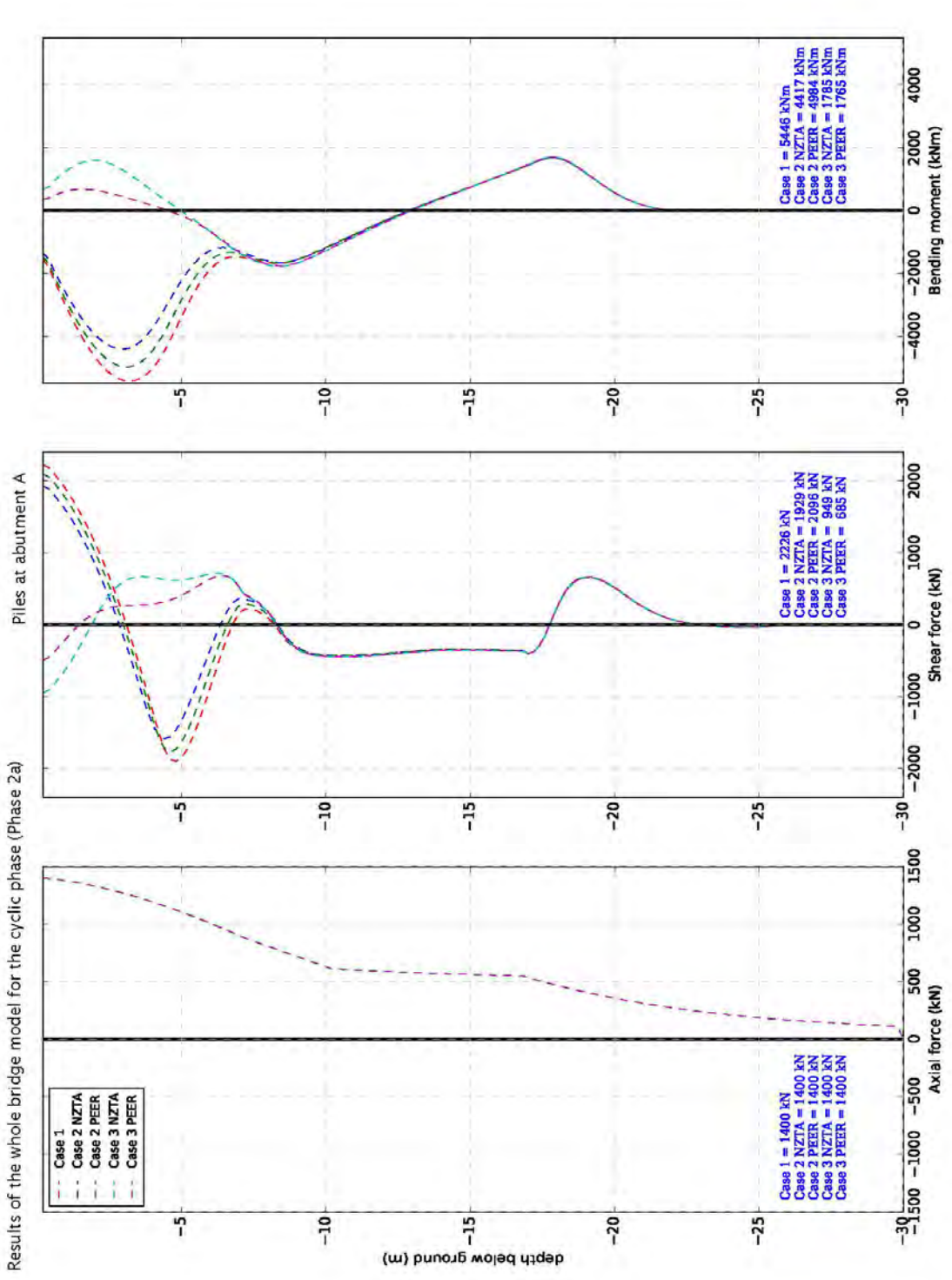
Results of the whole bridge model for the cyclic phase (Phase 2a)
Piles at abutment A
depth below ground (m)
Case 1
Case 2 NZTA
Case 2 PEER
Case 3 NZTA
Case 3 PEER
Case 1 = 1400 kN
Case 2 NZTA = 1400 kN
Case 2 PEER = 1400 kN
Case 3 NZTA = 1400 kN
Case 3 PEER = 1400 kN
Axial force (kN)
Case 1 = 2226 kN
Case 2 NZTA = 1929 kN
Case 2 PEER = 2096 kN
Case 3 NZTA = 949 kN
Case 3 PEER = 685 kN
Shear force (kN)
Case 1 = 5446 kNm
Case 2 NZTA = 4417 kNm
Case 2 PEER = 4984 kNm
Case 3 NZTA = 1785 kNm
Case 3 PEER = 1765 kNm
Bending moment (kNm)

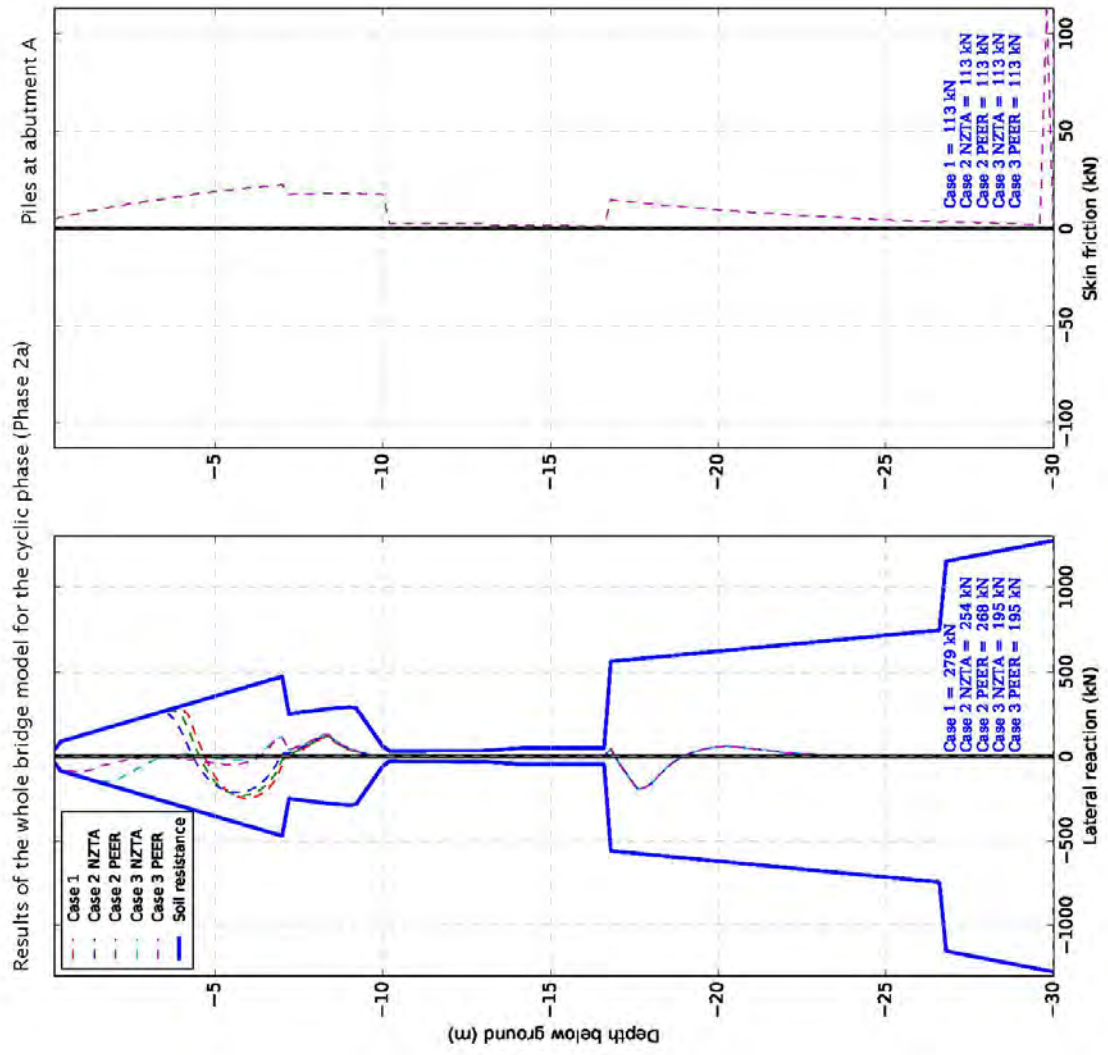
Results of the whole bridge model for the cyclic phase (Phase 2a)
Piles at abutment A
Depth below ground (m)
Lateral reaction (kN)
Skin friction (kN)
Case 1
Case 2 NZTA
Case 2 PEER
Case 3 NZTA
Case 3 PEER
Soil resistance
Case 1 = 279 kN
Case 2 NZTA = 254 kN
Case 2 PEER = 268 kN
Case 3 NZTA = 195 kN
Case 3 PEER = 195 kN
Case 1 = 113 kN
Case 2 NZTA = 113 kN
Case 2 PEER = 113 kN
Case 3 NZTA = 113 kN
Case 3 PEER = 113 kN

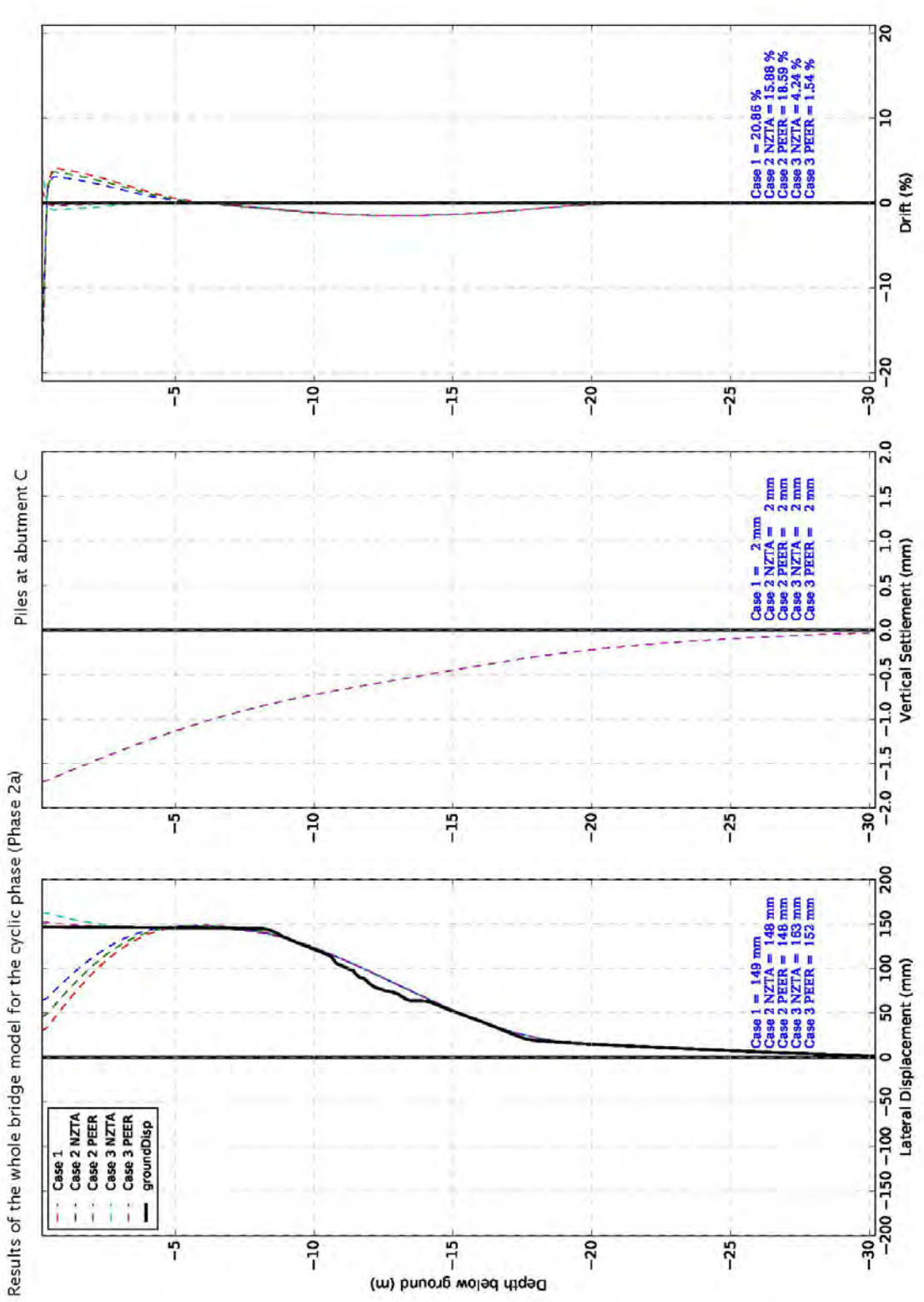
Results of the whole bridge model for the cyclic phase (Phase 2a)
Piles at abutment C
Depth below ground (m)
Lateral Displacement (mm)
Vertical Settlement (mm)
Drift (%)
Case 1
Case 2 NZTA
Case 2 PEER
Case 3 NZTA
Case 3 PEER
groundDisp
Case 1 = 149 mm
Case 2 NZTA = 148 mm
Case 2 PEER = 148 mm
Case 3 NZTA = 163 mm
Case 3 PEER = 152 mm
Case 1 = 2 mm
Case 2 NZTA = 2 mm
Case 2 PEER = 2 mm
Case 3 NZTA = 2 mm
Case 3 PEER = 2 mm
Case 1 = 20.86 %
Case 2 NZTA = 15.88 %
Case 2 PEER = 18.59 %
Case 3 NZTA = 4.24 %
Case 3 PEER = 1.54 %

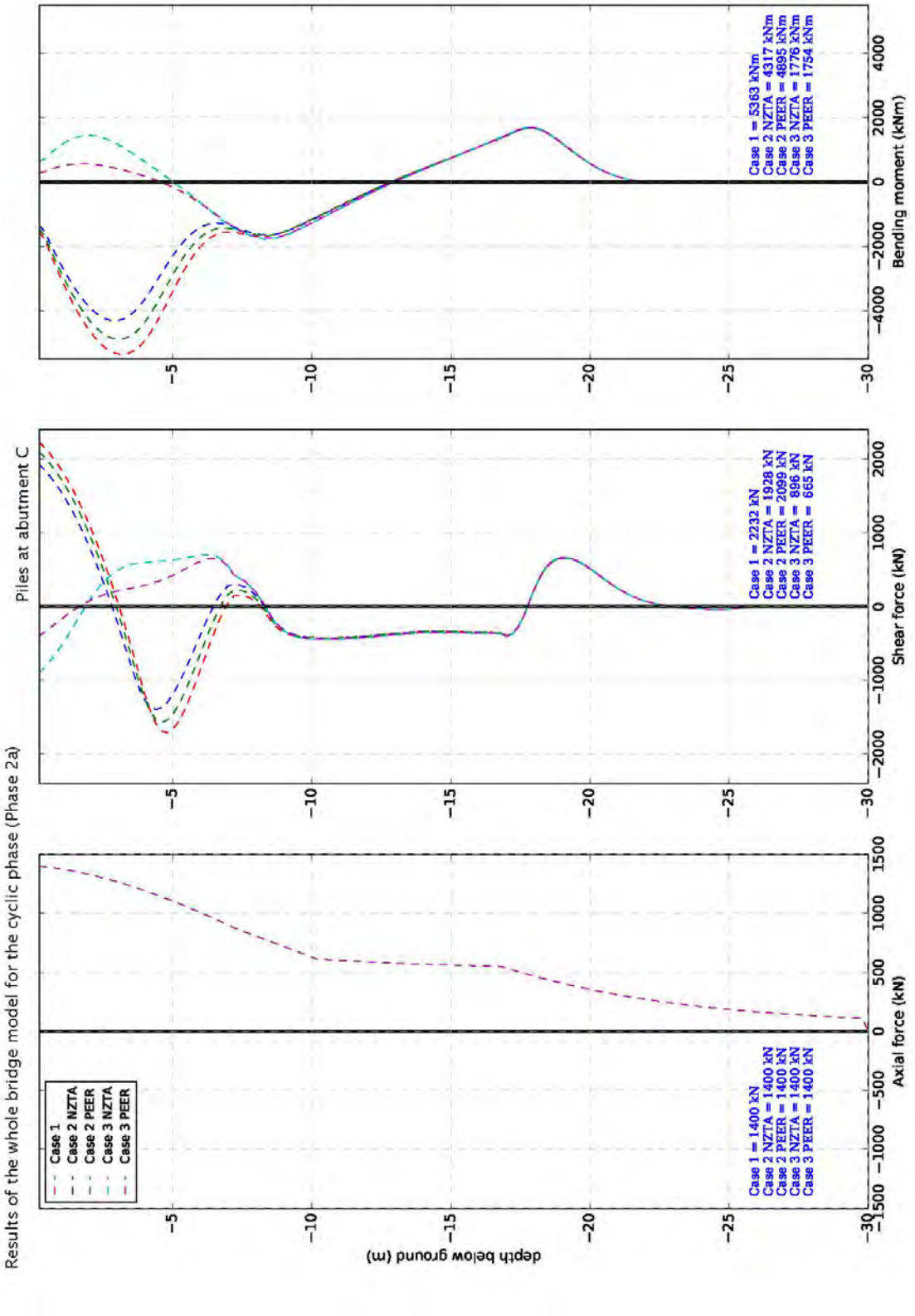
Results of the whole bridge model for the cyclic phase (Phase 2a)
Piles at abutment C
depth below ground (m)
Axial force (kN)
Shear force (kN)
Bending moment (kNm)
Case 1
Case 2 NZTA
Case 2 PEER
Case 3 NZTA
Case 3 PEER
Case 1 = 1400 kN
Case 2 NZTA = 1400 kN
Case 2 PEER = 1400 kN
Case 3 NZTA = 1400 kN
Case 3 PEER = 1400 kN
Case 1 = 2232 kN
Case 2 NZTA = 1928 kN
Case 2 PEER = 2099 kN
Case 3 NZTA = 896 kN
Case 3 PEER = 665 kN
Case 1 = 5363 kNm
Case 2 NZTA = 4317 kNm
Case 2 PEER = 4895 kNm
Case 3 NZTA = 1776 kNm
Case 3 PEER = 1754 kNm

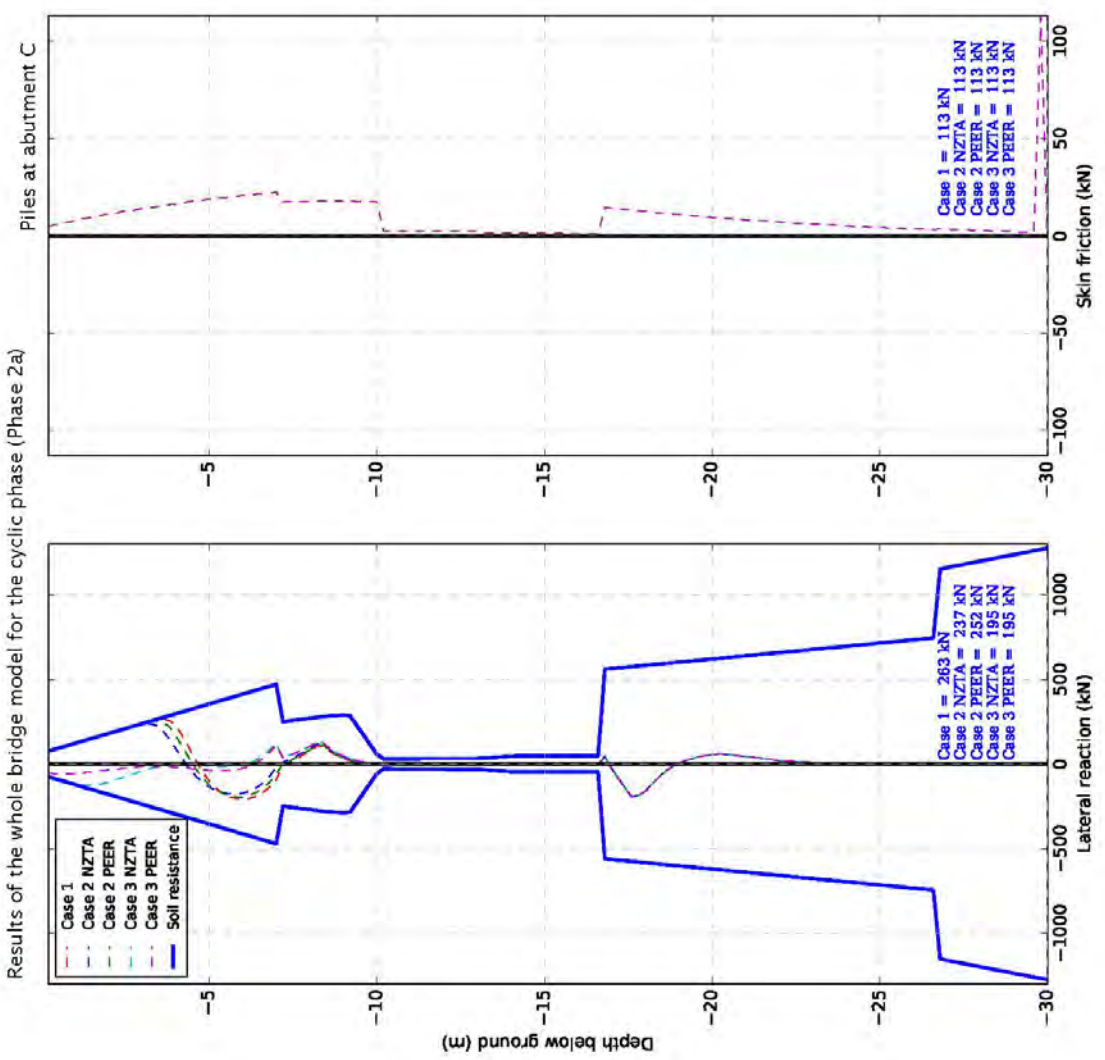
Results of the whole bridge model for the cyclic phase (Phase 2a)
Piles at abutment C
Depth below ground (m)
Lateral reaction (kN)
Skin friction (kN)
Case 1
Case 2 NZTA
Case 2 PEER
Case 3 NZTA
Case 3 PEER
Soil resistance
Case 1 = 263 kN
Case 2 NZTA = 237 kN
Case 2 PEER = 252 kN
Case 3 NZTA = 195 kN
Case 3 PEER = 195 kN
Case 1 = 113 kN
Case 2 NZTA = 113 kN
Case 2 PEER = 113 kN
Case 3 NZTA = 113 kN
Case 3 PEER = 113 kN

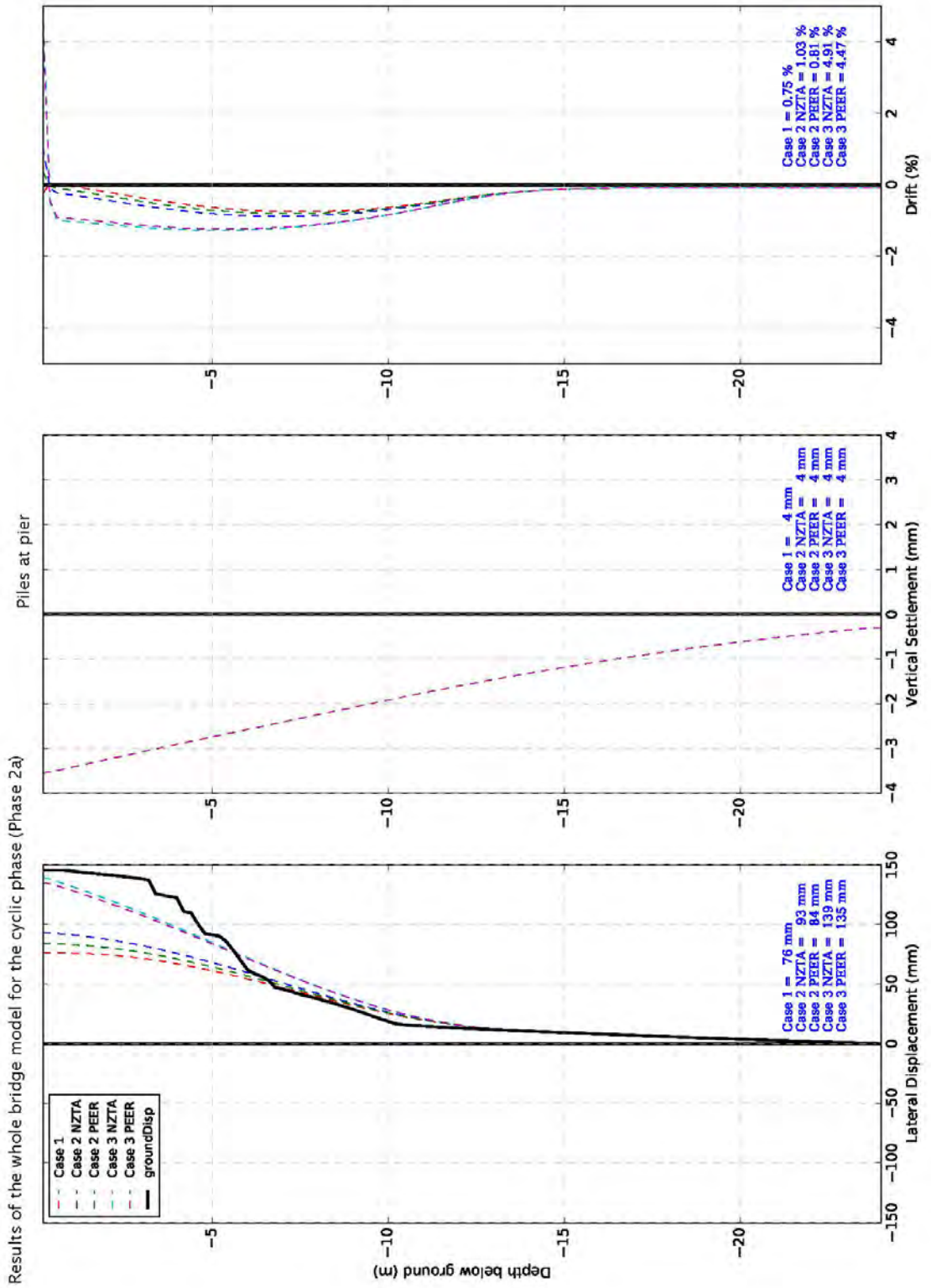
Results of the whole bridge model for the cyclic phase (Phase 2a)
Piles at pier
Depth below ground (m)
Lateral Displacement (mm)
Vertical Settlement (mm)
Drift (%)
Case 1
Case 2 NZTA
Case 2 PEER
Case 3 NZTA
Case 3 PEER
groundDisp
Case 1 = 76 mm
Case 2 NZTA = 93 mm
Case 2 PEER = 84 mm
Case 3 NZTA = 139 mm
Case 3 PEER = 135 mm
Case 1 = 4 mm
Case 2 NZTA = 4 mm
Case 2 PEER = 4 mm
Case 3 NZTA = 4 mm
Case 3 PEER = 4 mm
Case 1 = 0.75 %
Case 2 NZTA = 1.03 %
Case 2 PEER = 0.81 %
Case 3 NZTA = 4.91 %
Case 3 PEER = 4.47 %

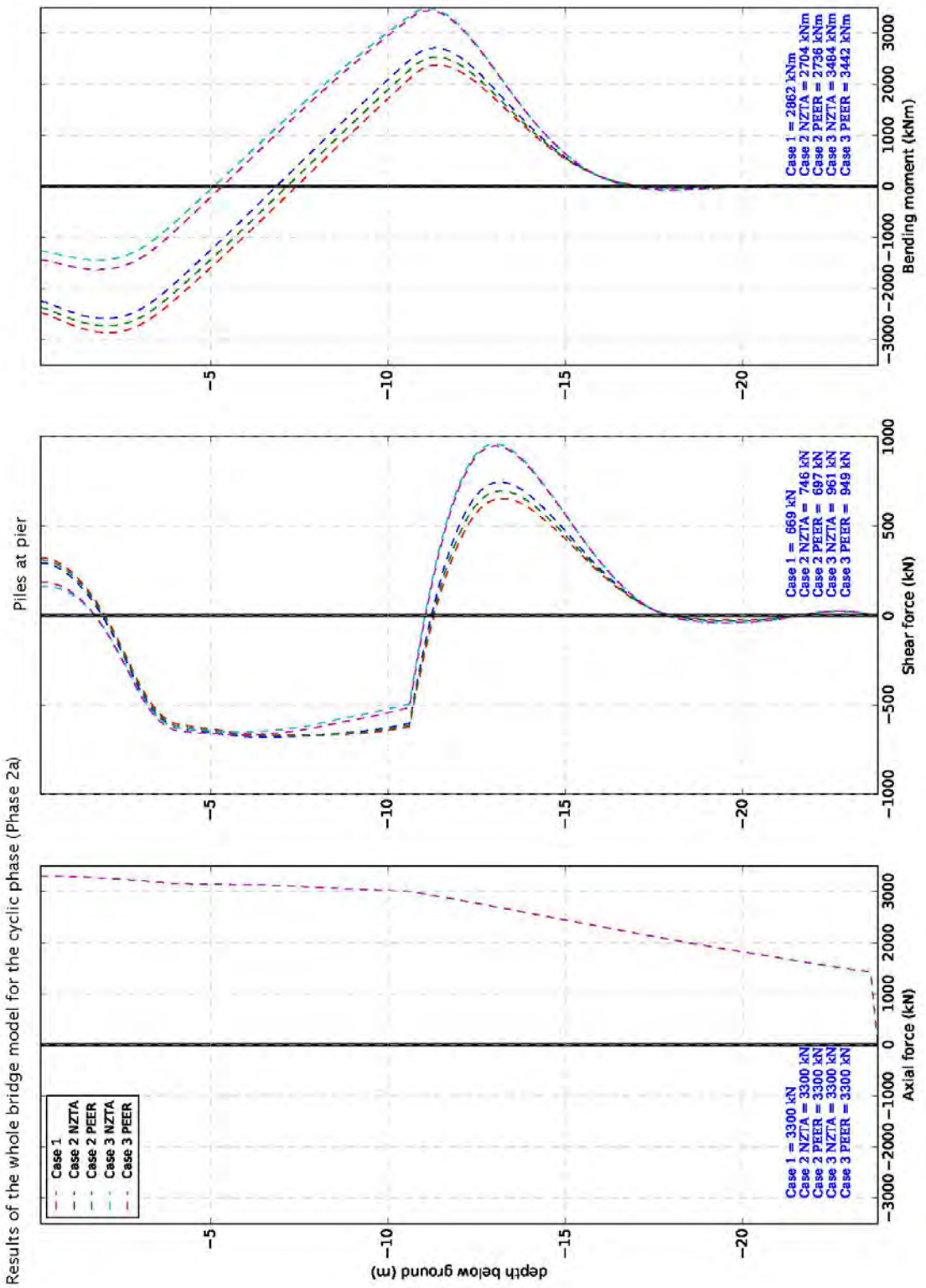
Results of the whole bridge model for the cyclic phase (Phase 2a)
Piles at pier
depth below ground (m)
Axial force (kN)
Shear force (kN)
Bending moment (kNm)
Case 1
Case 2 NZTA
Case 2 PEER
Case 3 NZTA
Case 3 PEER
Case 1 = 3300 kN
Case 2 NZTA = 3300 kN
Case 2 PEER = 3300 kN
Case 3 NZTA = 3300 kN
Case 3 PEER = 3300 kN
Case 1 = 669 kN
Case 2 NZTA = 746 kN
Case 2 PEER = 697 kN
Case 3 NZTA = 961 kN
Case 3 PEER = 949 kN
Case 1 = 2862 kNm
Case 2 NZTA = 2704 kNm
Case 2 PEER = 2736 kNm
Case 3 NZTA = 3464 kNm
Case 3 PEER = 3442 kNm

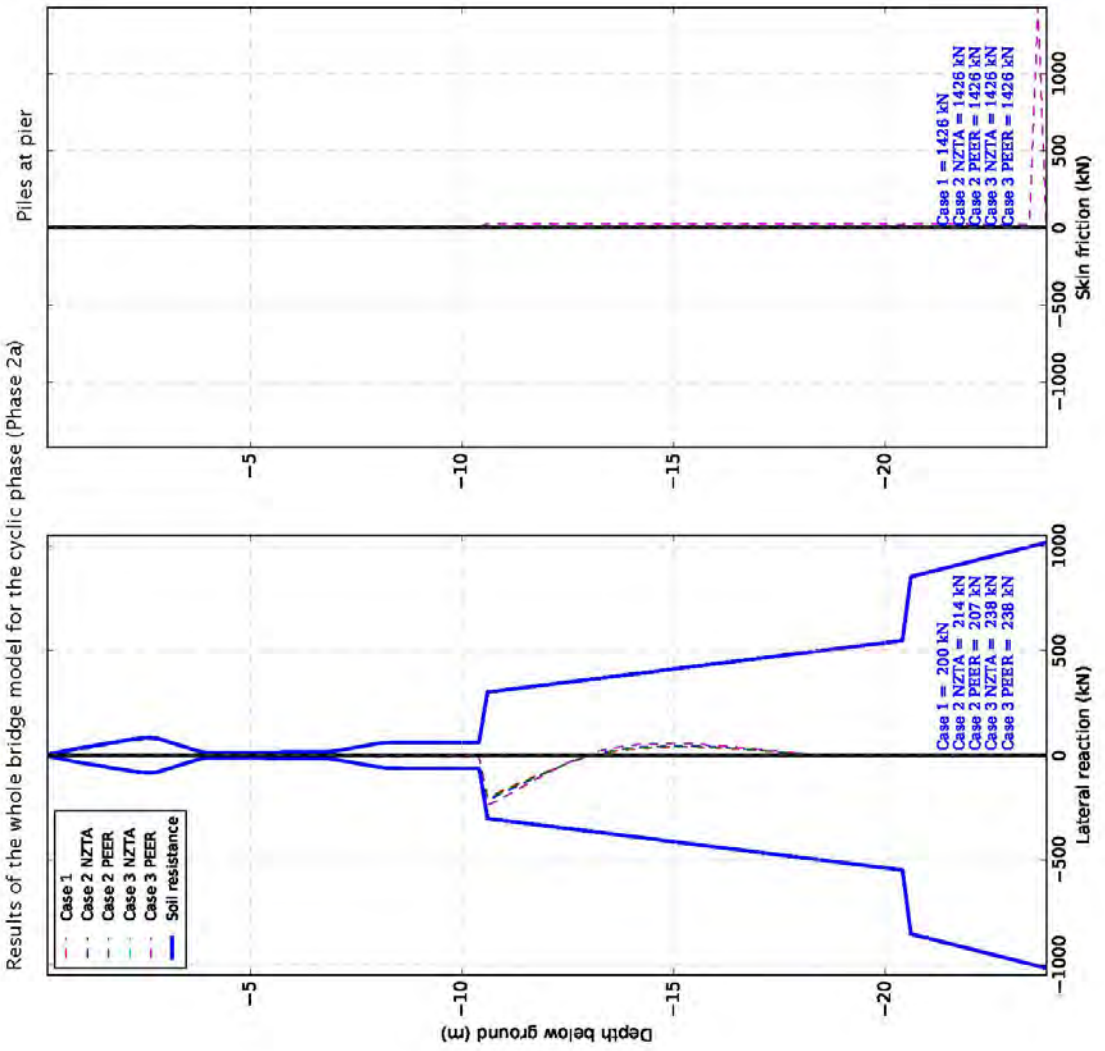
Results of the whole bridge model for the cyclic phase (Phase 2a)
Piles at pier
Depth below ground (m)
Lateral reaction (kN)
Skin friction (kN)
Case 1
Case 2 NZTA
Case 2 PEER
Case 3 NZTA
Case 3 PEER
Soil resistance
Case 1 = 200 kN
Case 2 NZTA = 214 kN
Case 2 PEER = 207 kN
Case 3 NZTA = 238 kN
Case 3 PEER = 238 kN
Case 1 = 1426 kN
Case 2 NZTA = 1426 kN
Case 2 PEER = 1426 kN
Case 3 NZTA = 1426 kN
Case 3 PEER = 1426 kN

A4 Results of the whole bridge model for the cyclic phase (Phase 2b)

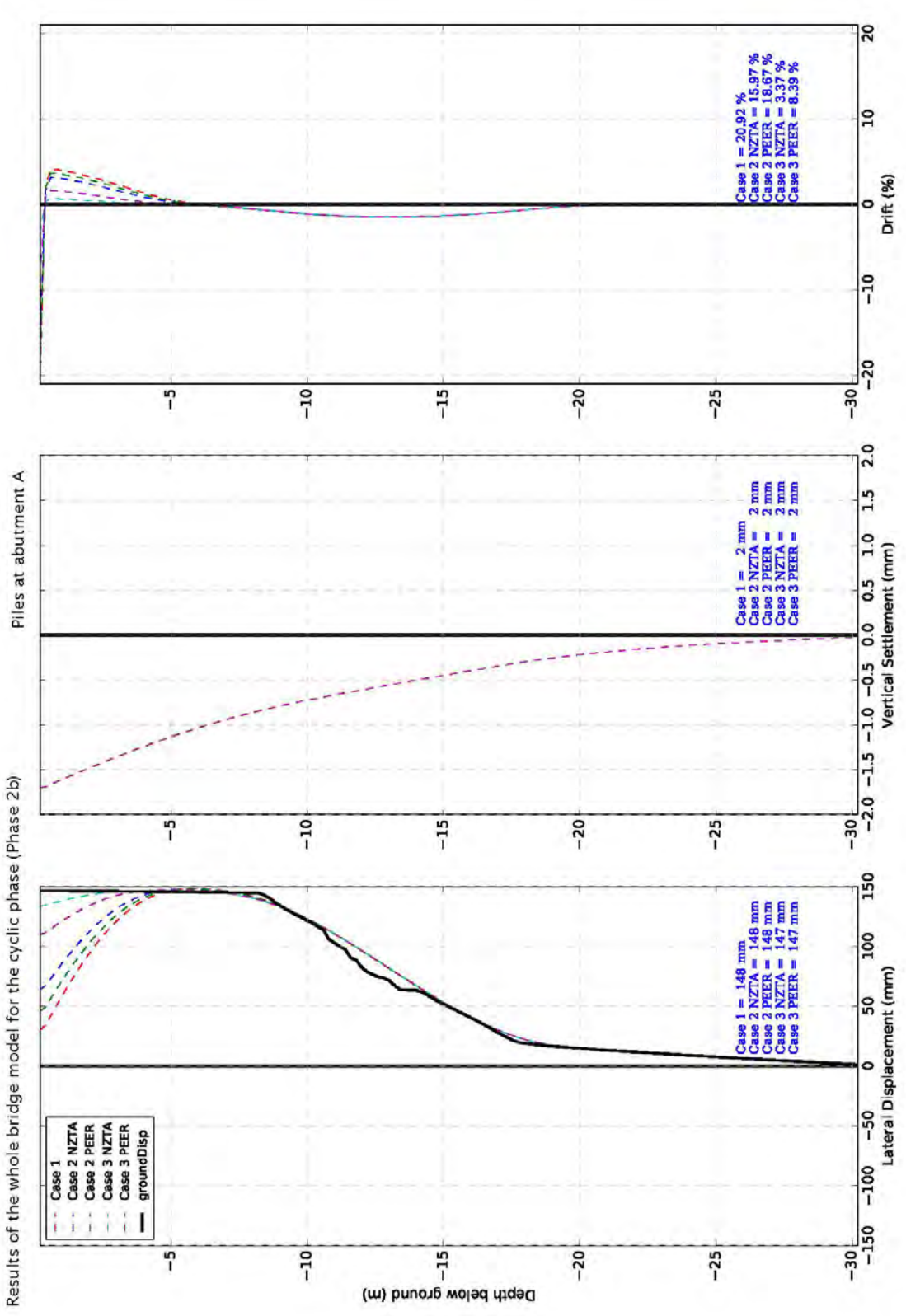

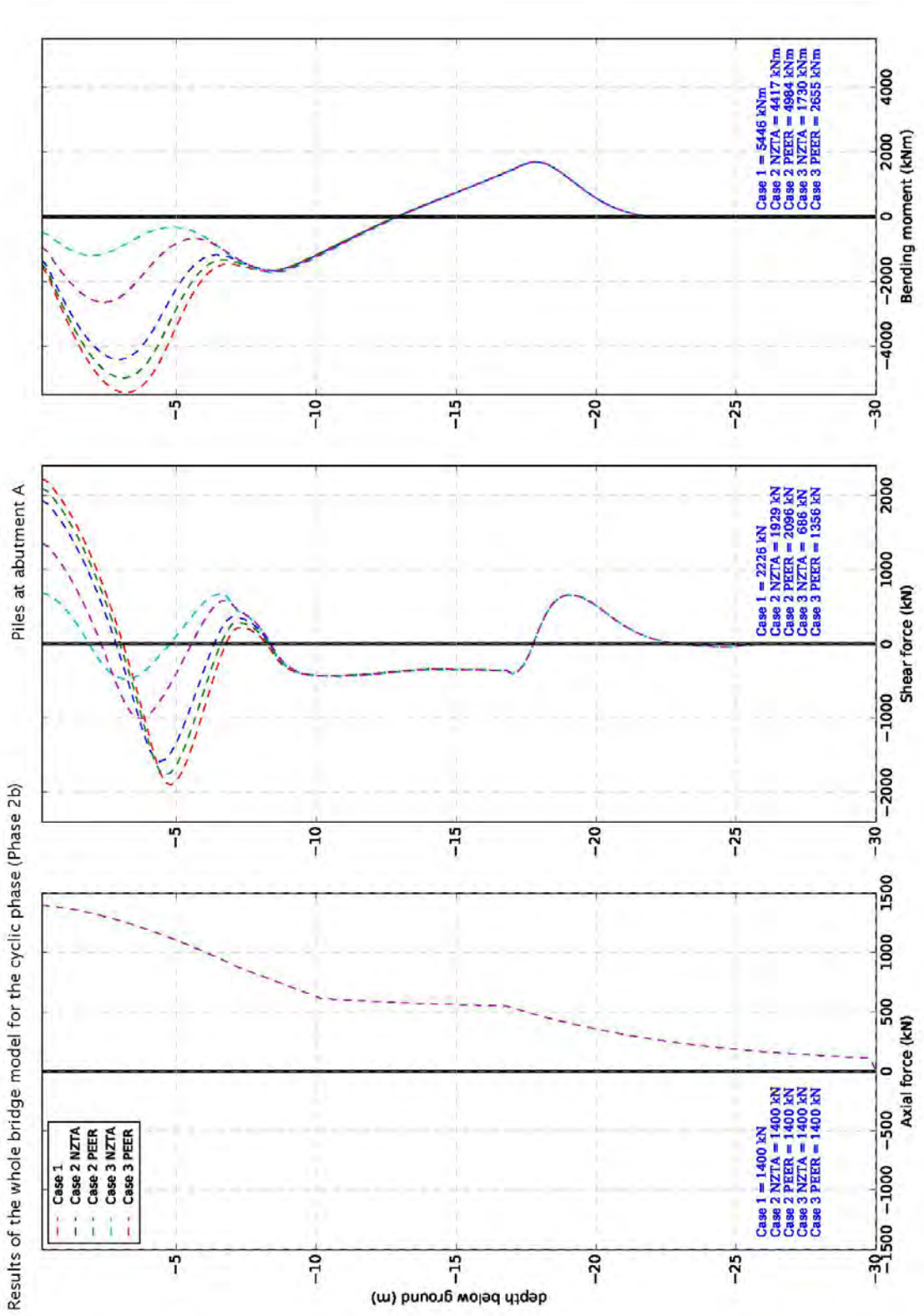
Results of the whole bridge model for the cyclic phase (Phase 2b)
Piles at abutment A
depth below ground (m)
Axial force (kN)
Shear force (kN)
Bending moment (kNm)
Case 1
Case 2 NZTA
Case 2 PEER
Case 3 NZTA
Case 3 PEER
Case 1 = 1400 kN
Case 2 NZTA = 1400 kN
Case 2 PEER = 1400 kN
Case 3 NZTA = 1400 kN
Case 3 PEER = 1400 kN
Case 1 = 2226 kN
Case 2 NZTA = 1929 kN
Case 2 PEER = 2096 kN
Case 3 NZTA = 686 kN
Case 3 PEER = 1356 kN
Case 1 = 5446 kNm
Case 2 NZTA = 4417 kNm
Case 2 PEER = 4984 kNm
Case 3 NZTA = 1730 kNm
Case 3 PEER = 2655 kNm

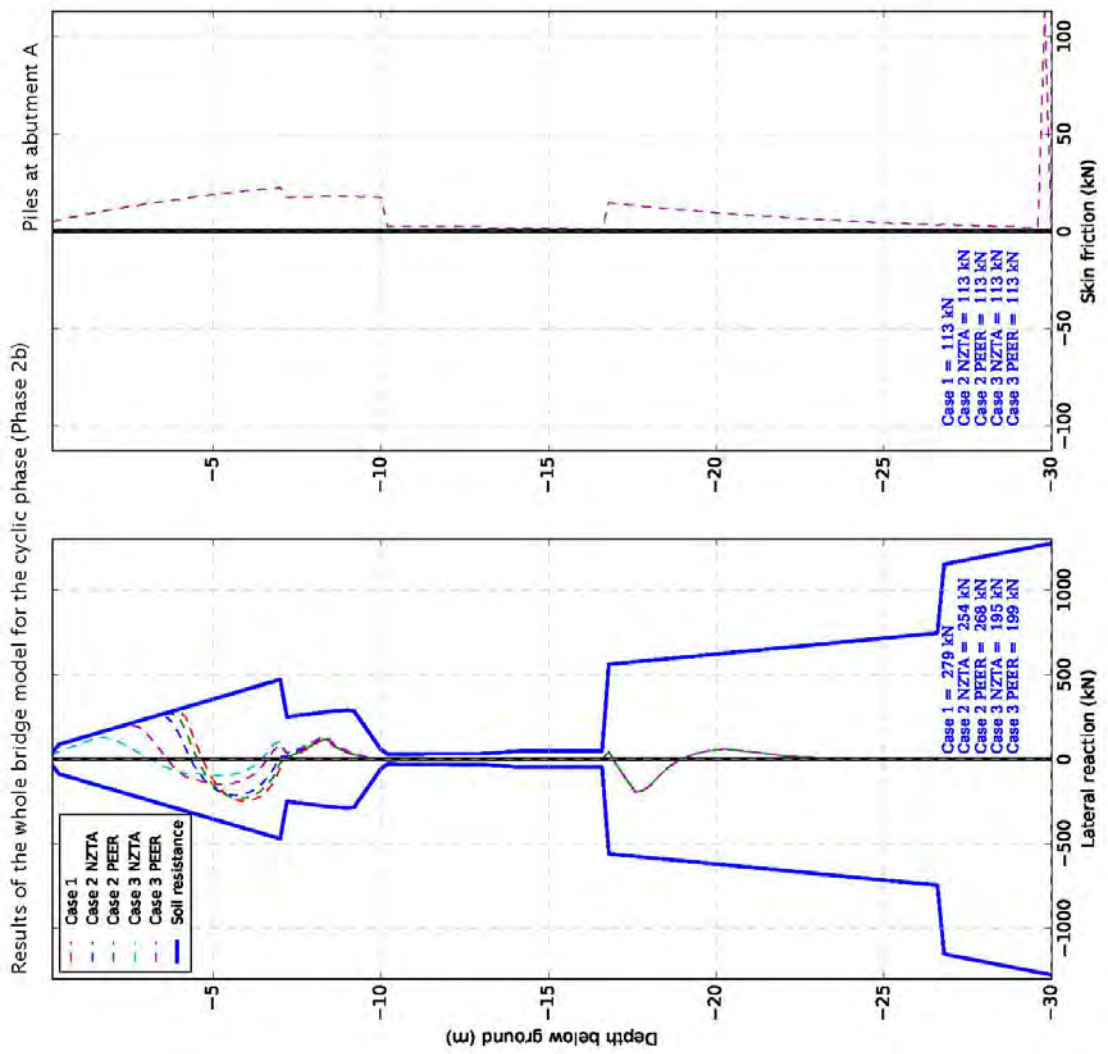
Results of the whole bridge model for the cyclic phase (Phase 2b)
Piles at abutment A
Depth below ground (m)
Lateral reaction (kN)
Skin friction (kN)
Case 1
Case 2 NZTA
Case 2 PEER
Case 3 NZTA
Case 3 PEER
Soil resistance
Case 1 = 279 kN
Case 2 NZTA = 254 kN
Case 2 PEER = 268 kN
Case 3 NZTA = 195 kN
Case 3 PEER = 199 kN
Case 1 = 113 kN
Case 2 NZTA = 113 kN
Case 2 PEER = 113 kN
Case 3 NZTA = 113 kN
Case 3 PEER = 113 kN

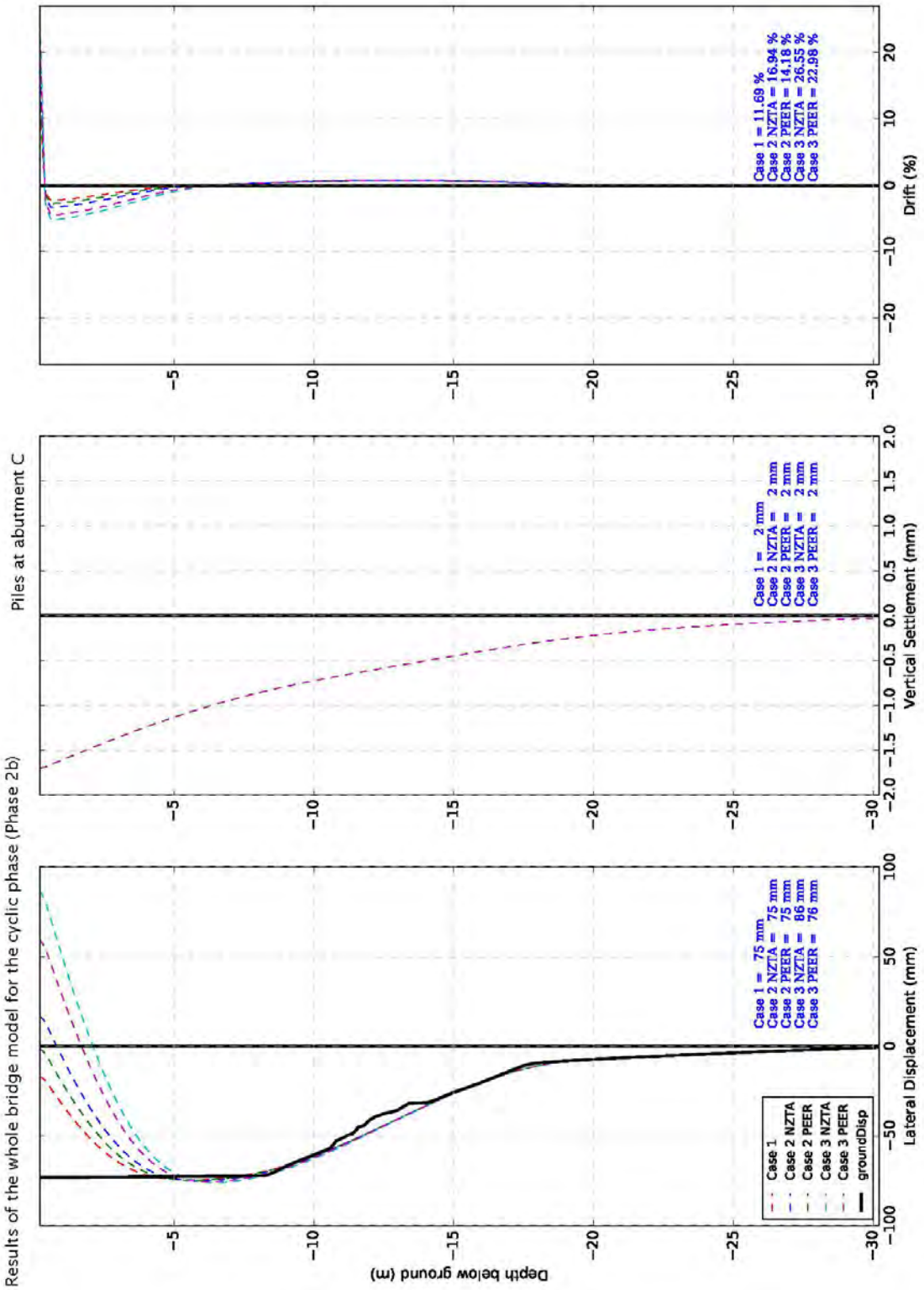
Results of the whole bridge model for the cyclic phase (Phase 2b)
Piles at abutment C
Depth below ground (m)
Lateral Displacement (mm)
Vertical Settlement (mm)
Drift (%)
Case 1
Case 2 NZTA
Case 2 PEER
Case 3 NZTA
Case 3 PEER
groundDisp
Case 1 = 75 mm
Case 2 NZTA = 75 mm
Case 2 PEER = 75 mm
Case 3 NZTA = 86 mm
Case 3 PEER = 76 mm
Case 1 = 2 mm
Case 2 NZTA = 2 mm
Case 2 PEER = 2 mm
Case 3 NZTA = 2 mm
Case 3 PEER = 2 mm
Case 1 = 11.69 %
Case 2 NZTA = 16.94 %
Case 2 PEER = 14.18 %
Case 3 NZTA = 26.55 %
Case 3 PEER = 22.98 %

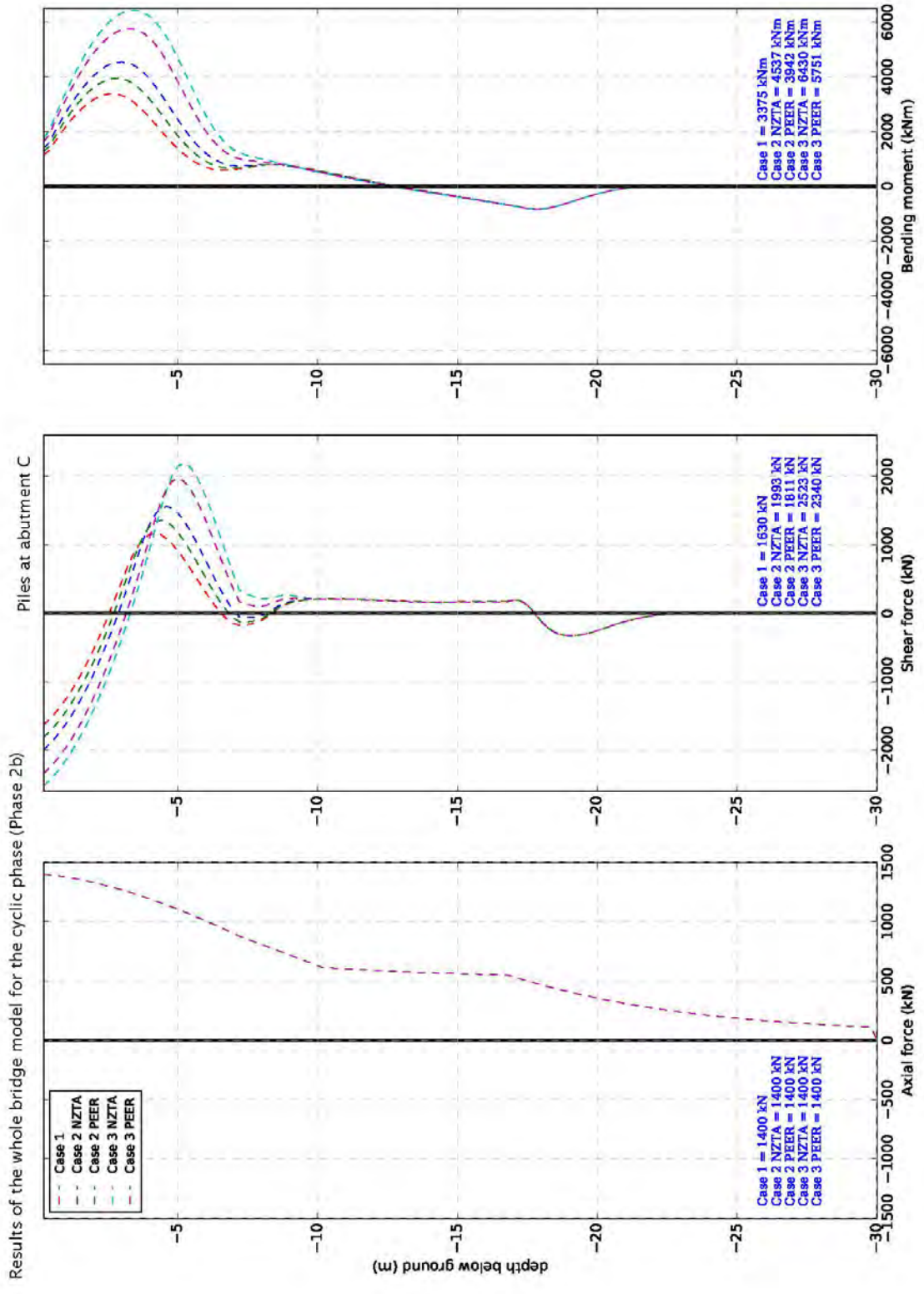
Results of the whole bridge model for the cyclic phase (Phase 2b)
Piles at abutment C
depth below ground (m)
Axial force (kN)
Shear force (kN)
Bending moment (kNm)
Case 1
Case 2 NZTA
Case 2 PEER
Case 3 NZTA
Case 3 PEER
Case 1 = 1400 kN
Case 2 NZTA = 1400 kN
Case 2 PEER = 1400 kN
Case 3 NZTA = 1400 kN
Case 3 PEER = 1400 kN
Case 1 = 1630 kN
Case 2 NZTA = 1993 kN
Case 2 PEER = 1611 kN
Case 3 NZTA = 2523 kN
Case 3 PEER = 2340 kN
Case 1 = 3375 kNm
Case 2 NZTA = 4537 kNm
Case 2 PEER = 3942 kNm
Case 3 NZTA = 6430 kNm
Case 3 PEER = 5751 kNm

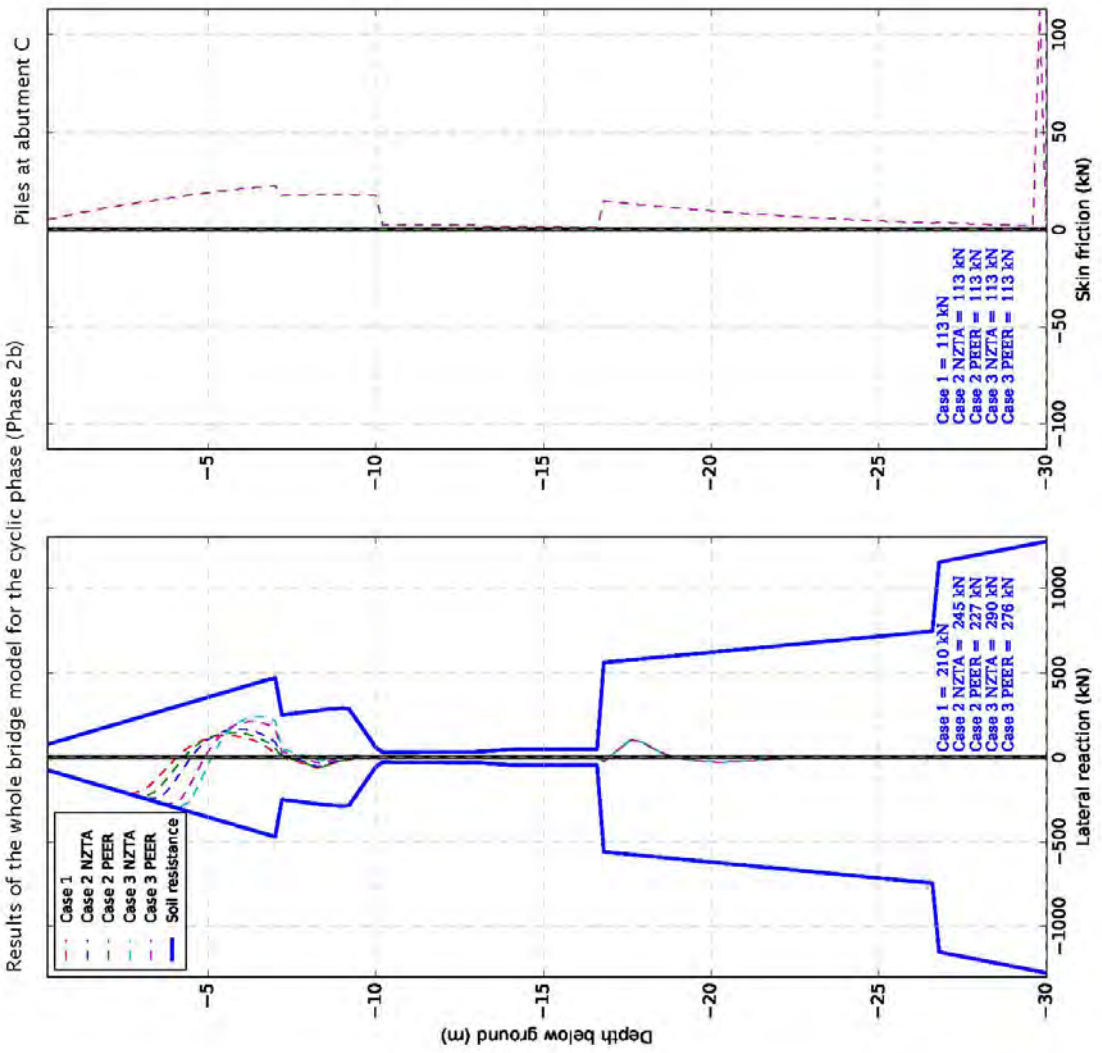
Results of the whole bridge model for the cyclic phase (Phase 2b)
Piles at abutment C
Depth below ground (m)
Lateral reaction (kN)
Skin friction (kN)
Case 1
Case 2 NZTA
Case 2 PEER
Case 3 NZTA
Case 3 PEER
Soil resistance
Case 1 = 210 kN
Case 2 NZTA = 245 kN
Case 2 PEER = 227 kN
Case 3 NZTA = 290 kN
Case 3 PEER = 276 kN
Case 1 = 113 kN
Case 2 NZTA = 113 kN
Case 2 PEER = 113 kN
Case 3 NZTA = 113 kN
Case 3 PEER = 113 kN

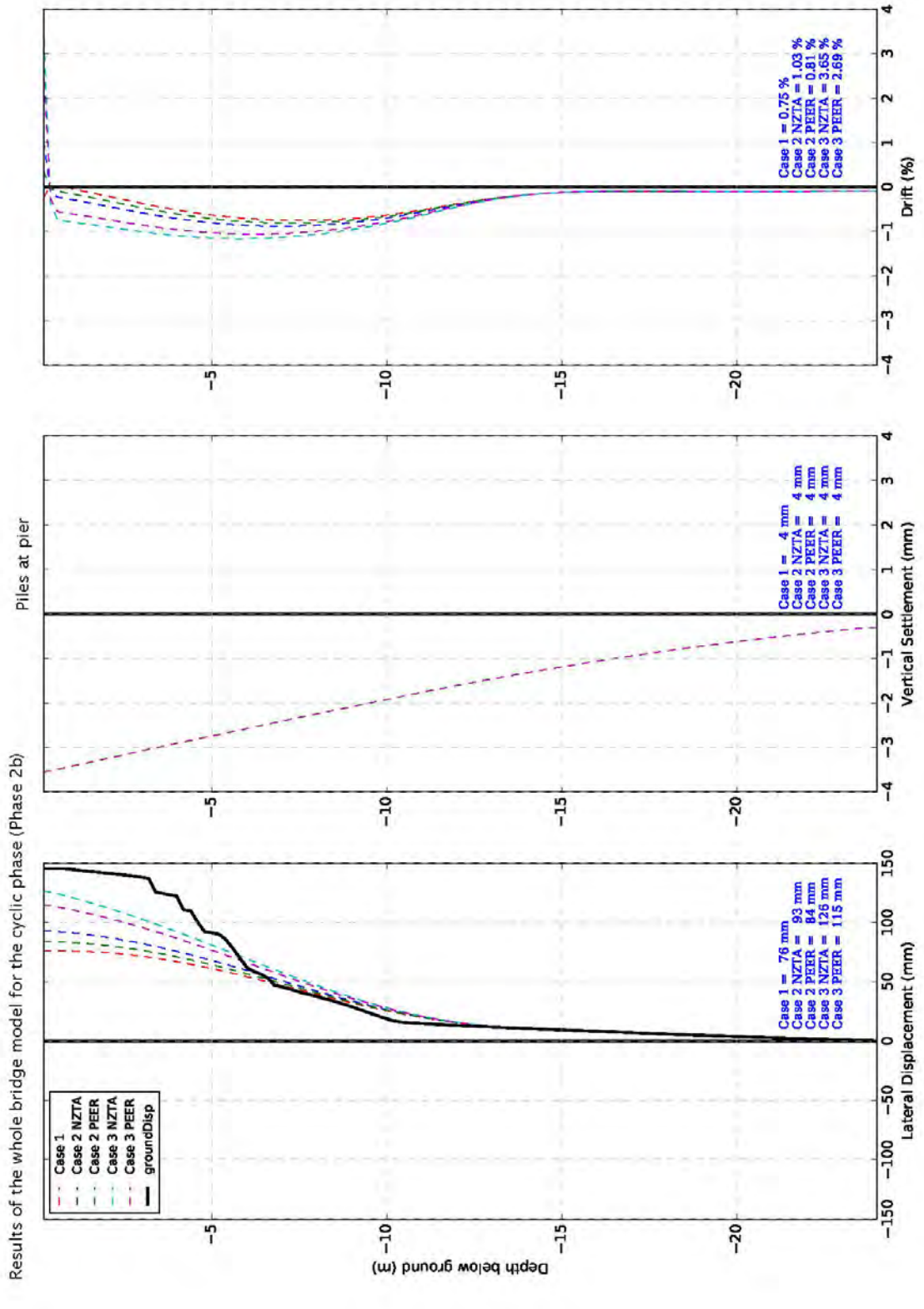
Results of the whole bridge model for the cyclic phase (Phase 2b)
Piles at pier
Depth below ground (m)
Lateral Displacement (mm)
Vertical Settlement (mm)
Drift (%)
Case 1
Case 2 NZTA
Case 2 PEER
Case 3 NZTA
Case 3 PEER
groundDisp
Case 1 = 76 mm
Case 2 NZTA = 93 mm
Case 2 PEER = 84 mm
Case 3 NZTA = 126 mm
Case 3 PEER = 115 mm
Case 1 = 4 mm
Case 2 NZTA = 4 mm
Case 2 PEER = 4 mm
Case 3 NZTA = 4 mm
Case 3 PEER = 4 mm
Case 1 = 0.75 %
Case 2 NZTA = 1.03 %
Case 2 PEER = 0.81 %
Case 3 NZTA = 3.65 %
Case 3 PEER = 2.69 %

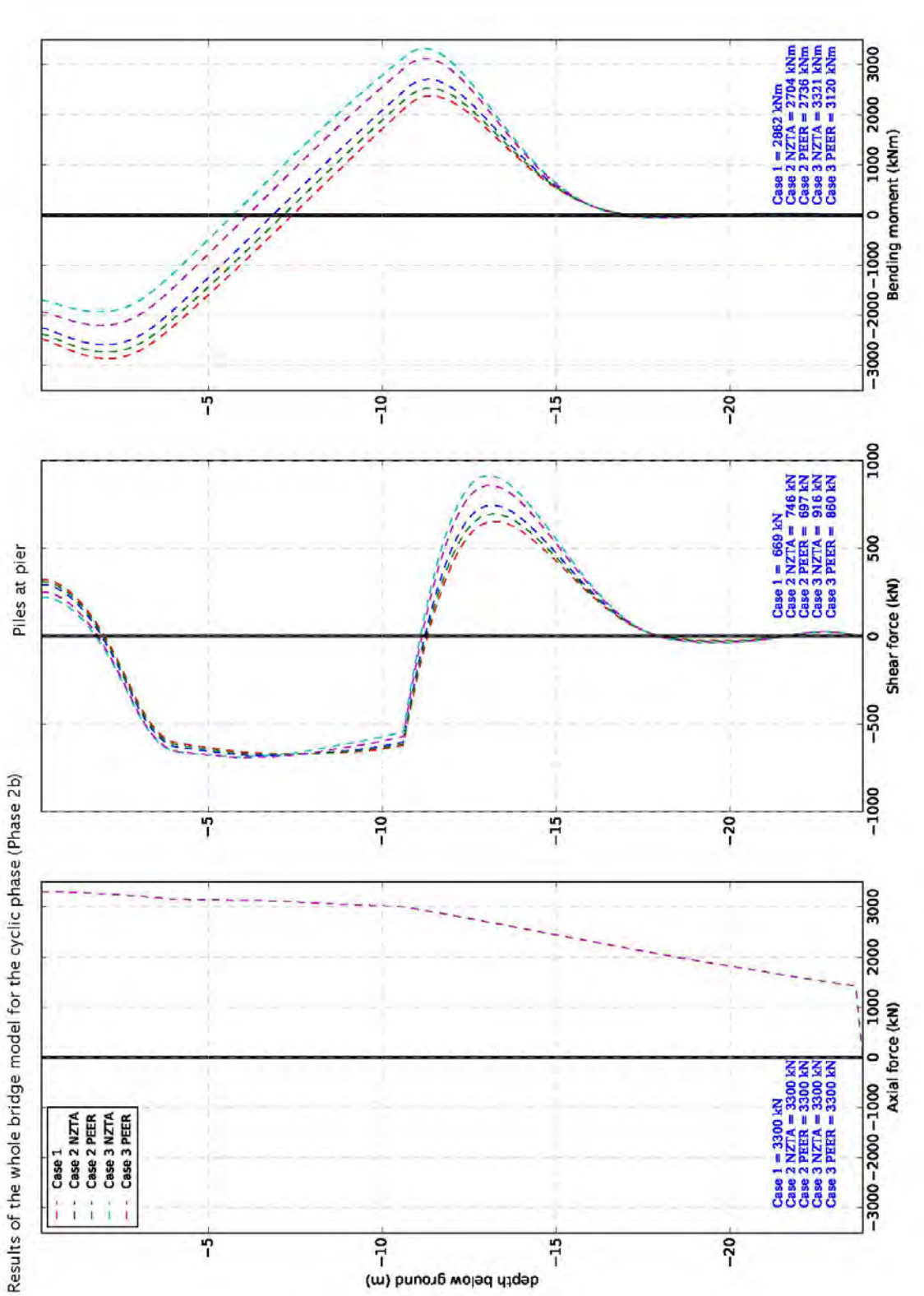
Results of the whole bridge model for the cyclic phase (Phase 2b)
Piles at pier
depth below ground (m)
Axial force (kN)
Shear force (kN)
Bending moment (kNm)
Case 1
Case 2 NZTA
Case 2 PEER
Case 3 NZTA
Case 3 PEER
Case 1 = 3300 kN
Case 2 NZTA = 3300 kN
Case 2 PEER = 3300 kN
Case 3 NZTA = 3300 kN
Case 3 PEER = 3300 kN
Case 1 = 669 kN
Case 2 NZTA = 746 kN
Case 2 PEER = 697 kN
Case 3 NZTA = 916 kN
Case 3 PEER = 860 kN
Case 1 = 2862 kNm
Case 2 NZTA = 2704 kNm
Case 2 PEER = 2736 kNm
Case 3 NZTA = 3321 kNm
Case 3 PEER = 3120 kNm

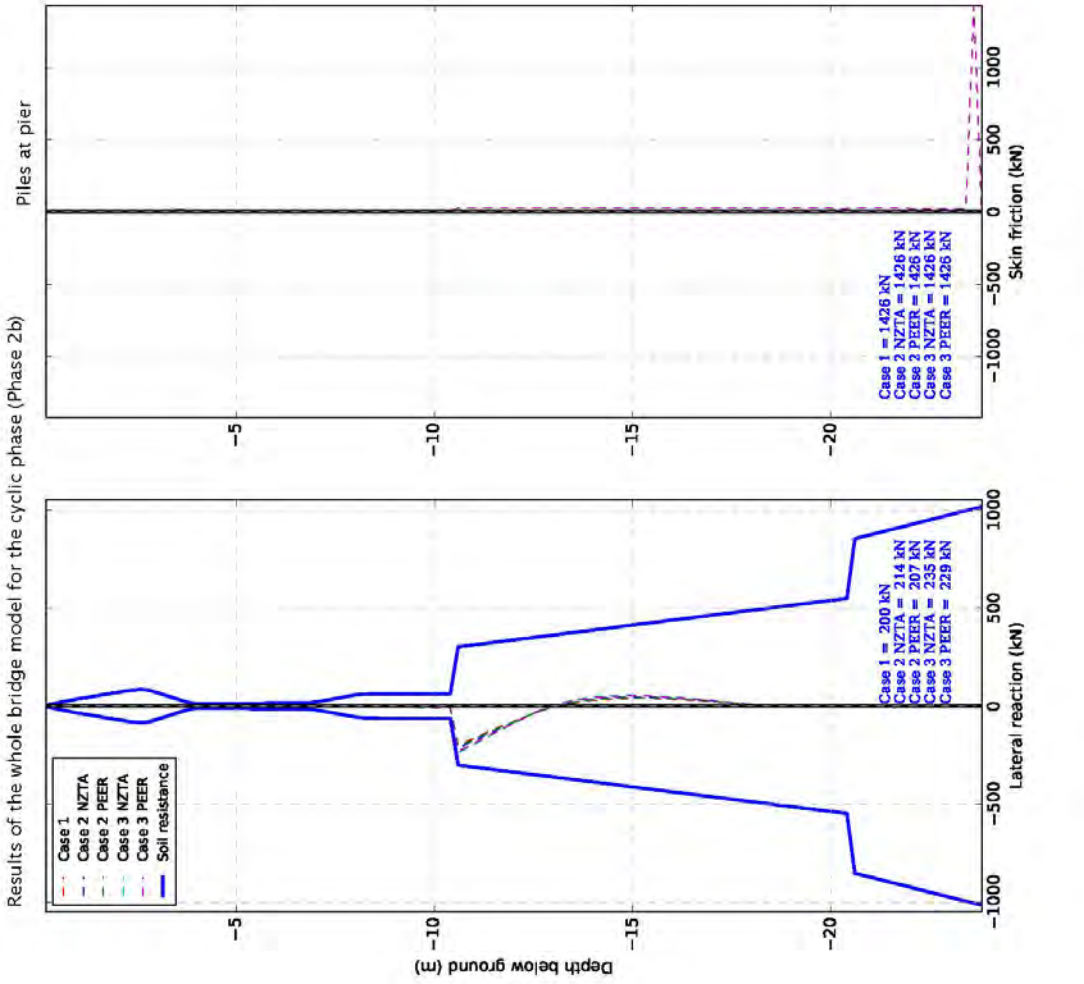
Results of the whole bridge model for the cyclic phase (Phase 2b)
Piles at pier
Depth below ground (m)
Lateral reaction (kN)
Skin friction (kN)
Case 1
Case 2 NZTA
Case 2 PEER
Case 3 NZTA
Case 3 PEER
Soil resistance
Case 1 = 200 kN
Case 2 NZTA = 214 kN
Case 2 PEER = 207 kN
Case 3 NZTA = 235 kN
Case 3 PEER = 229 kN
Case 1 = 1426 kN
Case 2 NZTA = 1426 kN
Case 2 PEER = 1426 kN
Case 3 NZTA = 1426 kN
Case 3 PEER = 1426 kN

A5 Results of the single model for the lateral spreading phase (Phase 3)

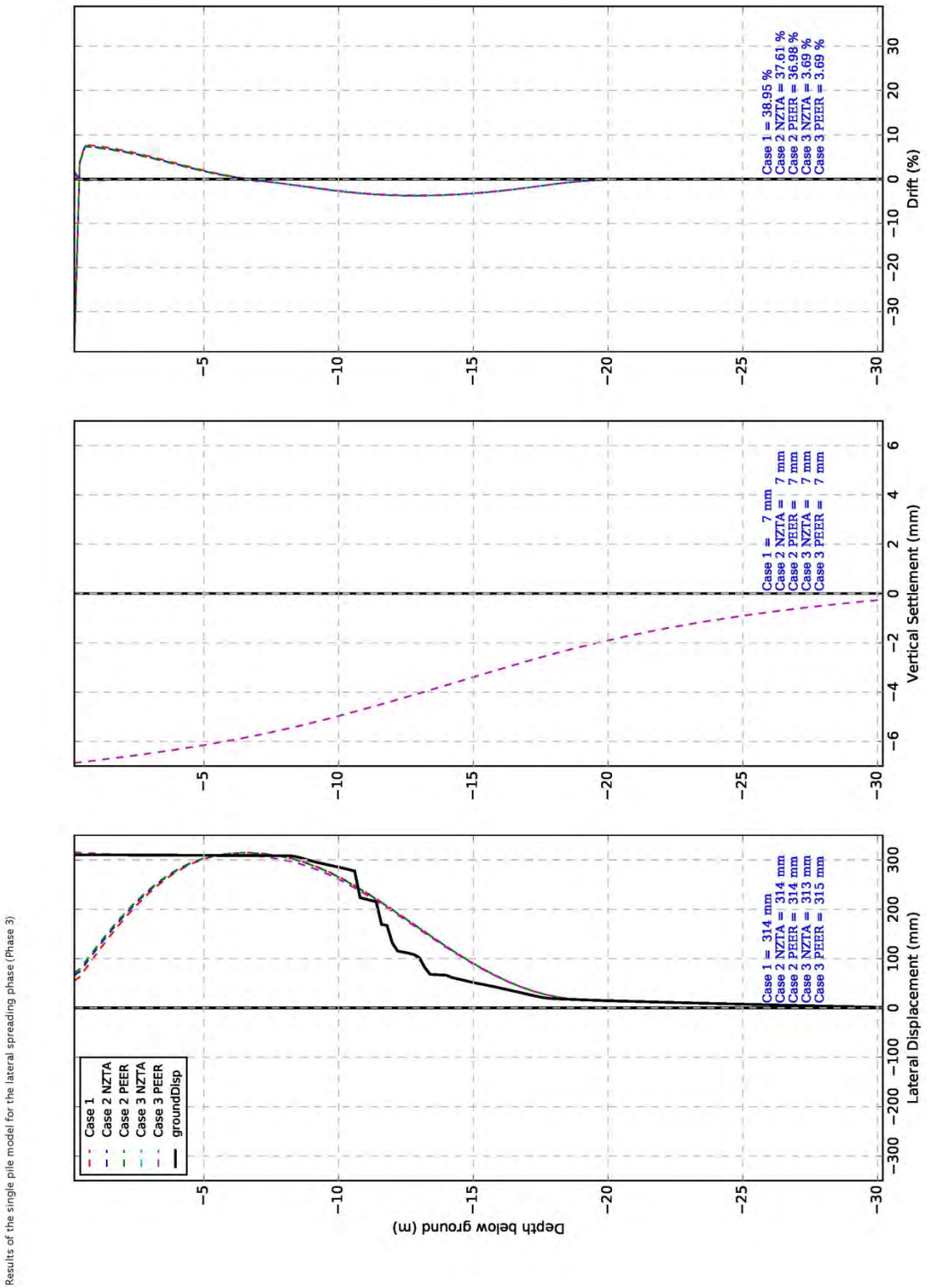

Results of the single pile model for the lateral spreading phase (Phase 3)

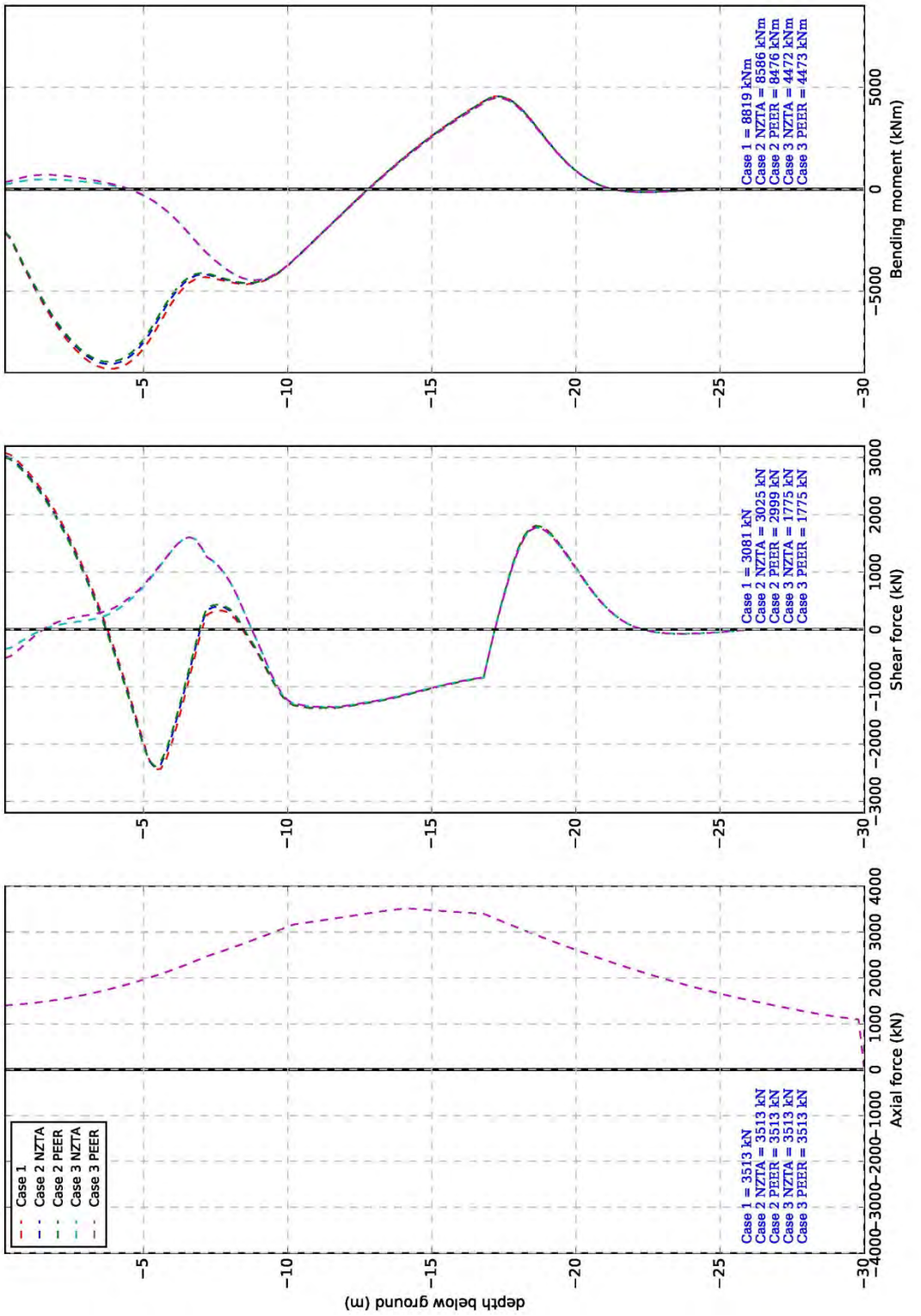

Results of the single pile model for the lateral spreading phase (Phase 3)

Results of the single pile model for the lateral spreading phase (Phase 3)

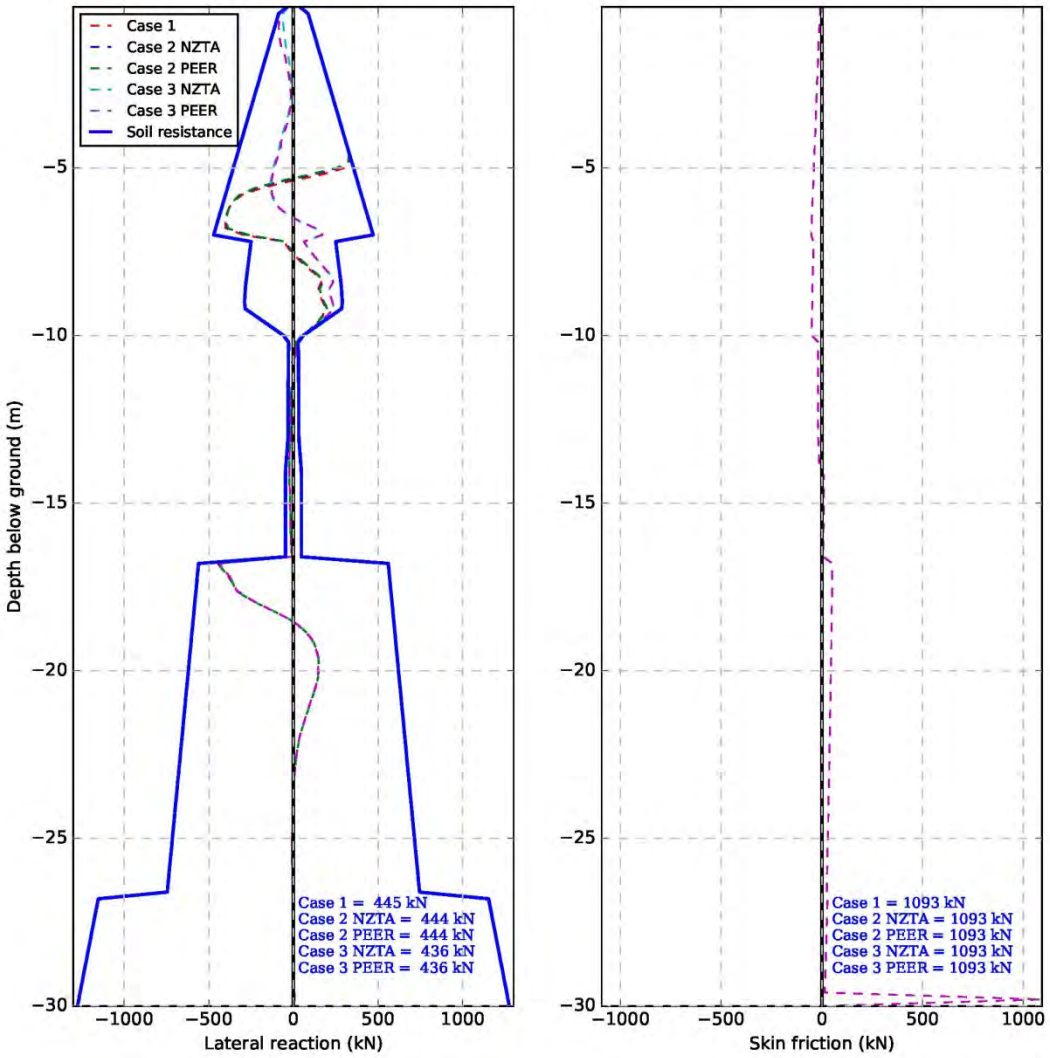

A6 Results of the whole bridge model for the lateral spreading phase (Phase 3a)

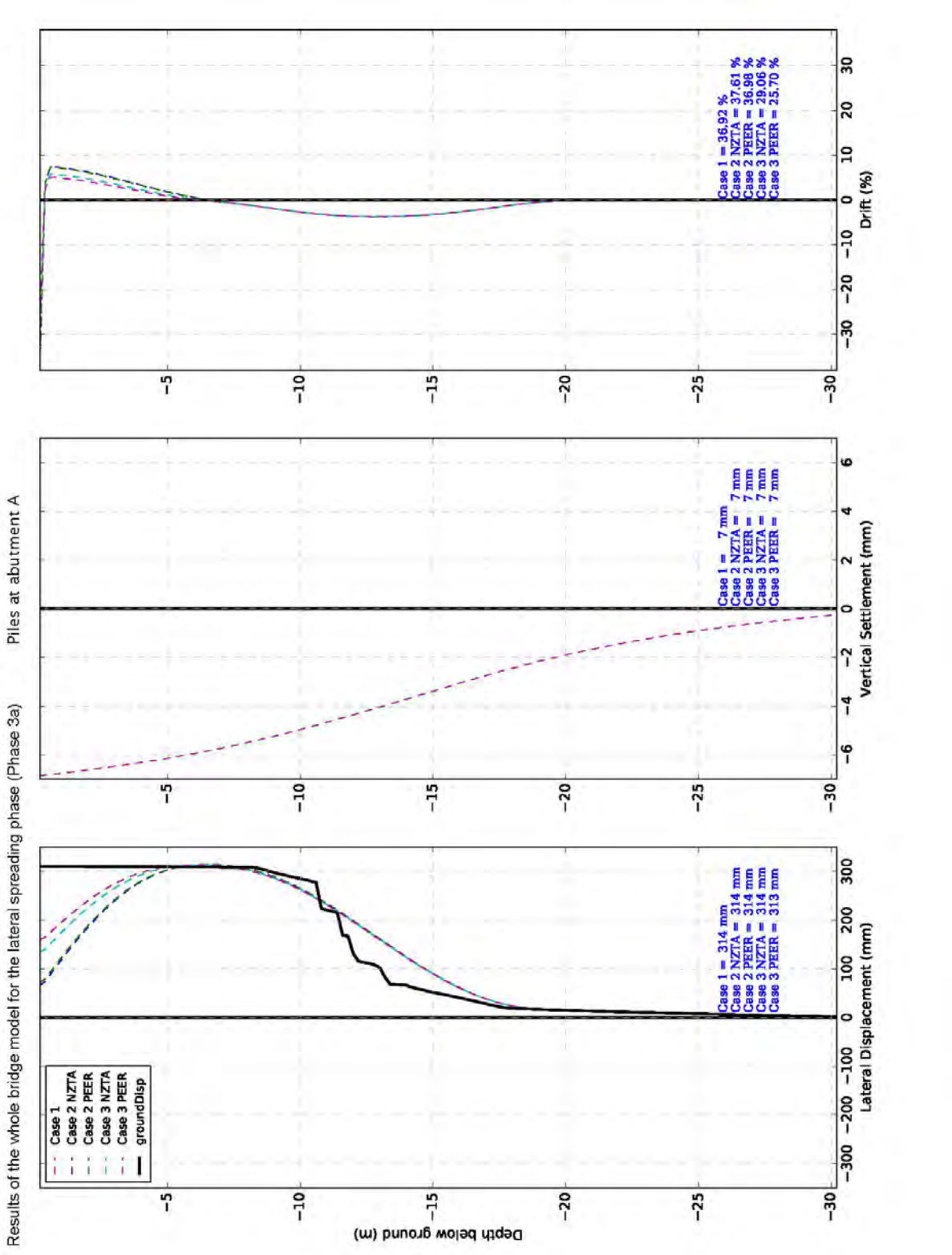

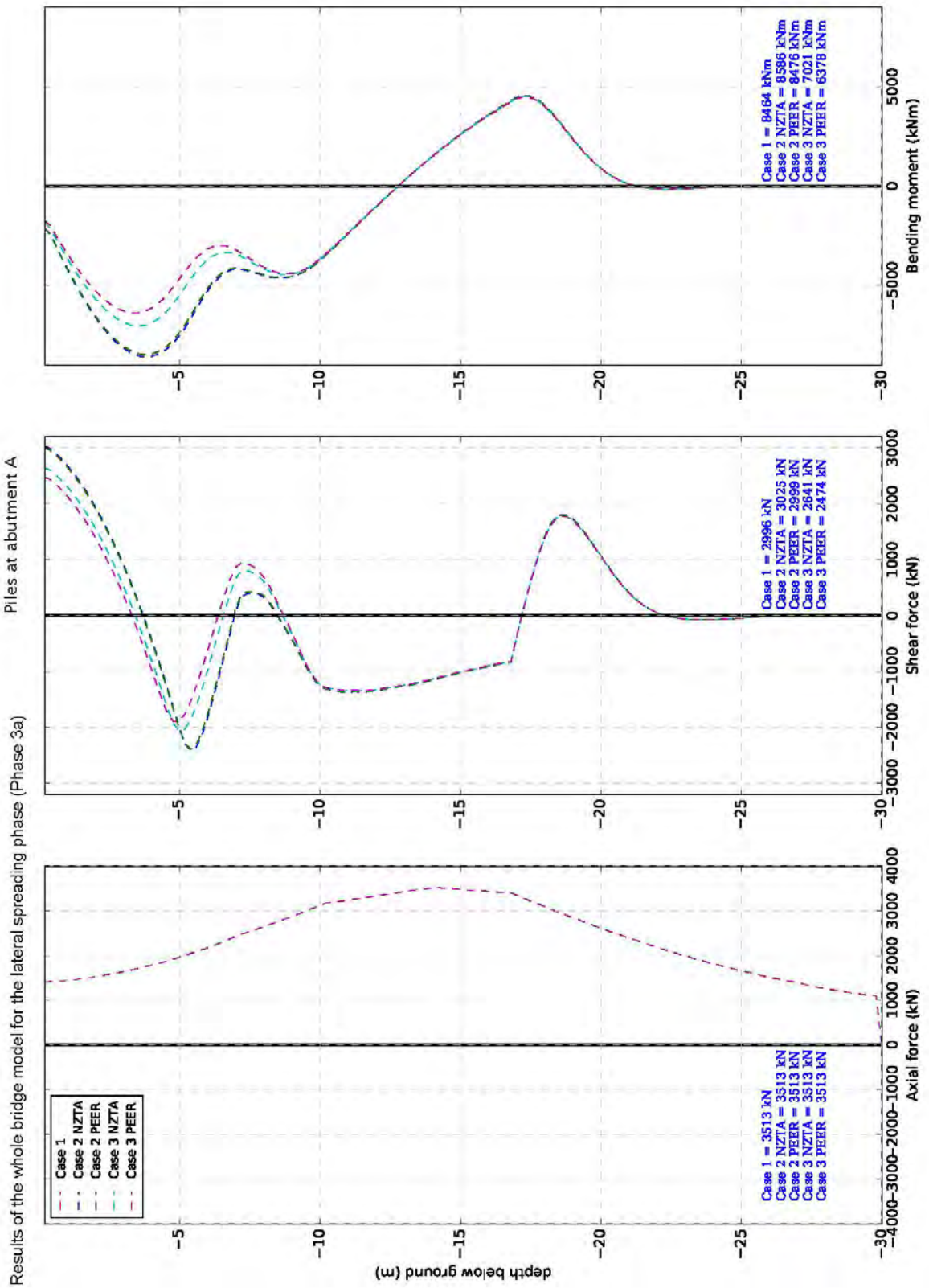
Results of the whole bridge model for the lateral spreading phase (Phase 3a)
Piles at abutment A
depth below ground (m)
Axial force (kN)
Shear force (kN)
Bending moment (kNm)
Case 1
Case 2 NZTA
Case 2 PEER
Case 3 NZTA
Case 3 PEER
Case 1 = 3513 kN
Case 2 NZTA = 3513 kN
Case 2 PEER = 3513 kN
Case 3 NZTA = 3513 kN
Case 3 PEER = 3513 kN
Case 1 = 2996 kN
Case 2 NZTA = 3025 kN
Case 2 PEER = 2999 kN
Case 3 NZTA = 2641 kN
Case 3 PEER = 2474 kN
Case 1 = 8464 kNm
Case 2 NZTA = 8586 kNm
Case 2 PEER = 8476 kNm
Case 3 NZTA = 7021 kNm
Case 3 PEER = 6378 kNm

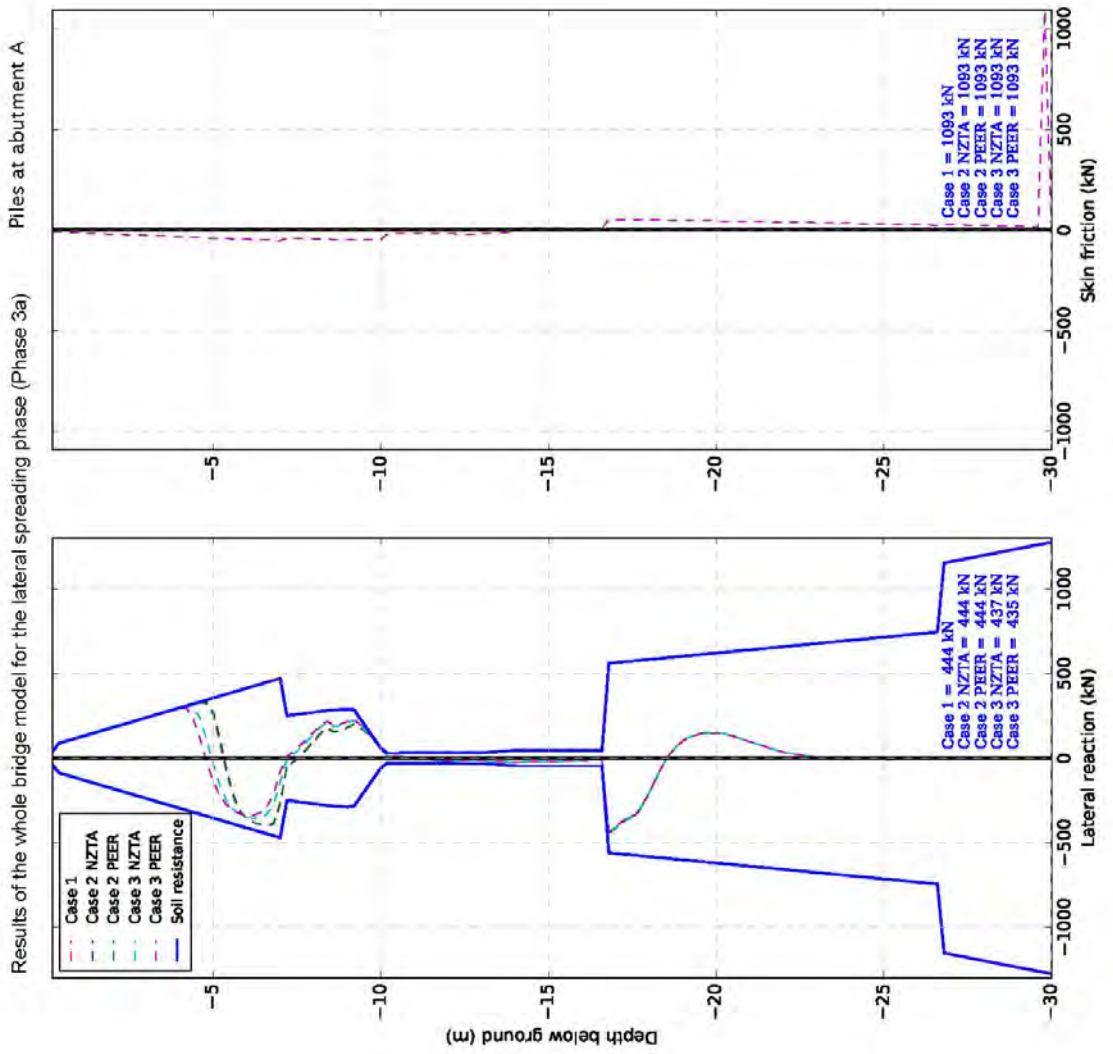
Results of the whole bridge model for the lateral spreading phase (Phase 3a)
Piles at abutment A
Depth below ground (m)
Lateral reaction (kN)
Skin friction (kN)
Case 1
Case 2 NZTA
Case 2 PEER
Case 3 NZTA
Case 3 PEER
Soil resistance
Case 1 = 444 kN
Case 2 NZTA = 444 kN
Case 2 PEER = 444 kN
Case 3 NZTA = 437 kN
Case 3 PEER = 435 kN
Case 1 = 1093 kN
Case 2 NZTA = 1093 kN
Case 2 PEER = 1093 kN
Case 3 NZTA = 1093 kN
Case 3 PEER = 1093 kN

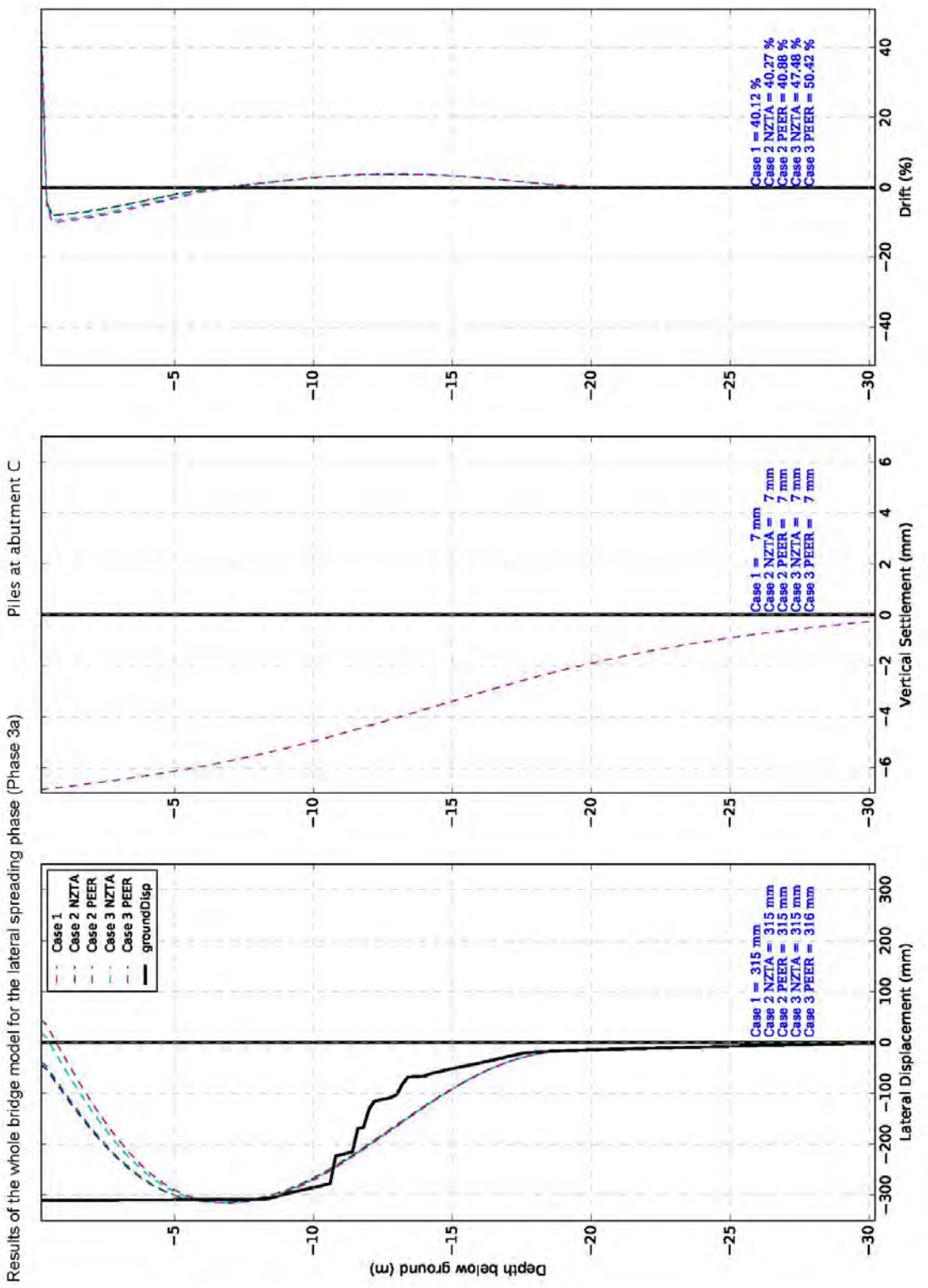
Results of the whole bridge model for the lateral spreading phase (Phase 3a)
Piles at abutment C
Depth below ground (m)
Lateral Displacement (mm)
Vertical Settlement (mm)
Drift (%)
Case 1
Case 2 NZTA
Case 2 PEER
Case 3 NZTA
Case 3 PEER
groundDisp
Case 1 = 315 mm
Case 2 NZTA = 315 mm
Case 2 PEER = 315 mm
Case 3 NZTA = 315 mm
Case 3 PEER = 316 mm
Case 1 = 7 mm
Case 2 NZTA = 7 mm
Case 2 PEER = 7 mm
Case 3 NZTA = 7 mm
Case 3 PEER = 7 mm
Case 1 = 40.12 %
Case 2 NZTA = 40.27 %
Case 2 PEER = 40.88 %
Case 3 NZTA = 47.48 %
Case 3 PEER = 50.42 %

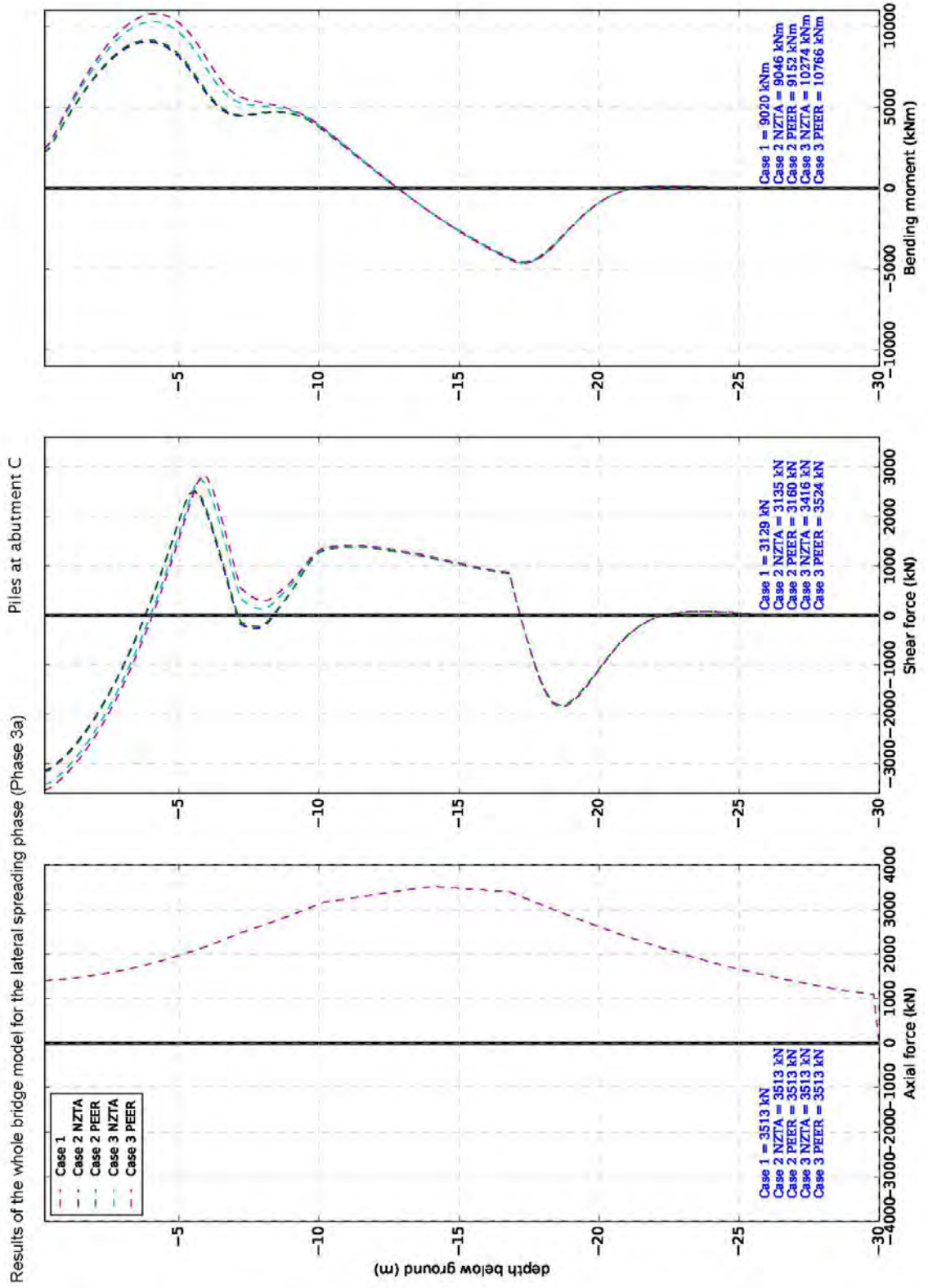
Results of the whole bridge model for the lateral spreading phase (Phase 3a)
Piles at abutment C
depth below ground (m)
Axial force (kN)
Shear force (kN)
Bending moment (kNm)
Case 1
Case 2 NZTA
Case 2 PEER
Case 3 NZTA
Case 3 PEER
Case 1 = 3513 kN
Case 2 NZTA = 3513 kN
Case 2 PEER = 3513 kN
Case 3 NZTA = 3513 kN
Case 3 PEER = 3513 kN
Case 1 = 3129 kN
Case 2 NZTA = 3135 kN
Case 2 PEER = 3160 kN
Case 3 NZTA = 3416 kN
Case 3 PEER = 3524 kN
Case 1 = 9020 kNm
Case 2 NZTA = 9046 kNm
Case 2 PEER = 9152 kNm
Case 3 NZTA = 10274 kNm
Case 3 PEER = 10766 kNm

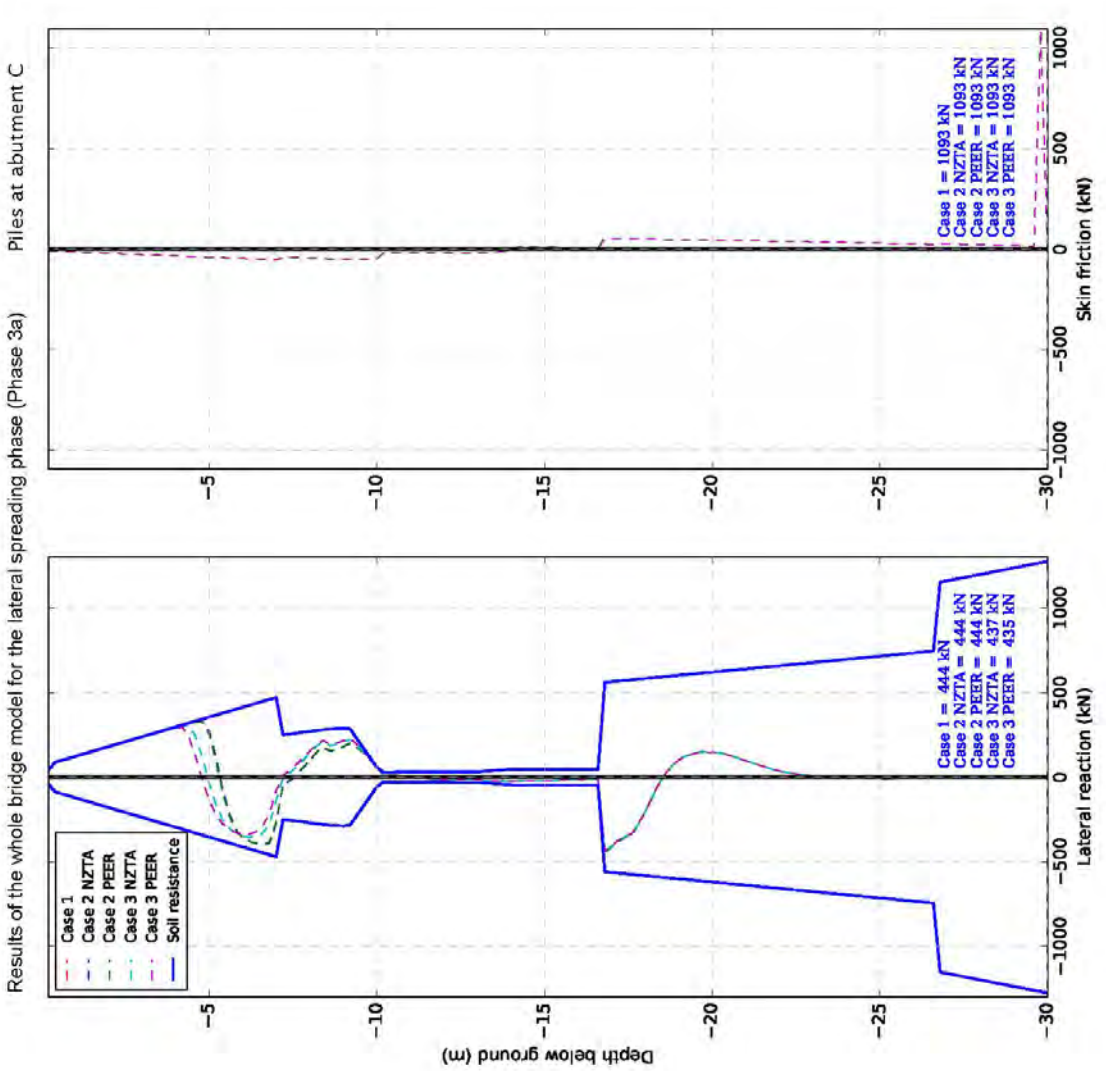
Results of the whole bridge model for the lateral spreading phase (Phase 3a)
Piles at abutment C
Depth below ground (m)
Lateral reaction (kN)
Skin friction (kN)
Case 1
Case 2 NZTA
Case 2 PEER
Case 3 NZTA
Case 3 PEER
Soil resistance
Case 1 = 444 kN
Case 2 NZTA = 444 kN
Case 2 PEER = 444 kN
Case 3 NZTA = 437 kN
Case 3 PEER = 435 kN
Case 1 = 1093 kN
Case 2 NZTA = 1093 kN
Case 2 PEER = 1093 kN
Case 3 NZTA = 1093 kN
Case 3 PEER = 1093 kN

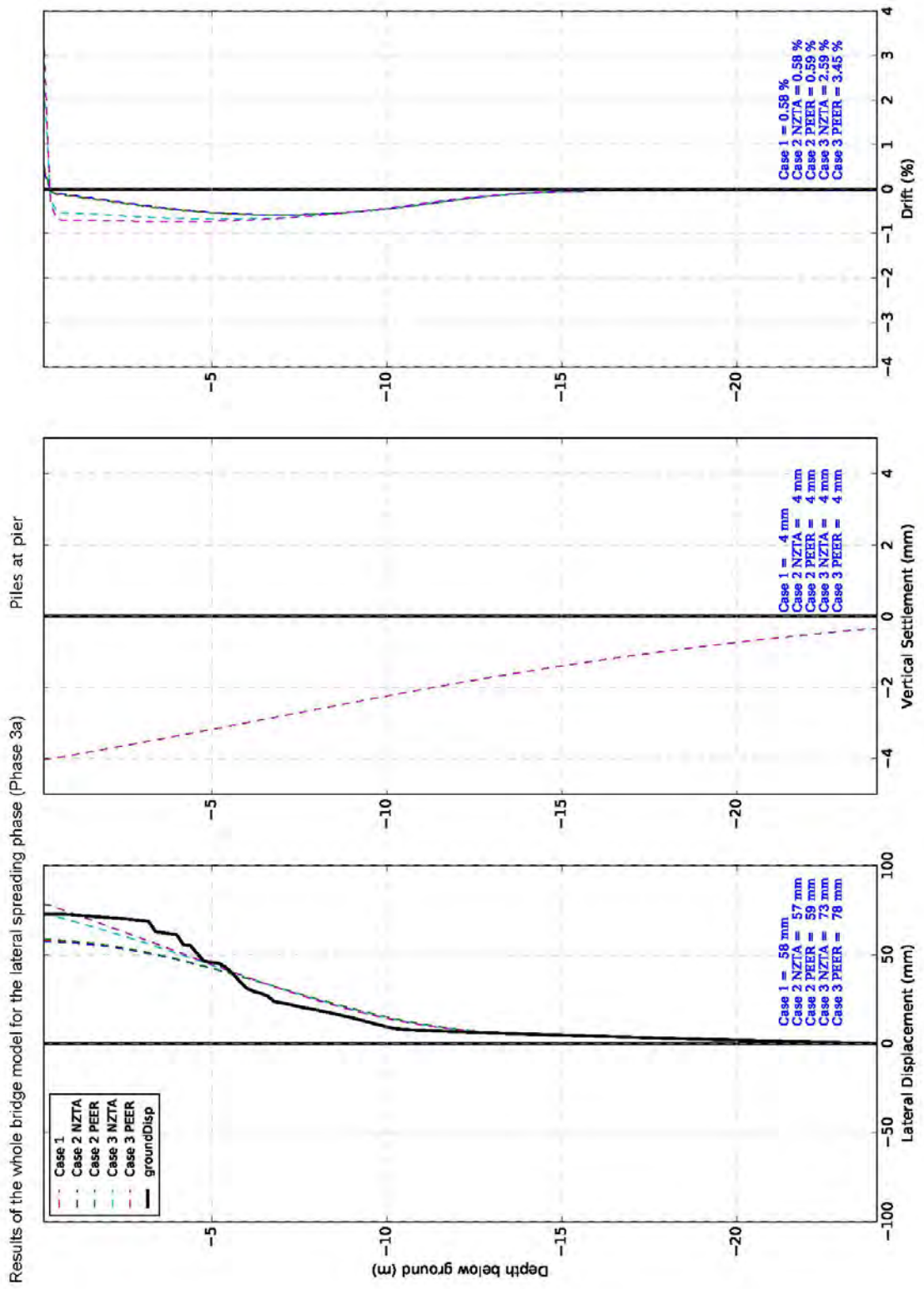
Results of the whole bridge model for the lateral spreading phase (Phase 3a)
Piles at pier
Depth below ground (m)
Lateral Displacement (mm)
Vertical Settlement (mm)
Drift (%)
Case 1
Case 2 NZTA
Case 2 PEER
Case 3 NZTA
Case 3 PEER
groundDisp
Case 1 = 58 mm
Case 2 NZTA = 57 mm
Case 2 PEER = 59 mm
Case 3 NZTA = 73 mm
Case 3 PEER = 78 mm
Case 1 = 4 mm
Case 2 NZTA = 4 mm
Case 2 PEER = 4 mm
Case 3 NZTA = 4 mm
Case 3 PEER = 4 mm
Case 1 = 0.58 %
Case 2 NZTA = 0.58 %
Case 2 PEER = 0.59 %
Case 3 NZTA = 2.59 %
Case 3 PEER = 3.45 %

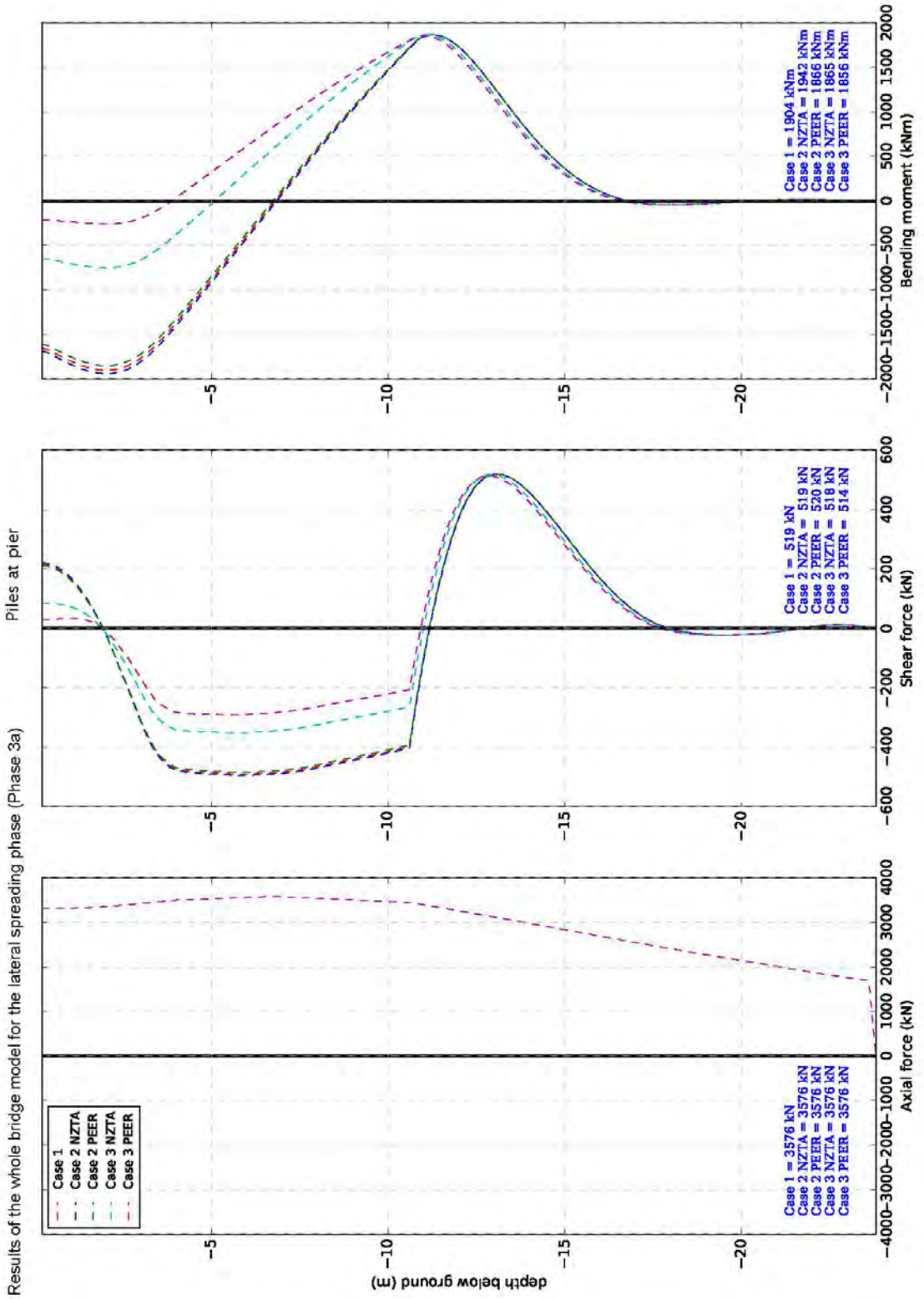
Results of the whole bridge model for the lateral spreading phase (Phase 3a)
Piles at pier
depth below ground (m)
Axial force (kN)
Shear force (kN)
Bending moment (kNm)
Case 1
Case 2 NZTA
Case 2 PEER
Case 3 NZTA
Case 3 PEER
Case 1 = 3576 kN
Case 2 NZTA = 3576 kN
Case 2 PEER = 3576 kN
Case 3 NZTA = 3576 kN
Case 3 PEER = 3576 kN
Case 1 = 519 kN
Case 2 NZTA = 519 kN
Case 2 PEER = 520 kN
Case 3 NZTA = 518 kN
Case 3 PEER = 514 kN
Case 1 = 1904 kNm
Case 2 NZTA = 1942 kNm
Case 2 PEER = 1866 kNm
Case 3 NZTA = 1865 kNm
Case 3 PEER = 1856 kNm

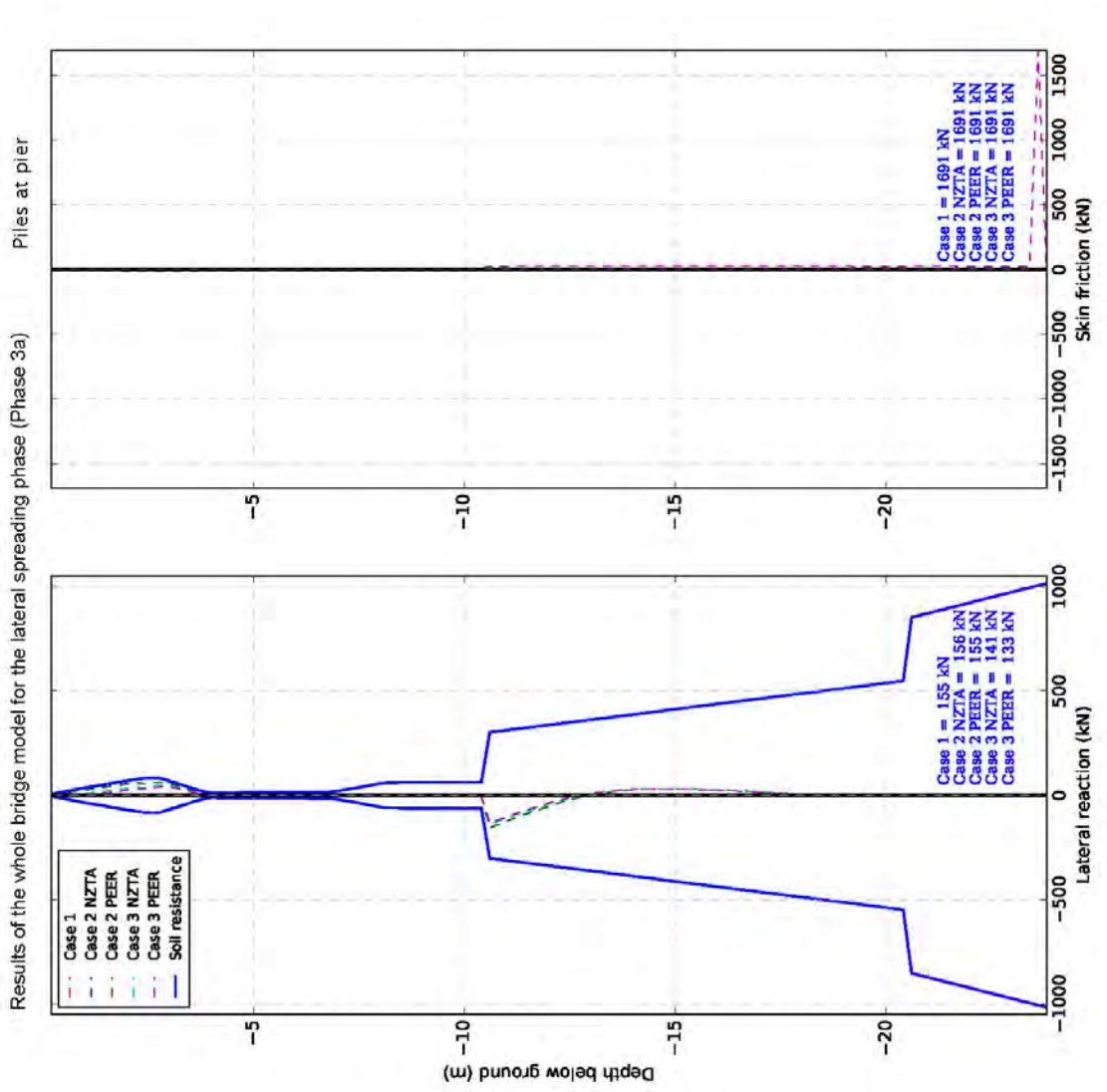
Results of the whole bridge model for the lateral spreading phase (Phase 3a)
Piles at pier
Depth below ground (m)
Lateral reaction (kN)
Skin friction (kN)
Case 1
Case 2 NZTA
Case 2 PEER
Case 3 NZTA
Case 3 PEER
Soil resistance
Case 1 = 155 kN
Case 2 NZTA = 156 kN
Case 2 PEER = 155 kN
Case 3 NZTA = 141 kN
Case 3 PEER = 133 kN
Case 1 = 1691 kN
Case 2 NZTA = 1691 kN
Case 2 PEER = 1691 kN
Case 3 NZTA = 1691 kN
Case 3 PEER = 1691 kN

A7 Results of the whole bridge model for the lateral spreading phase (Phase 3b)

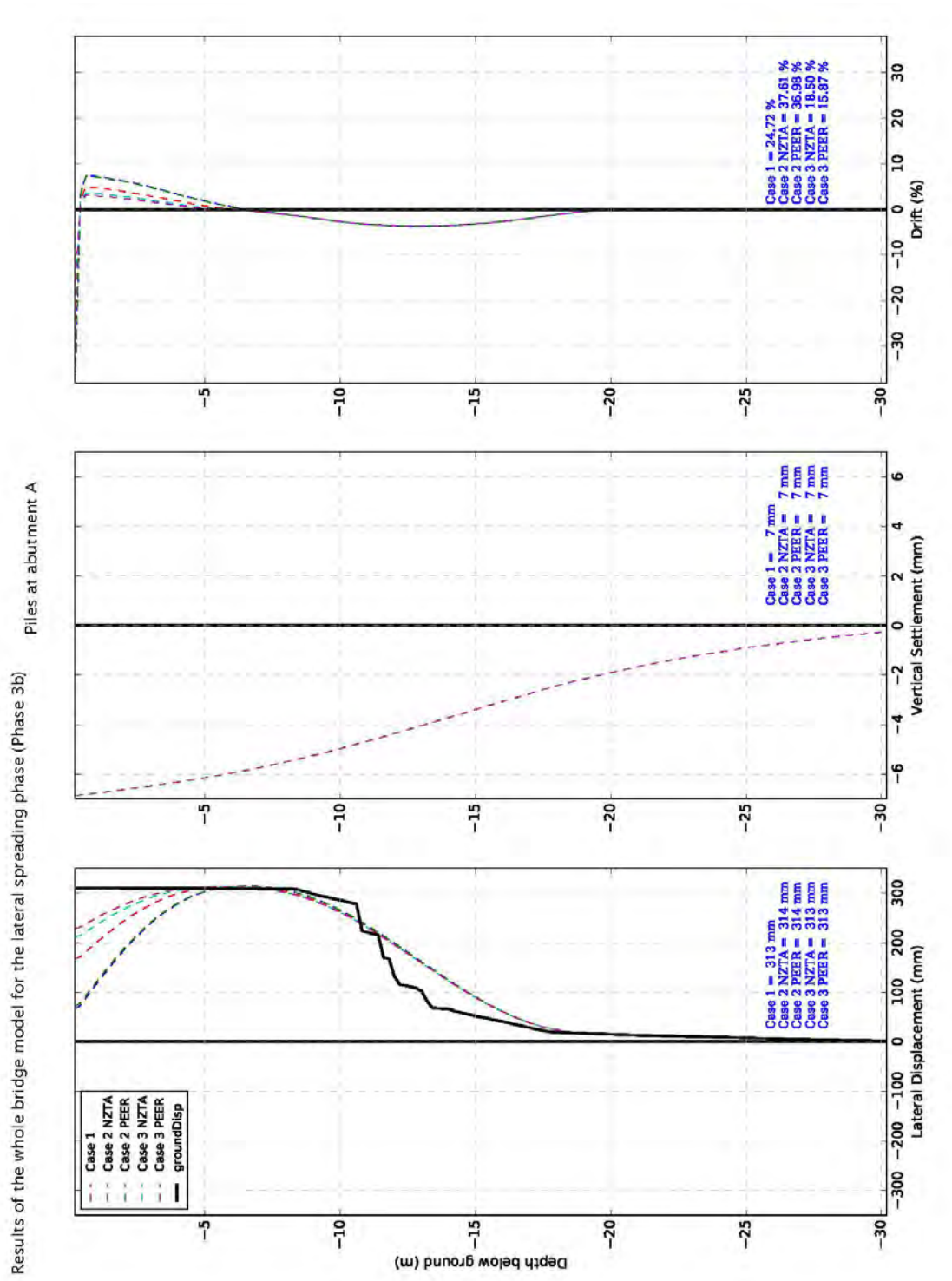

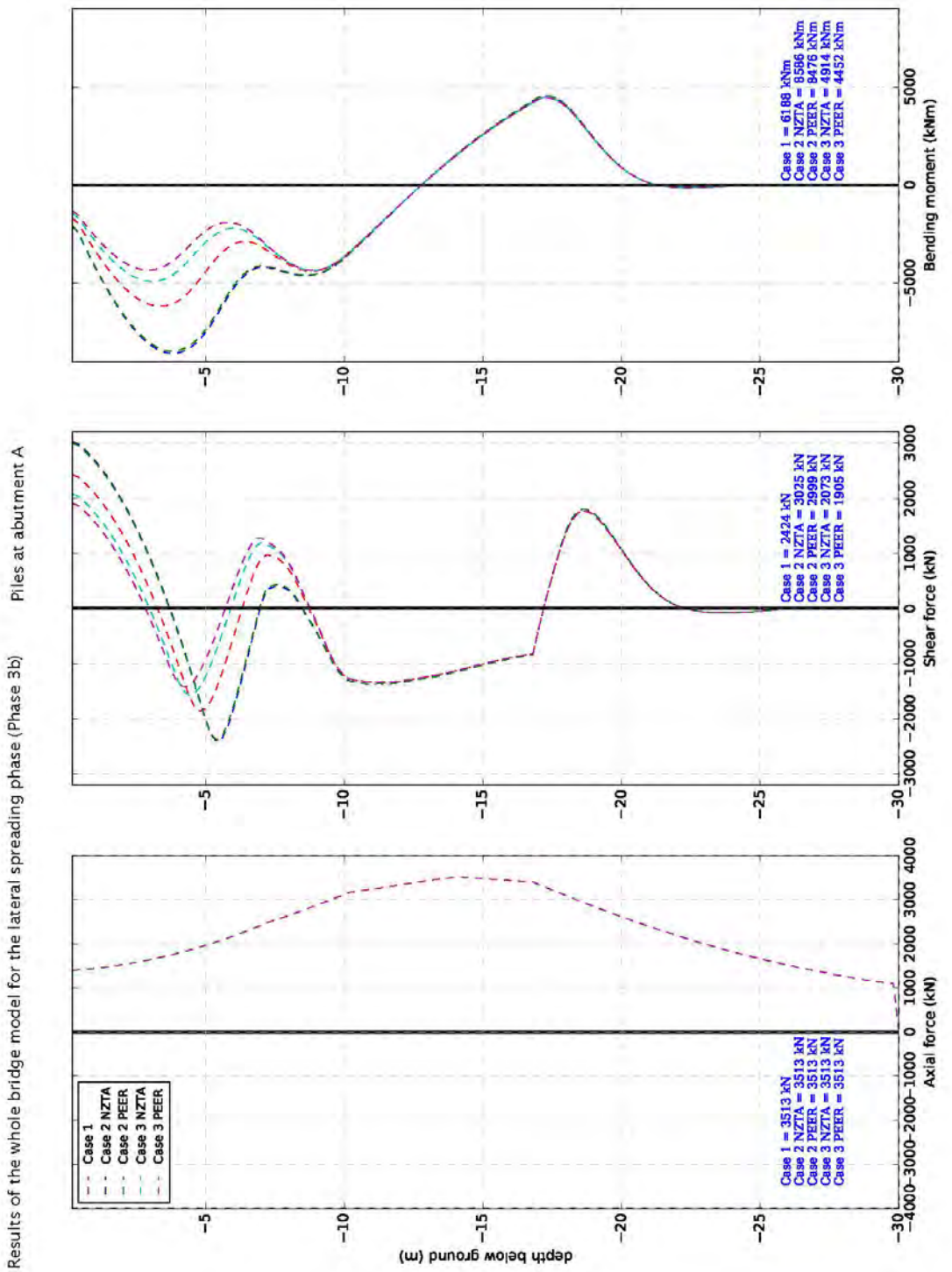
Results of the whole bridge model for the lateral spreading phase (Phase 3b)
Piles at abutment A
Case 1
Case 2 NZTA
Case 2 PEER
Case 3 NZTA
Case 3 PEER
Case 1 = 3513 kN
Case 2 NZTA = 3513 kN
Case 2 PEER = 3513 kN
Case 3 NZTA = 3513 kN
Case 3 PEER = 3513 kN
Axial force (kN)
Case 1 = 2424 kN
Case 2 NZTA = 3025 kN
Case 2 PEER = 2999 kN
Case 3 NZTA = 2073 kN
Case 3 PEER = 1905 kN
Shear force (kN)
Case 1 = 6188 kNm
Case 2 NZTA = 8586 kNm
Case 2 PEER = 8476 kNm
Case 3 NZTA = 4914 kNm
Case 3 PEER = 4452 kNm
Bending moment (kNm)
depth below ground (m)

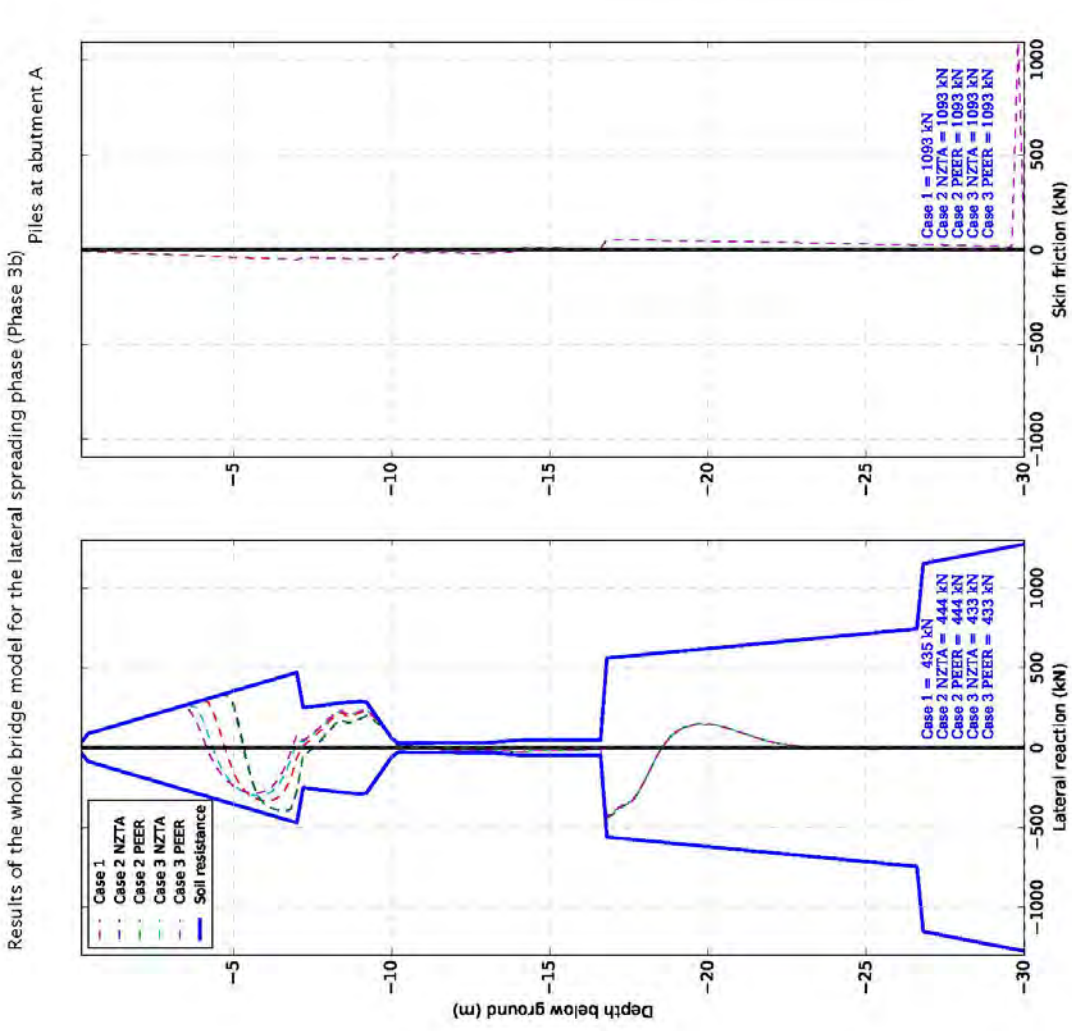
Results of the whole bridge model for the lateral spreading phase (Phase 3b)
Piles at abutment A
Depth below ground (m)
Lateral reaction (kN)
Skin friction (kN)
Case 1
Case 2 NZTA
Case 2 PEER
Case 3 NZTA
Case 3 PEER
Soil resistance
Case 1 = 435 kN
Case 2 NZTA = 444 kN
Case 2 PEER = 444 kN
Case 3 NZTA = 433 kN
Case 3 PEER = 433 kN
Case 1 = 1093 kN
Case 2 NZTA = 1093 kN
Case 2 PEER = 1093 kN
Case 3 NZTA = 1093 kN
Case 3 PEER = 1093 kN

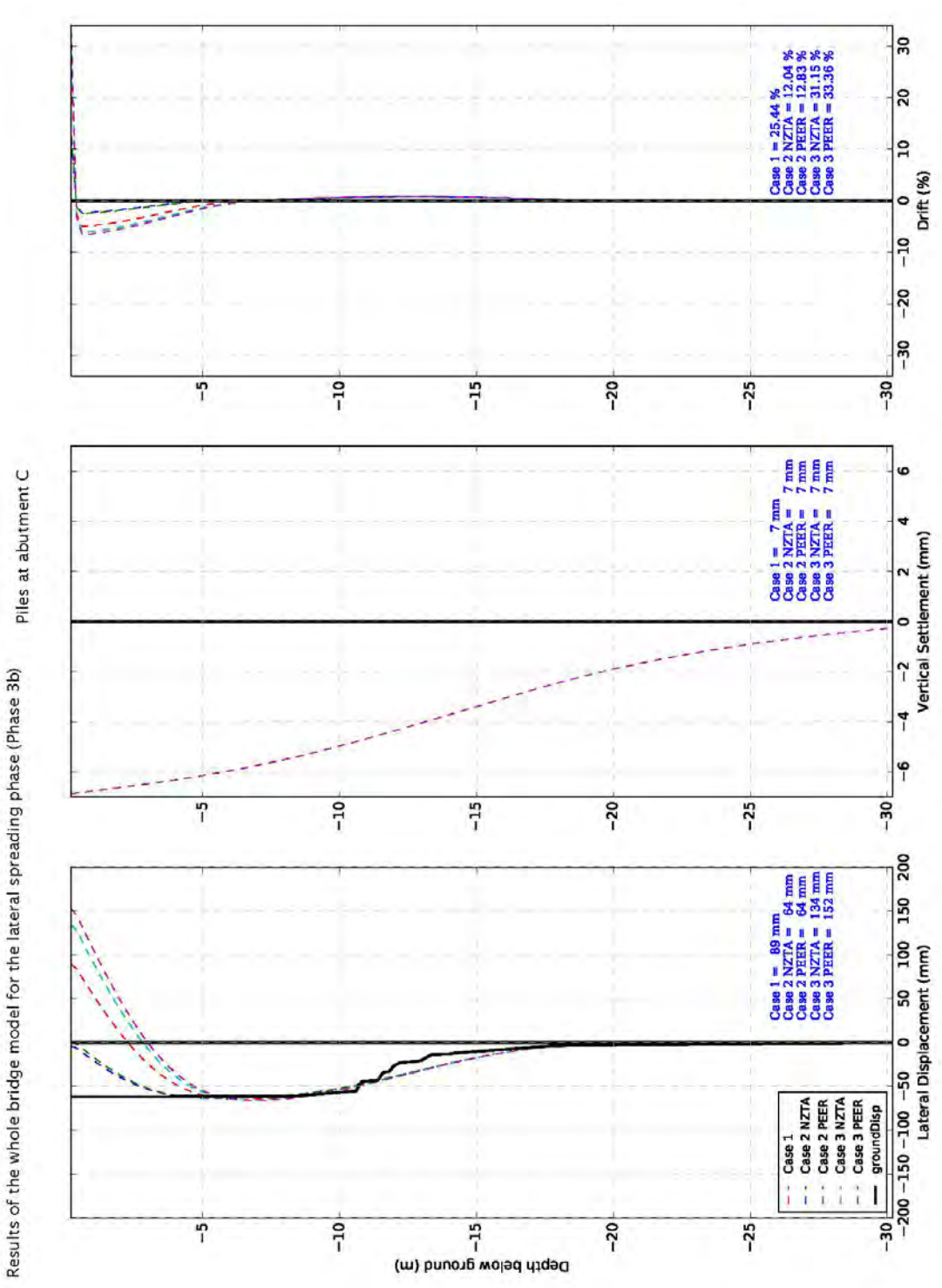
Results of the whole bridge model for the lateral spreading phase (Phase 3b)
Piles at abutment C
Depth below ground (m)
Lateral Displacement (mm)
Vertical Settlement (mm)
Drift (%)
Case 1 = 89 mm
Case 2 NZTA = 64 mm
Case 2 PEER = 64 mm
Case 3 NZTA = 134 mm
Case 3 PEER = 152 mm
Case 1 = 7 mm
Case 2 NZTA = 7 mm
Case 2 PEER = 7 mm
Case 3 NZTA = 7 mm
Case 3 PEER = 7 mm
Case 1 = 25.44 %
Case 2 NZTA = 12.04 %
Case 2 PEER = 12.83 %
Case 3 NZTA = 31.15 %
Case 3 PEER = 33.36 %
Case 1
Case 2 NZTA
Case 2 PEER
Case 3 NZTA
Case 3 PEER
groundDisp

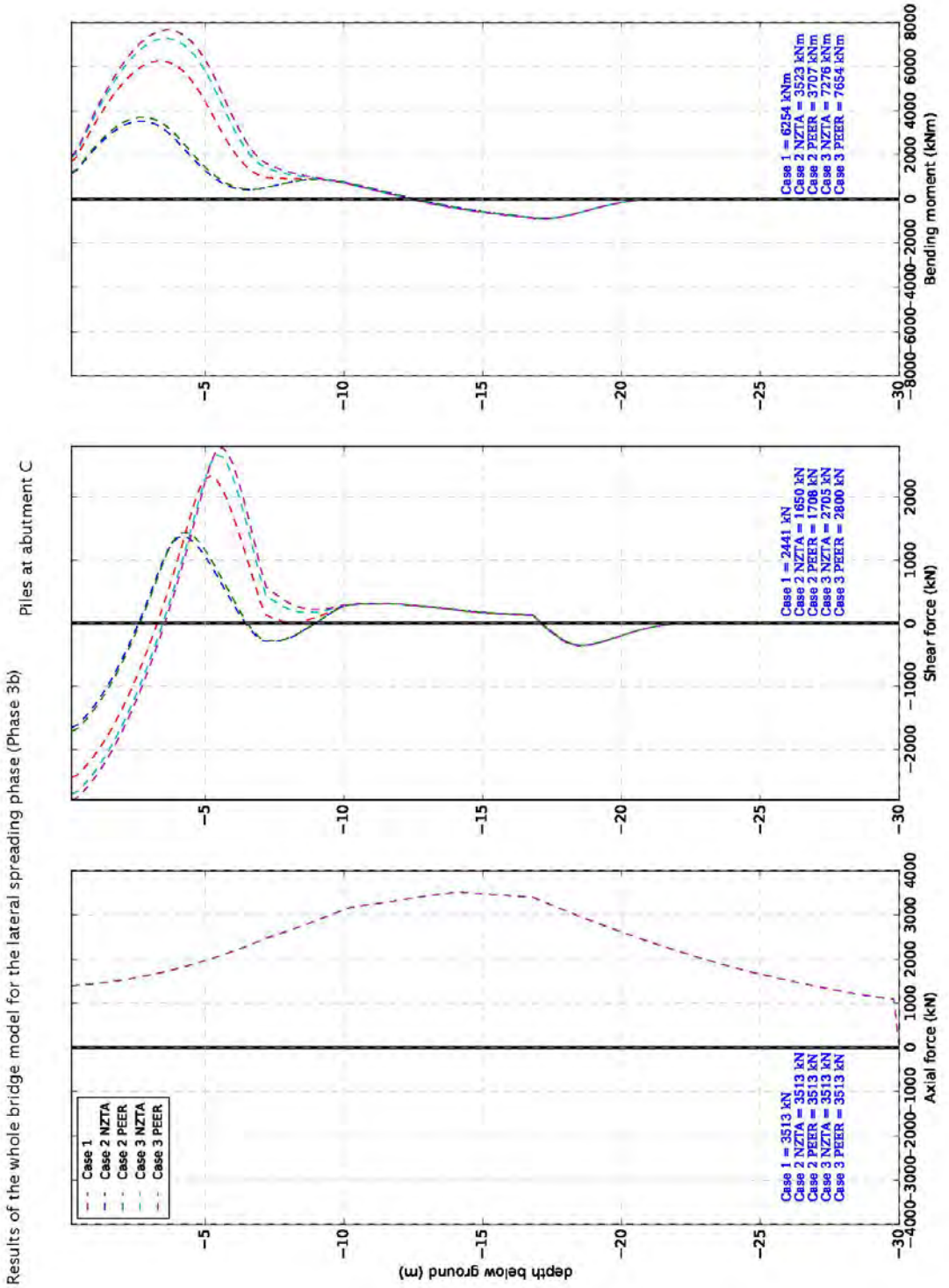
Results of the whole bridge model for the lateral spreading phase (Phase 3b)
Piles at abutment C
depth below ground (m)
Axial force (kN)
Shear force (kN)
Bending moment (kNm)
Case 1
Case 2 NZTA
Case 2 PEER
Case 3 NZTA
Case 3 PEER
Case 1 = 3513 kN
Case 2 NZTA = 3513 kN
Case 2 PEER = 3513 kN
Case 3 NZTA = 3513 kN
Case 3 PEER = 3513 kN
Case 1 = 2441 kN
Case 2 NZTA = 1650 kN
Case 2 PEER = 1706 kN
Case 3 NZTA = 2705 kN
Case 3 PEER = 2800 kN
Case 1 = 6254 kNm
Case 2 NZTA = 3523 kNm
Case 2 PEER = 3707 kNm
Case 3 NZTA = 7276 kNm
Case 3 PEER = 7654 kNm

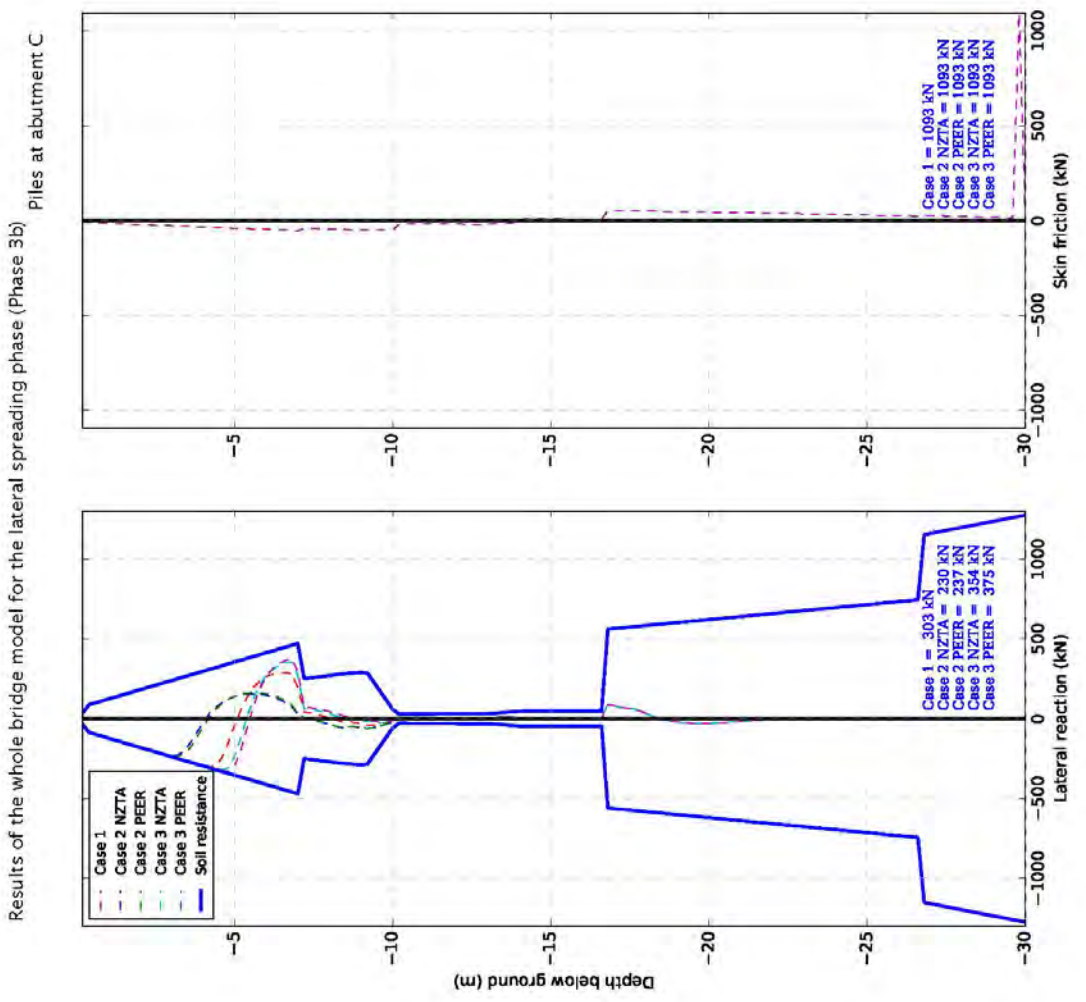
Results of the whole bridge model for the lateral spreading phase (Phase 3b)
Piles at abutment C
Depth below ground (m)
Lateral reaction (kN)
Skin friction (kN)
Case 1
Case 2 NZTA
Case 2 PEER
Case 3 NZTA
Case 3 PEER
Soil resistance
Case 1 = 303 kN
Case 2 NZTA = 230 kN
Case 2 PEER = 237 kN
Case 3 NZTA = 354 kN
Case 3 PEER = 375 kN
Case 1 = 1093 kN
Case 2 NZTA = 1093 kN
Case 2 PEER = 1093 kN
Case 3 NZTA = 1093 kN
Case 3 PEER = 1093 kN

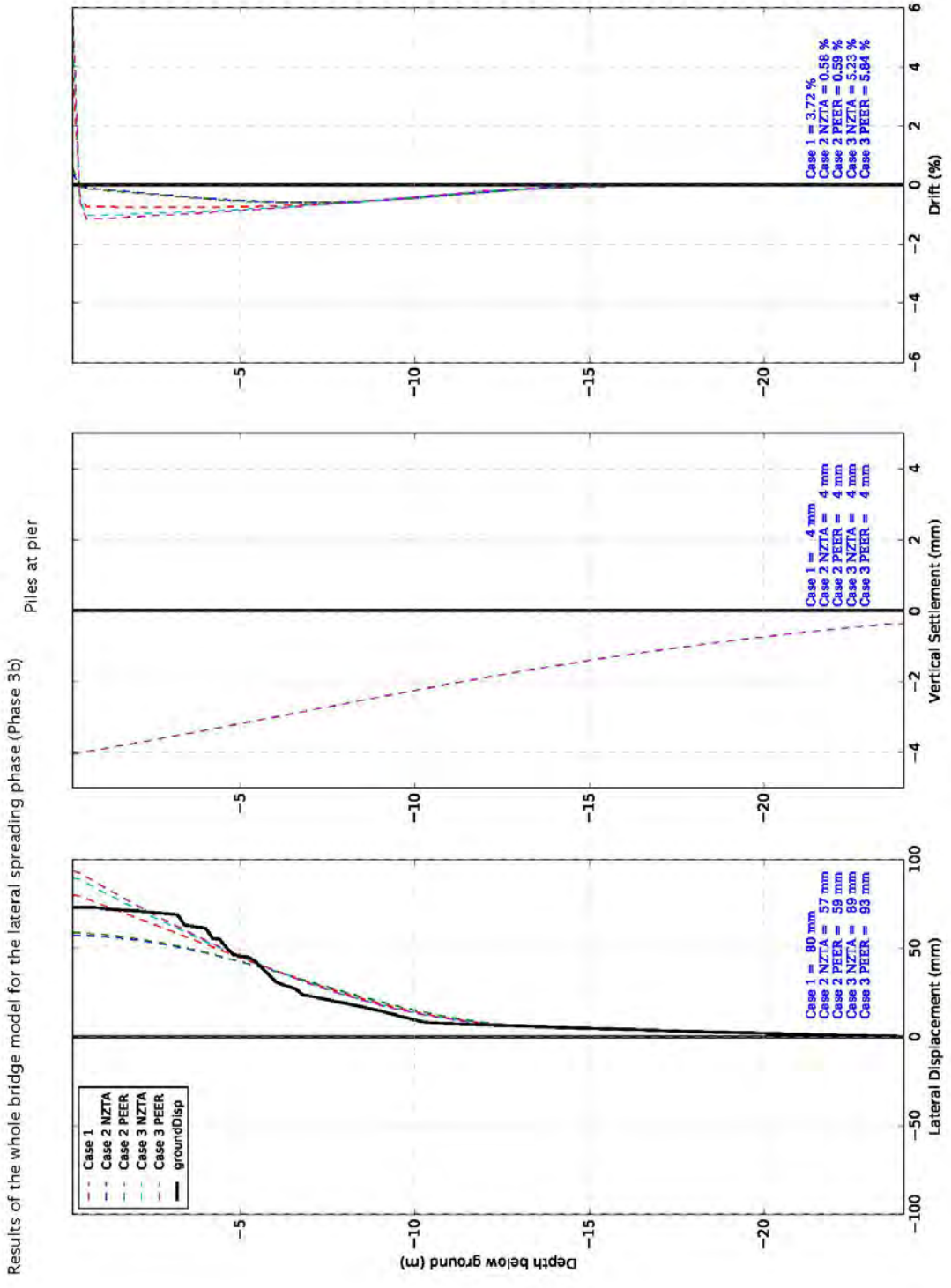
Results of the whole bridge model for the lateral spreading phase (Phase 3b)
Piles at pier
Depth below ground (m)
Lateral Displacement (mm)
Vertical Settlement (mm)
Drift (%)
Case 1
Case 2 NZTA
Case 2 PEER
Case 3 NZTA
Case 3 PEER
groundDisp
Case 1 = 80 mm
Case 2 NZTA = 57 mm
Case 2 PEER = 59 mm
Case 3 NZTA = 89 mm
Case 3 PEER = 93 mm
Case 1 = -4 mm
Case 2 NZTA = 4 mm
Case 2 PEER = 4 mm
Case 3 NZTA = 4 mm
Case 3 PEER = 4 mm
Case 1 = 3.72 %
Case 2 NZTA = 0.58 %
Case 2 PEER = 0.59 %
Case 3 NZTA = 5.23 %
Case 3 PEER = 5.84 %

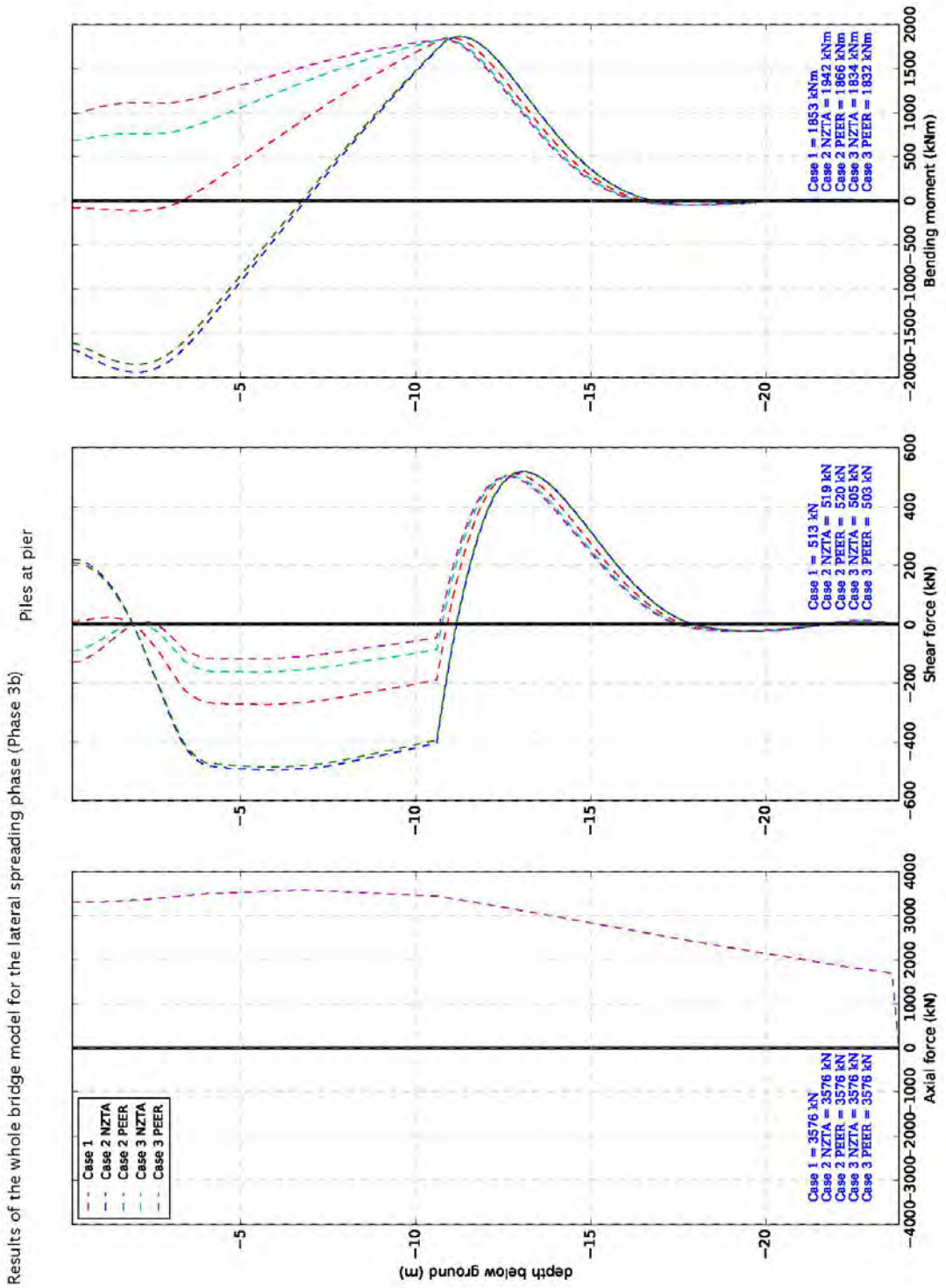
Results of the whole bridge model for the lateral spreading phase (Phase 3b)
Piles at pier
depth below ground (m)
Bending moment (kNm)
Shear force (kN)
Axial force (kN)
Case 1
Case 2 NZTA
Case 2 PEER
Case 3 NZTA
Case 3 PEER
Case 1 = 1853 kNm
Case 2 NZTA = 1942 kNm
Case 2 PEER = 1866 kNm
Case 3 NZTA = 1834 kNm
Case 3 PEER = 1832 kNm
Case 1 = 513 kN
Case 2 NZTA = 519 kN
Case 2 PEER = 520 kN
Case 3 NZTA = 505 kN
Case 3 PEER = 503 kN
Case 1 = 3576 kN
Case 2 NZTA = 3576 kN
Case 2 PEER = 3576 kN
Case 3 NZTA = 3576 kN
Case 3 PEER = 3576 kN

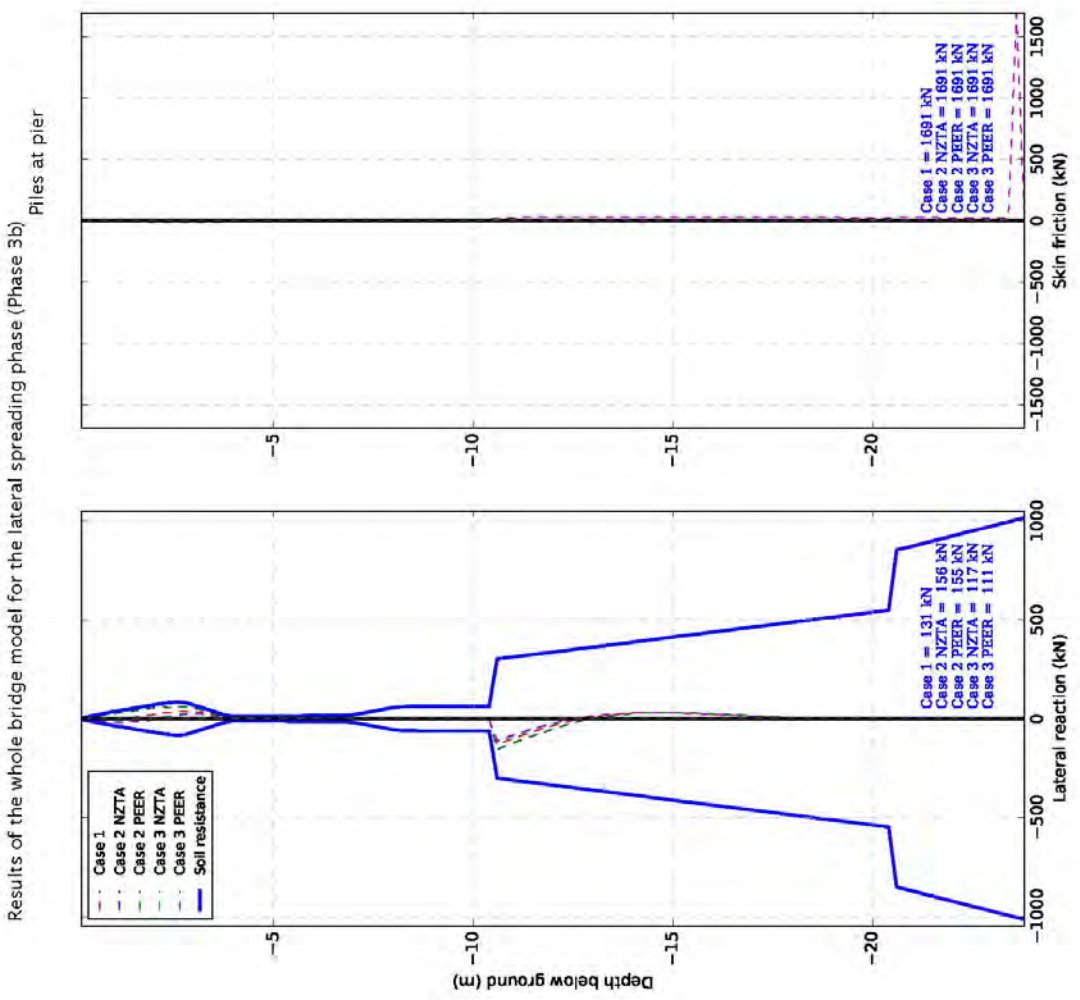
Results of the whole bridge model for the lateral spreading phase (Phase 3b)
Piles at pier
Depth below ground (m)
Lateral reaction (kN)
Skin friction (kN)
Case 1
Case 2 NZTA
Case 2 PEER
Case 3 NZTA
Case 3 PEER
Soil resistance
Case 1 = 131 kN
Case 2 NZTA = 156 kN
Case 2 PEER = 155 kN
Case 3 NZTA = 117 kN
Case 3 PEER = 111 kN
Case 1 = 1691 kN
Case 2 NZTA = 1691 kN
Case 2 PEER = 1691 kN
Case 3 NZTA = 1691 kN
Case 3 PEER = 1691 kN